STRESSES AND DEFORMATIONS IN FLEXIBLE LAYERED PAVEMENT SYSTEMS SUBJECTED TO DYNAMIC LOADS

by

S. F. Brown, B.Sc.

Thesis submitted to the University of Nottingham for the degree of Doctor of Philosophy, May, 1967.

STRESSES AND DEFORMATIONS IN FLEXIBLE LAYERED PAVEMENT SYSTEMS SUBJECTED TO DYNAMIC LOADS

by S.F. Brown, B.Sc.

Abstract

Many of the proposed rational design methods for flexible pavements are concerned with the stresses and strains which occur in the various layers of the structure. The purpose of the work reported is to investigate, in the laboratory, the complete stress and strain distributions set up in the different layers under dynamic loads.

Two systems have been investigated, a single layer of clay and a two layer system consisting of a granular base on a clay subgrade. The loading in each case consisted of a single pulse having a duration of loading between 0.1 and 2 sec. The load was uniformly distributed over a circular area and of varying magnitude.

In-situ measurements of stress and strain were made using pressure and strain cells, at various orientations. Surface deflection was measured with a rectilinear potentiometer.

Stress and strain distributions were determined by

moving the load relative to the buried transducers. By superimposing results, values of principal stresses and strains and maximum shear were derived. By combining stress and strain measurements, values of in-situ elastic modulus and Poisson's ratio were calculated.

Results were compared with elastic theory, both Boussinesq and layered system, the latter being computed using a recently developed program. Stresses showed good agreement with theory in both systems, but strains, being dependent on modulus, were less easy to predict theoretically.

In-situ values of modulus were stress dependent for both materials. For the clay, at low stress levels, the modulus increased sharply with decreasing stress, while for the granular material modulus increased with stress level.

In the two layer system results compared less favourably with theory, but the important values of tensile horizontal stress above the interface and vertical strain below the interface appear to be predicted adequately. The values of modular ratio were near to unity and hence Boussinesq theory was equally as adequate as the layered system approach for most effects.

Strains were predicted with fair accuracy when local values of modulus were used i.e., those in the neighbourhood of the points concerned. The assumption of perfect roughness at the interface, used in most theoretical solutions, was shown to be valid.

The stress dependence of modulus is thought to be one of the main problems at present in the application of layered system theory and, for the calculation of strains, in the use of the Boussinesq approach also.

SYNOPSIS

An experimental investigation to determine stresses, strains and deflections in model road pavement test sections is being conducted at the University of Nottingham as part of a major effort to establish a rational approach to the design of flexible pavements.

This thesis describes the second phase of the project and deals with a single layer subgrade of Keuper marl and a two layer system incorporating a granular base layer as well.

A great deal of work has been done to investigate the behaviour of the earth pressure cell and the strain cell, both of which instruments were of primary importance in the main investigation.

Measurements of stress and strain were made in both the systems described above, when they were subjected to dynamic load analogous to that provided by a passing vehicle.

Both the clay and granular materials were found

to have non-linear stress/strain relationships, but stresses were in general predicted well by linear elastic theory. For the prediction of strain by this means, a knowledge of the stress/strain relationship for the material is required.

CONTENTS

INTRODUCTION

The work described in this thesis is the Author's main contribution to a major experimental research project in the field of flexible pavement design, being undertaken at Nottingham University.

The majority of highway pavements, today, are designed largely by empirical rules based on simple tests carried out on subgrade soils, and on experience. The most common design method is that based on the California Bearing Ratio (C.B.R.) of the subgrade and is the one recommended for use in the U.K.[1] While it has been claimed that the C.B.R. design method, because of improvements made in recent years is a "rational" approach to flexible pavement design,[2] no one disputes the fact that it is largely empirical. There is some confusion, therefore, in the literature as to the definition of the word "rational" when applied to design methods. It is generally taken as being descriptive of design methods, not yet used extensively in practice, which are analogous to those used in the design of structures, and this is the definition used in what follows.

The Nottingham University project is part of a world wide effort now being made, particularly in N. America and Western Europe to try and evolve structural design, or "rational" design methods for flexible pavements.

The main shortcoming of the C.B.R. method is that it takes little or no account of the strength of the upper layers in a pavement structure. Since it is based on experience under certain conditions, there is a danger in extrapolating the results to new conditions, either of climate, loading or type of construction. The best of the various proposed rational design methods aim to determine the critical stresses and strains in the various layers, and to ensure that these do not exceed permissible values for the materials being used. This is the usual approach in problems of structural design, but it is much more complicated when the structure is a flexible pavement, because of the complex behaviour of road making materials and underlying soils.

Most of the suggested rational design methods are based on the theory of elasticity and its application to what is known as a "three-layer system". This is a

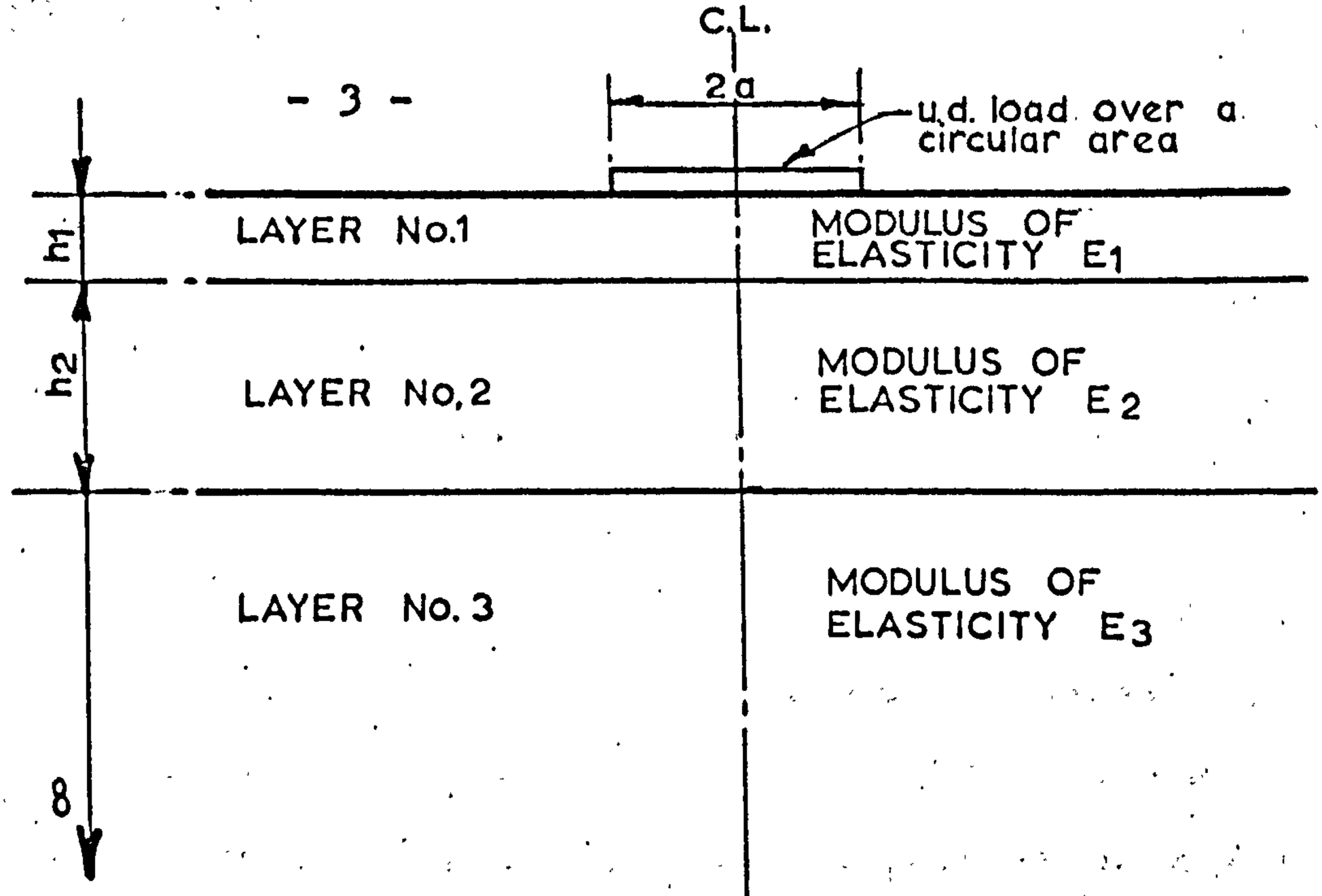

FIG. 1 THE THREE LAYER SYSTEM

simplified model of an actual pavement (Fig. 1) and expressions for stress and deformation resulting from the application of a circular uniformly distributed load were first derived by Burmister.[3] Most theoretical analyses have used his equations, or their numerical solutions, to calculate the important values of stress, strain or deflection.

The critical points in the structure would appear to be the top of the subgrade and the bottom of the upper layers.[4] If the vertical strain in the subgrade is excessive, large deformations of the whole structure result, causing an uneven riding surface and probably

cracking in the upper layers. Road making materials, particularly unbound granular bases, cannot carry very much tension, particularly in the case of bound bases when subjected to repeated loading, because of the possibility of fatigue failure. Tensile stresses, which have their maximum values at the bottom of the surface and/or base layers, must therefore be limited to avoid cracking. Apart from the obvious structural weakness caused by the presence of cracks, they also allow moisture to enter the pavement resulting in additional weakness, particularly to unbound bases, and to all materials in the event of frost.

These theoretical design methods have, in many cases, assumed elastic behaviour of the pavement without sufficient justification. Bituminous materials are known to be visco-elastic[5] and most fine grained soils and granular materials have non-linear stress-strain relationships,[6] so the assumption of linear elasticity is, on the face of it, a sweeping one. Whiffin and Lister[7] in a paper concerned with the applicability of elastic theory showed that under dynamic conditions i.e. vehicle speeds in excess of 15 m.p.h., pavements appear to behave elastically, provided that failure is not imminent.

If pavement materials are approximately elastic in behaviour under traffic loading conditions, then there is justification for using theories based on this assumption. At the present time these are the only ones available, although work is progressing on a visco-elastic approach, which would more completely describe the behaviour of the bituminous materials in particular.[8]

Two elastic constants are used to define each material in the theory of elasticity approach. These are Young's modulus (E) and Poisson's ratio (ν). The effectiveness of the theory then depends on how well these values can be predicted, and various suggestions have been made for methods to determine, in particular, the in-situ moduli of pavement materials. Poisson's ratio has less effect on stresses in a layered system than modulus, Peattie[9] having shown that a reduction from 0.5 to 0.35 only seriously affects horizontal stress at the bottom of the top layer.

There are three main interdependent topics which require investigation before a rational approach to the design of flexible pavements can be successful. There needs to be an adequate theoretical understanding of the

behaviour of layered systems, and this subject has already received a good deal of attention although it has been somewhat isolated from experimental work. Secondly controlled laboratory testing of model pavements and paving materials needs to be conducted. The validity of theoretical approaches can be checked by comparison with measurements on model pavements. The strength characteristics of soils, and base and surface layer materials subjected to repeated dynamic loading can be evaluated using suitable specimens. This could provide the appropriate elastic constants for use in theoretical analyses and also indicate safe working stresses or strains. Finally full scale road tests are required to check whether design procedures evolved from a combinations of theory and laboratory testing are satisfactory in practice.

The main aim of the Nottingham University project, of which this thesis describes a part, is to check the validity of linear elastic solutions to three layer systems, by testing model pavements in the laboratory. The procedure consists essentially of applying a single dynamic load pulse to the structure and measuring, by means of buried transducers, stresses strains and deflections at different locations.

By testing a model pavement made up of typical road making materials, important information can be obtained about the performance of different types of material. The present programme includes a typical clay subgrade, a granular material which may be used as a sub-base on main roads or a base on minor roads, and a bituminous material found in surface and base layers. Several typical materials have therefore been catered for and others could be included in future pavement structures.

While endeavouring to make the pavement as realistic as possible, it has been necessary to make certain compromises. The granular base layer was of a smaller particle size ($\frac{3}{8}$ in maximum) than found in practice, so that the transducers which were developed for use in clay, could work satisfactorily. This thesis does not deal with the bituminous layer, but it is possible that a sandsheet mix would have to be used, again to facilitate instrumentation.

Since theoretical solutions were to be checked, it was necessary to make the pavement follow, as closely as possible, the assumptions involved in these solutions. The loading system was therefore arranged so that a uniformly distributed load was applied over

a circular area through a flexible platen. In practice the contact area is usually elliptical[7,10] although it depends on the type of tyre and its inflation pressure.

If a wheel load were applied to the model pavement, it would be difficult to control the load and especially the rate of loading if the wheel was to be rolled across the surface. The circular platen which was adopted is kept stationary and a single load pulse applied. This produces the gradual increase, and then decrease, of stress at a point in the pavement as occurs when a wheel passes over it. The difference between the two types of loading is greater at the surface since under a rolling load there is an instantaneous increase in contact pressure as the wheel arrives. Another difference is that of rate of loading which beneath a rolling load decreases with depth, while for the stationary pulse it is constant.

Early work on this project was described by Tory[11] and his contribution consisted mainly of developing suitable apparatus and techniques for tackling the experimental work. An important contribution was the development of a soil strain cell for measuring in-situ

dynamic strains, and it was realised that this instrument, in conjunction with the less novel earth pressure cell, could provide important information about the in-situ moduli of subgrade soils and possibly granular bases, as well as indicating strain distributions.

This thesis deals with tests on single and two layer systems. The single layer work is an extension of Tory's contribution. He obtained stress, strain and surface deflection measurements but they were not comprehensive enough to calculate many other effects. The present work includes measurements from which the complete description of stress and strain at a large number of points has been obtained both for the single and two layer systems. Other, more important derived results, were values of modulus and Poisson's ratio at these same points, so that the variation of these elastic "constants" could be studied.

Prior to Tory's work, in-situ strains had not been successfully measured. The main contribution of this thesis is, therefore, to present in-situ dynamic strain measurements and values of principal strains and also values of elastic constants for a clay and a granular material calculated from in-situ measurements of stress and strain. These items have not previously

been presented, but other workers have produced comprehensive information about stress distributions although not under dynamic conditions, and only for either a single layer system[12,13] or the subgrade of a two[14,15] or three layer system.[16] The work herein presents measurements at the interface and within the base layer for the first time.

Incidental to the main project but equally important, is the work described in Chapters 3 and 4 on calibration of the pressure and strain cells used in the main investigation. These instruments were originally developed by Sparrow and Tory,[17] and they have now been thoroughly tested and their performance assessed in a clay and a granular material. The most important point illustrated by the pressure cell tests is that since the instrument has to work in a three dimensional stress field it must not be cross-sensitive i.e., stresses other than normal to the direction of measurement should have no effect on the cell output. This point is emphasised because it is believed that many of the pressure cells which have been used in the past are cross-sensitive.

CHAPTER 1 REVIEW OF CONTRIBUTIONS TO THE PROBLEM OF LAYERED SYSTEMS

1.1 Theoretical solutions to layered systems

Almost all the papers published in the last twenty years dealing either theoretically or experimentally with the problem of layered systems have used as their starting point the important paper by Professor Burmister published in 1943.[3] In this paper, Burmister applied the principles of the theory of elasticity to a two-layer system and later extended his work to the more useful three-layer problem.[18] Details of these two systems are shown in figs. 1 and 1.1. Since the appearance of Burmister's paper a good deal of work has been carried out in several countries to try and establish a rational approach to the design of flexible pavements, but now, over twenty years later, the semi-empirical California Bearing Ratio method is still the most widely used.

With the increasing use of the electronic computer, theoretical solutions based on Burmister's original equations have become more numerous and general, while experimental work on component materials and model pavements has provided a better understanding of the

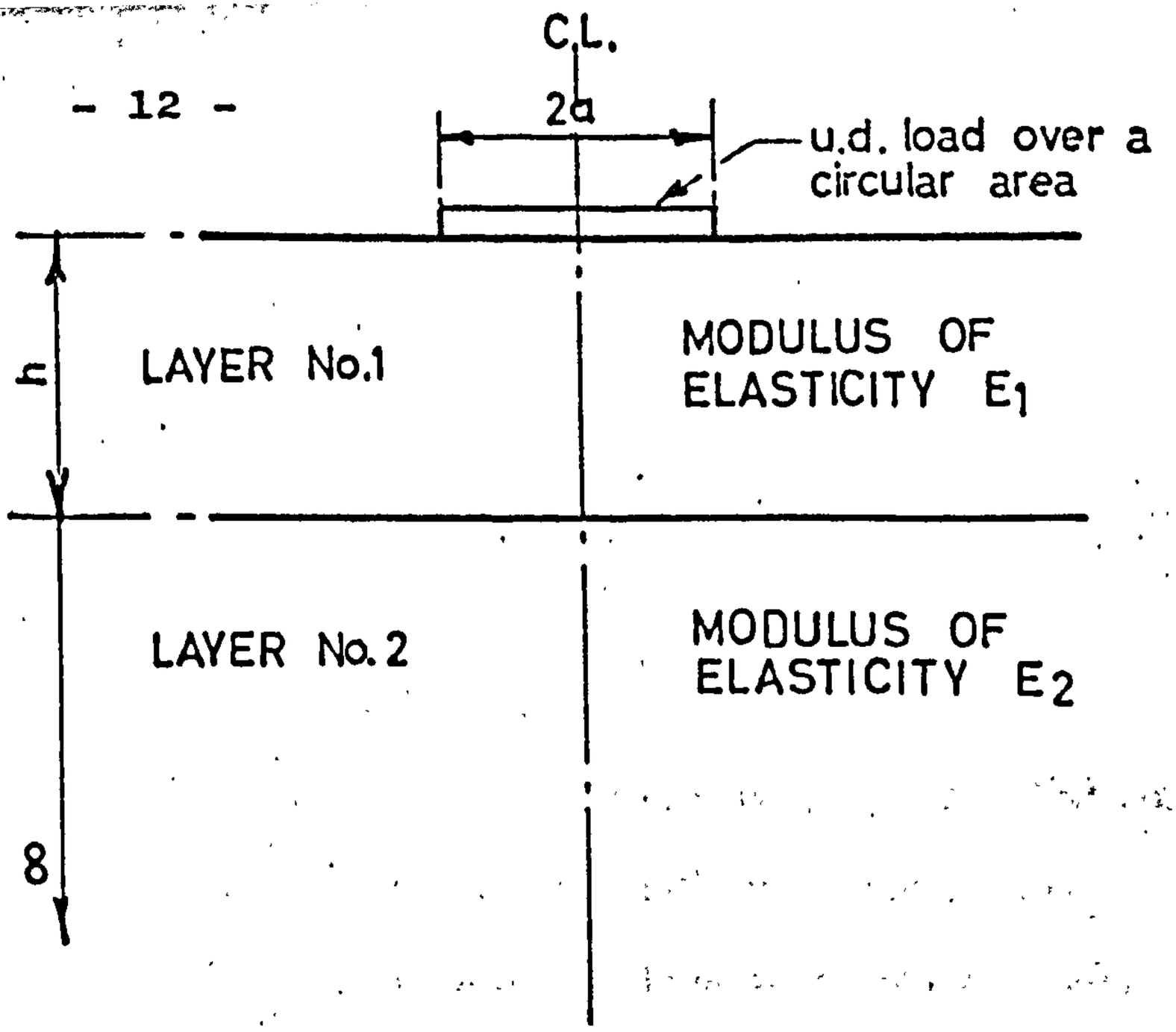

FIG. 1.1 THE TWO LAYER SYSTEM

behaviour of flexible pavement structures under dynamic load.

Burmister[3] used his two layer equations to calculate surface deflections in various cases, but Fox[19] in 1948 was the first to evaluate stresses in a two layered system for various values of the governing parameters E1/E2 and a/h. These results were restricted to positions on the axis of the load, but he also used a relaxation method to provide more comprehensive information about stresses at various depths and radii in four different two layered systems.

The same year Hank and Scrivner[20] also produced a limited number of solutions to the Burmister equations,

calculating vertical and radial stress just above and below the interface for various two layered systems and also either side of the top interface of a three layer system.

Three years later, Acum and Fox[21] extended Fox's original work to a three layered system by calculating stresses on the axis for several different systems, but the values were only those at the two interfaces, just above and below in each case. The important parameters were $k_1 = E1/E2$, $k_2 = E2/E3$, $a_1 = a/h_2$ and $H = h1/h_2$. They considered 6 values of k_1, 5 values of k_2, 2 values of a_1 and 4 values of H, producing results for most combinations of the chosen values.

It was not until 1962 that more comprehensive results were published by Jones,[22] who with the aid of a digital computer, the Ferranti Mark I, extended the work of Acum and Fox. Jones increased the number of values of the four parameters and his results occupied 28 tables against the 8 of Acum and Fox.

Despite this apparently comprehensive set of results, the three layer problem was still not completely solved since the available values were restricted to those at the interfaces and on the axis of the load. While maximum and therefore critical values occur on the axis

under a single wheel, for a dual wheel the worst condition may occur midway between wheels and this effect can only be calculated by superposition of two results off the axis. A further restriction to the use of these tables is that they are only suitable if the dimensions and elastic constants of a particular pavement correspond to those tabulated. It was, however, clear from Jones' paper that complete tables of results, universally applicable, would not be practicable and that the computer should be programmed to solve the particular problem required.

This was further illustrated by the even greater volume of results, mainly for two layered systems, produced by Mehta and Veletsos.[23] They computed stresses and deformations at various depths and radii for systems with 8 different values of a/h using an Illiac computer. Poisson's ratio was taken as 0.25 in both layers, whereas Jones et al had used 0.5. Mehta and Veletsos did, however, produce some stress results on the axis for varying Poisson's ratio, the values taken being 0, 0.25 and 0.5. Their 44 tables of results included some for three, four and five layered systems, and they also considered some problems with perfectly smooth conditions at the interface.

Jones[24] also produced in 1962, tables to calculate vertical surface deflection for three layered systems. The parameter values he used were slightly more numerous than for his stress results published earlier and he took Poisson's ratio as 0.35 instead of 0.5 for each layer. Results were again restricted to the axis of the load.

The equations for calculating the stress distribution in a semi-infinite soil mass, as opposed to the more complicated layered systems, were originally presented by Boussinesq.[25] His theory has however been used to predict stresses beneath a pavement, although it ignores the greater stiffness of the upper layers. Fröhlich[26] overcame this by including a concentration factor to take account of the extra strength of these layers. A lot of interest over the years has centred on the original Boussinesq problem with a view to trying to verify his equations by experiment. This "single layer" system has been studied in detail by several workers as well as the Author, but the Waterways Experiment Station made a major contribution both experimentally and theoretically. Again with the aid of a computer, Ahlvin and Ulery[27] produced a very comprehensive and useful set of tables to calculate stresses, strains and displacements in a semi-

infinite mass subjected to a circular U.D. load. Values of modulus and Poisson's ratio for the material are not built into the tables, but can be chosen appropriately by the user. Because of the smaller number of variables involved in this single layer problem, a set of tables is suitable for solving most systems whereas for two or three layered systems it is not.

When work on the Author's two layered system was in progress, Shell made available a computer program developed by Jones[28] using a UNIVAC 1107 computer to solve the multilayer problem completely. The only drawback was that of all elastic solutions, namely the assumption of linear elastic behaviour for all layers. A program dealing with a variable modulus is being developed at the time of writing.[29] The program which was used, can deal with any number of layers up to about ten, although in practice, anything greater than four occupies a great deal of computing time, but this snag is being overcome.[29] Values of modulus and Poisson's ratio can be specified for each layer and results, consisting of a full description of stress and strain, plus vertical and radial displacement, can be computed for any desired location. This is hence, a major advance on previously published solutions, which were necessarily restrictive.

The future development of Jones' program to cater for a variation of modulus with depth should be even more useful, since one of the major conclusions of this thesis is that the granular base layer and subgrade materials have stress dependent moduli. As shown in Chapter 7 and elsewhere,[6] modulus can be taken approximately as varying with depth, provided the radius is restricted to less than that of the loaded area. An approximate method for dealing with the variable modulus problem has also been outlined by Cummings and Gerrard.[30]

1.2 Experimental determination of stresses in layered systems

Useful and relevant laboratory tests on model pavements have been comparatively few in number. One reason for this is the practical difficulty of measuring in-situ stresses and strains. The single layer system was dealt with in a fairly comprehensive way by the Waterways Experiment Station.[12,13] They studied two test sections, one of sand and the other of silty clay and produced stress distribution plots which showed good agreement with the Boussinesq solution. There were two main shortcomings to this work when thought of in terms of pavement behaviour. Firstly, no reliable strain

measurements were taken so that in-situ values of modulus and Poisson's ratio could not be calculated direct and, secondly, the loading was applied statically.

Work on pressure measurements in sand as a single layer system, beneath a base layer and beneath a base with asphalt surfacing has been carried out by Allwood,[31] Hu[32] and Buck[33] at Birmingham University. Again static loading was applied and no strain measurements were taken. In the single layer system studied by Hu, a lot of stress measurements were taken on various planes and the results presented in the form of pressure bulbs. A lot of time was spent in calibrating the pressure cells, but as pointed out by Tory[11] alluding to Allwood's work with the same cells, no attention appears to have been paid to cross-sensitivity, which could introduce large errors particularly to horizontal stress measurements.

In the two and three layer systems which Hu and Buck worked with, no measurements were taken in the upper layers, the argument being that in a pavement structure the layers above the subgrade are stronger and, therefore, any failure will take place in the subgrade. This argument clearly ignores the different modes of failure which are possible in the more highly

stressed upper layers.

An artificial interface in the form of waterproof paper was introduced between the layers which departs from practice, and makes comparison with layered theory difficult, since perfectly rough conditions are generally assumed at the interface.

Although stress measurements were superimposed in order to calculate shear stresses and principal stresses, no check appears to have been made on whether stresses at a point produce an equilibrium condition. This is particularly necessary since Hu concludes that the sand is not homogeneous or isotropic and presumably superposition introduces errors, which need correcting before using the stresses to derive other values.

One of the main conclusions of Hu's thesis is that since the sand behaves in an "elastic-plastic" manner, no solution is possible by the theory of elasticity. While this may well be true for static conditions, under dynamic traffic loading, the theory of elasticity may well be valid, and because of this it is important that conditions of loading on model pavements should be dynamic in character. Buck, however, pointed out the possibility that results under static conditions may not be applicable for "live loads".

McMahon and Yoder[14] measured vertical stress resulting from the application of a static load through a rigid platen. Both single layer (clay subgrade) and two layer (granular base on clay) systems were tested, but the results did not correlate particularly well either with Boussinesq or Burmister two layer solutions. Again only subgrade stresses were measured.

Sowers and Vesic[16] also measured vertical subgrade stress beneath various types of base layer subjected to static load applied through single and dual vehicle tyres. They concluded that for unbound bases, Boussinesq's theory predicted vertical stresses adequately, but for bound bases with significant tensile strength two layer theory was more accurate. The systems they tested were in fact three layers although the theoretical solutions were based on two layer theory. The values of modulus used to determine theoretical values were based on laboratory tests and were not necessarily the appropriate values for the materials in-situ.

Measurements of vertical stress in a sand subgrade beneath different types of base layer were also reported by Trollope, Lee and Morris.[15] Repeated static loading was applied and the stress distributions were compared with Boussinesq and with Burmister two layer theory. In

order to apply the latter a rather curious method was used to obtain values of modulus for the two layers. For concrete and soil cement bases, modulus was determined from beam tests and using this value in conjunction with measurements of surface deflection, the subgrade modulus was calculated using two layer theory. Armed with the values of modulus thus obtained, two layer theory was used to predict vertical subgrade stresses. Very good agreement was not surprisingly reported. A test of the applicability of two layer theory would have been demonstrated better by calculating E_2 from the vertical stress measurements and then using them to predict surface deflections. The reason for this is that deflection is far more dependent on modular ratio than vertical stress. Either way, the approach is not very satisfactory and emphasises the need for in-situ measurements of modulus for both layers.

1.3 Determination of In-situ Elastic Constants

Because in-situ strains have not been successfully measured in the past (except by Tory), values of modulus for the pavement materials have not been calculated from stress and strain measurements and hence other methods have had to be adopted. Three approaches have been used

by various experimentors in this field. They are ; repeated load triaxial tests on undisturbed samples, usually of subgrade soil, plate loading tests, both static and dynamic, and vibration testing of pavements.

A considerable amount of work on repeated loading of clay triaxial specimens has been carried out at the University of California under Professor Seed. He and his colleagues have pointed out the various factors affecting the modulus of clay,[34] not least of which is that of stress level, a conclusion also reached by the Author from in-situ measurements. One criticism of repeated load triaxial tests is that the specimen is not subjected to the same sequence of stress as occurs under a pavement. The passage of a wheel load produces a shear reversal which cannot be reproduced in a triaxial cell. Sparrow[35] has designed an apparatus which is an attempt to overcome this difficulty.

Repeated load tests have also been carried out on granular materials under Seed[6] and elsewhere[15] and here again the stress dependence of modulus makes the application of triaxial tests to pavement performance very difficult.

Not much work appears to have been done on bound base course mixes, but the behaviour of asphalt surface

layer materials has been extensively investigated. The stiffness of asphalt mixes can be obtained from the Nomograph presented by Van der Poel,[36] which was the result of testing a considerable number of asphalt specimens. The most important factors affecting the modulus of asphalt mixes are rate of loading and temperature, both of which are likely to vary significantly in an actual pavement.

Static plate load tests have been used extensively, particularly by Burmister,[37] to determine values of in-situ modulus, both for a homogeneous soil mass and for a two layer system. For the latter, modulus is calculated with the aid of Burmister's theoretical work on two layered systems.

Vibration, or "non-destructive" testing of pavements and pavement subgrades has been carried out by the Koninklijke-Shell Laboratorium in Amsterdam[38 to 41] and by the Road Research Laboratory in England.[42 to 46] Shell have used two methods to evaluate pavement strength, using a heavy vibrator at relatively low frequencies (5 to 60 c.p.s.) and a light electrodynamic vibrator at higher frequencies (up to 3,000 c.p.s.). The heavy vibrator has been used to determine the stiffness of a pavement structure simply by relating the applied force

to the deflection. It has also been used as a source of deeply penetrating waves, from whose velocity of propagation, the subgrade modulus can be calculated. The high frequency light vibrator with very much lower penetration was also used as a source of waves to determine the dynamic moduli of surface layers, or of the subgrade when placed directly thereon before construction. The Road Research Laboratory have also used this latter method and extensive work on the problems of wave propagation in layered systems has been done by Jones in connection with their test programs.[42 to 46] A convenient, if somewhat approximate, result of the Shell work is a simple relationship between dynamic modulus and C.B.R. of subgrade namely E = 1400 (C.B.R.) (lb/sq.in.).

Although vibration methods can determine the in-situ modulus of each layer in a pavement, since neither stress nor strain have been measured in the pavements tested, it is not yet clear whether these values of modulus can be used in layered system theory to accurately predict stresses and strains. Heukelom and Klomp[41] have checked the deflection measurements taken with their heavy vibrator against calculated values based on wave propagation measurements of modulus, with some success. This type

of vibration is, however, not exactly analogous to traffic loading because the rate of loading is constant with depth, whereas under traffic it decreases with depth. The rate of loading may also be faster than the worst conditions in a real pavement. Since it appears from results by Seed et al[6] as well as those herein, that the modulus of both fine grained and granular materials is stress dependent, results from the light vibrator are open to question, because little or no stress is applied to the system.

Cyclical plate loading tests[47] have also been carried out, since these were considered to represent traffic loading better than either static plate load tests or vibration methods. Once again, however, the values of modulus which resulted have not been proved to be reliable for use in layered system theory, except in some cases for the calculation of surface deflections.

The determination of in-situ values of modulus from stress and strain measurements is likely to be more accurate and realistic than any of the methods detailed above, and this is the approach adopted herein. The values of modulus thus obtained have been used in both single and two layer theory in order to determine stress and strain distributions which were then compared with

measured values. This approach does not produce unique values of modulus for the construction materials being used, but allows a study of the variation of modulus and, incidentally, of Poisson's ratio to be made. The results may well be only applicable for the particular installation from which they were obtained, but a good deal of fundamental information about the applicability of layered system theory to actual layered systems has been obtained.

1.4 Proposed Rational Design Methods

The method which at present comes closest to the ideal structural design approach is that developed by Shell and presented by Peattie[4] and Dorman,[48] appropriately, at the International Conference on the Structural Design of Asphalt Pavements in 1962. It was improved by Dorman and Metcalf[49] in 1964 and has been presented in other forms elsewhere.[50,51]

The Shell design method is based on the three layer elastic theory results of Jones[22] and their interpretation by Peattie.[52] The latter suggested[4] that pavements should be designed in order to limit vertical strain in the subgrade and tensile stresses and strains in the upper layers. The design method also uses the results

obtained by Heukelom and Klomp[41] for dynamic moduli of typical bases and subgrades from vibration testing, and in particular the correlation they reported between dynamic modulus and C.B.R.

The permissible vertical strain in the subgrade is taken as 650 micro-strain.[48] The problem of fatigue arises as the result of repeated applications of tensile stress to the bituminous layers, the suggested permissible tensile stress being 700 lb/sq.in. Dorman and Metcalf improved the design curves based on the above criteria to allow for different traffic intensities, by incorporating fatigue life results.

Burmister[37] has proposed a design method wherein the critical effects are deflection and shear stresses. On the reasonable assumption that there is perfect continuity at interfaces, he points out that if the modular ratios between adjoining layers are high, then large shear stresses will result. These shear stresses will only be mobilised by deflection taking place. Plate bearing tests are used to calculate elastic moduli and then using layered system theory vertical and shear stresses are calculated. These, and the overall deflection should not exceed certain permissible values. A small difference in modulus between adjacent layers is recommended.

In Burmister's approach there is no mention of the important fatigue aspect, although many writers, in particular Hveem,[53] have shown that there is a correlation between transient deflection and the occurrence of surface cracks, which are explained in terms of fatigue. This deduction is based on the fact that the pavement is adequate in other ways, there being no permanent deformation of any magnitude.

Most papers, other than those mentioned above, have admitted that while a rational design method is desirable it is not yet attainable, and the majority of contributions have therefore not attempted to present a complete design procedure. The difficulty with the Shell approach is that their design is based on theoretical calculations of stress and in particular strain, which have in the past been very difficult to measure in-situ. Checks on the design figures have not therefore been reported yet. This problem is being overcome by the Nottingham University project and by Shell laboratories in Holland and Germany. Papers are to be presented at the Second Internation Conference on the Structural Design of Asphalt Pavements[8] showing strain measurements in bituminous layers. The measurements so far at Nottingham are those presented herein dealing with an

unbound base and a clay subgrade.

From a selection of the many papers contrubuting to the problem of flexible pavement design by rational methods, several points emerge which are of interest. In North America, particularly, State Highway Authorities have recently revised their design procedures in the light of developments, and in particular as a result of the A.A.S.H.O. road test findings. The Asphalt Institute have produced revised recommendations for thickness design,[54] the background to which was described by Shook and Finn[55] and extensions have been presented by Shook.[56] The main short-coming of the A.A.S.H.O. test is that while surface deflections were measured, very few in-situ stresses, and no strains, were recorded.[57] Typical of the present outlook is that of North Carolina and Massachusetts. Hicks[58] describes how the thickness of pavements in North Carolina is determined by using Boussinesq stress distributions. The variation of stress with depth is plotted for the required wheel load. The depth at which the stress equals the allowable bearing stress for the soil is noted and the pavement constructed to a thickness equal to this depth. This procedure is little better than the C.B.R. approach, since it ignores the strength of the pavement structure itself. In

Massachusetts,[59] layered system theory is used as an indication of pavement thickness but details are based on the A.A.S.H.O. test findings. Current design practice in England is based on the recommendations of Road Note 29.[1] This method depends on subgrade C.B.R. values, which are tabulated for a variety of soils. These recommendations are based on experience and on full scale tests carried out by the Road Research Laboratory.

Several writers have expressed doubt about the validity of elastic layered system theory,[2,60] one important criticism being that since road making materials are very weak in tension, the tensile modulus is nearly zero. Elastic theory assumes it to be equal in tension and compression. Another criticism is that the materials are not elastic, but visco-elastic, and Baker[61] has suggested that a visco-elastic theory, when available, should be more accurate than the present elastic one. The programme for the Second International Conference at Ann Arbor[8] lists several papers on this topic. Any visco-elastic theory is going to be more complicated than the already complex elastic approach, and while an exact theoretical model is desirable, it is doubtful whether a visco-elastic solution will be practicable at this stage. This point is emphasised by the fact that visco-

elastic materials will behave elastically, if the rate of loading is sufficiently high, and the applications of load frequent enough.

Heukelom and Klomp[41] have shown that an unbound base is not likely to have a modulus more than twice that of the subgrade, although they show that theoretically it could be three times larger. The strength of the base layer can be improved by using a binder and there is now an increasing trend towards bituminous bound bases. McLeod[62] has pointed out that the choice could well be an economic one depending on the availability of suitable aggregates for unbound construction. If there is a shortage, then a thinner bound layer is likely to be used. The possibility of wastage of aggregate is also illustrated, since there would appear to be an optimum thickness of pavement above which the load carrying capacity per inch is greatly reduced. This optimum thickness, which is the total pavement depth, is given as 1.5 to 2 times the radius of the loaded area.

A great deal of effort, particularly in the United States has been put into investigations concerning deflection of layered systems. This is chiefly because of the ease with which it can be measured, using such means as the Benkelman beam,[63] and hence checked against

theoretical predictions. It also follows from the correlations shown by Hveem[53] and also the A.A.S.H.O.[57] and W.A.S.H.O.[64] tests between deflection and the incidence of cracking.

The University of California[6] have extensively investigated the factors affecting deflection and the way in which it can be accurately predicted. They have used elastic theory, but realised the problems involved, particularly in regard to the correct choice of values of modulus for each layer. A thorough review of the factors affecting modulus of various pavement materials is presented, the main conclusion being that modulus varies within a layer, whereas elastic theory assumes it to be constant.

If the radius is restricted, Seed et al show that modulus may be taken as varying with depth alone. In predicting the deformation of a two layer system consisting of an unbound granular base on a fine grained subgrade, the structure is divided into layers of different, constant modulus. Since modulus is stress dependent, the stress levels are first determined using Boussinesq theory. The corresponding modulus is then determined from relationships between stress and modulus for each material

obtained from repeated load triaxial tests and plate loading tests. By considering points at the top and bottom of each layer an average value of modulus for the layer is found. The vertical deformation of each layer is calculated as the difference between vertical deflections at top and bottom of the layer. These calculations are performed with the aid of Ahlvin and Ulery's tables.[27] The total pavement deflection is then obtained by summing the contribution of individual layers.

The procedure used for the two layer system is based on Boussinesq stress distributions since other workers have shown this to be appropriate for an unbound base. A three layer system was also tackled, but in this case Boussinesq theory was not considered adequate, because of the greater stiffness of the top layer. A method of successive approximation was used to determine surface deflections in this case. The procedure involves estimating the modulus of each layer, calculating the resulting stresses above and below each interface from Jones' three-layer tables[22] and then checking the assumed moduli by reference to the relationships between stress and modulus. If there is a discrepancy, then new values of modulus are taken and the procedure repeated. Seed et al[6] showed that there was good correlation between

deflections calculated as described above and those measured on trial pavement sections. One of the points arising from this excellent paper is that since the modulus of granular materials increases with stress and that of clays decreases, there is a possibility that, for thick base layers the granular material may have a lower modulus at the subgrade interface than the underlying soil. Increasing the thickness of base layer will not under these circumstances, greatly reduce deflection, and this effect provides a possible explanation for the "optimum" base thickness described by McLeod.[62]

Many other contributions have been made on the subject of pavement deflection and the Association of Asphalt Paving Technologists held a symposium on the subject at their annual meeting in 1962.[65]

While not wishing to dispute the wealth of information relating transient deflection to pavement cracking it should be pointed out that if cracking is caused by fatigue of the bituminous material, deflection is not the best measure of likely fatigue failure. Considerable work on the fatigue of bituminous mixes reported by Pell[66,67] and others[68,69] has shown that failure is related to maximum principal tensile strain. The maximum tensile strain in a surface layer for instance, occurs at its

underside, but its magnitude is not proportional to pavement deflection. Dehlen[70] has shown that radius of curvature is a better criterion, but Pell[71] has pointed out that this too is not an accurate guide, since the tensile strain will depend on the thickness of the layer. This argument lends support to the need for more in-situ measurements in pavement structures under appropriate conditions. The work described herein is intended to be a small contribution to this end.

CHAPTER 2 DETAILS OF THE SYSTEMS INVESTIGATED

2.1 Test pit and loading head

A full description of the test pit, in which the model pavement was constructed, as well as the loading head, used to apply the dynamic load pulse, has been given by Tory.[11] A brief description is, however, included here for the sake of completeness.

The test pit was 8ft. square in plan and 5ft. deep, the top being level with the laboratory floor. Side pieces were made in order to increase the depth by a further 12 in. In fact the subgrade was made 5ft. deep and a 12 in. thick base layer placed above this. The pneumatic loading head was mounted at the base of a large portal frame as can be seen in fig. 2.1 which shows a general view of the apparatus as it appeared for testing the single layer system. The loading head was capable of delivering a uniform pressure over a circular area in the form of a single pulse having a maximum possible amplitude of 5 tons and a fastest time to peak of 0.05 sec. approximately. The load could be applied almost anywhere on the surface of the pit, by moving the loading head transversely along the base of the portal frame which in turn could be cranked along the rails in the

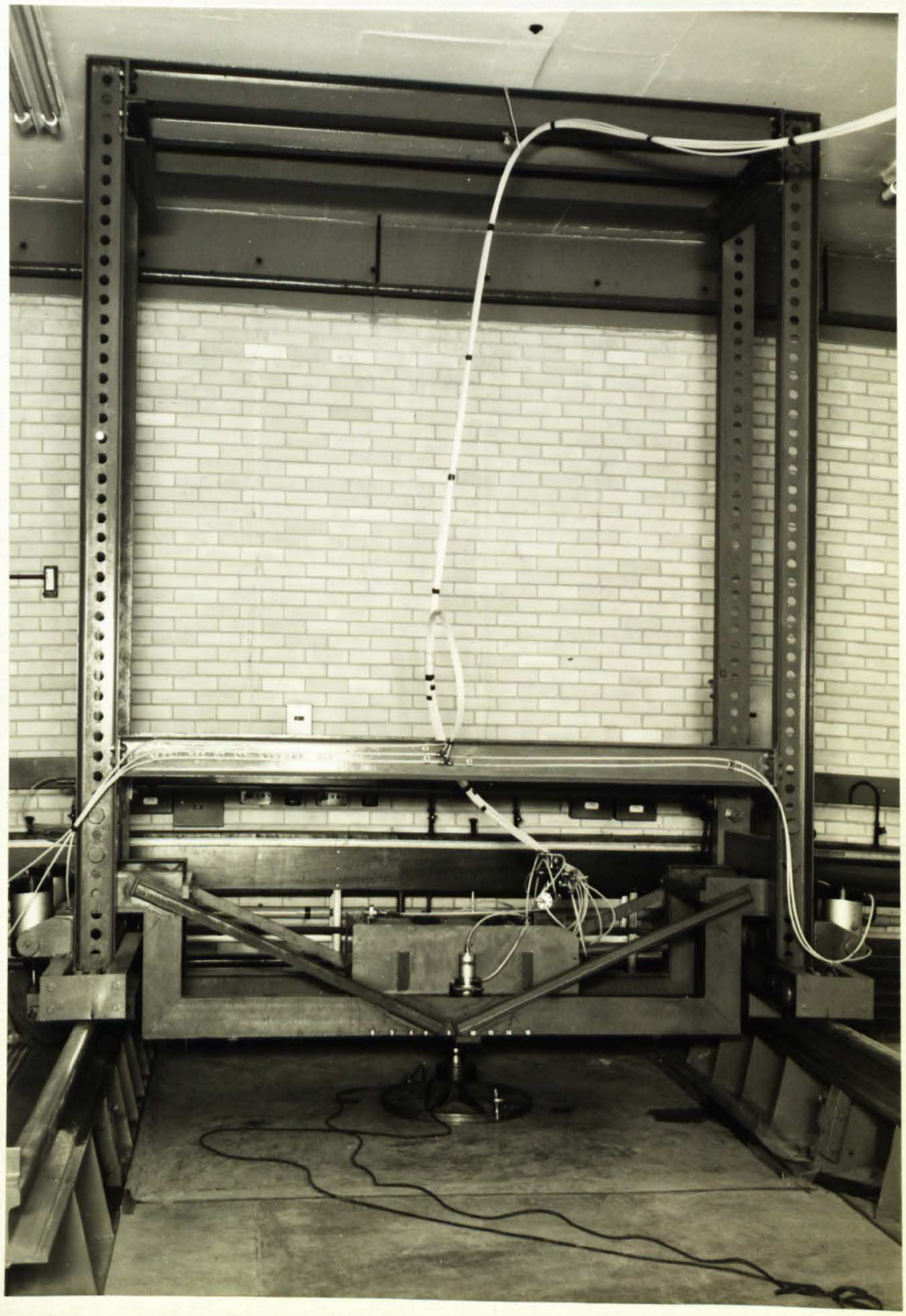

FIG. 2.1 TEST PIT AND LOADING HEAD -

SINGLE LAYER SYSTEM

perpendicular direction. Once in the desired position both the trolley and the portal frame could be clamped by a pneumatic system connected to the control circuit of the loading head in such a way as to provide a safety device, since the load could not be applied unless the clamps were on.

A system of cartesian co-ordinates was used to locate positions on the test pit as shown in fig. 2.2. One unit on each axis was equal to $1\frac{1}{2}$ in., this module being chosen so as to arrange for all likely reference points to be at a node, i.e. to have integer co-ordinates.

The loading head was operated by remote control from a small room off the main laboratory. All the control equipment was located here, and a general view of the apparatus for the two layer system is shown in fig. 2.3. The loading head controls are on the left of the photograph.

The load was applied to the pavement through a flexible platen devised by Tory[11] (fig. 2.4). The object of this arrangement, was to ensure that the contact pressure was uniformly distributed over the circular area. Three different sizes of loaded area were used; 6 in., 9 in., and 12 in. radius. The total load applied to the pavement was determined by a load cell mounted above the rigid platen and the pressure of water within

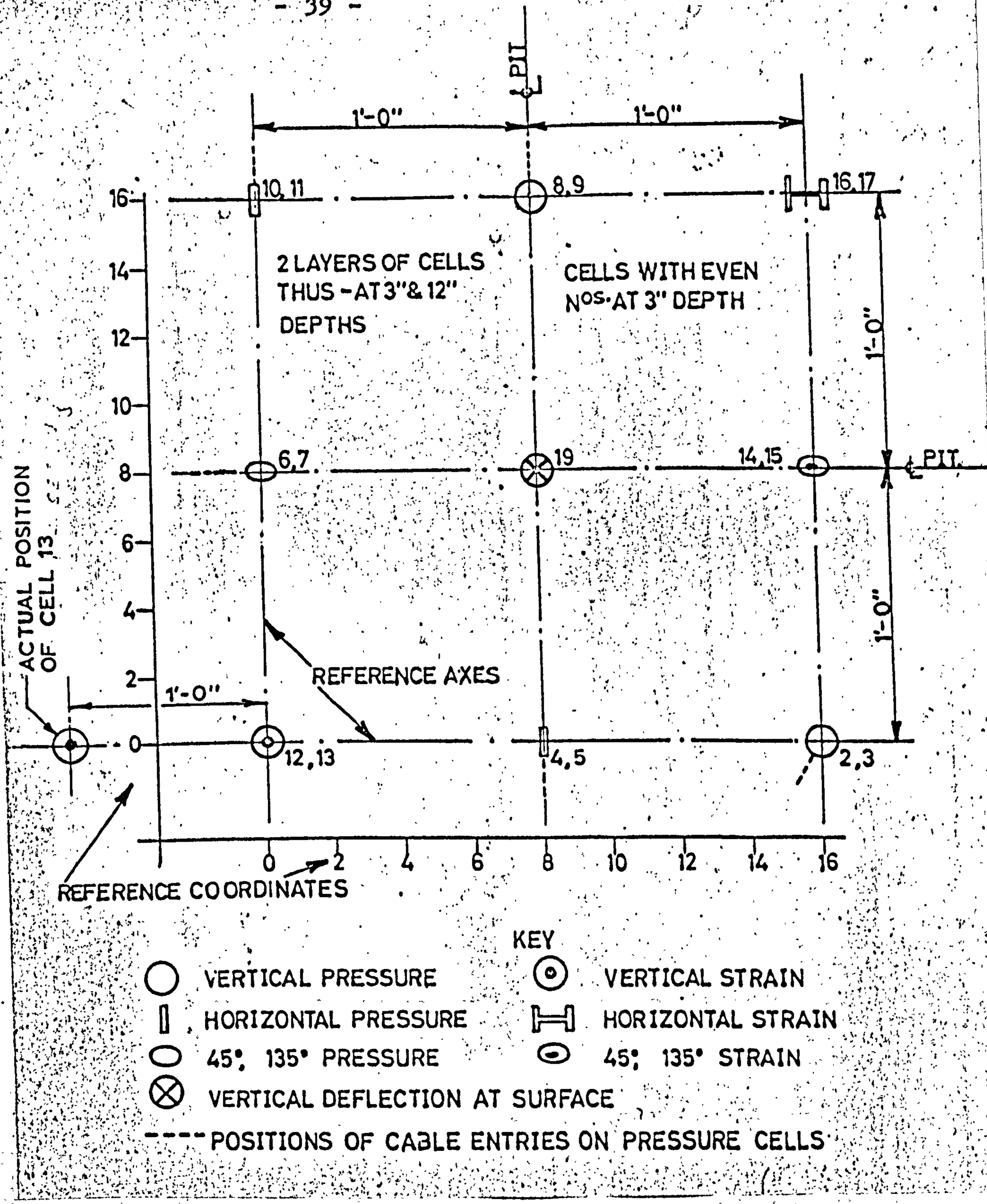

FIG. 2.2 LAYOUT OF INSTRUMENTS - SINGLE LAYER SYSTEM

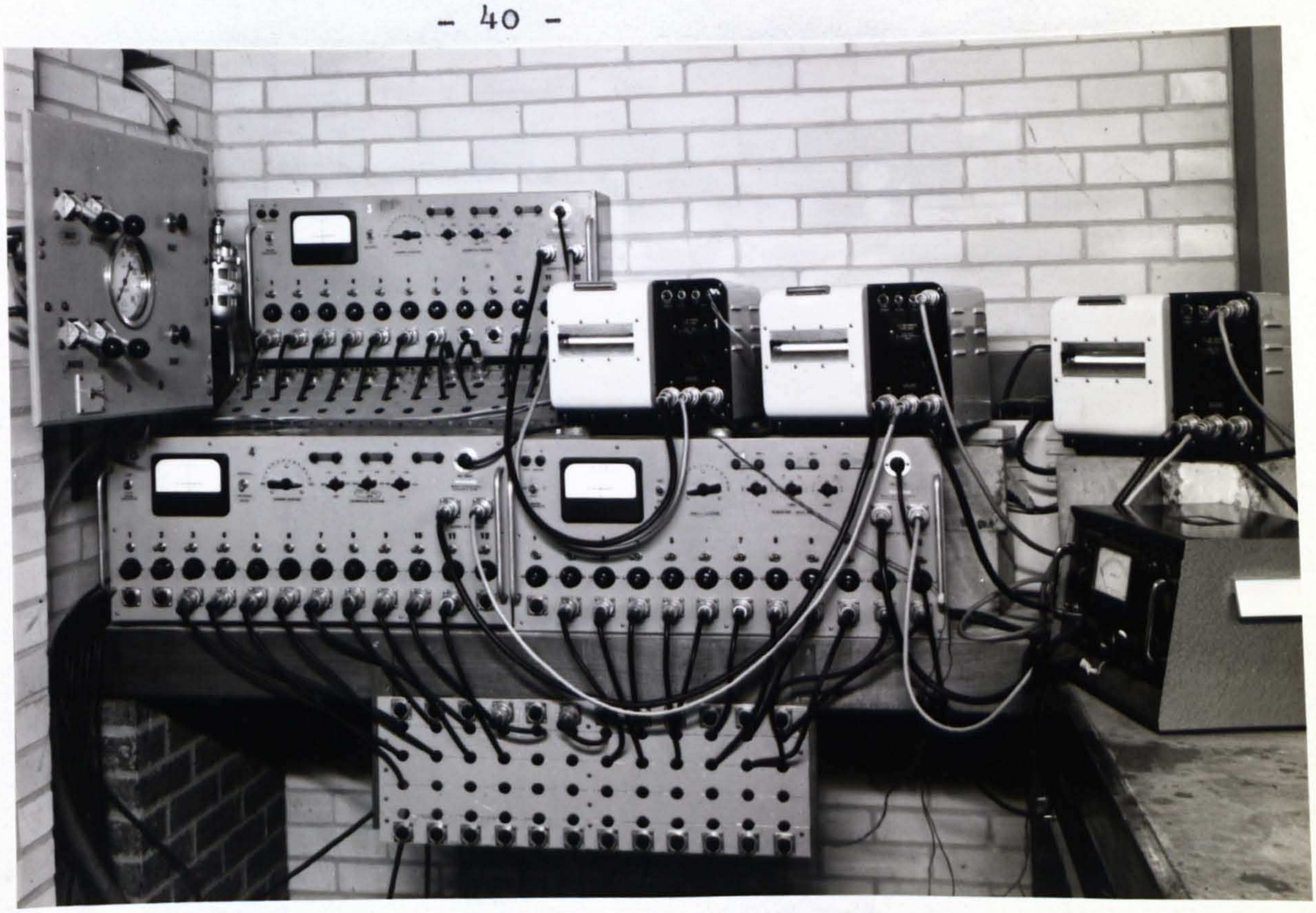

FIG. 2.3 CONTROL EQUIPMENT

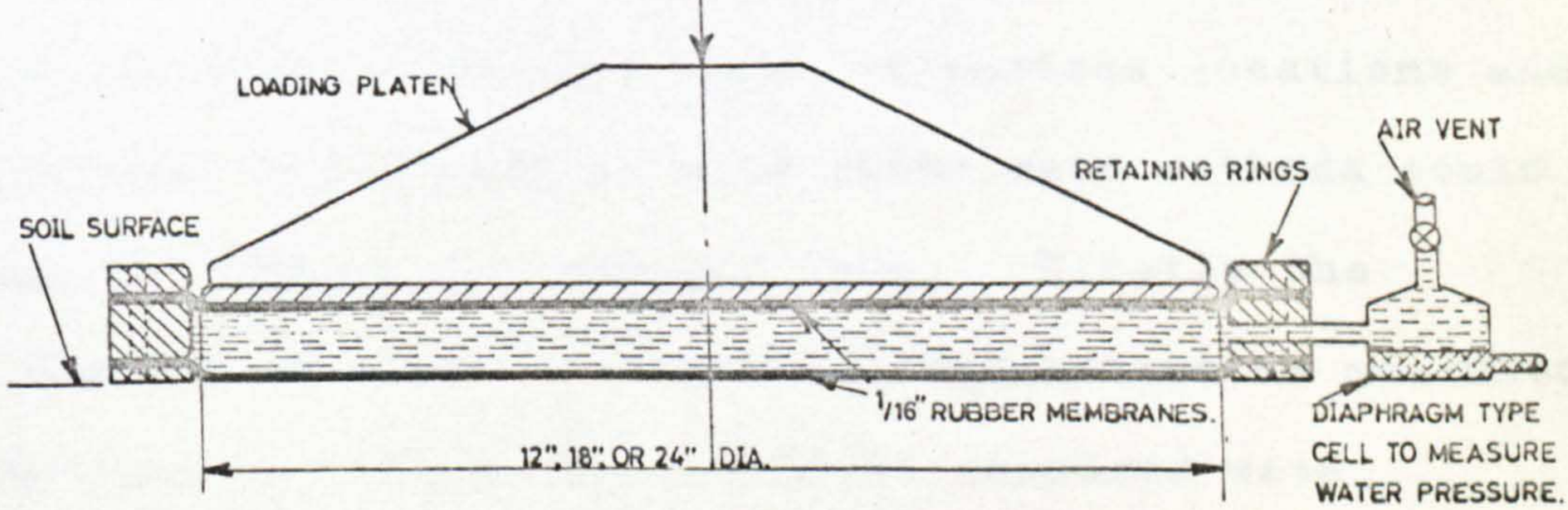

FIG. 2.4. FLEXIBLE LOADING PLATEN

the flexible platen, being equal to the contact pressure, was recorded by a diaphragm type cell as shown in fig. 2.4. Both these instruments were calibrated before each series of tests, the results being almost identical each time.

Two systems were investigated using this apparatus, a single layer consisting of a clay subgrade and a two layer system obtained by laying a granular base over the clay subgrade.

2.2 Measurements taken in both systems

The main object of the experimental work carried out on the test pit was to check the validity of linear elastic theoretical solutions to the layered system problem. In order to do this, measurements of stress, strain and deflection were taken at various locations and in different directions so that three main methods could be used to achieve the desired ends. Firstly the distribution of stress, strain and deflection as measured by appropriate transducers could be compared with theoretical predictions. Secondly, these measurements could be analysed to determine principal stresses and strains and the directions in which they act. Finally, stress and strain measurements could be combined to calculate

values for the modulus of elasticity and Poisson's ratio of the materials in-situ.

Fig. 2.5 shows the measurements intended to be taken on the single layer system. A full set of results at a point consisted of vertical, radial, tangential, 45° and 135° measurements of both stress and strain. Similar results were taken for the two layer system, but in addition, certain important effects were measured at the interface. These interfacial measurements consisted of vertical strain in the subgrade, radial strain just above and below the interface and radial stress in the base layer. Arrangements were also made to measure vertical stress and deflection in the subgrade, but the relevent instruments broke down before any results were obtained. The object of these interfacial measurements was to check certain effects which are believed to contribute to the failure of flexible pavements and to decide whether the theoretical assumption of a perfectly rough interface is justified. Large vertical strains in the subgrade soil and tensile stresses at the bottom of the base layer are believed to be possible causes of failure and the measurement of horizontal strains either side of the interface could check the theoretical assumption of perfect roughness.

Excavation of the transducers carried out just before

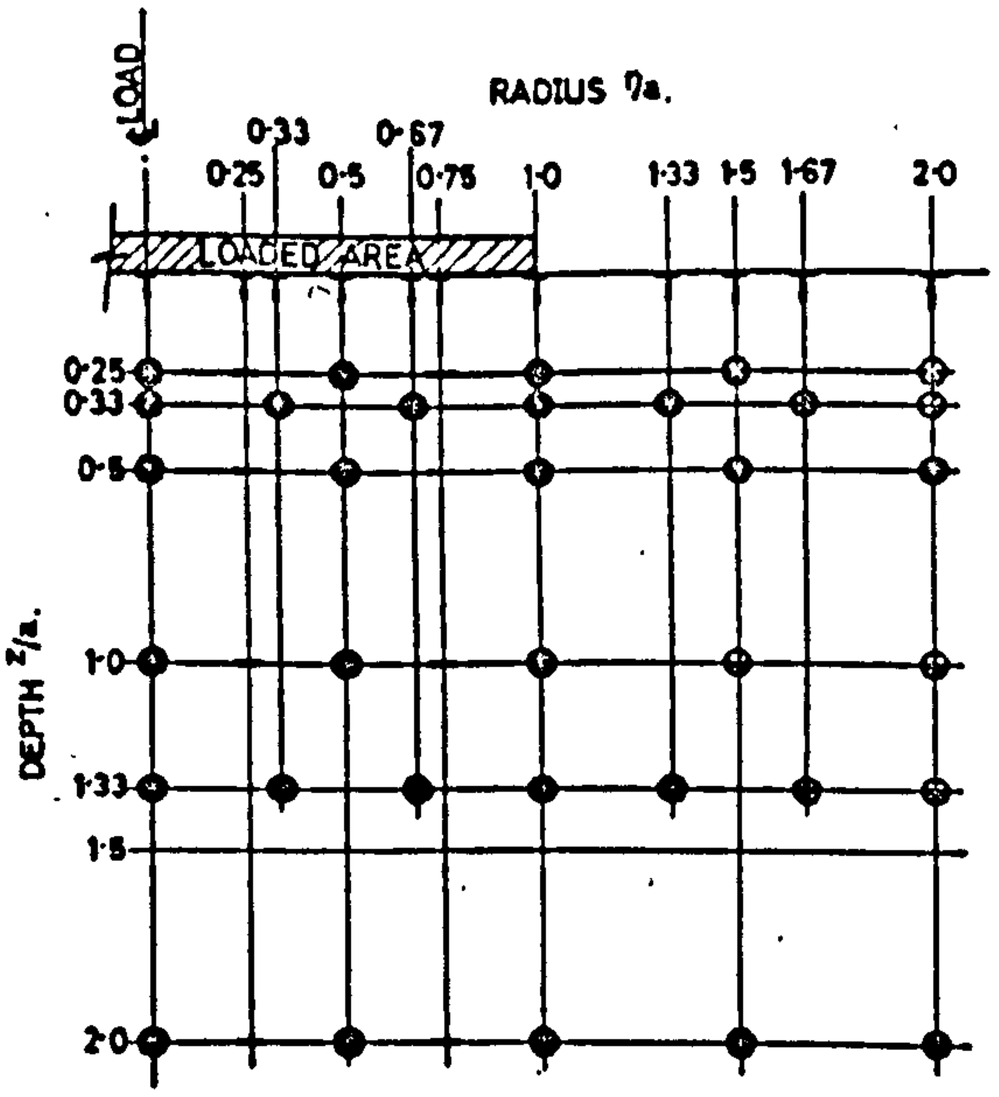

KEY

● FULL SET OFSTRESSES AND STRAINS AT POINTS SHOWN THUS MEASUREMENTS ELSEWHERE ONLY ON PLANES INDICATED.

T VERTICAL SURFACE DEFLECTION.

FIG. 2.5 LOCATION OF MEASURING POINTS - SINGLE LAYER SYSTEM

completion of this thesis showed that the instrument measuring vertical strain in the clay at a depth of 12 in. (cell 13) was 12 in. out of position in plan as shown in fig. 2.2. This meant that full sets of strains at this depth could not be obtained, although stresses were unaffected. By the time this discovery was made, calculations based on the assumed position of cell 13 had been completed. These have since been corrected and their effects as far as possible eliminated.

Stress measurements were obtained by the use of a number of diaphragm type pressure cells, strain was determined by use of a strain cell and surface deflection by a rectilinear potentiometer. These instruments were developed by Sparrow and Tory[11,17] and the pressure and strain cells are dealt with in detail in Chapters 3 and 4.

It would have been impossible to obtain all the various measurements outlined above at such close spacing by loading the soil in one place. Instruments, even when present singly, upset the stress distribution, so that clearly a large number of them close together would be valueless. It would also be impossible to measure more than one effect at one point. The procedure therefore adopted was to install almost a minimum number of instruments separated by 12 in. horizontally and 9 in. vertically. The instruments at the interface in the two layer system are closer than this, being in some cases only 6 in. apart. This could not be easily avoided as a study of fig. 2.6 indicates that they had to be displaced in plan from the main arrangement of instruments. The load was moved relative to the instruments and applied in a sufficient number of positions to be able to obtain the desired results by superposition. Hence, the effects shown in fig. 2.5 were obtained by superimposing results

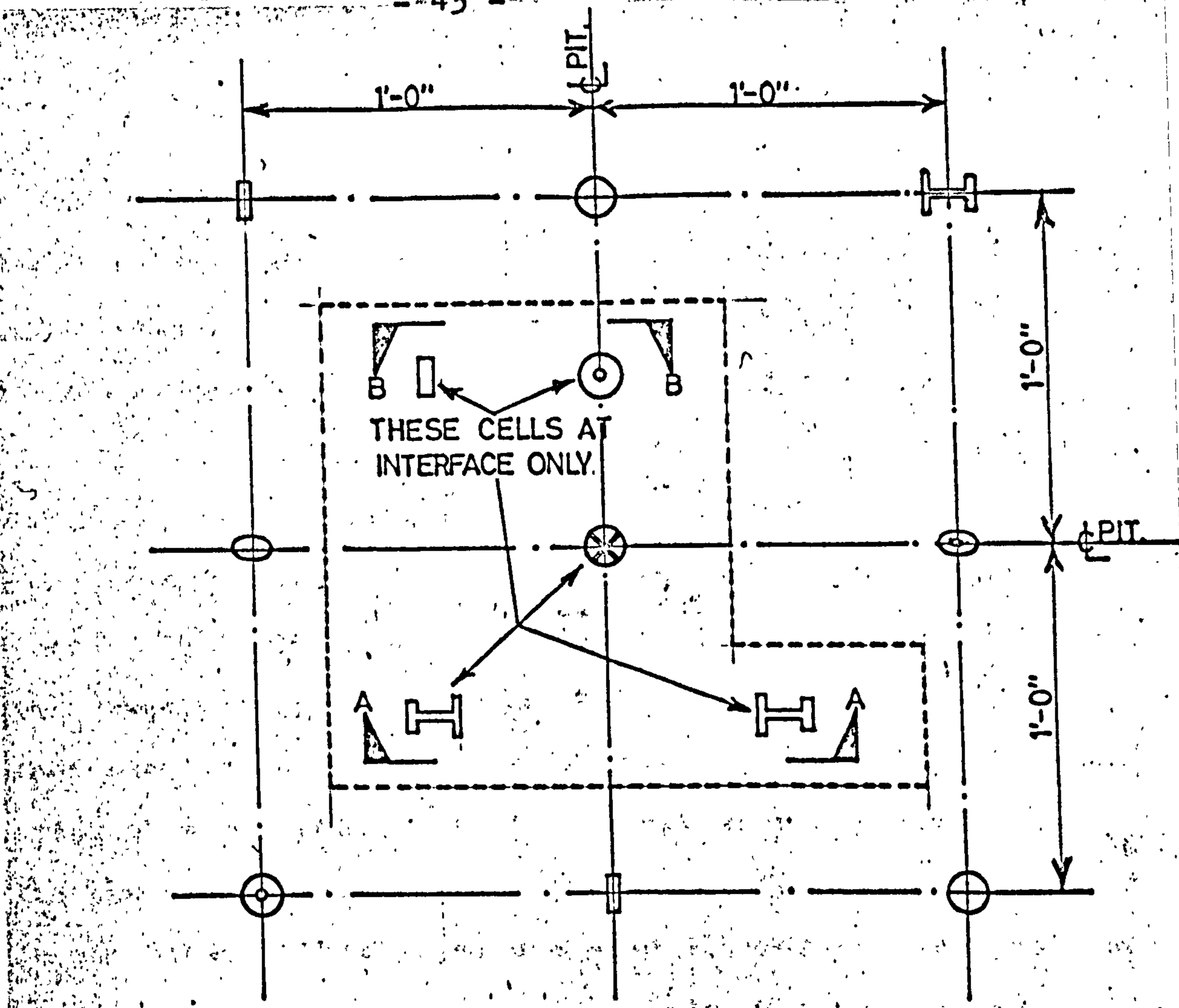

SYMBOL	MEASUREMENT
⊙	P_z
▯	P_r, P_θ
⊙	P_{45}, P_{135}
⊙	e_z
H	e_r, e_θ
⊙	e_{45}, e_{135}
⊗	w_z, AT SURFACE OF SUBGRADE

NOTES.

1. OVERALL TEST PIT DIMENSIONS 8'-0"x 8'-0"x 5'-0" DEEP.
2. DEPTH OF BASE LAYER = 12 In.
3. MAIN LAYOUT OF CELLS AT DEPTHS OF 6", 15"&24".

FIG. 2.6 LAYOUT OF INSTRUMENTS -

taken in different parts of the pit, their positions being determined by reference to the loaded area. Radial and vertical distances are expressed as fractions of the radius of the loaded area as indicated in fig. 2.5.

By using different sizes of loaded area, one absolute depth assumed several different "effective" depths. This was the main reason for varying the radius of the loaded area. In the two layer system, it also meant that the thickness of the upper layer took different values when expressed in this way. It was clearly far simpler to adopt this procedure than to install more instruments on the one hand, or change the thickness of the base layer on the other. This procedure also depends on superposition of different systems, but this in itself is something which is possible in the theoretical approach and had therefore to be checked.

2.3 The Single Layer System.

The single layer system consisted of a clay subgrade of Keuper Marl. This soil is an inorganic clay of medium plasticity and occurs widely in the midlands of England, its distribution being roughly in a diagonal band between the Humber and Severn estuaries. The properties of the material were discussed by Tory[11] who carried out standard

TABLE 2.1 PROPERTIES OF KEUPER MARL

Liquid Limit	41%
Plastic Limit	18%
Plasticity Index	23%
Optimum moisture content	13.2%
Maximum dry density	122 lb/cu.ft.
C.B.R. at O.M.C.	12%
Apparent cohesion	34 lb/sq.in.
Angle of shearing resistance	9.5°
In-situ moisture content	14%
In-situ dry density	121 lb/cu.ft.
In-situ C.B.R.	9.6%

tests to define it. The only one of these tests which has been repeated is that to determine the Atterberg limits, since the liquid limit in particular, can assume a wide range of values depending on the sample chosen. The properties of the Keuper Marl used in this investigation are summarised in Table 2.1. "In-situ" values quoted in the table are based on tests carried out on samples in standard moulds. No in-situ measurements of dry density were made due to an oversight. The assumption is, therefore, that the compaction was the same in-situ as in the moulds, which is not necessarily true.

The original installation of the single layer system has been described by Tory. When the author started work on the project a large number of the transducers had failed, chiefly because the apparatus had lain idle for about 12 months. A brief test program was carried out with this original installation, the only useful results being vertical stress measurements. The decision was then taken to excavate all the cells, investigate the failures and install a new arrangement.

The new installation is shown in fig. 2.2 and was arrived at in the light of experience gained by Tory. The chief differences between his installation and the

new one can be summarised as follows:

1. Cells were installed at 3 in. and 12 in. depths only, instead of basically 9 in., 18 in. and 27 in. The original test results indicated very small measurements, particularly of strain, at the lower depths.
2. The strain cells, which were largely experimental in the original layout, proved reliable so that in addition to measuring vertical and horizontal strain the new layout provided additionally for 45° strain readings.
3. Vertical deflection in the old layout was measured at the surface and at a depth of 13½ in. thus allowing a check to be made on the vertical strain cell readings. Because of the success of these cells and the failure of one of the linear potentiometers used for measuring vertical deflection, the 13½ in. deep measurement was abandoned. The actual results obtained by Tory with this instrument were too small to be of use.
4. Because of possible pressure cell failures, the new layout included duplicate cells to measure vertical and horizontal stresses. These extra cells also provided additional stress measurements,

thereby making for more reliable results.

The compaction procedure for Keuper Marl involved placing a 6 in. layer of the clay in well broken form, the maximum size of pieces being approximately 2 in. across. Two pneumatic tampers were used, one with a single 5 in. diameter head and the other with three 5 in. diameter heads. This latter machine was particularly effective. The surface was sealed with polythene sheeting to keep the moisture content constant, at about 14%.

Samples taken from various depths in the test pit a few months after testing indicated a higher moisture content at the surface, a much lower value, 2 in. below and a slight increase down to 10 in., which was the maximum depth investigated, (fig. 2.7). The average value was 14.1%. The large value at the surface was caused by condensation forming on the underside of the polythene cover where it was not completely in contact with the soil. When the cover was removed, moisture tended to be deposited on the soil surface. Further samples taken at the surface nearly a year later indicated this same above average figure of over 16%.

2.4 The Two Layer System

The only specification originally laid down for the

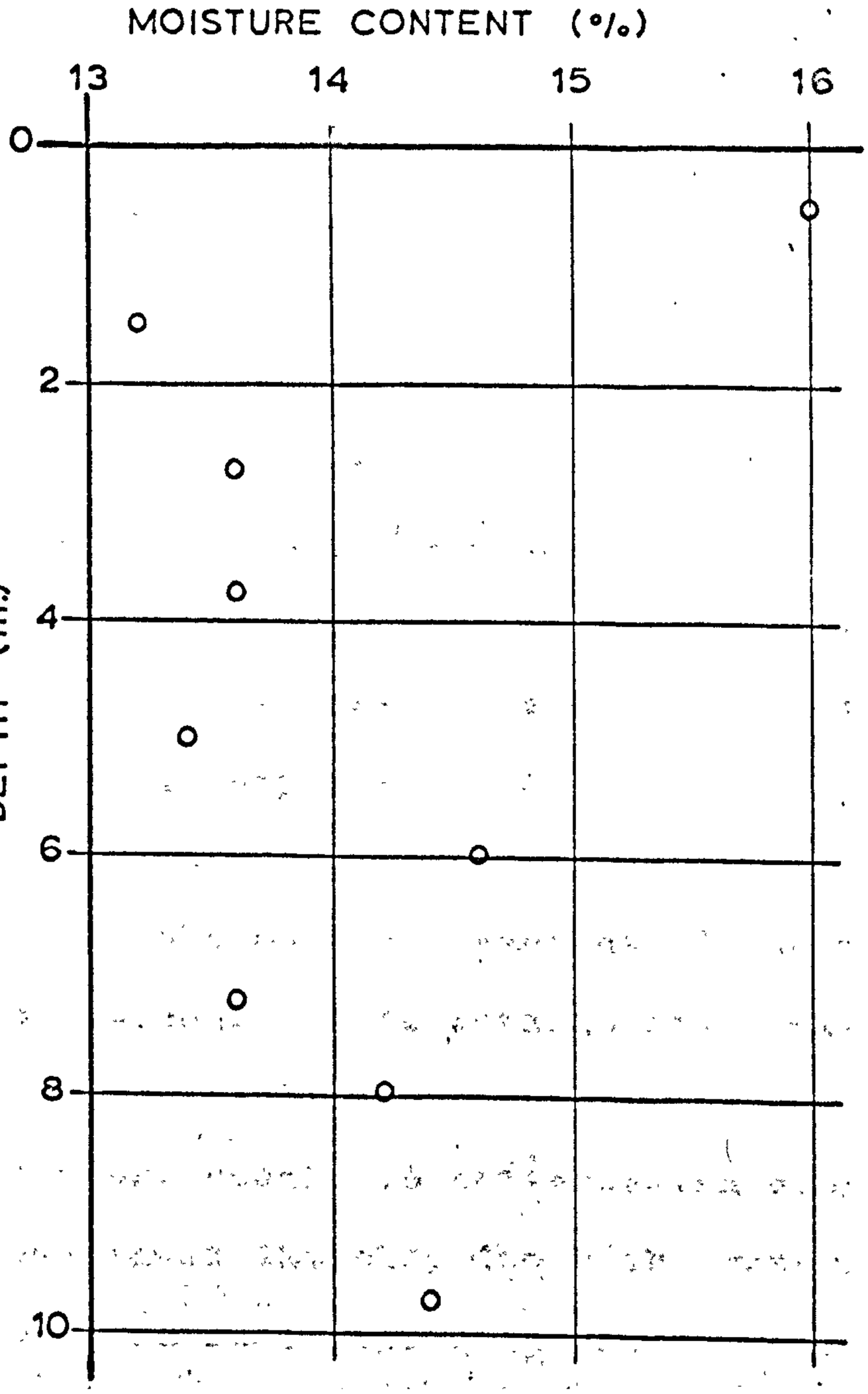

FIG. 2:7 VARIATION OF MOISTURE CONTENT WITH DEPTH

upper layer in the two layer system was that it should consist of an unbound granular material, about 10 in. thick. Certain other requirements followed when a material had eventually to be chosen.

It was desirable to be able to use the same transducers as for the Keuper Marl, and this dictated that a small particle size should be used. The interface should be as realistic as possible and this meant no artificial membrane of any sort. If the clay subgrade was to remain at the same moisture content as in the single layer tests, the moisture content of the upper layer had to be chosen so as to arrange for equilibrium of soil suction across the interface. It was decided that this requirement should be satisfied in order to compare measurements in the clay for both systems. The material had to be as realistic as possible while still satisfying these requirements so clearly a compromise had to be reached.

One of the requirements of a road base material is that it should have a grading curve approximating to that derived by Fuller[72] which provides a maximum dry density for the largest particle size chosen. This curve is based on the relationship:

$$\% \text{ passing any sieve} = 100 \sqrt{\left[\frac{\text{The apperture size of the sieve}}{\text{Largest particle size}} \right.}$$

upper layer in the two layer system was that it should consist of an unbound granular material, about 10 in. thick. Certain other requirements followed when a material had eventually to be chosen.

It was desirable to be able to use the same transducers as for the Keuper Marl, and this dictated that a small particle size should be used. The interface should be as realistic as possible and this meant no artificial membrane of any sort. If the clay subgrade was to remain at the same moisture content as in the single layer tests, the moisture content of the upper layer had to be chosen so as to arrange for equilibrium of soil suction across the interface. It was decided that this requirement should be satisfied in order to compare measurements in the clay for both systems. The material had to be as realistic as possible while still satisfying these requirements so clearly a compromise had to be reached.

One of the requirements of a road base material is that it should have a grading curve approximating to that derived by Fuller[72] which provides a maximum dry density for the largest particle size chosen. This curve is based on the relationship:

$$\% \text{ passing any sieve} = 100 \sqrt{\left[\frac{\text{The apperture size of the sieve}}{\text{Largest particle size}} \right.}$$

A sample of Meldon Dust, which is a crushed stone of $\frac{3}{8}$ in. maximum particle size, was obtained from British Railways Research Department. It is a material from the B.R. quarry near Okehampton in Devon which has been used extensively as a blanket material beneath rail tracks. Geological details of Meldon Dust are given in reference 73.

The first test conducted in the laboratory on this material was a sieve analysis and the resulting grading curve, shown in fig. 2.8, was considered near enough to the Fuller specification to be satisfactory.

One of the requirements to be satisfied for this material was that it should develop the same soil suction as already existed in the clay. During tests on the single layer system, a horticultural soil tensiometer had been used to monitor any changes in moisture content, so that the soil suction for the clay was known and was equal to 20 cm. of Mercury (3.85 lb/sq.in.). Since a unique relationship exists between soil suction and moisture content for a particular soil, this relationship was determined for the Meldon Dust to decide whether the moisture content required to balance soil suctions at the interface was a sensible one.

The horticultural soil tensiometer was used for this

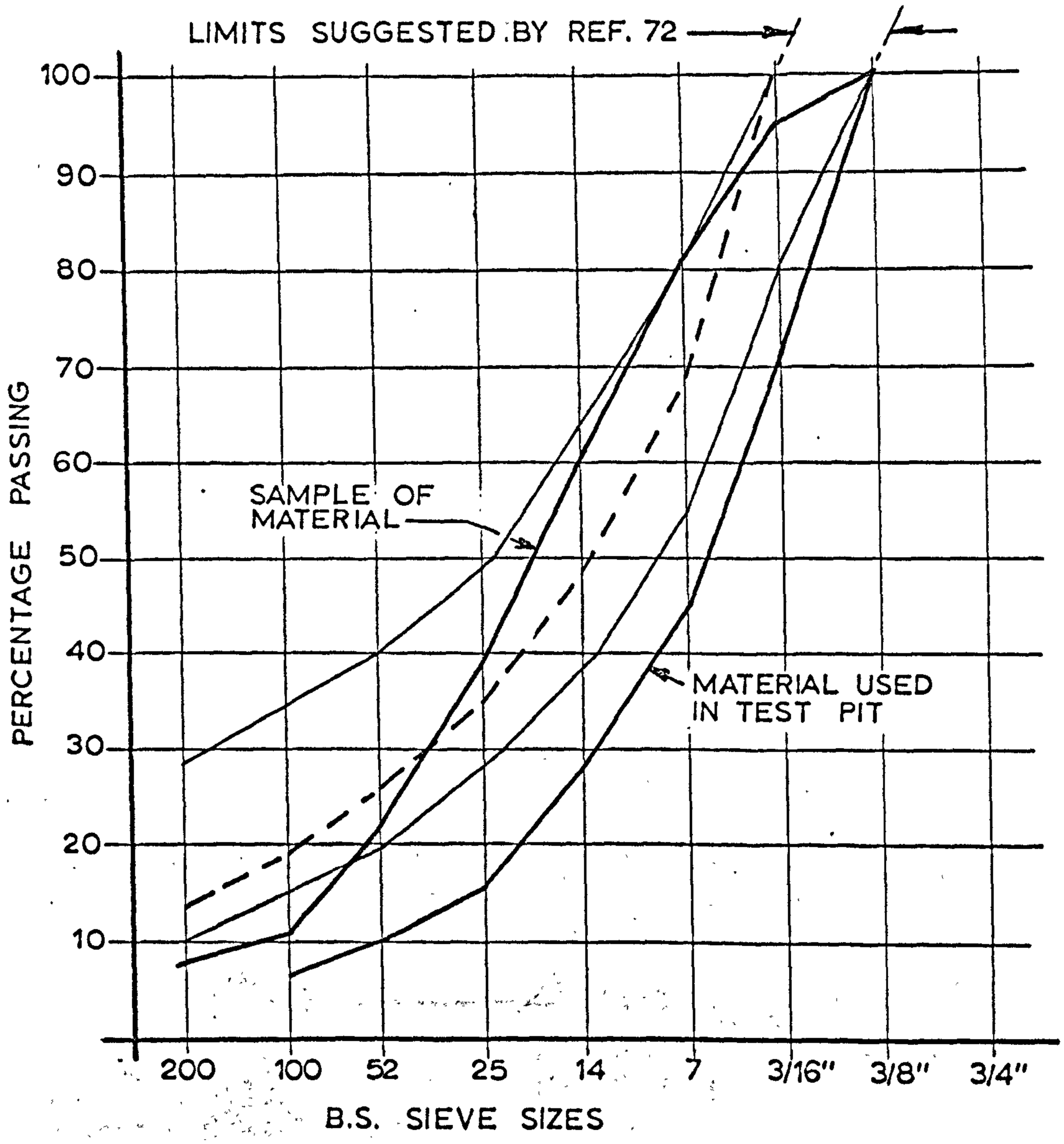

FIG. 2.8 GRADING CURVES FOR MELDON DUST

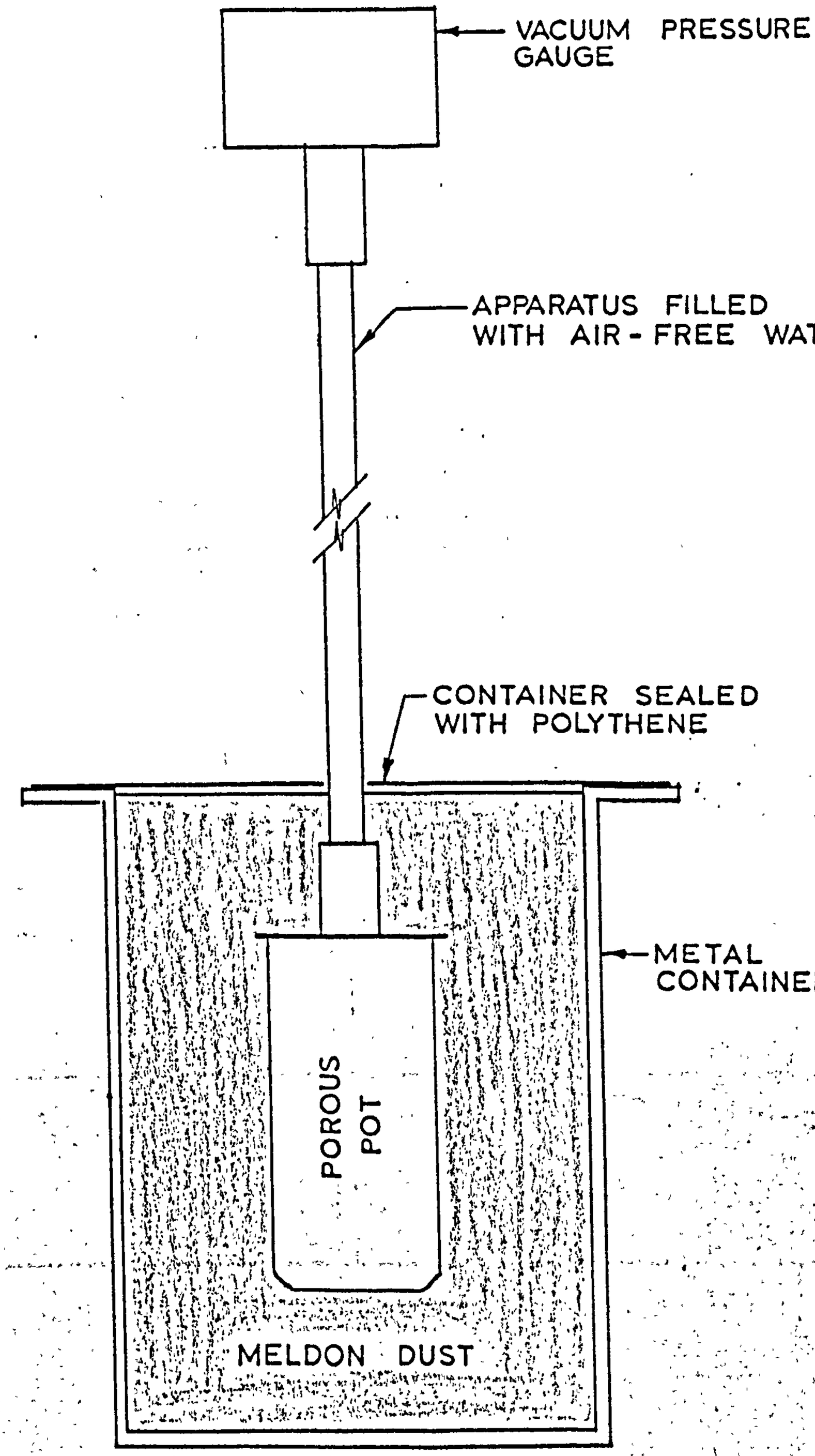

FIG. 2.9 APPARATUS FOR SOIL SUCTION TESTS ON MELDON DUST

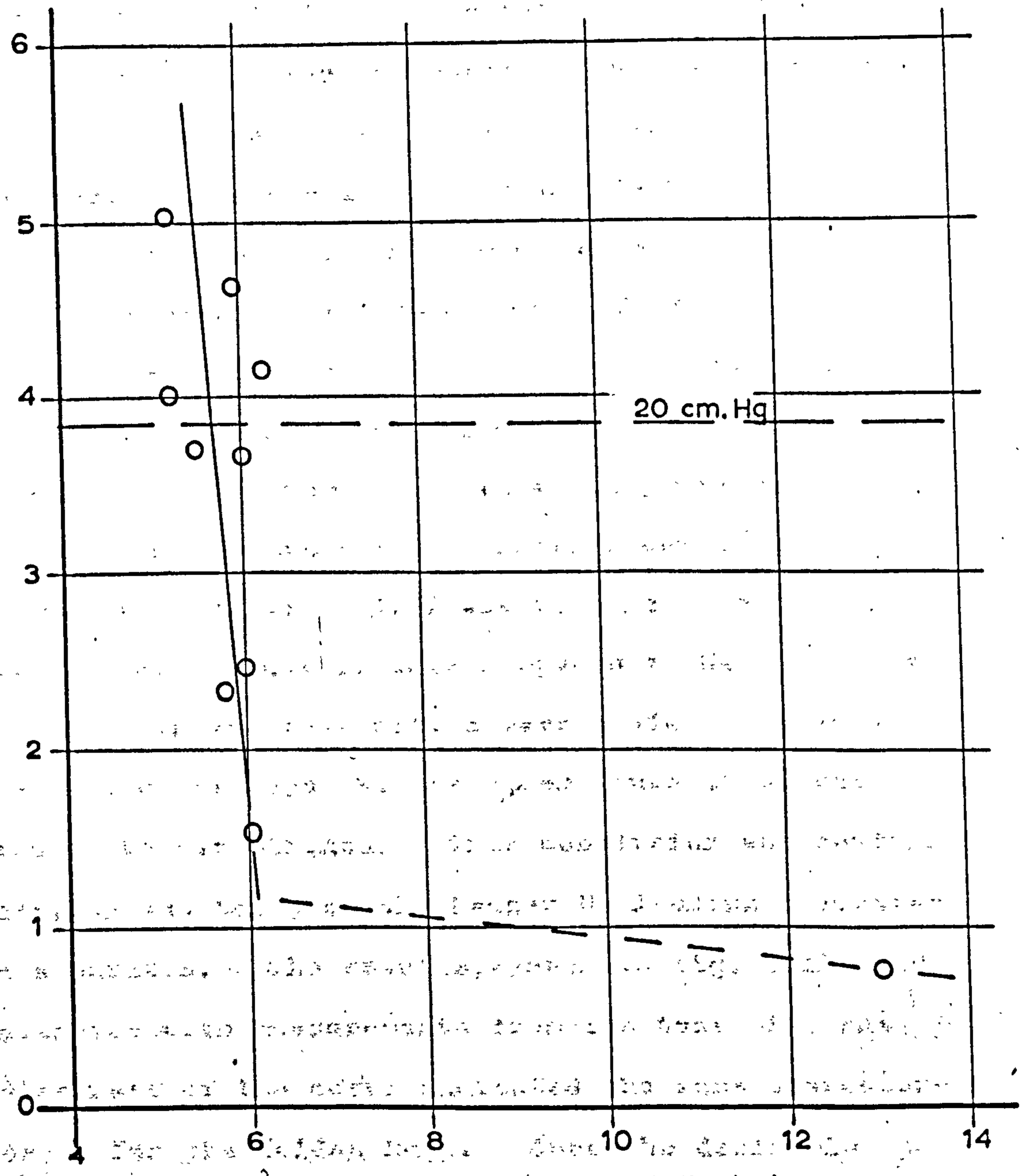

FIG. 2.10 SOIL SUCTION AGAINST MOISTURE CONTENT - MELDON DUST

purpose. It was "planted" in a specimen of the Meldon Dust as shown in fig. 2.9. The surface was sealed to keep the moisture content constant and the apparatus was left until a steady reading was obtained on the tensiometer. This usually took about 24 hours. The reading was noted and the moisture content determined, before the procedure was repeated at a different moisture content. The resulting curve is shown in fig. 2.10.

It was clear that the soil suction near the value which was being aimed at (3.85 lb/sq.in.) was very sensitive to slight changes in moisture content, but it appeared that a value of 5.7% was the one to be used. It was also clear that if this happened to be the wrong value to use in the test pit, a very small transfer of moisture from one layer to the other would cause equilibrium to be established. This conclusion was confirmed by carrying out tests on the Keuper Marl using a suction plate apparatus. The results, shown in fig. 2.11, did not coincide with measurements from the test pit, but the steepness of the curve indicated the same characteristics as for the Meldon Dust. Once the desirable moisture content had been determined, standard strength and compaction tests could proceed.

It was thought that when compacting a granular

material in the test pit, a vibrating plate would give the best results. Standard laboratory tests for compaction and C.B.R. were, therefore, conducted using this compaction technique. The vibrator which was normally used for compacting concrete, was fitted with a $5\frac{7}{8}$ in. diameter plate which just fitted into the standard 6 in. diameter C.B.R. mould. Specimens were compacted in three layers allowing one minute's vibration per layer. Results of compaction and C.B.R. tests are shown in fig. 2.12, and the properties of Meldon Dust are detailed in Table 2.2.

Undrained triaxial tests to failure on standard $1\frac{1}{2}$ in. diameter x 3 in. long specimens indicated that the material had an apparent cohesion of 8 lb/sq.in., based on total stress. These tests were carried out at 5.5% moisture content, being the working value indicated from soil suction tests. Stress/strain curves obtained from similar samples indicated that the secant modulus was approximately 9,000 lb/sq.in. under a confining stress of 10 lb/sq.in.

The Meldon Dust was approved for use in the upper layer of the two layer system on the basis of the tests described above which were carried out on a sample of the material. When the bulk delivery arrived, it was found to have a different grading curve from the sample, (see fig.2

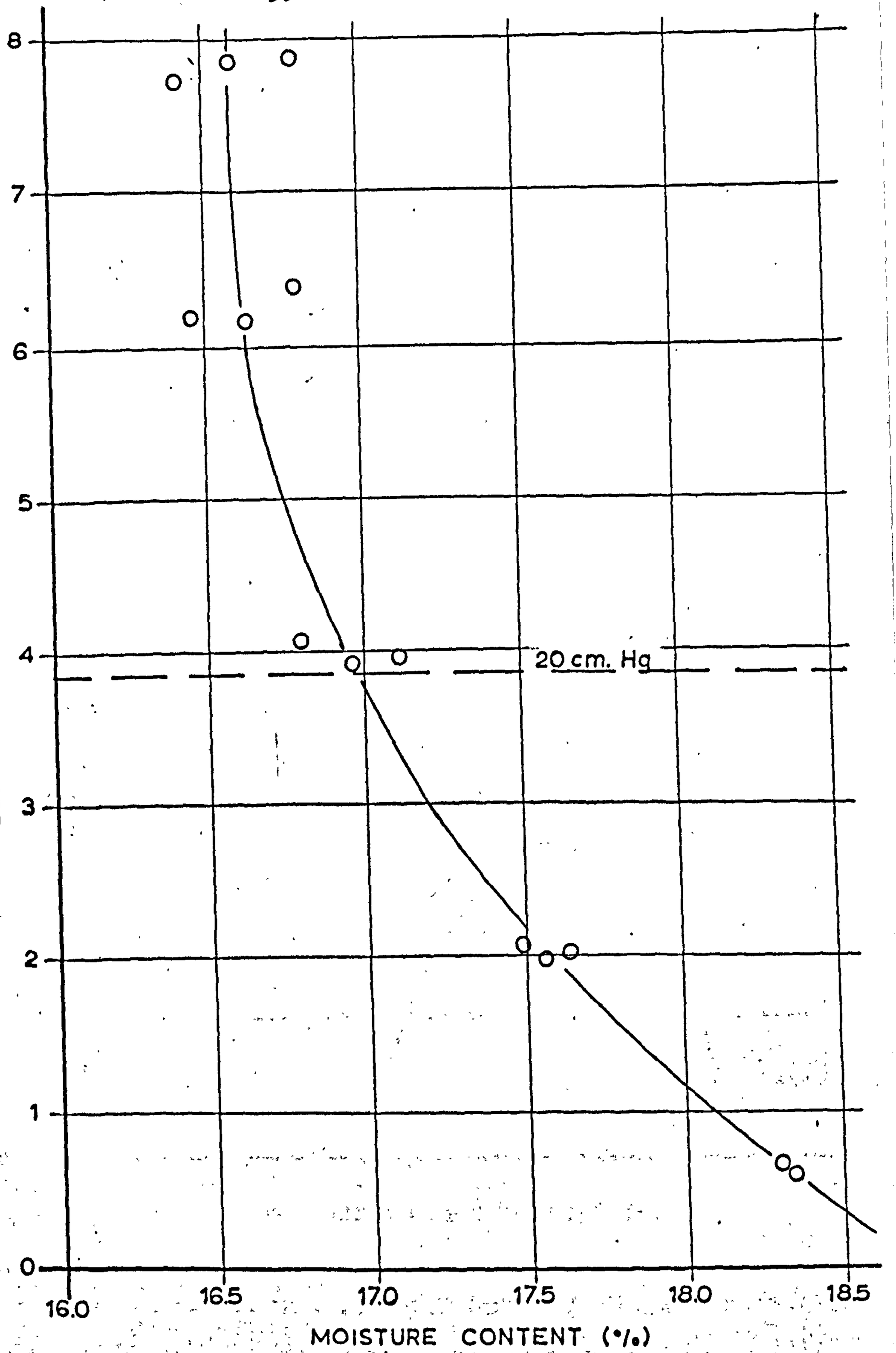

FIG. 2.11 SOIL SUCTION AGAINST MOISTURE CONTENT

KEUPER MARL

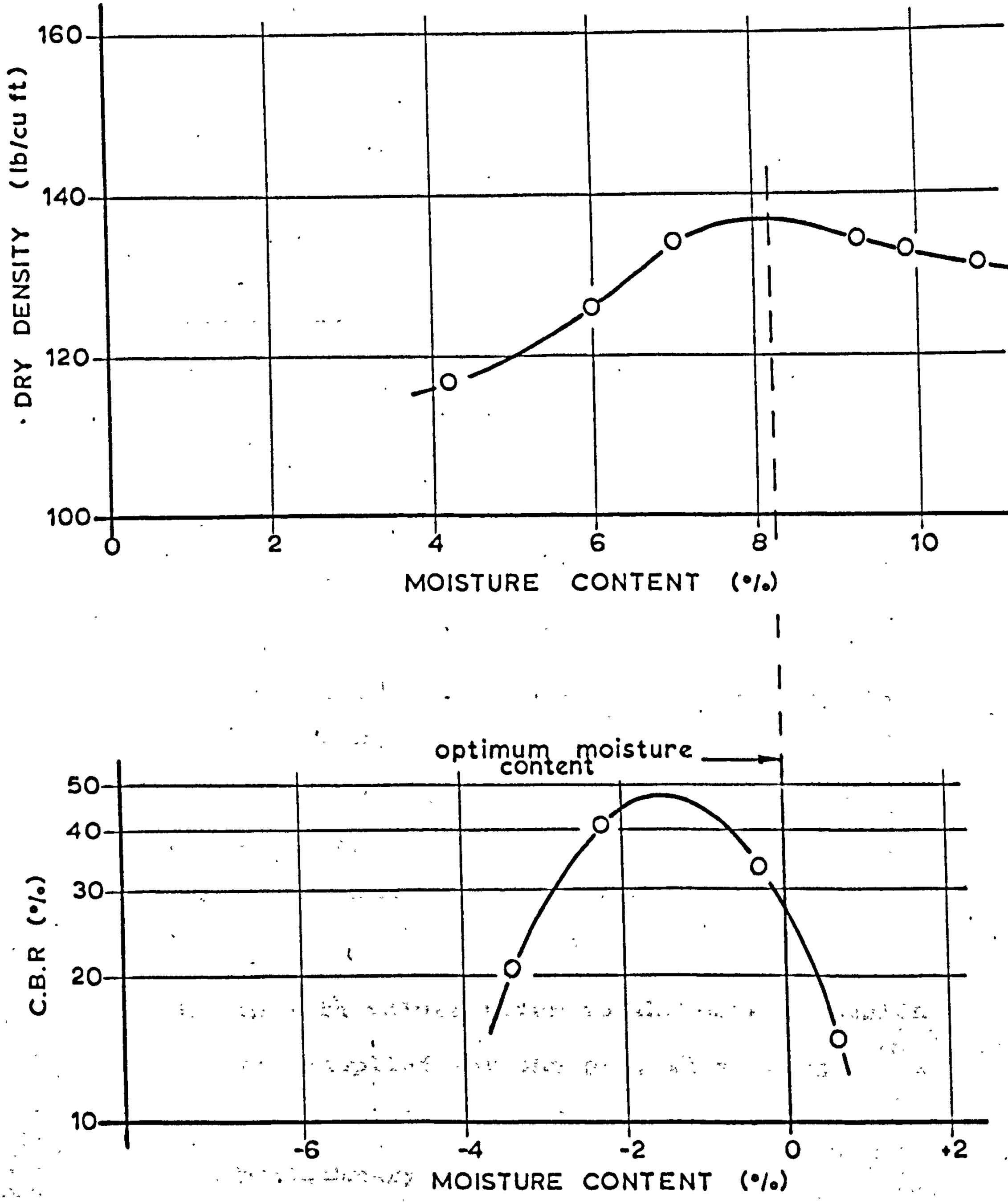

FIG. 2.12 C.B.R. AND DRY DENSITY AGAINST MOISTURE CONTENT - MELDON DUST SAMPLE

TABLE 2.2 PROPERTIES OF MELDON DUST

Maximum particle size	$\frac{3}{8}$ in.
Optimum moisture content	8.2%
Maximum dry density	136 lb/cu.ft.
C.B.R. at O.M.C.	28.8%
Apparent cohesion	8 lb/sq.in.
Angle of shearing resistance	45.7°
In-situ moisture content	5.4%
In-situ dry density	113 lb/cu.ft.
In-situ C.B.R.	20%

N.B. In-situ values refer to the material which was supplied for the pit, this being slightly different from that used for preliminary tests.

and because its grading departed from the Fuller curve on the large side, poorer compaction and a slightly weaker base layer resulted. Tests conducted some 9 months after laying this material indicated a lower moisture content than had been thought necessary for soil suction equilibrium, a lower dry density in-situ and a poorer C.B.R. All these findings were in line with the behaviour suggested by the grading curve and details are shown in fig. 2.13.

The thickness of layer eventually chosen was 12 in. This arose from considerations of the geometry of the system, so as to allow tabulated values of theoretical results to be used. This criterion became unnecessary later on when Jones' multilayer computer program[28] was made available, since any dimensions could then be catered for. A view of the test pit, with the two layer system installed, is shown in fig. 2.14.

The arrangement of instruments in the two layer system is shown in fig. 2.6. It consisted of a pattern identical in plan to that already installed at two levels in the subgrade and was placed in the centre of the layer, i.e. 6 in. below the surface. In addition, certain instruments were arranged just above or below the interface as discussed under 2.2. Since one layer

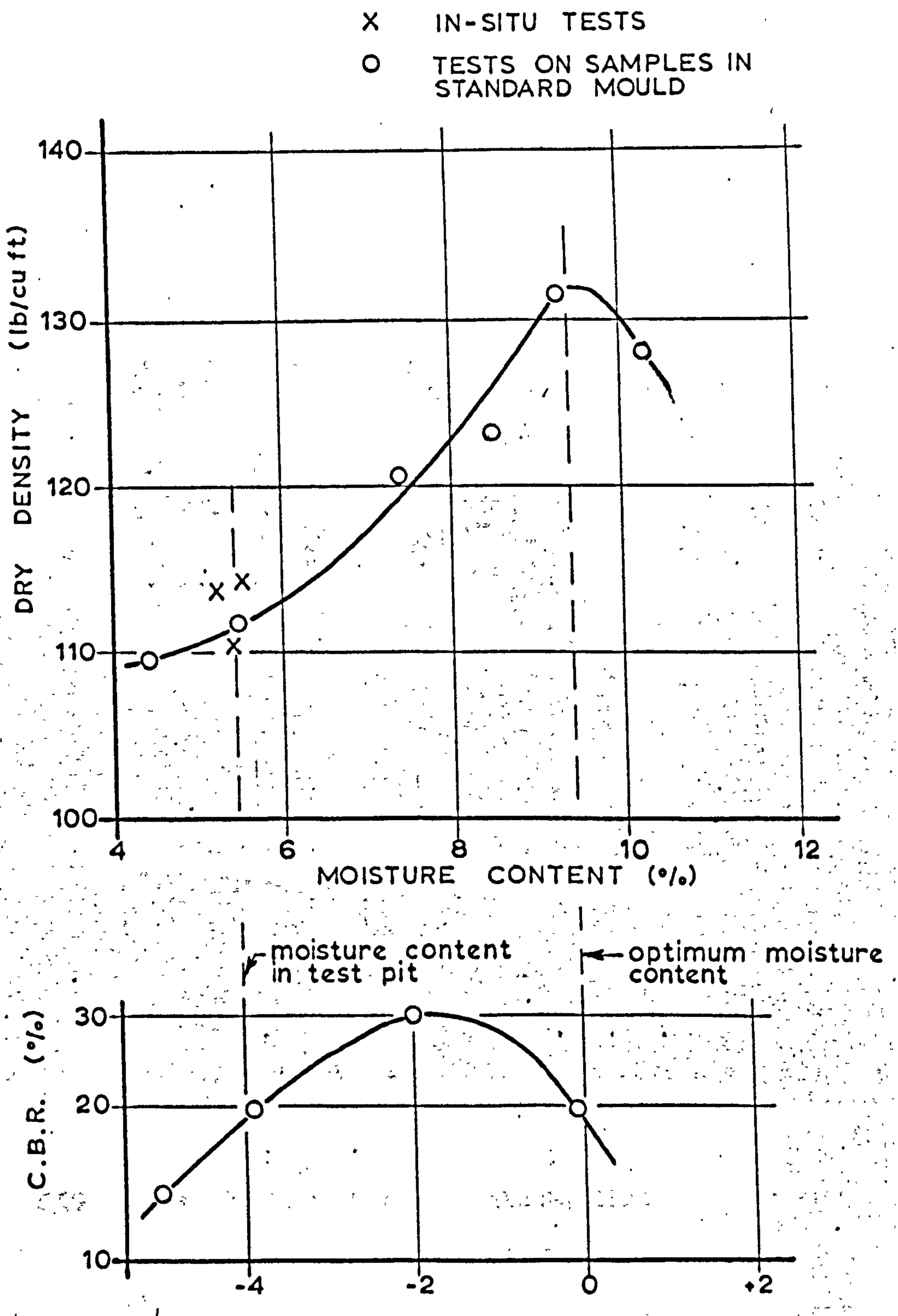

FIG. 2.13 C.B.R. AND DRY DENSITY AGAINST MOISTURE CONTENT - MELDON DUST USED IN TEST PIT

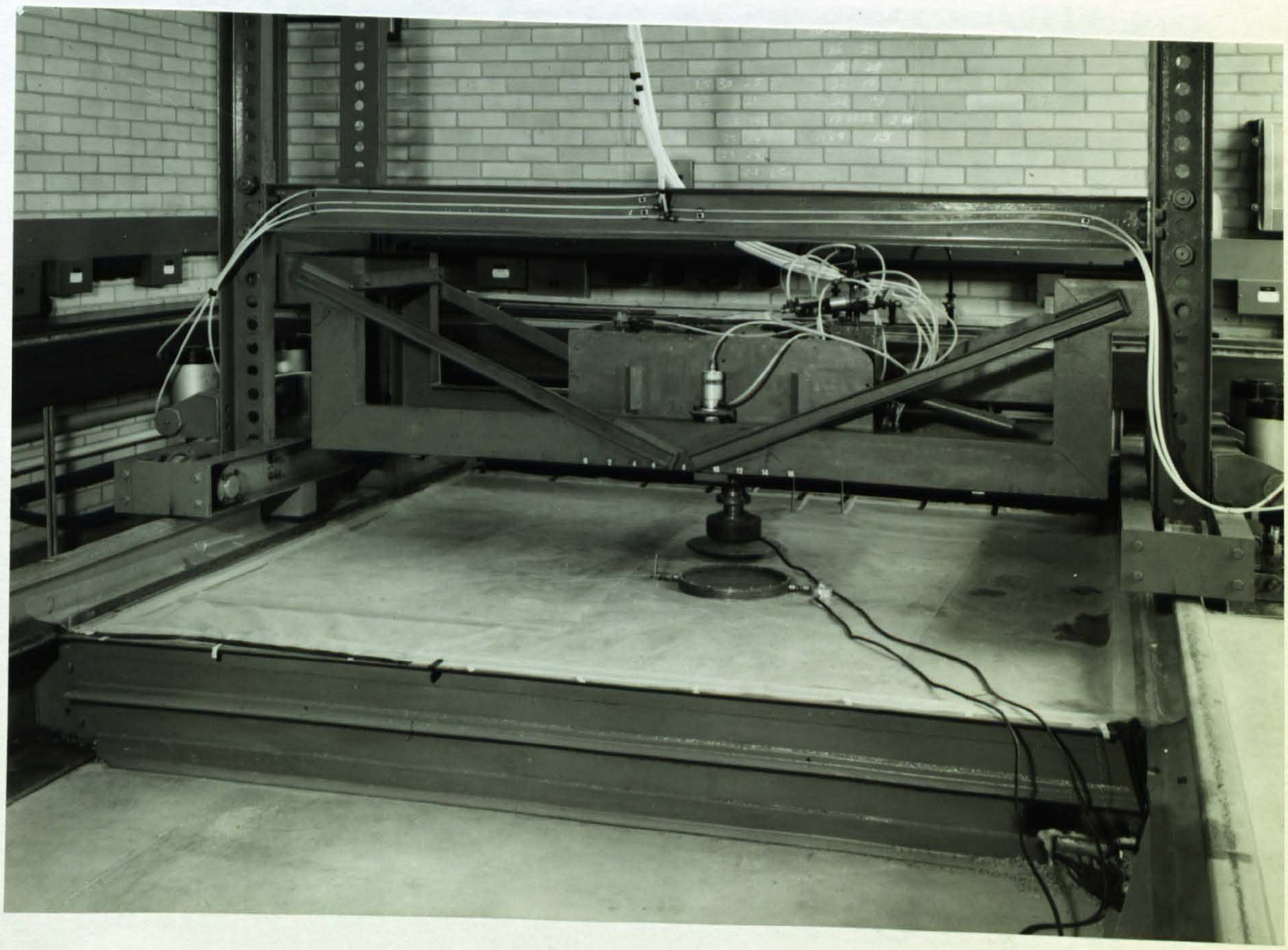

FIG. 2.14 TEST PIT AND LOADING HEAD -

TWO LAYER SYSTEM

of cells in the subgrade was only 3 in. below the interface, interfacial cells had to be displaced in plan and were therefore arranged on a 1ft. square grid about the centre of the pit.

It was impossible to take measurements exactly just above or below the interface, the positions used in theoretical analyses, but to get as close as possible with the horizontal strain cells, the two instruments which were used had end plates of a smaller diameter than the standard model.

The rod attached to the base of the pit which was used by Tory,[11] for mounting a deflection gauge to take measurements at a depth of $13\frac{1}{2}$ in. was extended and a new gauge attached to measure surface deflection for the two layer system. The gauge used for this measurement in the single layer tests remained to measure the deflection of the interface. Unfortunately both these instruments failed before any tests were completed, so no deflection measurements were taken in the two layer system.

The failure of several pressure cells in the upper layer was more disconcerting, since waterproofing and insulation were considered far better on these instruments than on the deflection gauges. When they were "exhumed" 12 months after installation the strain gauge cement was

found to have failed.

A soil tensiometer was installed to measure soil suction and hence monitor moisture content in each layer of the two layer system. Before sealing the top of the pit, the Meldon Dust was dried and subsequently wetted until the suction in each layer was at 20 cm. of Mercury, the value measured for the single layer system. With time, however, readings from the two gauges fluctuated and eventually diverged, but this happened well after the tests had been completed. The variation of soil suction and moisture content during testing is dealt with in Chapter 5. Despite the indication of the tensiometer that the Meldon Dust had dried out, samples taken from a few inches beneath the surface 9 months after installation had a moisture content of 5.4%. Tests on the samples of Meldon Dust had indicated 5.7% for equilibrium, but the material used in the pit being slightly coarser, would require a smaller moisture content.

Because of the problem of condensation on the underside of the polythene sheet, care was taken to keep it flat and hence in contact with the surface as much as possible. When the pit was out of use old sacks and similar weighting were used to improve the situation.

The procedure for installing both strain and pressure cells in the Meldon Dust was generally similar to that used in the Keuper Marl and is described in detail in Chapters 3 and 4. The material was compacted to a level about 2 in. above that at which the instruments were to be installed, and recesses were then dug to accommodate them. The main difference in procedure with Meldon Dust was that fine material, passing a No. 7 sieve, was used next to the instruments to prevent large particles from causing false readings. Since this same procedure was used for the calibration tests described in Chapters 3 and 4, the presence of this finer material should not itself have caused errors in the measurements.

A vibrating plate about 12 in. x 6 in. was used to compact the Meldon Dust. This was done in layers 3 in. (uncompacted) thick and measurements of in-situ dry density have been shown to be comparable with values obtained in a C.B.R. mould (fig. 2.13).

The equipment used during installation of the layer of Meldon Dust is shown in fig. 2.15. A close up of a pressure cell being installed is shown in fig. 2.16, its correct position and orientation being ensured by means of the plumb bob and spirit level.

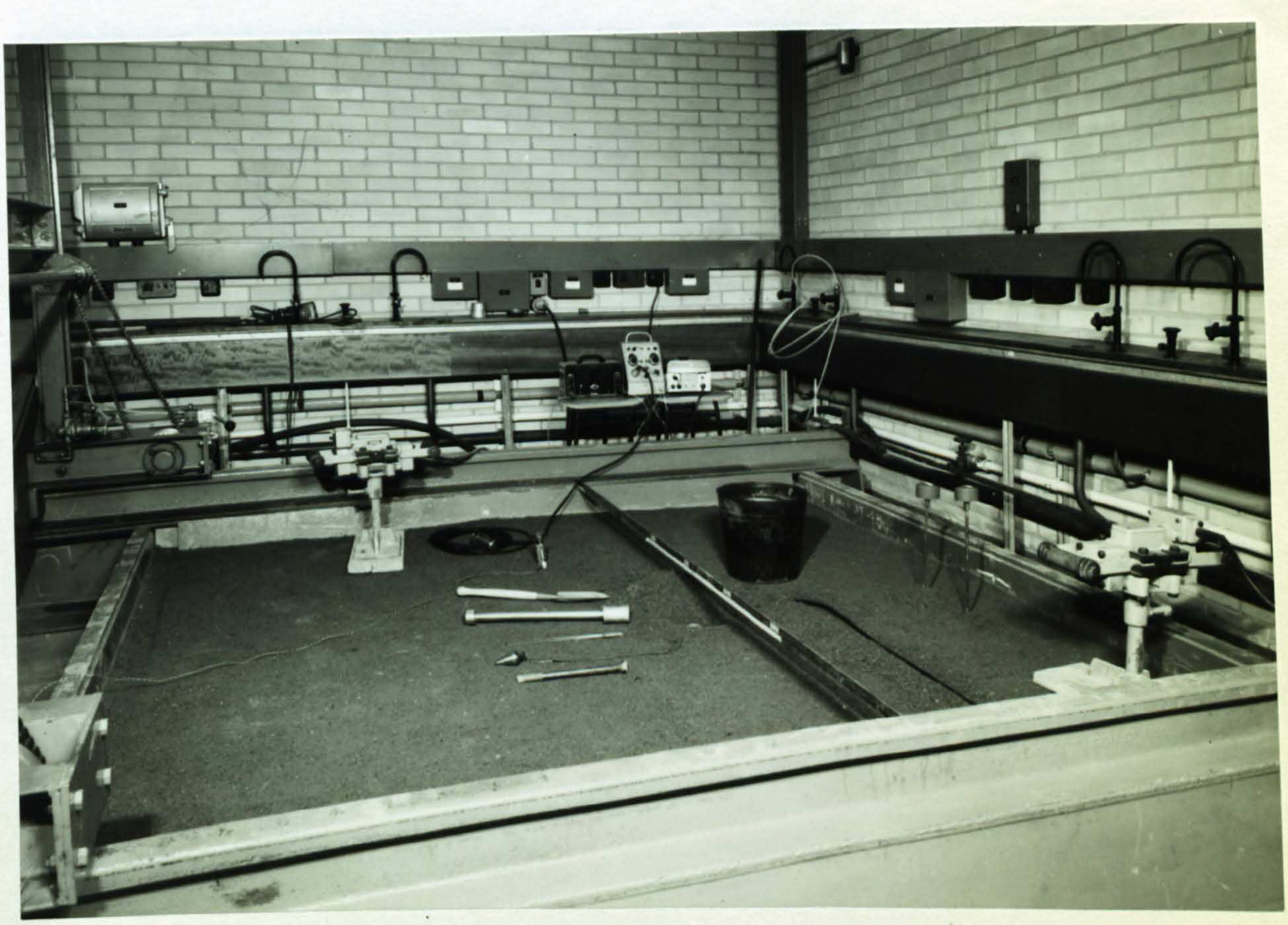

FIG. 2.15 INSTALLATION OF BASE LAYER

FIG. 2.16 INSTALLATION OF A PRESSURE CELL

CHAPTER 3 THE PRESSURE CELL

3.1 Introduction

The pressure cell used to determine stresses in both the single and two layer systems was developed by Sparrow and Tory[11,17] and its design embodies the principles suggested by Peattie and Sparrow.[74] Details are shown in fig. 3.1. It is a diaphragm type cell, $2\frac{1}{2}$ in. diameter x 0.43 in. thick, the sensing device consisting of a four arm active Wheatstone bridge circuit, each arm made up of a 200 ohm "Tinsley 1 CF" strain gauge.

At the outset of his work, the Author was, therefore, provided with a pressure cell well proven in practice, having been used by British Railways[75] as well as on this project, and which appeared to satisfy the various theoretical requirements for pressure cell design. The most important of these may be enumerated as:-

1) A small depth to diameter ratio,

2) High stiffness relative to the soil,

3) A sensitive area of cell face less than 45% of the total area,

and 4) The cell should be insensitive to stresses other than normal to the diaphragm, i.e. not cross-sensitive.

The first three of these requirements were fulfilled and from the construction of the instrument the fourth was assumed to be satisfied also. The investigations into pressure cell performance described herein show that in its original form, the cell was in fact cross-sensitive, and steps were takn to correct this.

Most investigators have appreciated the need to fulfill the requirements listed above and even to calibrate their pressure cells in specimens of the soil to be used for a particular project.[14,16] In general, however, calibration tests have consisted either of applying a uniaxial stress at right angles to the diaphragm, sometimes with the cell in the appropriate medium, or of applying a hydrostatic pressure with the cell not necessarily in the soil to be used in practice. There appears to have been no satisfactory check on whether a particular pressure cell was cross-sensitive. Dunn and Billam[76] calibrated a modified Redshaw pressure cell[77] in a large triaxial specimen of an appropriate soil, but although they list cross-sensitivity as something undesirable in pressure cells, their tests do not establish whether this is present in their instrument.

Cross-sensitivity is of particular importance when measuring stresses equal, or approximately equal, to the minor principal stress, since in this case the cross-stresses

will be large and there is the possibility of introducing a significant error to the measurement. Dunn and Billam related cell performance to the ratio p1/p3 but the minimum value of this ratio was taken as 1 i.e. the hydrostatic case. Hence the most important values from the point of view of cross-sensitivity, ($p1/p3 < 1$) were not investigated.

To emphasise the fact that most pressure cells, which have been used by various investigators in the past, are probably cross-sensitive, the Road Research Laboratory have shown that their piezoelectric cell, which is very stiff in the plane of the diaphragm, is cross-sensitive. This cell is stiffer than most which have been reported on, but it is thought by the R.R.L., that the weakening effect of the cable entry may have some bearing on the problem.[78]

The pressure cells used in this project were only subjected to a simple calibration test prior to their installation in the test pit. This test involved applying a uniaxial stress normal to the diaphragm using oil pressure, and hence no check on possible cross-sensitivity was obtained. Further, since the test was performed by applying pressure directly to the cell, no information was obtained about the cell's performance

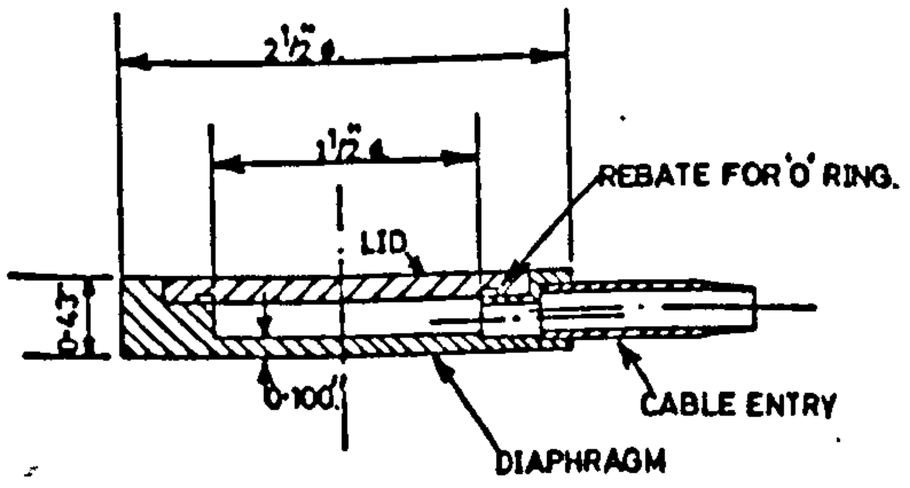

SECTION THROUGH CELL

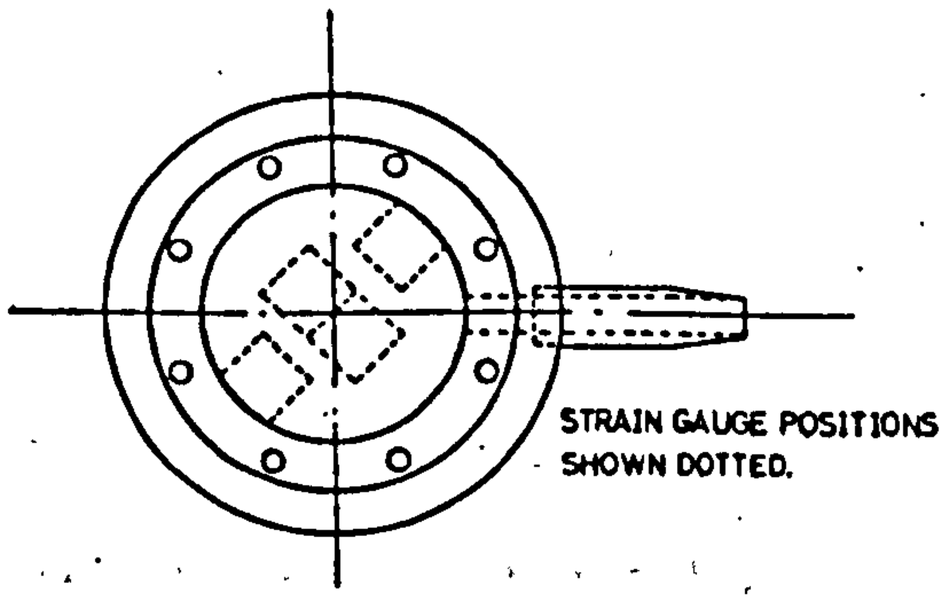

PLAN OF CELL WITH LID REMOVED

FIG. 3.1 DETAILS OF PRESSURE CELL

when installed in a soil mass.

Thus it was proposed to calibrate the cell by installing it in a 9 in. dia. triaxial specimen, and subjecting this to various combinations of ambient pressure and axial stress. A number of such tests were carried out with the cell at various orientations relative to the vertical axis of the soil specimen, and installed in each case, using the same procedure as that adopted in the test pit.

The method used to convert cell output current into stress involved switching a 500 k Ω calibration resistor across one arm of the Wheatstone bridge circuit. The stress producing an equivalent deflection was determined at the time of the uniaxial calibration test, and thereafter, cell readings were calculated by comparing the actual galvanometer deflection to that caused by the 500 k Ω resistor, which was switched in immediately before taking a reading from the pressure cell. The advantage of this system is that any changes in voltage or temperature on the bridge, affect both the calibration deflection and the reading in the same way and are therefore eliminated.

3.2 1st Series of Calibration Tests

The 9 in. dia. soil specimens were made by mounting a three piece split perspex mould around the triaxial cell pedestal, and compacting the soil in layers after first placing the lower loading platen in position. The inside surface of the mould was smeared with a thin layer of silicone grease before use to prevent adhesion with the soil.

The first series of tests were carried out on 18 in. long specimens with the pressure cell installed horiz-

ontally in the centre. The soil was compacted in 3 in. (compacted) layers using a pneumatic tamper with a rounded hammer head, so as to provide an uneven surface in an attempt to prevent interfaces forming between layers. After compacting 3 layers of soil, the pressure cell was installed, diaphragm up, in a slight recess dug in the surface of the soil. Selected fine soil was compacted by hand around and over the cell and cable, which passed through a hole in the perspex mould. When a layer of about $1\frac{1}{2}$ in. had been hand compacted over the cell, the remainder of the specimen was made up in 3 in. layers pneumatically tamped as before.

The pressure cell cable passed through a special waterproof cable entry in the rubber membrane around the specimen, and then through another cable entry in the triaxial cell base.

The object of the tests was to compare the pressure cell output with that from a load cell measuring the direct axial stress applied to the specimen and hence to the pressure cell. This procedure was adopted with varying ambient pressures between 0 and 10 lb/sq.in.

The results of this first test series showed, apparently, that the pressure cell was under-registering by 30%, whereas previous test results from the pit and

the theoretical analysis[11] indicated that the cell should over-register by 0 to 10%. One test was carried out by applying increasing ambient pressure alone, to the specimen, and this resulted in the pressure cell indicating the applied pressure almost exactly.

At this stage, the low figure obtained when applying axial stress to the specimen was put down to the possible effect of soil "arching" across the cell diaphragm, thereby relieving the stress at this important point. This argument was reinforced by the fact that the various layers of soil tended to separate very easily when dismantling the specimen after testing and also, as a result of using a rounded head on the tamper, the surface of each layer tended to "creep" up the side of the mould during compaction thereby forming the layer into an "arch".

The next few tests were carried out on specimens 9 in. long. These were quicker to make and since greased loading platens were used, no "end effects" were expected to interfere with the stress distribution in the centre of the specimen.[79] In order to try and prevent the "arching effect" from taking place, the soil layers were compacted using a flat ended tamper and after compaction the surface was levelled and roughened slightly

to try and form a key for the next layer. The test procedure was, otherwise, the same as before and again a very low result was obtained with the pressure cell in the centre of the specimen (50% of applied stress).

A test was carried out with the pressure cell mounted near the edge of the specimen, but still horizontal and at mid-height. This indicated, as had been anticipated, a higher result; in fact the pressure cell registered the applied stress exactly.

Hence it had become apparent that the stress distribution across the soil specimen was not uniform as had previously been assumed. Having eliminated the arching effect, the reason appeared to be differential compaction, causing the soil to be stiffer at the edge than in the centre, thus causing a non-uniform stress distribution across a section, high at the edge and low in the centre. A different method of compaction was therefore adopted for the next series of tests.

By compacting the specimen statically using a stiff plate, it was hoped to eliminate the previous troubles. Again a 9 in. long specimen was used and this was made up in 4 layers, with the cell again installed in the centre. The compacting procedure, was to mount the triaxial cell base with the mould in position, in the

testing machine, place the soil and apply a load by means of a substantial piston which fitted closely in the mould. It was found necessary to apply 100 lb/sq.in. to each layer to obtain the required degree of compaction, the load being determined by proving ring. Before placing in the mould, the soil was broken down into small pieces in a slicing machine, whereas, in previous tests it had been considered sufficient to cut up the soil by hand to pieces up to 2 in. dia. The top of each layer was well pitted and roughened using a trowel and no trouble resulted from separation of the layers. The pressure cell was installed by placing it diaphragm up on the flat surface resulting from the compaction of the second layer, and then compacting fine soil around and above it by hand as before. The soil surface around the cell was roughened before compacting a thin layer by hand to bring the level about $\frac{1}{2}$ in. above the pressure cell diaphragm. The remainder of the specimen was then made up in two layers in the usual way.

After compacting the top layer the usual procedure had been to trim the end of the specimen level with the top of the mould leaving a flat horizontal surface on which to place the loading platen. After compacting a specimen statically the resulting surface was smooth,

but slightly convex.. While this curvature was observed, it was not corrected for in the first two tests, with the result that an uneven stress distribution resulted. A specimen with the pressure cell centrally placed gave a result indicating an over-registration of 11%, while a similar specimen with the cell installed near the edge showed it under-registering by 18%.. A further two tests were carried out on specimens whose tops had been trimmed flat and level, and again by placing a central cell in one and a cell near the edge in the other, it was possible to check the stress distribution across the central section of the specimen. This time the cells gave almost the same result, indicating over-registrations of 3% and 1% respectively. Thus it was considered that a statically compacted specimen with flat ends was suitable for calibrating the pressure cells, since the stress distribution was sensibly constant across the central section.

3.3 Second Series of Calibration Tests

The two unconfined tests on statically compacted specimens described above, constituted the first tests of the second series. There followed a further seven tests, three with the cell vertical, three at 45° to the vertical axis and a further one with the cell horizontal.

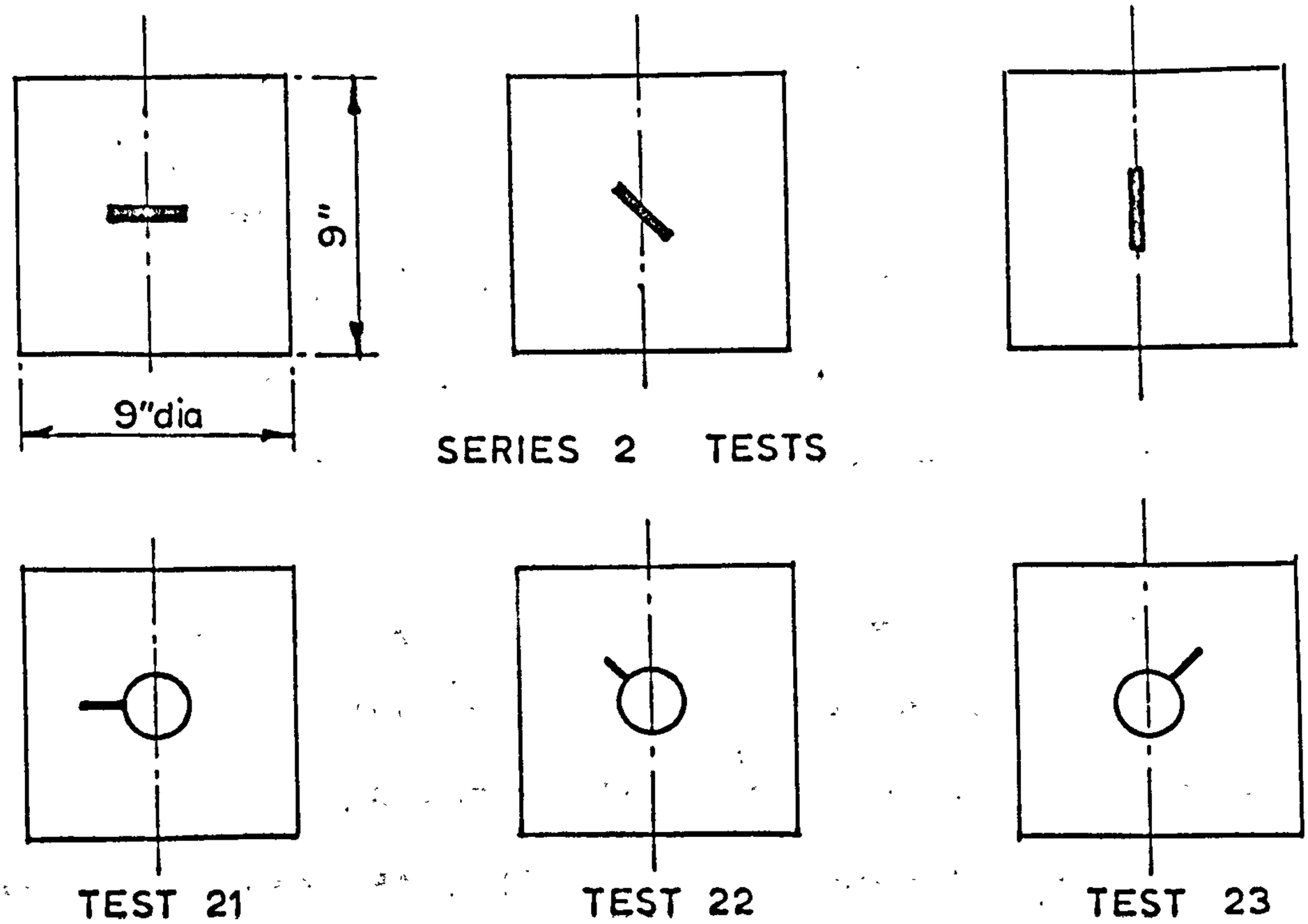

FIG. 3.2 CALIBRATION TESTS ON PRESSURE CELL

In all cases the cell was installed at the centre of the soil specimen, as shown in fig.3.2.

In general the axial stress was cycled from 0 to 30 lb/sq.in. twice before taking results. The output from both pressure cell and load cell were fed onto an Ultra Violet recorder and a proving ring was used to determine visually the approximate load increments. Three sets of results were generally taken for each test

using ambient pressures of 0, 5 and 10 lb/sq.in. Having applied the ambient presure, which was, for the sake of convenience, air pressure, the axial stress was increased in six increments to 18 lb/sq.in. and reduced similarly.

When dismantling the specimen the orientation of the cell was carefully checked to give an indication of how accurately the cells in the test pit may have been installed. This was particularly important in the case of the 45° cells, as discussed later when considering the apparent lack of equilibrium in the test pit results. It was also important in these triaxial tests, since the results at 45° were more sensitive to orientation than those with the pressure cell either vertical or horizontal.

Since the load cell calibration was based on the load being applied to an area 9 in. in diameter, the circumference of each specimen at mid-height was checked after testing, so as to provide a correction to the figure for applied stress.

From these results plots of load cell output against pressure cell output were obtained, and hence a figure for stress as indicated by p. cell

$$\frac{\text{true stress}}{}$$

TABLE 3.1 2ND SERIES OF PRESSURE CELL CALIBRATION TESTS IN KEUPER MARL - PRESSURE CELL P.17

Test No.	Nominal Ambient Pressure (lb/sq.in.)	Result $\frac{\text{Cell output}}{\text{True stress}}$	Cell Position	Moisture content of soil (%)
5/1 5/2 5/5	unconfined	1.05 1.03 1.02	Horizontal in centre	15.0
6/1 6/2 6/5	unconfined	1.01 1.00 1.02	Horizontal. Edge $\frac{1}{8}$" from side of specimen	15.5
7/5 7/6 7/9 7/10 7/11	unconfined 5 lb/in^2 10 lb/in^2	1.11 1.08 1.06 1.10 1.08	43° to horizontal in centre	15.3
8/3 8/4 8/7	unconfined	1.30 1.26 1.26	45° to horizontal in centre	15.2
9/5 9/6 9/7	unconfined 5 lb/in^2 10 lb/in^2	0.24 0.23 0.28	89° to horizontal in centre	-
10/3 10/4 10/5	unconfined 5 lb/in^2 10 lb/in^2	0.10 0.12 0.14	Vertical in centre	15.1
11/3 11/4 11/5	unconfined 5 lb/in^2 10 lb/in^2	0.11 0.14 0.11	92° to horizontal in centre	14.7
12/3 12/4 12/5	unconfined 5 lb/in^2 10 lb/in^2	1.02 1.00 1.04	47° to horizontal in centre	15.2
13/A 13/B 13/C	unconfined 5 lb/in^2 10 lb/in^2	1.07 1.02 1.03	Horizontal in centre	-
-	amb. press. loading	0.94	Horizontal	-
-	amb. press. loading	0.92	Vertical	-

$\frac{\text{cell output}}{\text{cross stress}}$

These results are presented in Table 3.1 and discussed in detail later in section 3.5.

3.4 Third Series of Calibration Tests

In the light of results from the second series of tests, a further three tests were carried out with the pressure cell installed vertically. It had become apparent that the pressure cell was cross-sensitive and that the orientation of the cell in the plane of the diaphragm had an important bearing on this. Hence in these three tests this orientation was varied. It was also thought that different cells may behave slightly differently, so a different pressure cell was used.

The only difference in test procedure from series 2 was that an additional test was performed whereby each specimen was loaded by increasing ambient pressure alone up to 25 lb/sq.in.

A further direct calibration test was carried out on each of the two cells which had been used in the triaxial specimens. This involved subjecting the cell to ambient air pressure by placing it in the triaxial cell. It was thus possible to compare the results of this test with the triaxial tests on the pressure cell in soil and with the simple uniaxial tests carried out originally.

Results from this series of tests are summarised in Table 3.2.

3.5 Discussion of Calibration Tests in Keuper Marl

All readings taken from the pressure cells were based on the original uniaxial calibration figures, and over or under registrations are, therefore, relative to these figures.

The ambient pressures indicated in Tables 3.1 and 3.2 are those registered by the pressure gauge attached to the pressure control system. Subsequent calibration of this instrument showed that it had a substantial zero error, and in fact the two values of ambient pressure used were 7.0 lb/sq.in. and 12.1 lb/sq.in.

In the second series, tests carried out with the cell horizontal gave consistent results indicating an over-registration of 3%. With the cell installed vertically, inconsistent results were obtained, but they showed evidence of considerable cross-sensitivity. The results are expressed in the form:

$$\frac{\text{pressure cell output}}{\text{"out of balance" cross-stress}}$$

i.e. if cross-stresses are p_z and p_y where $p_z > p_y$

TA TABLE 3.25 PRESSURE CELL CALIBRATION TESTS ION IN MELDON DUST - PRESSURE CELL P.18

Test No.	Nominal Ambient Pressure (lb/sq.in)	Result Cell output / Cross stress	Cell Position		Moisture content (%)
			Orientation of plane of diaphragm	Orientation in plane of diaphragm	
2	Ambient Pressure loading 10 15 20	1.46 1.08 1.02 1.02	Horizontal in centre	-	6.9
3	Ambient Pressure loading 10 15 20	1.33 0.94 0.89 0.85	Horizontal in centre	-	6.9
4	Ambient Pressure loading 10, 15 and 20	1.10 Cell output / Cross stress = 0.035	Vertical in centre	Cable entry horizontal	7.0
5	Ambient Pressure loading 10 and 20	1.15 Cell output / Cross stress = 0.02	89° to horizontal in centre	Cable entry 45° below horizontal	6.8
6	Ambient Pressure loading 10 20	1.28 0.95 0.93	45° to horizontal in centre	-	6.9
7	Ambient Pressure loading 10 20	1.14 1.02 0.95	48° to horizontal in centre	-	6.4
8	Ambient Pressure loading 10 20	1.38 0.98 0.89	Horizontal in centre	-	6.8
9	Ambient Pressure loading 10 20	1.21 0.90 0.81	Horizontal near edge	-	6.6

"out of balance" cross-stress = $(p_z - p_y)$.
Mean results show pressure cell output = 25%, 12% and 12% of this cross-stress. For no cross-sensitivity these results should all be zero.

The results of tests with the pressure cell set at 45° are again inconsistent showing over-registrations of 9%, 27% and 2%. The orientation of the cell was correct to $\pm$ 2°.

The third series of tests confirmed that the cross-sensitivity was dependent on the orientation of the cell in the plane of the diaphragm, relative to the direction of maximum cross-stress. Mean results from the three tests gave -5%, 33% and -41% of "out of balance cross-stress" with the cell cable entry making angles of 0°, 45° and 135° with the horizontal in each case respectively (see fig. 3.2).

Each individual test in series 2 and 3 was generally repeated three times at different ambient pressures as described elsewhere. The procedure adopted, was to apply the ambient pressure, take a zero reading and then increase the axial stress on the specimen. The results show no variation with ambient pressure, and consequently final mean figures quoted above refer to the average result of the three tests in each case.

Five tests were carried out (3 in series 3, and 2 in series 2) by applying ambient pressure only, to the specimen, and the mean value obtained for $\frac{\text{pressure cell output}}{\text{applied pressure}}$ was 0.87. There were differences in the results obtained from the two cells, P.17 (series 2) giving 0.93 and P.16 (series 3) giving 0.83.

When the cells were loaded directly by ambient air pressure P.16 indicated 0.97 and P.17 1.02 giving a mean of 1.0. This means that calibrating the cell under ambient air pressure gives the same result as the uniaxial test. Fig. 33 shows these calibration.

The maximum values of cross-sensitivity were obtained when the cross-stress was applied at 45° to each side of the cable entry; positive to one side and negative to the other. These directions correspond with the diameters on which the diaphragm strain gauges are mounted. Fig. 3.4 shows the disposition of these strain gauges, with one pair about the centre and one pair at opposite edges of the diaphragm. With the stress applied in direction 1, cell output = -0.41 x (cross-stress) and in direction 2 cell output = +0.33 x (cross-stress).

Because of the stiffening effect of the outer ring of the cell, most of the deformation will be concentrated at the

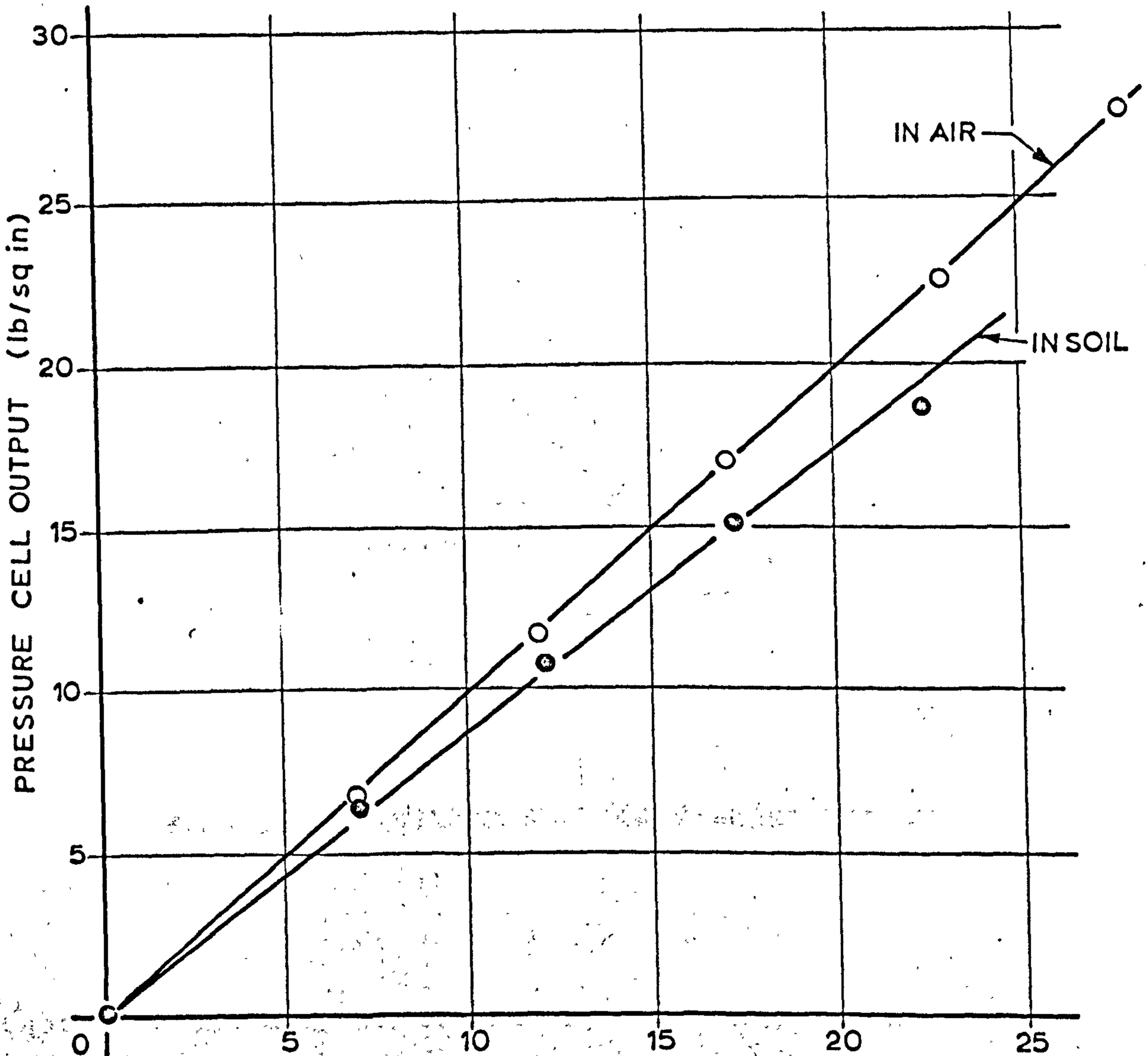

FIG. 3.3 PRESSURE CELL CALIBRATION UNDER AMBIENT PRESSURE - KEUPER MARL

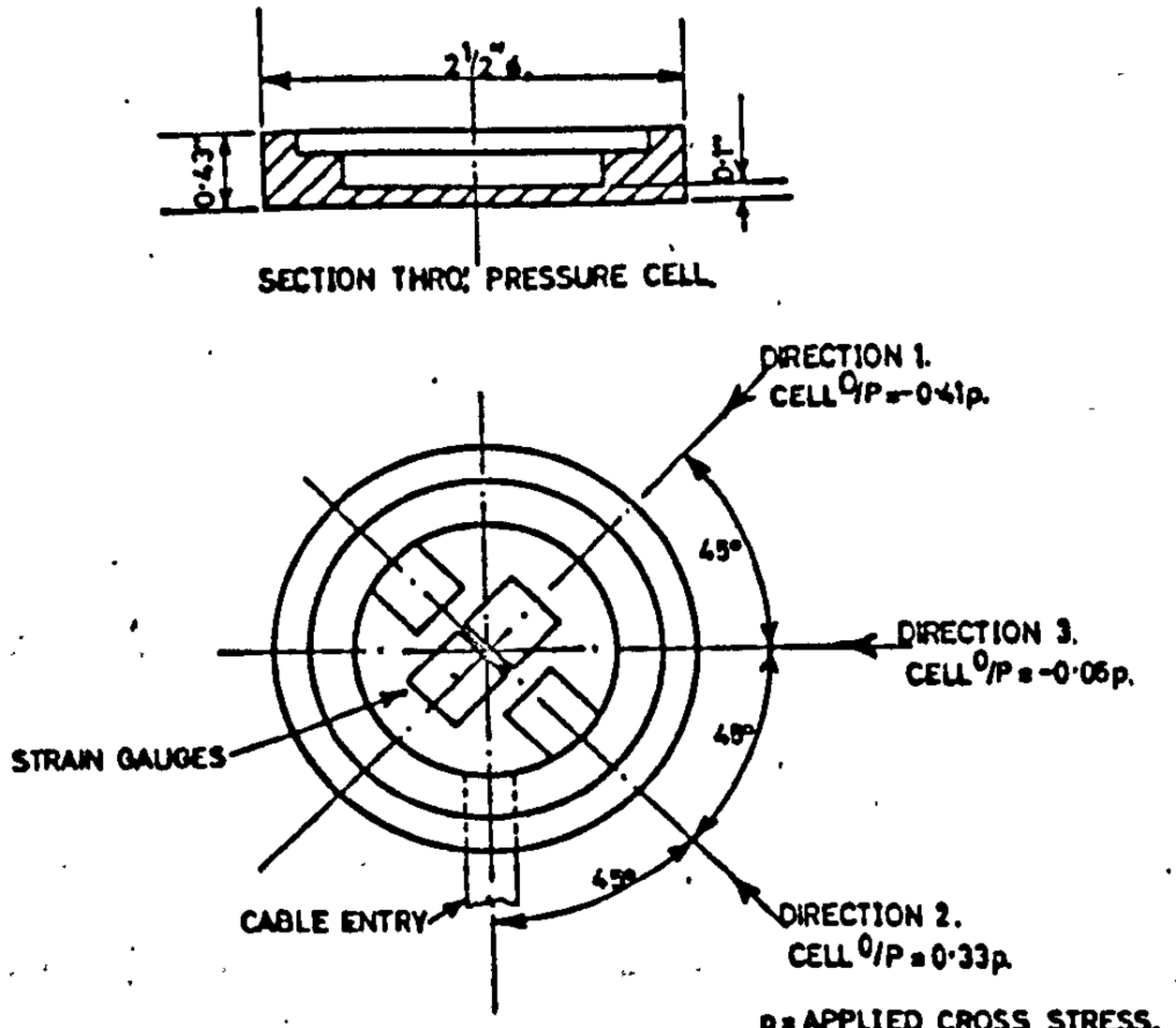

FIG. 3.4 PRESSURE CELL CROSS-SENSITIVITY

centre of the diaphragm, causing the gauges mounted there to govern the electrical output. The results indicate that the centre of the diaphragm is subjected to direct compression in the direction of the applied stress and tension due to the Poisson's ratio effect, at right angles to this. Hence, when the stress is applied in direction 1 the central strain gauges go into compression and in direction 2 they go into tension.

The diaphragm may also be bending, although the strains caused must be much less than those due to direct compression. With the applied stress in direction 2, the positive output would appear to be high if caused by the Poisson's ratio effect alone, however, if the diaphragm bends inwards as is likely since this happens in use, the outer strain gauges would assist in indicating a positive output. The same effect with the stress in direction 1 would tend to reduce the size of the negative output recorded.

There was a large discrepancy between the cell output under ambient pressure in air and in soil, (fig. 3.3), the latter giving an under-registration of 13%. If the equal all-round radial cross-stress is replaced by two equal stresses acting along the critical diameters of the cell, by superimposing the two relevant results of series 3 tests, the net output is -8%. This figure cannot be compared directly with the -13% of the ambient pressure tests, because of superposition effects, inaccuracy in the position of strain gauges and orientation of the cell in the soil specimens, but the fact that they are of the same order does help to explain the results of the tests under all-round pressure. Also, by considering the result of loading in direction 3 to apply also in a

direction at right angles to this the net output would be -10% if two equal stresses are applied in these directions. This again is comparable with the -13% recorded under ambient pressure.

The results for cross-sensitivity observed in tests 2 and 3 were confirmed by a simple dead-load test on each pressure cell. A weight of 11 lb. was applied to the cell on edge on a bench with the cable entry in the three positions used for series 3 tests. This point load of 11 lb. was very roughly equivalent to a U.D. load over the cell's projected area of 10 lb/sq.in., being the mean value generally used in the soil tests.

The apparently high errors caused by cross-stresses acting on the cell may be partly caused by "cell-action". The cell has a very adverse depth: breadth ratio in the direction of the cross-stresses and hence there will be a build up of stress on the edge of the cell, so that the actual cross-stress will be higher than that recorded during the tests. The simple dead load tests, while indicating the same behaviour as the tests in soil, gave slightly smaller results. While the application of a point load would probably tend to indicate higher results, the fact that there is no cell action operating more than nullifies this.

The inconsistent results obtained during series 2 tests with the cell vertical and at 45° were presumably caused by varying the position of the cable entry. No record was kept of the orientations in this direction, but the cable entries were probably nearer horizontal than 45°.

The two cells (P.16 and 17) used in these calibration tests had the same disposition of strain gauges (fig. 3.4) and the results of the dead load tests described above were, in fact, similar for both cells, in keeping with this strain gauge arrangement. It is possible, however, to arrange the gauges in the same position relative to each other, but 90° removed relative to the cable entry. (They are always placed on diameters approximately 45° each side of the cable entry to facilitate wiring.) Thus, it can be seen that the strain gauge positions on the pressure cells installed in the test pit may or may not be the same as P.16 and P.17. When the test pit was instrumented, no record was kept of the side on which the diaphragm was placed on vertical cells, or the angle made between the cable entry and the horizontal, since it was not considered important at that stage. Cells placed horizontally and at 45° will also be subject to cross-sensitivity, and while they were all placed "diaphragm up", the exact orientation of their cable entries is also

unknown. It thus becomes apparent that the stress measurements taken from the Keuper Marl in the test pit cannot be corrected for cross-sensitivity with any accuracy.

The cross-stress causing the greatest cross-sensitivity error will not necessarily be the largest stress acting in the plane of the diaphragm, since the error is also a function of the direction in which the stress acts relative to the strain gauge arrangement. Consequently a large stress acting at right angles to the cable entry may have less effect than a smaller stress acting at 45° to this. Hence, even if more information were available about the orientation of the cells and their strain gauge positions, as only two cross-stresses were measured, and these were obtained by superposition of results, there would still be insufficient information to correct the stress measurements accurately.

3.6 Approximate method for correction of stresses in Keuper Marl

Despite the foregoing remarks, which present the various problems baring an accurate application of the results of these calibration tests to the single layer system results, an approximate method to determine likely

errors in stress results can be evolved.

The following assumptions need to be made:

1. That cable entries to vertical cells and 45° cells are horizontal, and to horizontal cells are perpendicular to the grid layout. The cells likely to be most at variance with this assumption are 2 and 3 (see fig. 2.2).

2. That the result from series 3 tests with the cross-stress applied in position 3, applies equally well in the perpendicular direction.

3. The principle of superposition holds. This is a general assumption in this work to obtain stress distributions and to perform calculations on stresses in different directions at a point. In the present context it is likely to cause some error, so the assumption is repeated here.

These assumptions provide the simplified condition of the two known cross-stresses acting perpendicular to, and in line with, the cable entry, i.e. in the direction dealt with in assumption 2. This means that for a cell measuring vertical stress, for instance, the two cross-stresses will be the radial and tangential ones, whose values are known, and whose effects on the cell reading are known by virtue of the directions in which they act.

TABLE 3.3 ESTIMATED LIKELY ERRORS DUE TO CROSS-SENSITIVITY FOR STRESS MEASUREMENTS IN KEUPER MARL
Test S/A - Results at the 3" depth

Radius (in.)	Measured Stress, p. (% of contact pressure)	Error $-.05(J_1-p)$	Percentage Error $\frac{-5(J_1-p)}{p}\%$	Direction of stress
0	89	-4.4	-5	Vertical
3	84	-3.7	-4	
6	42	-1.7	-4	
9	2	-0.9	-45	
12	0	-0.6	-	
0	48	-6.5	-13	Radial
3	46	-5.6	-12	
6	39	-1.9	-5	
9	26	+0.4	+2	
12	14	+0.3	+2	
0	43	-6.7	-16	Tangential
3	28	-6.5	-23	
6	-3	-4.0	-133	
9	-8	-1.4	-18	
12	-3	-0.7	-23	
0	65	-5.6	-9	45°
3	76	-4.1	-5	
6	54	-1.1	-2	
9	18	-0.1	-10	
12	8	-0.2	-7	
0	65	-5.6	-9	135°
3	50	-5.4	-11	
6	18	-2.9	-17	
9	3	-0.8	-27	
12	5	-0.3	-6	

The appropriate result from series 3 tests indicates that the cell output due to a cross-stress in the direction concerned is -5% of that stress. Hence the error in vertical stress

$$= -.05\ p_r - .05\ p_\theta$$

$$= -.05\ (p_r + p_\theta)$$

$$= \underline{-.05\ (J_1 - p_z)} \qquad (\text{where } J_1 = p_z + p_r + p_\theta = p_{45} + p_{135} + p_\theta)$$

$$\therefore \text{Corrected vertical stress} = p_z + 0.05\ (J_1 - p_z)$$

$$= \underline{0.05(J_1 + 19p_z)}$$

with similar expressions for the other stresses.

In general this error will be negative since J_1 is greater than individual stresses (although there are exceptions to this), indicating that the pressure cells are under-registering nearly all stress measurements.

The stresses from test S/A at the 3 in. depth have been analysed by the above method and the results are shown in Table 3.3. The only positive errors appear for radial stress away from the loaded area, where the 1st stress invariant is small, because of negative tangential stresses.

A study of these results indicates that the most

accurate stresses are p_z under the load, p_r away from the load and p_{45}. The least accurate is p_θ.

Values of errors in p_1 and p_3 have been calculated for the same results of test S/A as used in Table 3.3. These are shown in Table 3.4, and they indicate smaller errors for p_1 than for p_3. This is in keeping with the general trend of smaller errors in stresses which are large relative to the cross-stresses.

Two other quantities are calculated from the measured stresses in the pit, these are maximum shear stress and elevation of major principal plane from the horizontal. The effect of cross-sensitivity errors on these quantities can be determined as follows:

Maximum shear stress = τ max

where τ max = $0.5\ (p_1 - p_3)$

Corrected τ max $= 0.5\ [0.05\ (J_1 + 19p_1) - 0.05(J_1 + 19p_3)]$

$= 0.5 \times 0.95\ (p_1 - p_3)$

$= 0.95 \times \tau$ max

i.e. Error in maximum shear stress is constant at +5%.

The angle of elevation of the major principal plane is given by

$$\tan 2\alpha = \frac{2p_{45} - p_z - p_r}{p_z - p_r}$$

Radius (in.)	Derived Stress p (% of contact pressure)	Error $-.05(J_1-p)$	Percentage Error $\frac{-5(J_1-p)}{p}$ %	Identification of stress
0	88	-4.5	-5	Major Principal
3	87	-3.5	-4	
6	57	-2.0	-4	
9	27	+0.4	+1	
12	14	+0.2	+1	
0	47	-6.5	-14	Minor Principal
3	41	-5.8	-14	
6	22	-2.7	-12	
9	-1	-1.0	-100	
12	0	-0.6	-	

TABLE 3.4 ESTIMATED LIKELY ERRORS DUE TO CROSS-SENSITIVITY FOR DERIVED STRESSES IN KEUPER MARL

Test S/A - Results at the 3" depth

$$\therefore \text{ corrected value of } \tan 2\alpha$$

$$= \frac{0.05\,[2(J_1 + 19p_{45}) - (J_1 + 19p_z) - (J_1 + 19p_r)]}{0.05\,[(J_1 + 19p_z) - (J_1 + 19p_r)]}$$

$$= \frac{2p_{45} - p_z - p_r}{p_z - p_r} = \tan 2\alpha$$

i.e., it is unaffected by errors in stresses.

3.7 Calibration tests in Meldon Dust

The granular material to be used for the second, or base layer, of the model pavement was chosen partly with the intention of using the same transducers as for the clay subgrade. Details of this base layer material have been presented in Chapter 2, and it will be noted that it is of relatively small particle size, thus enabling the existing instruments to be used. Because of the different properties of this material however, calibration tests on the same lines as those described for the cell in Keuper Marl, were conducted.

The pressure cells to be used in the Meldon Dust were modified in order to reduce the effects of cross-sensitivity, present with the cells used earlier. A different arrangement of strain gauges on the cell diaphragm was adopted as a result of the findings in the 3rd test series, and this is shown in fig. 3.5. Since

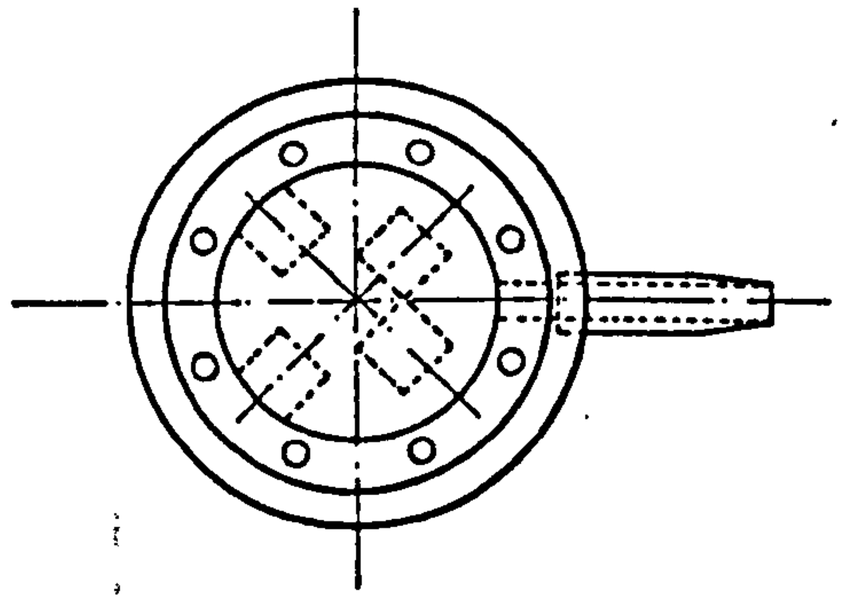

STRAIN GAUGE POSITIONS SHOWN DOTTED.

FIG. 3.5 NEW PRESSURE CELL

STRAIN GAUGE ARRANGEMENT

cross-sensitivity is caused mainly by the central strain gauges registering direct compression of the cell diaphragm, these gauges were now mounted at 90° to one another. This meant that one would register compression under a cross-stress as before, while the other was registering tension, tending to cancel the effect of the first. Similar relative positions were used for the strain gauges at the edge of the diaphragm.

Eight triaxial specimens 9 in. dia. x 9 in. long were tested with a pressure cell installed at different orientations in the centre. In general, after three preloading cycles, each specimen was loaded three or four times, firstly by ambient pressure alone and then by

Test No.	Nominal Ambient Pressure (lb/sq.in)	Result Cell output / Cross stress	Cell Position		Moisture content (%)
			Orientation of plane of diaphragm	Orientation in plane of diaphragm	
21/3	unconfined	-0.05	88° to horizontal in centre	Cable Entry Horizontal	15.9
21/5	5 lb/in^2	-0.04			
21/6	10 lb/in^2	-0.06			
21/7	Ambient Pressure loading	0.84*			
22/3	unconfined	0.30	92° to horizontal in centre	Cable Entry 45° above Horizontal	15.4
22/4	5 lb/in^2	0.33			
22/5	10 lb/in^2	0.33			
22/6	Ambient Pressure loading	0.85*			
23/3	unconfined	-0.43	Vertical in centre	Cable Entry 45° below Horizontal	15.1
23/4	5 lb/in^2	-0.36			
23/5	10 lb/in^2	-0.44			
23/6	Ambient Pressure loading	0.79*			

* Cell output / Applied Pressure

TABLE 3.12 3RD SERIES OF PRESSURE CELL CALIBRATION TESTS IN KEUPER MARL - PRESSURE CELL P.16

TABLE 3

IN

applying an axial stress at three different ambient pressures. Details of the results of these tests are shown in Table 3.5 and typical calibration plots in figs. 3.6 and 3.7.

Compaction of the triaxial specimens was by vibrating plate in approximately 2" (compacted) layers, allowing one minute continuous vibration per layer. The cell installation procedure was the same as used in the test pit, material passing a number 7 sieve being placed over the diaphragm to avoid larger particles from causing false readings.

The results were generally satisfactory despite the very high over-registration obtained when the specimen was loaded by ambient pressure alone. The mean value for stress as indicated by the pressure cell divided by the applied stress was 0.94 i.e. 6% under-registration. The mean value for this function when applying ambient pressure alone was 1.33, however, as soon as any deviator stress was applied this relationship disappeared. On the calibration plot in fig. 3.7 the deviator stress has been applied initially in very small increments and this plot shows that there was no transition from the higher over-registration to the normal behaviour. Some mechanism is presumably present under hydrostatic conditions, possibly

TEST 8

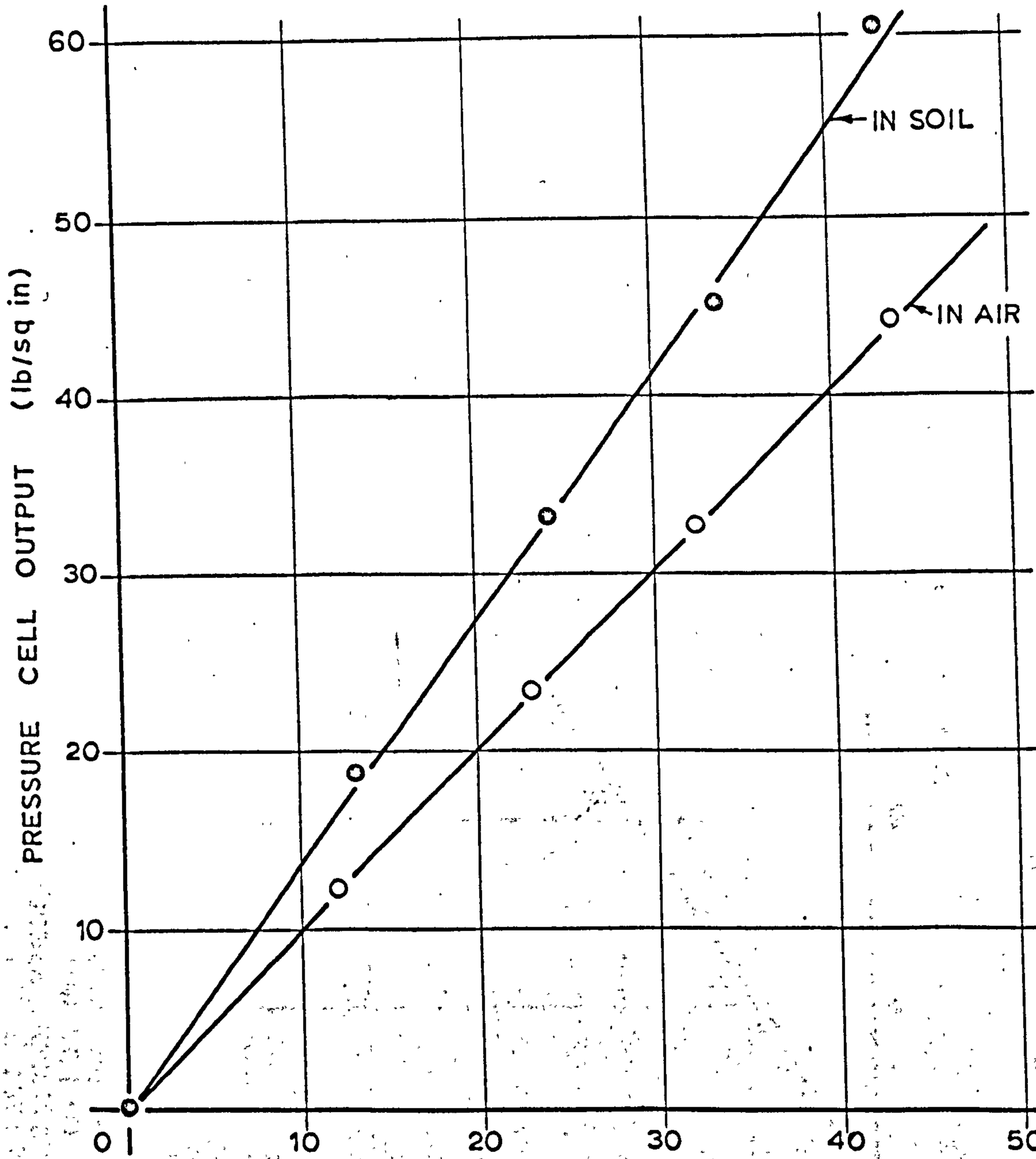

FIG. 3.6 PRESSURE CELL CALIBRATION UNDER AMBIENT PRESSURE - MELDON DUST

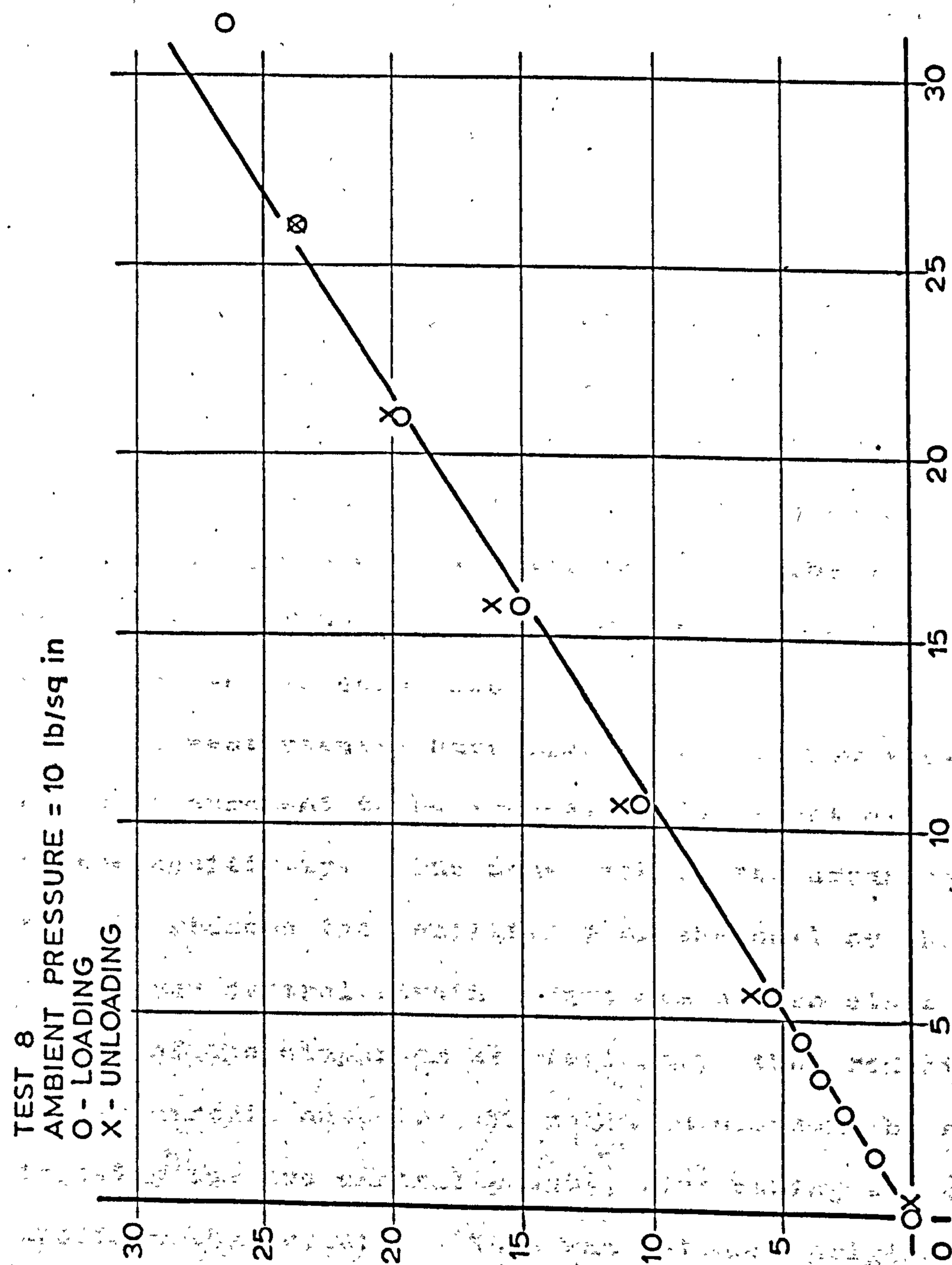

FIG. 3.7 TYPICAL PRESSURE CELL CALIBRATION IN MELDON DUST

as a result of the compaction technique, which breaks down as soon as any shear stress is applied to the system. It was assumed that since there will always be some shear stress present in practice, however small, this high calibration figure may be safely ignored. It seemed also to depend on the orientation of the cell since mean results with the cell horizontal gave a figure of 1.42, at 45°, 1.28 and vertical 1.19. The 45° result is approximately a mean of the other two. If the effect is caused indirectly by the compaction procedure, the above variation can be appreciated since the quantity and distribution of hard compacted material around the cell was different in each case.

The test results have also shown the new strain gauge arrangement to be successful in almost eliminating cross-sensitivity. One draw back of the arrangement is that it reduces the sensitivity of the cell by about 30%. as the two central strain gauges are not so close to the centre of the diaphragm as previously, thus reducing the bridge circuit output. This can be overcome by super-imposing the two central gauges, thus making the cell more accurate than before. This was not done originally because there was insufficient time to check whether the arrangement worked satisfactorily.

The accuracy of the results taken in the calibration tests in Meldon Dust may not be as good as for the Keuper Marl. Less care was taken in ensuring that a uniform stress distribution existed across the section of triaxial specimen where the cell was installed. One test (Test 9) was conducted with the cell situated near the edge of the specimen, and the results indicated a lower mean calibration figure, 0.85, than for other tests with the cell placed centrally. This suggests that the compaction was better at the centre than near the edge of the specimen, and, therefore, the mean calibration figure of 0.94 may be slightly high. This is not particularly significant in the context of applying these results to stress measurements from the test pit. The scatter of results on stress distribution plots, presented in Chapters 7 and 8, is much greater than the error introduced here. The calibration figure was in fact considered near enough to unity to use the original uniaxial calibration tests, which are much easier to carry out. A further reason for this is that only one pressure cell was calibrated in the granular material, and hence not too much emphasis was placed on the absolute value of the result.

CHAPTER 4 THE STRAIN CELL

4.1 Introduction

Since the development of suitable instruments for measuring earth pressures in-situ, it has been realised that a strain measuring device would provide a considerable amount of useful information, both on its own and in conjunction with pressure cells. Measurements of stress and strain when combined could produce values for the elastic constants of the material and these were of particular interest in the analysis of layered pavement systems. The various studies of layered system behaviour have in the past adopted indirect or approximate methods for determining the modulus of the various layers as outlined in Chapter 1.

In view of the great need for information about the in-situ modulus of pavement materials it is surprising that an effective strain measuring device has not previously been developed. The Waterways Experiment Station, realising the need for such an instrument when investigating the behaviour of their homogeneous test sections, developed, at their Ohio River Division Laboratory, a rather large strain cell which in practice gave

disappointing results.[80] This instrument was 10 in. long, having at one end a differential transformer and at the other a perspex disc. The disc was connected to a rod which moved one of the transformer coils. Because of their lack of success with this instrument which was only used in the sand test section, the W.E.S. relied on an indirect method of vertical strain determination from surface deflection measurements.

To the best of the Author's knowledge, no other, even moderately successful, strain cell was reported on, until Sparrow and Tory[11,17] began work on the early stages of the present project. The strain cell developed by them has been described in detail elsewhere,[11] but a drawing of it is included here in fig. 4.1. The main requirement for a successful strain cell is that it should be very flexible relative to the soil in the direction of measurement, in order not to provide any reinforcing action but to move with the soil.

When the Author began work on the project, the strain cell had been developed and used successfully in a single layer system of Keuper Marl. There was, however, not much information about its actual performance when buried in a soil mass. Before installation in the single layer system described herein, the strain cells had only been

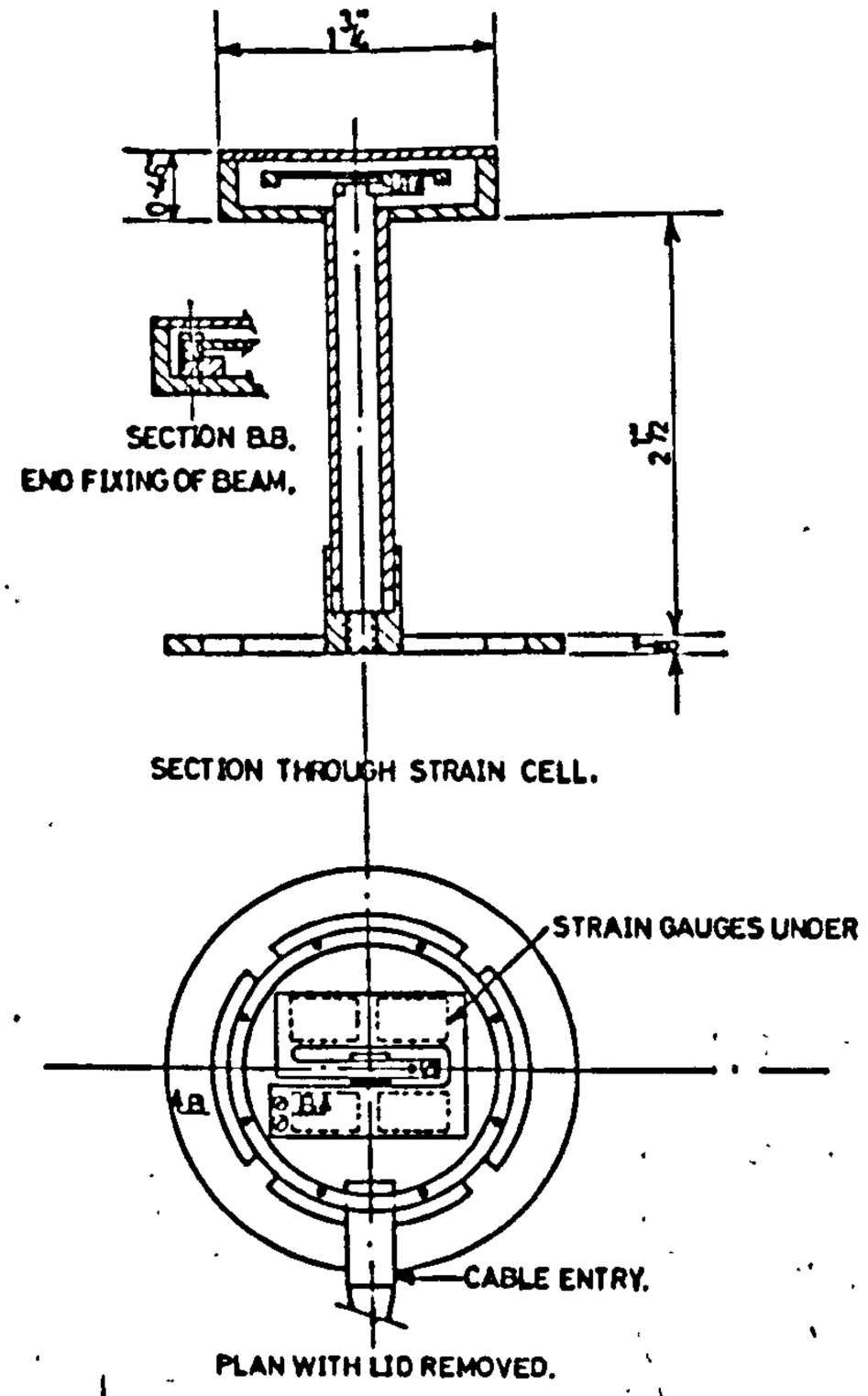

FIG. 4.1 DETAILS OF STRAIN CELL

subjected to a simple mechanical calibration test. This involved mounting the cell in a special bench micrometer and applying a known deflection while measuring the electrical output. In order to translate this "deflection" calibration into one of "strain", a gauge length had to be assumed, and this was taken as 3 in., being the over-all length of the instrument in its mid-travel position.

To decide whether this was in fact the gauge length when installed, and to generally obtain more accurate information about the behaviour of the strain cell when buried in a soil mass, a series of tests were carried out by installing the cell in a 9 in. dia. triaxial specimen, adopting a procedure similar to that used for the pressure cells. It was necessary to calibrate the instrument both in tension and compression and a total of five different tests were performed on two instruments, in unconfined specimens of Keuper Marl, once the experimental procedure had been satisfactorily developed.

4.2 Calibration tests in compression

The strain cell was installed in the centre of a 9 in. dia. triaxial specimen as shown in fig. 4.2. An 18 in. long specimen was used because of the larger size of the strain cell compared with the pressure cell. Greased loading platens were again adopted and with the longer specimen, it was thought that the neighbourhood of the cell would be free of end effects. The soil specimen was compacted statically, in the manner described for the pressure cell calibration tests.

The procedure for installing a cell in a triaxial specimen followed that adopted in the test pit. For

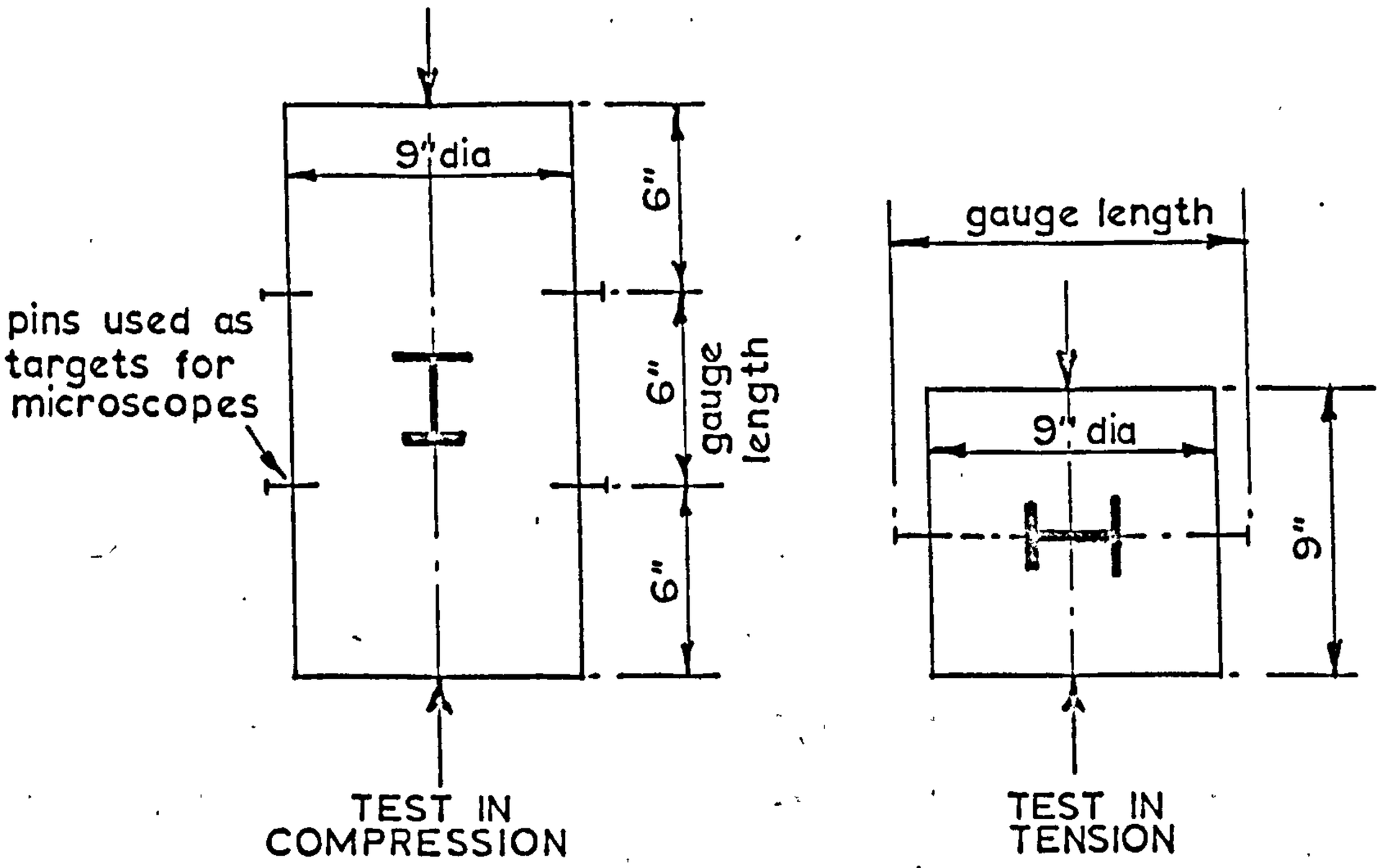

FIG. 4.2 CALIBRATION TESTS ON STRAIN CELL

this reason, it was fortuitous that experience with these cells in the test pit had in fact preceeded calibration tests.

During compaction and subsequently during the first few load cycles, large residual strains were set up in the soil, so it was necessary to ensure that the strain cell was not fully compressed before calibration tests were started. This was done by monitoring the cell output on a spot galvanometer during installation and arranging for the cell to be in its "fully open" position before completing the soil specimen. (The equipment for

this type of installation is shown in the background of fig. 2.15). After the instrument had been covered by soil, it could be opened or closed by tamping the soil to one side or above the instrument respectively.

Before installation the central tube of the instrument was well greased and fitted with a pliable rubber sleeve. The function of this sleeve was to prevent soil penetrating into the sliding fit between the end plate and the central tube and also to act as a shear break between the soil and rigid tube. This is further discussed later in this chapter. In order to facilitate compaction of soil around the instrument, the end plate was removed and replaced by a cap with the same dimensions as the hub of the end plate (see fig. 4.8).

The cell was installed in a recess about 3 in. deep with sloping sides in the centre of the soil specimen. The end containing the measuring beam was placed downwards and the cable allowed to pass along a small trench in the soil and thence through a hole in the split mould. After checking its position and level, fine soil was pressed around the base by hand and this was followed by further layers, compacted using a light tamper. When the soil had been compacted almost to the top of the instrument, the temporary cap was removed and the end plate screwed

on. Soil was then carefully pressed around the end plate and a layer about 1 in. thick was compacted over it.

Each specimen was left for at least 12 hours before testing, to allow the moisture content to become uniform. About three load cycles were then applied before taking any measurements, to allow residual strains to be eliminated.

The object of each calibration test was to compare the strain as indicated by the cell, assuming a 3 in. gauge length, with the true strain which was present in the soil. The problem was to obtain a reliable measure of this "true" strain. Early tests involved the measurement of overall strain in the conventional way by using a dial gauge outside the triaxial cell for a confined specimen. An attempt was made to obtain a plot of strain cell output against overall deflection of the specimen directly by using an X-Y plotter. In this case the overall deflection was measured using another strain cell acting as a deflection gauge and feeding its output onto one axis while that from the strain cell under test was amplified and fed onto the other axis. The main difficulty with this method was that the travel on the strain cell used for overall deflection measurements was

too small (0.1 in.).

All the methods involving the measurement of overall strain suffered from the same basic errors, those introduced by the end fittings and end effects in the specimen, which though minimised by using lubricated loading platens, were doubtless present. It was thus decided that an unconfined specimen would have to be used and the true strain measured over some suitable gauge length about the centre of the specimen, where the measurements would be free from the inaccuracies previously encountered.

Once again various methods of measuring the deformation over this new gauge length were tried. The first, rather crude, method involved driving 8 in. x $\frac{3}{4}$ in. x $\frac{1}{8}$ in. brass spikes, suitably pointed, into the side of the soil specimen at each end of two 6 in. vertical gauge lengths diametrically opposite one another. Deflection measurements were then affected by the use of four dial gauges, one on each spike. There were several errors involved here. It was difficult to drive the spikes in accurately, so that they usually ended up other than horizontal, making satisfactory contact with the dial gauge probes difficult. There was also the obviously dangerous practice of introducing

these spikes into the specimen, since this could have upset the strain distribution where it most mattered.

A travelling microscope was next tried. The 6 in. gauge lengths were marked by pins stuck into the side of the specimen, the microscope being focussed on each in turn as successive increments of load were applied. Originally this microscope could measure to a thousandth of an inch, but plots of the results indicated that this was not sufficiently accurate. The range of strain over which the strain cells were being calibrated was about 4,000 microstrain, so that over a 6 in. gauge length this produced a deflection of only 0.024 in. (24 thou.).

To overcome this inaccuracy the travelling microscope was fitted with a special eye piece permitting direct readings of 1/300 mm. (0.00013 in.) to be obtained. It was focussed on a pin stuck into the side of the soil specimen and suitably illuminated. The final procedure adopted for "true" strain was, therefore, to measure the deformation of two 6 in. diametrically opposite vertical gauge lengths (fig. 4.2) and take the mean, thus eliminating any bending strain and reducing any local effects which may have been present. Ideally, four microscopes should have been used, one at each end of each gauge length. However, only two of these instruments were available, so

two tests had to be performed, taking readings first on one gauge length and then on the other. The experimental set up is shown in fig. 4.3. The repeatability of the two tests had to be demonstrated, so that the two sets of "true" strain measurements could be considered as coming from the same test. This was done by measuring the overall deformation of the specimen each time, using two dial gauges mounted at each end of a diameter of the loading platen, and taking their mean readings. This was plotted against the strain cell output for each test and consistent results indicated sufficient repeatability to justify the procedure for obtaining the "true" strain measurements.

The strain cells were calibrated over the range 0 to 4000 microstrain which corresponded to a range of stress from 0 to 16 lb/sq.in. The stress was recorded during these tests both on a proving ring and from a load cell (fig. 4.3) so as to obtain a stress/strain relationship for the soil. The range of strain was covered in eight increments of stress, since it was easier to read stress directly using the proving ring. The various measurements described above were taken after each increment, both during loading and unloading. A summary of the results of these tests is given in Table 4.1 and typical plots

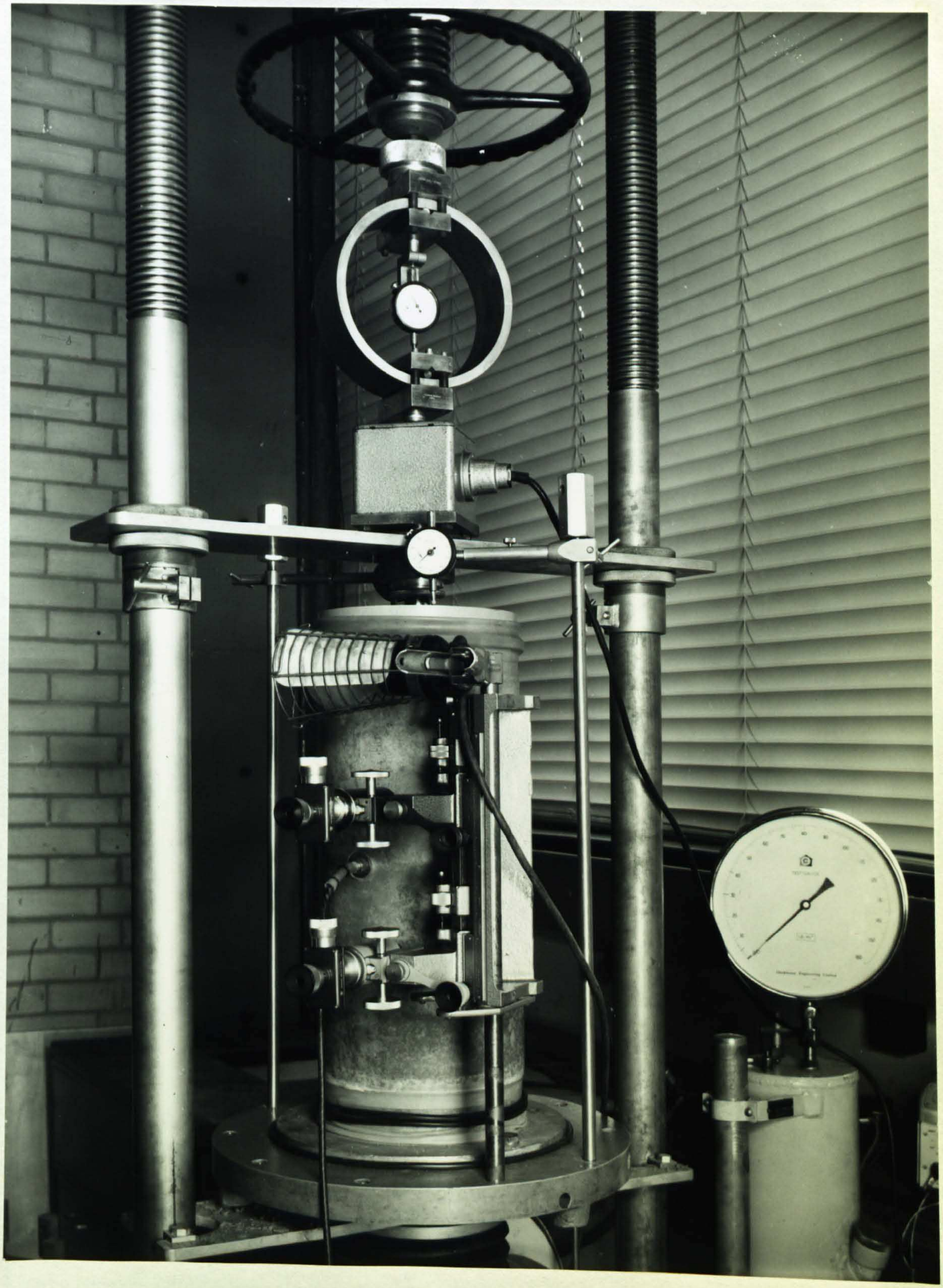

FIG. 4.3 APPARATUS FOR STRAIN CELL CALIBRATION

Test No.	Compression (loading)		Tension (unloading)		Remarks
	Cell output true strain	Zero error (micro-strain)	Cell output true strain	Zero error (micro-strain)	
1/5,6*	0.99	0	0.85	-54	S.Cell S.8 with membrane on soil
3/4,5*	1.03	0	0.99	132	
5/4,5	1.16	123	1.09	123	S.Cell S.9 with membrane on soil
5/6,7	1.11	45	1.07	78	
5/8,9	1.04	40	1.02	78	
5/10,11*	1.02	0	1.02	78	
6/4,5	1.03	163	1.02	174	S.Cell S.9 without membrane on soil
6/8,9	1.02	130	0.97	87	
6/10,11	1.02	109	0.90	141	
6/16,17*	0.95	87	0.90	119	

* Results used for calibration figures

TABLE 4.1 STRAIN CELL CALIBRATION TESTS IN COMPRESSION FOR KEUPER MARL

are included in figs. 4.4 and 4.5.

4.3 Calibration Tests in Tension

In the compression tests, the unloading half of the cycle was considered analogous to a tensile test, but in order to confirm the results thus obtained, "true" tensile tests were carried out on the strain cells.

For these tests the strain cells were installed horizontally in 9 in. long soil specimens (fig. 4.2). The true strain on the diameter of the specimen which coincided with the cell axis was measured using the microscopes. Because of the reorientation of the strain cell for these tests the shorter specimen was considered suitable since, with the lubricated loading platens, no end effects were expected to interfere with the results.

The procedure for installing the cell was again as used in the test pit. The end plate was screwed on before installation, since it no longer inhibited compaction and again the cell output was monitored to keep the instrument in the appropriate part of its travel. With the cell in the horizontal position, the residual strains were less and this did not present such a problem as in the compression tests.

During installation, care was taken to mark the ends

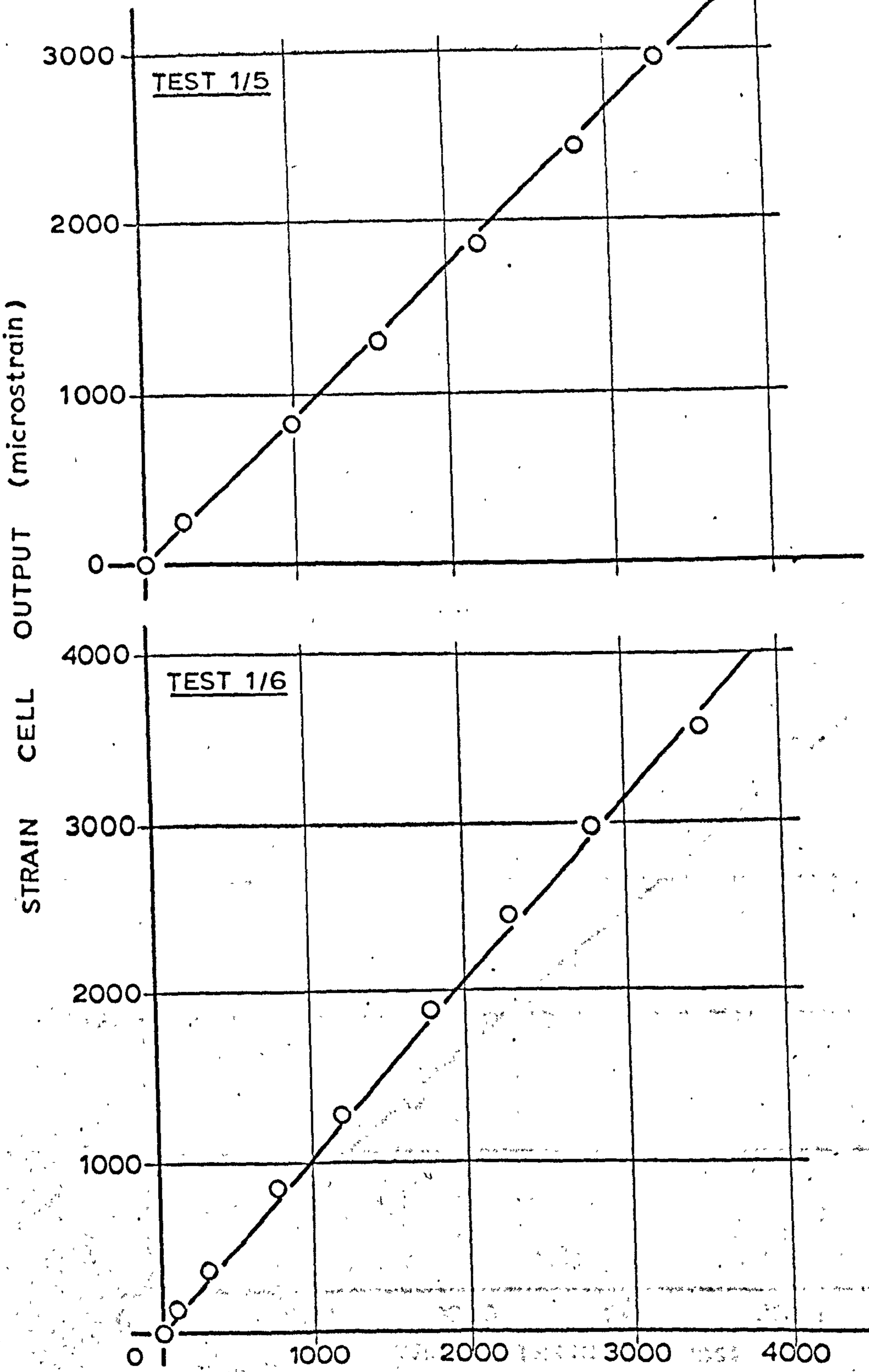

FIG. 4.4 STRAIN CELL CALIBRATION IN COMPRESSION.

COMPRESSION TEST IN KEUPER MARL

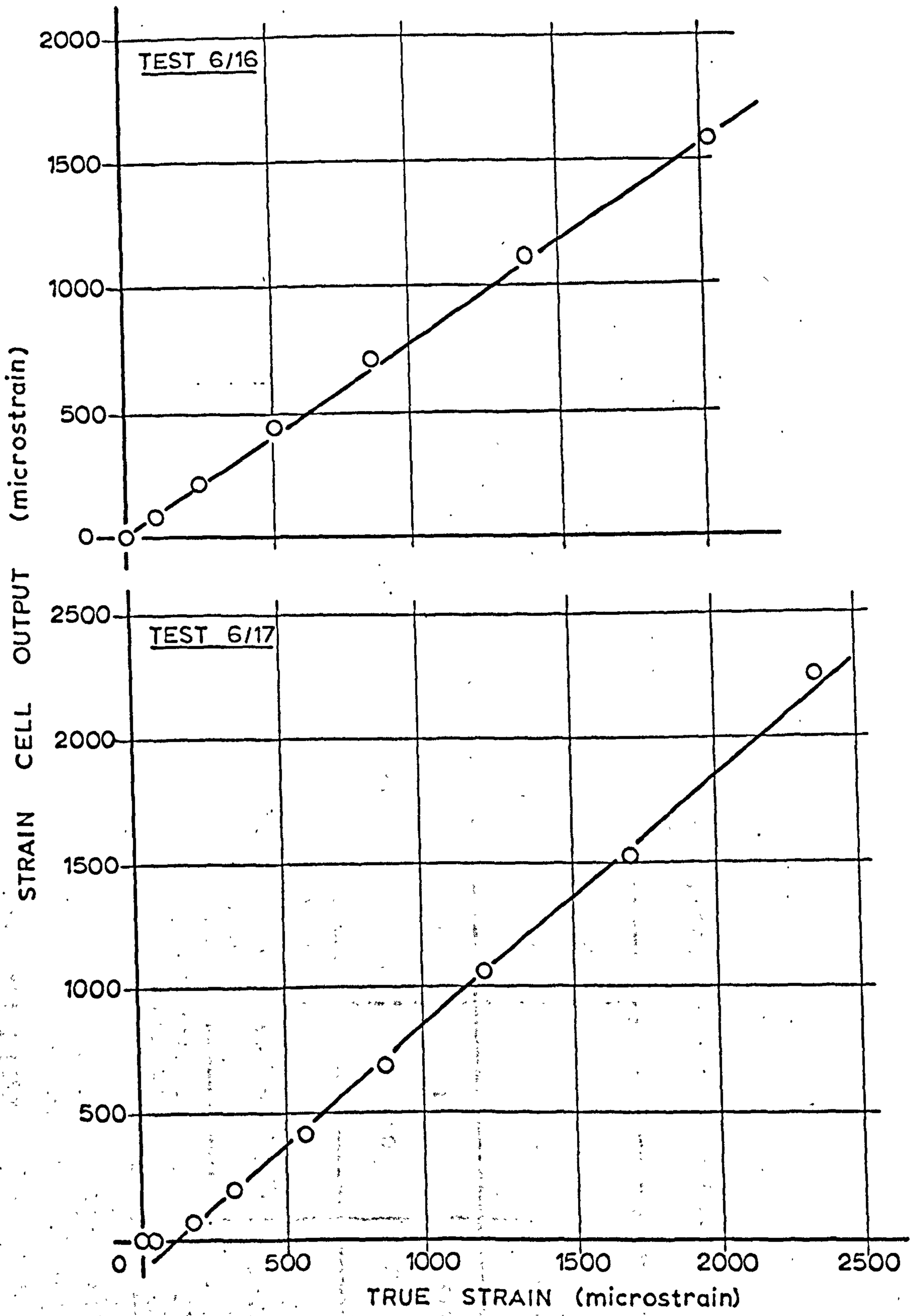

FIG. 4.5 STRAIN CELL CALIBRATION IN TENSION.

COMPRESSION TEST IN KEUPER MARL

TABLE 4.2 STRAIN CELL CALIBRATION TESTS IN TENSION FOR KEUPER MARL

Test No.	Compression (Unloading)		Tension (Loading)		Remarks
	Cell output / true strain	Zero error (micro-strain)	Cell output / true strain	Zero error (micro-strain)	
A/12	0.89	0	0.96	174	Cell S.8 without membrane on soil
A/16*	0.96	0	1.03	130	
B/5	0.86	88	0.97	150	Cell S.9 without membrane. Modified rubber sleeve on cell.
B/10*	0.87	38	0.94	180	

* Results used for calibration figures.

of the diameter on the cell axis so that the microscope targets could be placed as accurately as possible.

Overall vertical strain was measured during one test in the same way as for the compression tests, in order to obtain an approximate value of Poisson's ratio for the soil. The resulting value was 0.37, slightly lower than the 0.41 from in-situ measurements (Chapter 7).

The results of these "tensile" calibration tests are shown in Table 4.2, typical plots appearing in figs. 4.6 and 4.7.

4.4 Results of Calibration Tests in Keuper Marl

The strain, as indicated by the cell, was based on its original mechanical calibration. This test involved the application of a known deflection to the instrument, while measuring its electrical output, strain being introduced by using a 3 in. gauge length for the cell. This figure is the overall dimension of the instrument in its mid-travel position. The slopes of the calibration plots obtained on the tests in soil are, therefore, a measure of the accuracy of this initial assumption regarding gauge length. The figures obtained are fairly consistent from test to test, in tension and compression and using two separate instruments. This part of the

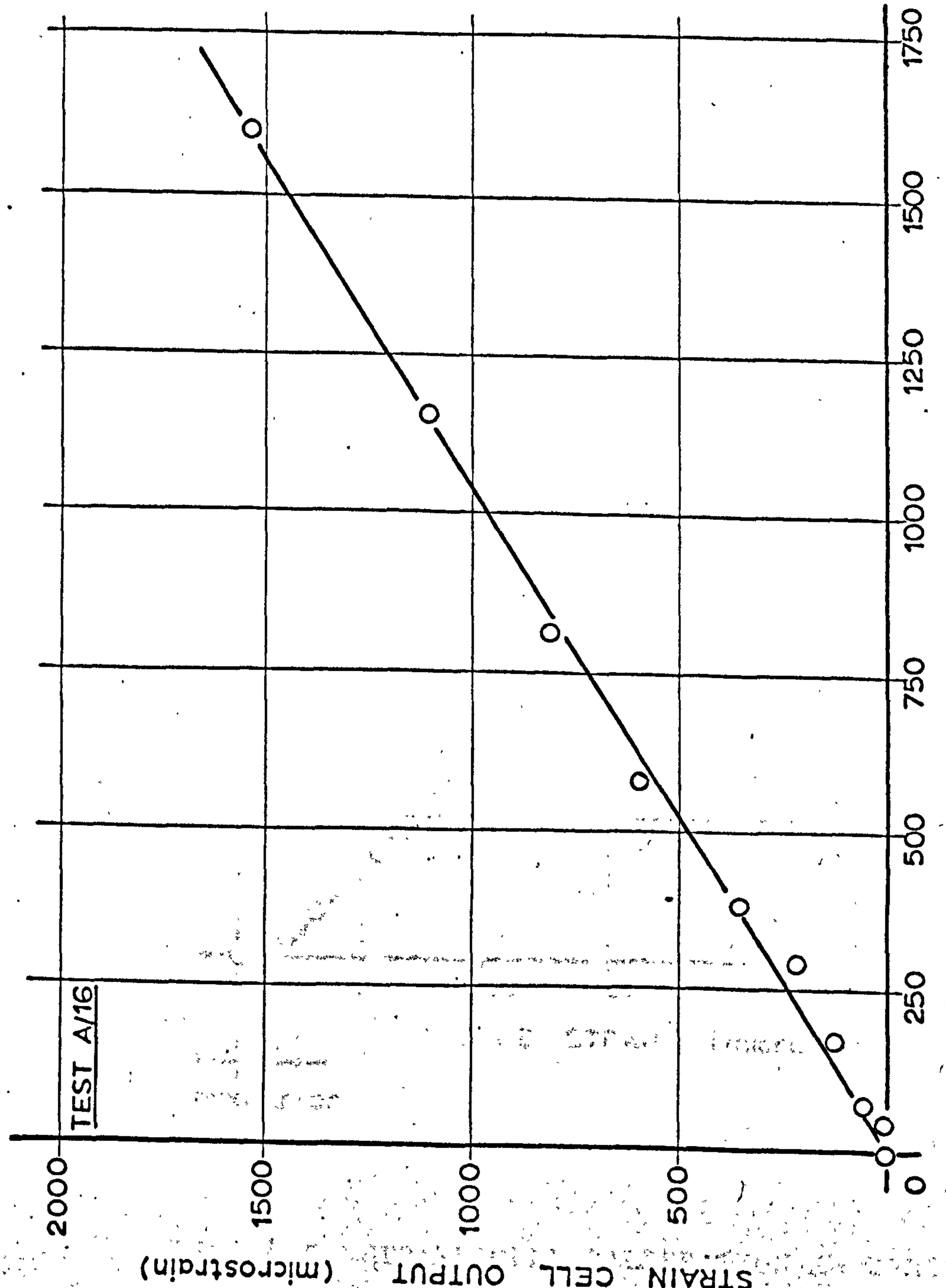

FIG. 4.6 STRAIN CELL CALIBRATION IN COMPRESSION IN KEUPER MARL TENSILE TEST

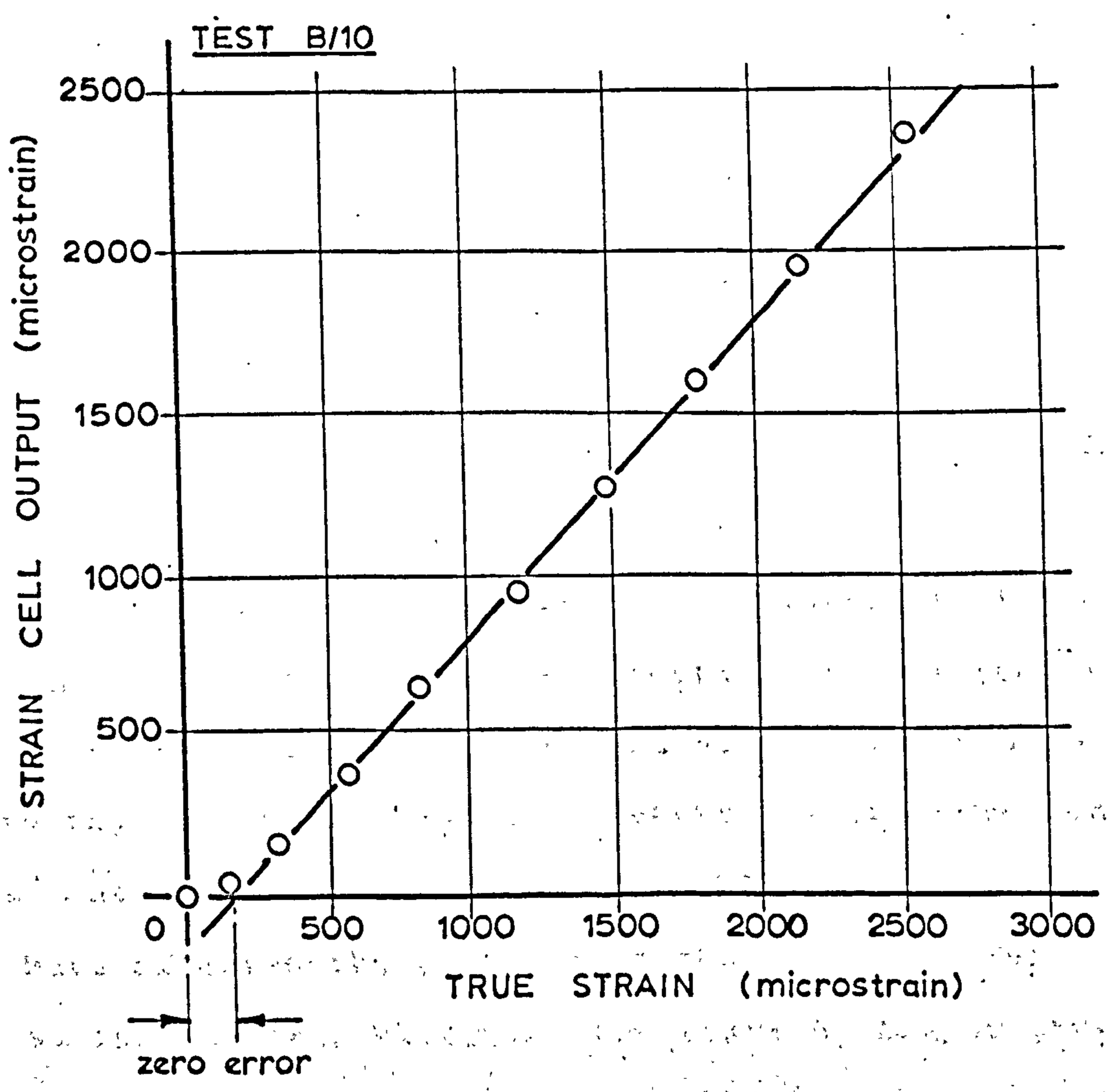

FIG. 4.7 STRAIN CELL CALIBRATION IN TENSION

TENSILE TEST IN KEUPER MARL

calibration testing was considered satisfactory and presented little problem.

The causes and magnitude of the zero error, defined as the intersection of the straight line of the calibration plot with the x-axis (see fig. 4.7), were more difficult to assess. Cell S.8 in compression consistently gave no zero error, whilst indicating an error in tension. Repeated tests on S.9 (tests 5) in the same specimen showed the zero error to grow successively smaller reaching zero in compression but remaining constant at 78 micro-strain in tension. The calibration figure (strain as indicated by cell/true strain) also diminished with successive tests. A delay of at least 4 hours was left between these tests. At the end of tests 5 it was decided to try the next tests on a specimen with the protective membrane removed for the duration of the test. It was considered possible for the membrane to have affected the movement of the pins used for measuring the true strain. For tests 6, longer pins were used, than before when there had been a penetration of only about $\frac{1}{4}$ in. in the radial direction, although the pins were in fact pushed into the soil about $\frac{1}{2}$ in. (Each pin was fixed normal to the line of sight of the microscope).

Tests 6 showed similar behaviour to tests 5, although there was still a zero error even after more cycles had been applied, and in tension, the reduction of zero error with successive tests was not wholly consistent.

Tensile tests A and B did not follow consistently the pattern of reducing zero error and calibration figure with successive tests. However, cell S.8 in compression showed no zero error. In an attempt to reduce the zero error, when present, the rubber sleeve fitted to the cells was replaced in tests B with two thin pieces of rubber membrane wrapped around the central tube and end plate hub, which were first coated with a layer of silicone grease. Grease was also applied between and outside the membranes.

4.5 Discussion of Calibration Test Results in Keuper Marl

Results taken during the unloading half of the cycle in compression tests have been taken as equivalent to applying a tension and vice versa for a tensile test. The justification for this is that the instrument has no fixed predetermined zero position. Zero is taken as the point in its travel which it happens to occupy after compaction and preloading of the specimen, i.e. at the beginning of a calibration test. The strain cell, thus,

measures relative strain, as is required under test conditions in the pit.

During a calibration test in compression for instance, a zero reading is taken and the specimen is compressed in increments over the range being studied. If the last reading taken is then regarded as a new zero, subsequent unloading must be tension relative to this new zero.

Results indicated similar behaviour in tension and in compression, both when the test was nominally compressive and when the loading half of the cycle produced tension, (i.e. nominally a tensile test). The best example of this was the compression result for cell S.8.

The magnitude and cause of the zero error was the chief concern of these tests since the calibration figure was fairly consistent and close to that assumed from the mechanical tests. The zero error is considered to be caused by friction between the soil and the central tube of the instrument. Once this friction is overcome, linear behaviour is obtained.

As a necessary result of the installation procedure, soil is tightly packed around the rubber sleeve covering the central tube (fig. 4.8). When the soil is strained

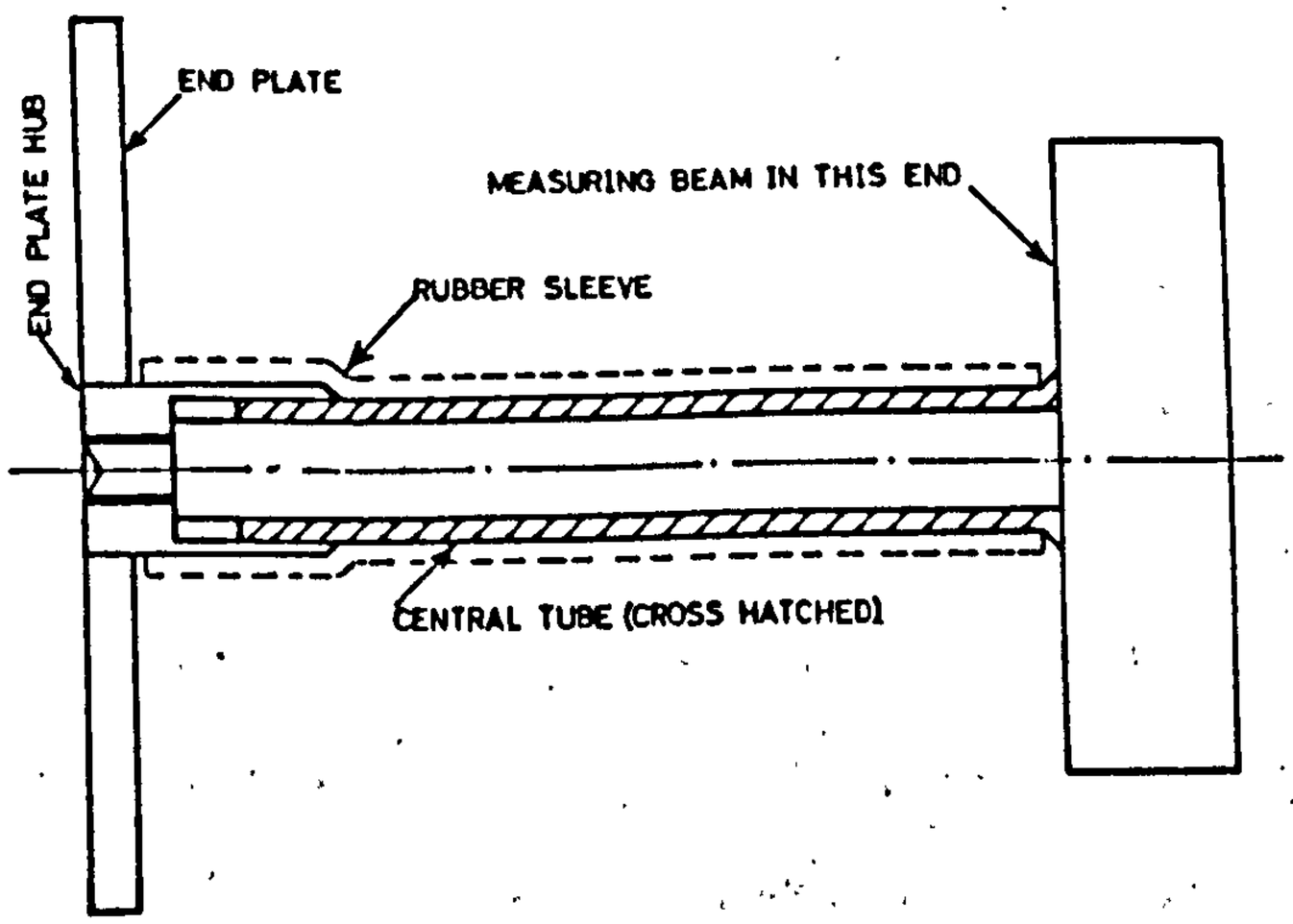

FIG. 4.8 STRAIN CELL SHOWING RUBBER SLEEVE

movement of the soil in the direction of measurement is spread evenly throughout its length, and consequently the soil immediately adjacent to the rubber sleeve will attempt to move uniformly. However, movement of the instrument is concentrated at one point, namely where the hub of the end plate fits over the tube. Therefore, either the soil movement has to also be concentrated at this one place, which is difficult to conceive, or there has to be relative movement between the soil and the central tube over its entire length, which is thought to be more likely. Some of this movement may be taken

up by the rubber sleeve shearing, but the majority of it must occur between the metal tube and the inside of the rubber sleeve. Friction on this surface was reduced to a minimum by the use of grease when fitting the rubber sleeve, but clearly there could still be a frictional force acting here, because of the pressure of soil around the tube. In tensile test B, an attempt was made to reduce the friction between the soil and the tube, without much success as the results indicate zero errors of similar magnitude to the other tests.

With this possible explanation in mind, the variation in zero error between tests can be appreciated, since it depends on the degree of soil compaction around the cell. The fact that the error appears to diminish with successive load cycles is less easy to explain except perhaps in terms of the friction reducing with use.

It should be borne in mind throughout this discussion that the movements referred to are very small and that the maximum strain of 0.004 only represents a deflection of 0.12 in. on the strain cell.

While the values of zero error varied from test to test when using cell S.9, the other cell, S.8, in compression consistently showed no zero error. A satisfactory explanation cannot be advanced for this, but it does under-

line the fact that the zero error varied from cell to cell and, therefore, cannot be predicted with any accuracy for a particular cell in the test pit. The negative zero error in Tests 1 on cell S.8 is the only one of its kind, and no better reason than experimental error can be advanced for this.

From the results of Tables 4.1 and 4.2, one set of figures from each specimen has been used to arrive at a suitable calibration. Because of the trend in the results with successive load cycles, the last one is taken in each case, since the cells in the test pit have undergone a large number of cycles. The means of these chosen figures are:-

	Compression	Tension
$\frac{\text{Strain Cell output}}{\text{True strain}}$	0.97	0.96
Zero Error (micro-strain)	21	98

If these results are applied over the range of strains indicated from the test pit results, the calibration graph shown in fig. 4.9 is obtained.

Clearly the zero error in compression can be ignored without causing any substantial error to the strain.

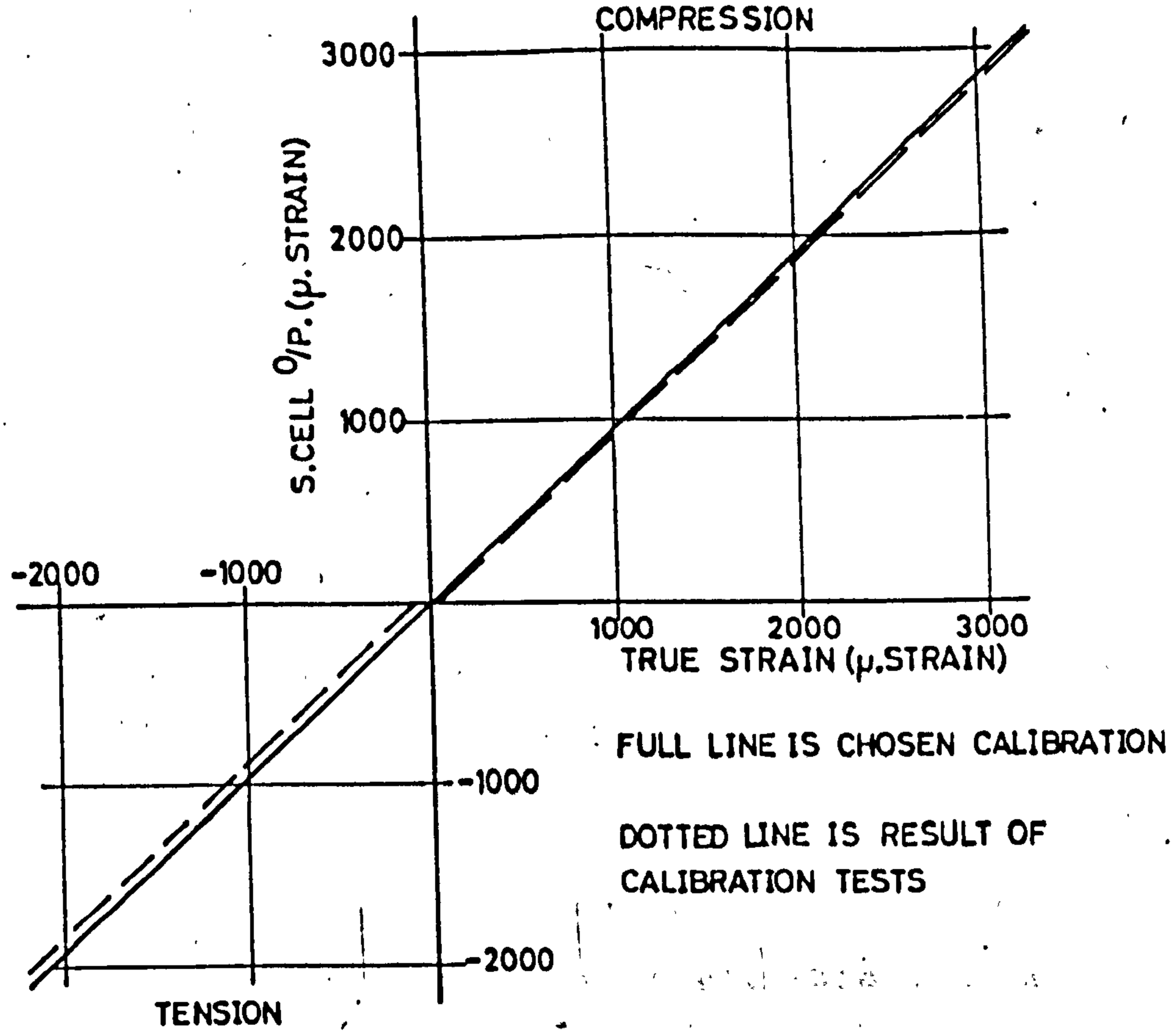

FIG. 4.9 CALIBRATION GRAPH FOR STRAIN CELL

readings. In tension, however, the mean error obtained from the two cells tested was 98 micro-strain and is of significant magnitude since a large number of strain results from the pit are of this order of magnitude or less. However, as mentioned above, this error varies from cell to cell so rather than apply the value obtained

from tests on only two cells, a straight line calibration has been used, bearing in mind that the test pit strains are minimum readings, particularly in tension, and that they could exceed their apparent value by about 100 micro-strain. This procedure, clearly, allows a simpler calibration figure, namely the slope of 0.97 to be applied to all strain readings.

If a zero error of 100 micro-strain (say) is assumed when correcting strain readings, then the minimum reading of the instrument becomes 100 micro-strain. There are a large number of strains less than 100 micro-strain, and by introducing a correction of the same order of magnitude, or larger, it is possible that a greater error will be introduced than exists already. A study of a typical calibration plot, fig. 4.7, shows that the zero error has been taken as the intercept formed by extrapolating the straight line portion of the plot. While this approximation is good enough for correcting large strains, it is rather inaccurate for the small strains which fall on the initial curved part of the plot. Another method would be to ignore results less than 100 micro-strain, but this eliminates so many readings, which may be of use, that it was decided just to apply the calibration factor of 0.97 to all readings and

then correct the results to the nearest 10 micro-strain, bearing in mind that small readings are likely to be inaccurate.

4.6 Calibration tests in Meldon Dust

The strain cell was tested in 9 in. diameter x 18 in. long specimens of Meldon Dust using the same procedure as described for the Keuper Marl. Results indicated very similar behaviour, the mean slope of the calibration plots in tension and in compression both indicating that strain as indicated by the cell, divided by true strain = 0.99 compared with 0.97 for the Keuper Marl. The mean zero error in compression was 70 micro-strain and in tension 81 micro-strain, compared with 21 and 98 micro-strain respectively for the Keuper Marl. In both materials, tests were carried out on two different strain cells, which was a minimum considering the conclusion earlier in this chapter that the zero error appeared to be a function of the individual cell as well as the way it was installed.

The calibration figure of 0.97 had already been used for strain readings in the Meldon Dust by the time these calibration tests had been completed. This was considered to be near enough to 0.99 to make correction

of strain readings from the two layer system unnecessary. The larger zero error in compression was likely to cause a greater discrepancy and this was borne in mind when discussing the results in Chapters 7 and 8.

CHAPTER 5 EXPERIMENTAL WORK ON THE TEST PIT

5.1 Tests on the single layer system

The philosophy behind the test procedure adopted for both systems is described in Chapter 2. The load was applied to the surface of the soil in various known positions relative to the buried instruments, output from those in the neighbourhood of the load being recorded. The arrangement of instruments in the single layer system is shown in fig. 2.2. A co-ordinate system was used to refer to any point where the load may be applied, or a cell located. To obtain the results indicated in fig. 2.5, it was necessary to load the pit in the positions shown on fig. 5.1. This involved 53 load applications for the 12 in. diameter loaded area, 45 for the 18 in. and 36 for the 24 in.

Tory[11] investigated the effects of contact pressure and rate of loading on the measured stresses and strains. His conclusions were that stress was virtually independent of rate of loading and proportional to contact pressure, while strain was not consistently proportional in either case. For the tests described herein, values at either end of the range used by Tory for both variables were used. The upper limit of contact pressure was in fact

TABLE 5.1 DETAILS OF TESTS ON SINGLE LAYER SYSTEM

Test No.	Symbol for plots	Contact pressure (lb/sq.in.)		Assumed contact area / Actual contact area (%)	Nominal loading time (sec.)	Radius of loaded area (in.)
		Nominal	Mean			
S/A	O	17.0	15.3	103	2.0	6
S/B	Δ	17.0	16.9	103	0.1	6
S/C	□	7.5	7.4	103	0.1	6
S/D	∇	7.5	7.0	104	2.0	6
S 18/A	O	17.0	15.7	98	2.0	9
S 18/B	Δ	17.0	16.8	101	0.1	9
S 18/C	□	7.5	7.6	95	0.1	9
S 18/D	∇	7.5	7.0	96	2.0	9
S 24/A	O	17.0	15.0	104	2.0	12
S 24/B	Δ	17.0	17.1	105	0.1	12
S 24/C	□	7.5	7.2	101	0.1	12
S 24/D	∇	7.5	7.3	100	2.0	12

increased, so that a wider range was covered. Three different sizes of loaded area were used and to obtain all the combinations of contact pressure and rate of loading, 12 tests were conducted, details of which are given in Table 5.1.

The mode of operation of the loading head has been fully described by Tory. It was developed so that by repeatedly charging a small reservoir with compressed air to the same pressure, consistent values were obtained for the force exerted by the loading platen for a particular rate of loading. This latter variable was also repeatable and controlled by two throttle valves. A pneumatic circuit diagram is shown in fig. 5.2.

Trial loadings with the apparatus over the concrete floor near the test pit produced a form of calibration. Before each test run, however, the rate of loading and contact pressure were checked by loading on the concrete. Some difficulty was experienced in getting the slow rates of loading to the desired values while making the pulse symmetrical, i.e., the same time to peak load as to unload. The actual contact pressures applied to the test pit were not exactly the same as the intended values which have consequently been termed "nominal". This occurred because of the difference between loading concrete

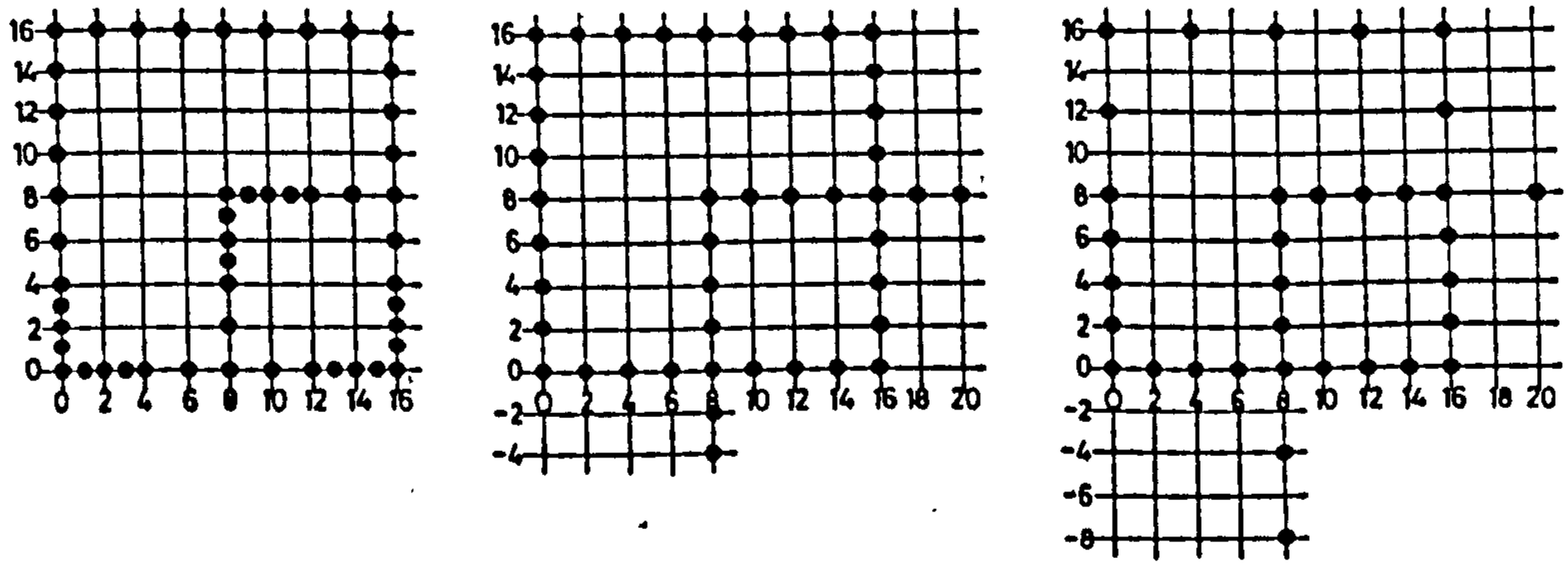

FIG. 5.1 LOADING POSITIONS - SINGLE LAYER SYSTEM

and soil and also because the trial loading traces were not measured exactly. The high contact pressure was sometimes difficult to achieve because of a drop in the line pressure on the compressed air supply. Exact values for loading time were not analysed since they were not required for this investigation.

One column of Table 5.1 indicates how far the actual contact area departed from that assumed from the platen diameter. The function shown is $\frac{p.\pi a^2}{W} \times 100\ \%$

$= \frac{\text{assumed area}}{\text{actual area}}$, where p = measured contact pressure, a = assumed radius of loaded area and W = measured load.

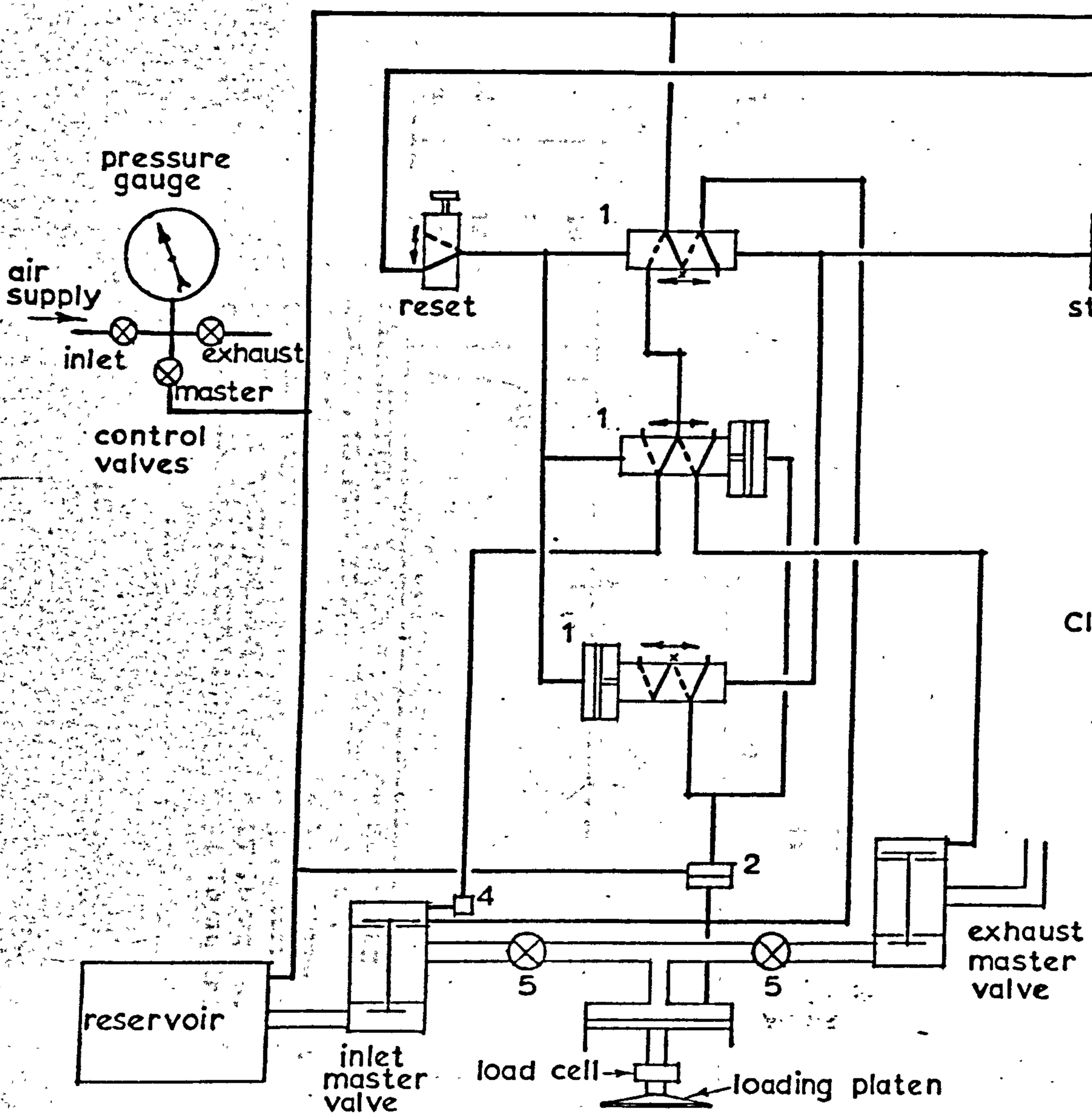

CIRCUIT IN RESET POSITION
UNCLAMPED

1. shuttle valves
2. pressure switch
3. clamp controls
4. quick exhaust valve
5. throttle valves

FIG. 5.2 PNEUMATIC CIRCUIT DIAGRAM FOR LOADING HEAD

TEST S/A		DATE 28-4-64
TEST NO.	COORDINATES	CELLS
1	0,0	4 5 6 7 12 13
2	0,1	12 13
3	0,2	6 7 12 13
4	0,3	12 13
5	0,4	6 7 12 13
6	0,6	6 7 12 13
7	0,8	6 7 10 11 12 13
8	0,10	6 7 10 11
9	0,12	6 7 10 11
10	0,14	6 7 10 11
11	0,16	6 7 8 9 10 11
12	2,16	8 9 10 11
13	4,16	8 9 10 11
14	6,16	8 9 10 11
	e.t.c	
50	10,8	19
51	12,8	
52	14,8	
53	16,8	

SOIL SUCTION = 22 cm. Hg
NOMINAL LOADING TIME = 2 sec.
INLET VALVE = 3/32 turns open
EXHAUST VALVE = 3/16 turns open
NOMINAL CONTACT PRESSURE = 17 lb/sq in.
GAUGE PRESSURE (RESERVOIR) = 94 lb/sq in.

FIG. 5.3 TYPICAL LOADING PROGRAMME

Both this function and the actual contact pressure are mean values for each test run. They deviated very little from this mean.

A loading programme sheet as shown in fig. 5.3 was used for each test run on the pit to provide information regarding the loading head position and the cells to be used at each load application. As described earlier the loading head can be moved in one direction by cranking the portal frame along its rails, and in a perpendicular direction by moving the trolley along the base of the portal frame. On the loading sheet, the left hand column gives the number of the "test" (one test run consisting in this case of 53 "tests" or load applications), the centre column the co-ordinates of the loading position and the right hand column, the cells whose outputs are required for this "test". In addition to the cells indicated here, numbers 0 and 1 were always used, since they represented the applied load and contact pressure respectively. Reference numbers of the other cells appear in fig. 2.2. To assist in positioning the loading head for a point with given co-ordinates, the abscissae were marked on the portal frame base, and the ordinates on one of the rails

The control and recording equipment used for the

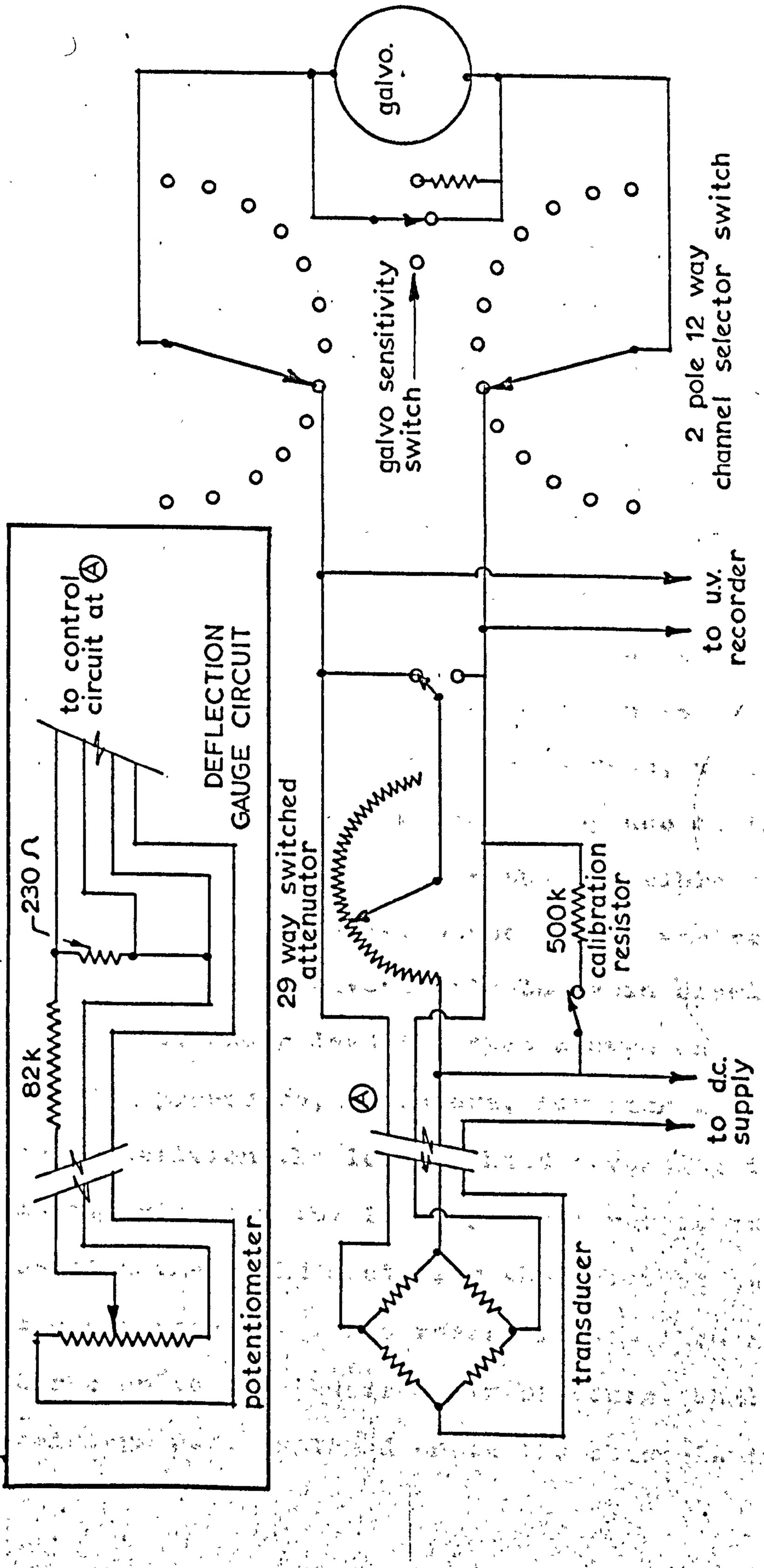

FIG. 5.4 CIRCUIT DIAGRAM FOR TRANSDUCERS

transducers is also described by Tory,[11] but a typical circuit diagram is included here in fig. 5.4. All cells had identical circuitry, except for the deflection gauge shown in the inset. 19 channels were utilised for these tests and they were split between two 12 channel balance boxes and two N.E.P. ultra violet recorders. The strain cells were confined to one recorder and balance box while the remainder of the instruments were connected to the others. All cells were kept permanently connected to the recorder for the duration of a test run. The miniature spot galvanometer connected to each cell provided a spot of light on the recorder screen, which could be moved in fairly large increments by use of the attenuator on the control box. It was thus possible to position the spots for the cells, whose output was required for a particular test, conveniently to avoid crowding and to ensure that under load the spot stayed on the screen.

The procedure, therefore, for each load application was to position the loading head according to the co-ordinates given on the loading sheet and identify and position the light spots for the relevant cells on the recorder screens. The reservoir was then allowed to charge up to the required air pressure, while calibration resistors were switched on to the channels in use and the

resulting deflections recorded. The loading head control circuit (fig. 5.2) was put in the "reset" position, the reservoir pressure adjusted to the correct value and the recorders started by means of a common remote control switch on the loading head control panel. The load was applied by operating the "start" button and the traces recorded. The recording paper was then removed and processed. For the first few test runs, Kodak Linagraph R.P. 12 paper, which required to be passed through a single stabilizing solution, was used, but for later tests the newer Kodak Linagraph Direct Print paper became available. The image on this paper emerged on subjection to fluorescent light and remained permanent if not left for too long in bright light or sunshine, so was clearly far quicker and more convenient to use.

The above procedure was repeated for each loading position. Certain additional information was recorded for each test run and this appears at the end of the loading sheet (fig. 5.3). Once the operator was proficient, a test run could be completed in about 1½ hours. The reading of the soil tensiometer was recorded before each test run and varied very little throughout the series of tests indicating that the moisture content had remained sensibly constant. The other information

recorded on the loading sheet, refers to the setting of the loading head.

When the new cell layout was installed the central deflection gauge was found to be out of position by $\frac{3}{8}$ in. in the "y direction" and $1\frac{1}{4}$ in. in the "x direction" referred to the co-ordinate system used on the pit. When taking deflection measurements during a test run, the loading head was positioned appropriately to allow for this error. Hence, cell 19, which is the deflection gauge, is the only instrument featuring towards the end of the loading programme.

At the end of a test run, all the results were in analogue form on the paper from the U.V. recorders. These traces were "read" with a special trace reader and converted into digital form on punched tape, prior to processing by digital computer. Details of the data processing procedure, and of the computer programs involved are given in Appendix I.

5.2 Tests on the two layer system

Two sizes of loaded area were used for tests on the two layer system, and since the thickness of the upper layer remained constant at 12 in., this meant that two different systems were tested. The measurements which

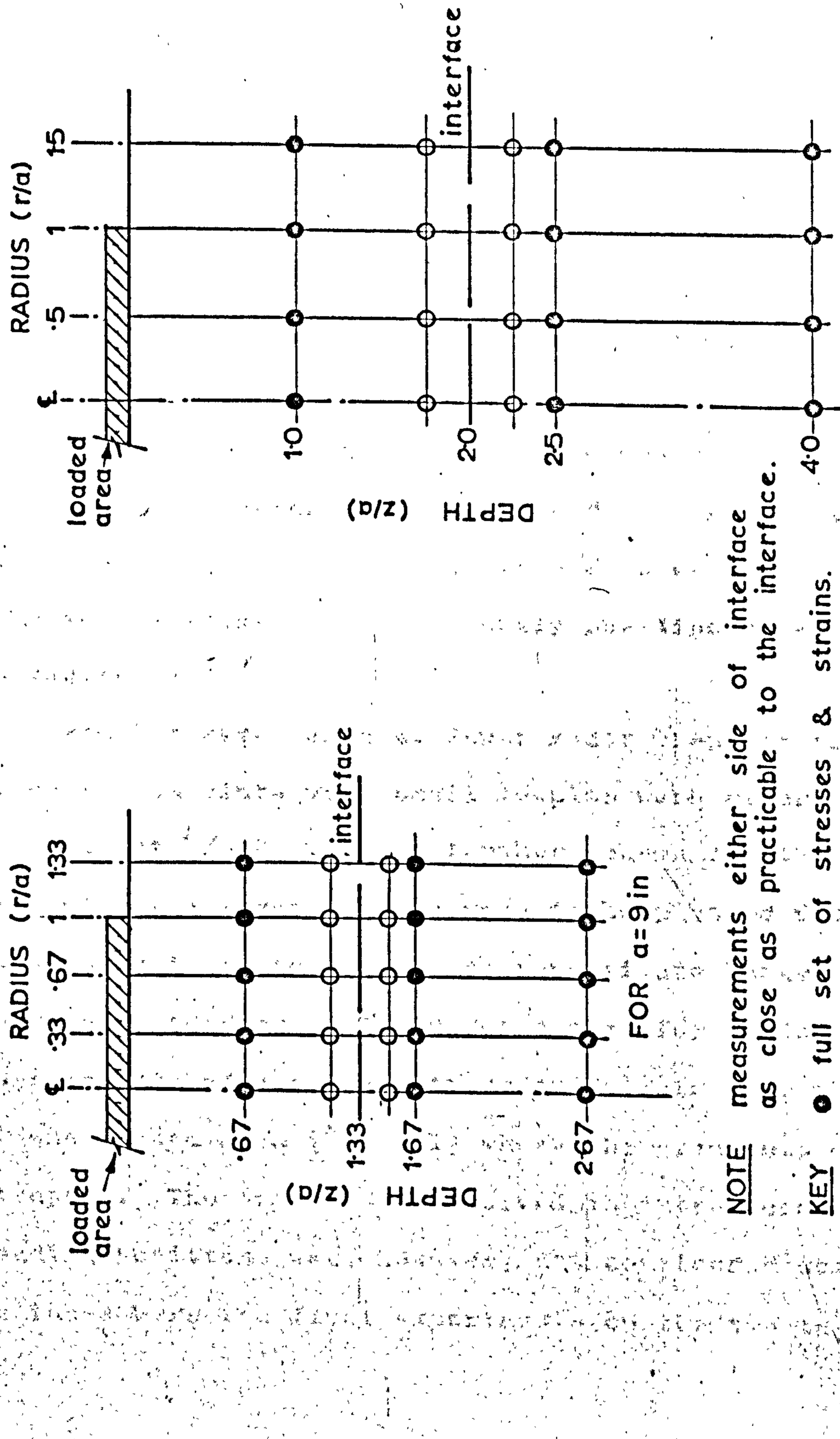

NOTE measurements either side of interface as close as practicable to the interface.

KEY ● full set of stresses & strains.
○ limited number of results.

FIG. 5.5 LOCATION OF MEASURING POINTS - TWO LAYER SYSTEM

were intended to be taken are shown in fig. 5.5. Because of the failure of certain transducers, the following measurements were not made:

1. 45° and 135° stress 3 in. below the interface.
2. Vertical deflection.
3. Vertical stress at the interface.
4. Radial stress just below the interface.

In addition, the strain cell measuring horizontal strain 6 in. below the surface did not work properly in tension. This is discussed later in Chapter 8. Vertical strain measurements 12 in. below the interface were in error because the transducer was wrongly positioned as explained in section 2.2.

Results were taken at fewer radii than for the single layer system since very small results were generally recorded at $^{r}/_{a} > 1.5$. A further reason for this was that more two layer results were to be plotted with depth, as opposed to radius, so as to investigate behaviour near the interface. There was a case for taking more measurements of vertical stress and strain near the edge of the loaded area ($^{r}/_{a} \approx 1$) where the gradients were steepest. The extra work involved in introducing extra loading positions was, however, not considered worth-while as these were the first experiments on the two layer system.

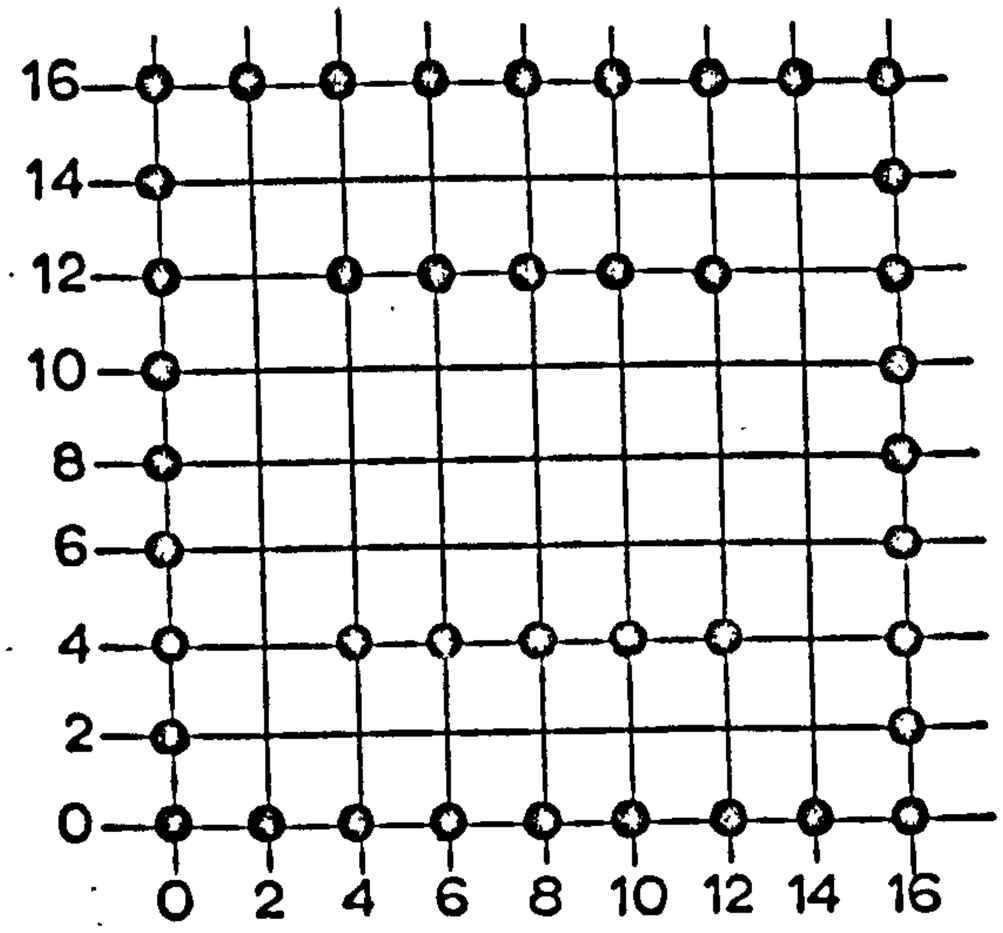

12" dia LOADED AREA

NOTE reference coordinates are based on a 1 1/2" square grid.

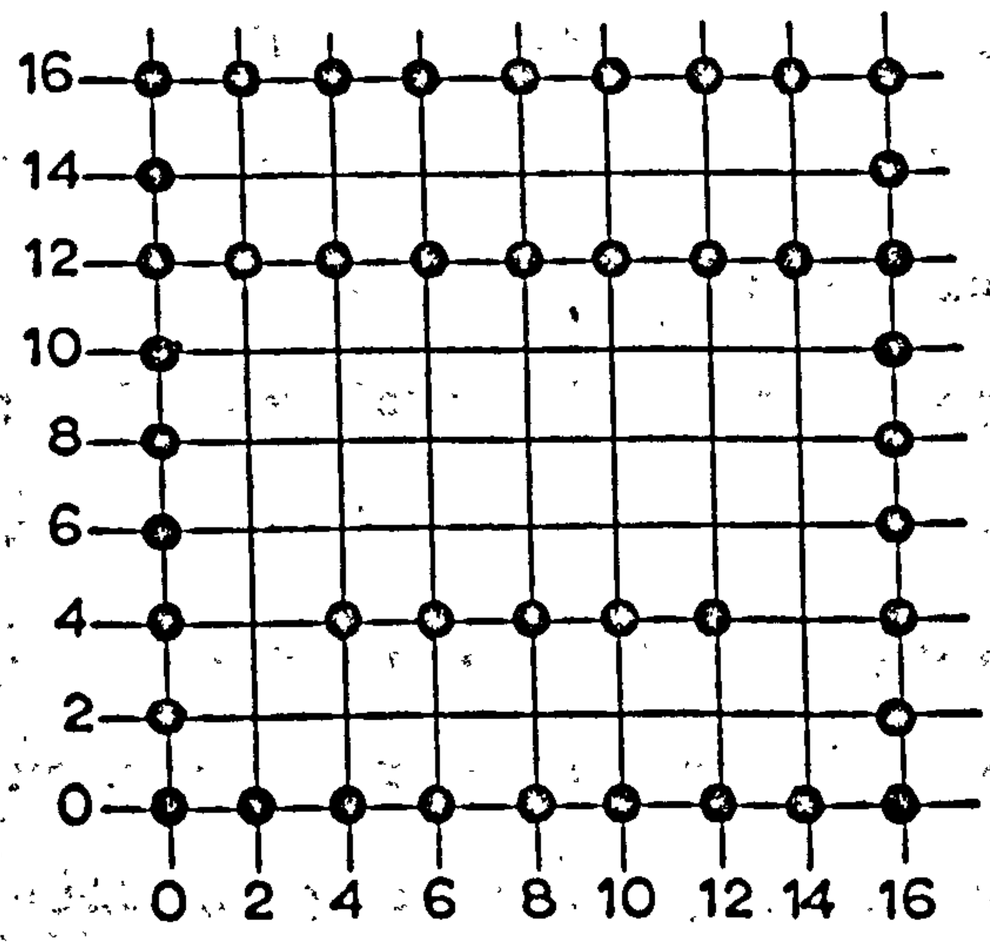

18" dia LOADED AREA

FIG. 5.6 LOADING POSITIONS - TWO LAYER SYSTEM

The test procedure was similar to that adopted for the single layer system, but involved more transducers. 28 channels were in use as opposed to 19 for the single layer system. They were connected to three 12 channel balance boxes and three U.V. recorders were utilised during the tests. The number of loading positions for the 12 in. diameter loaded area was 42 and for the 18 in. diameter area, 44. These are shown in fig. 5.6.

The choice of contact pressures and rates of loading to be used, were arrived at by similar considerations to those used for the single layer. The contact pressures were chosen so as to produce, approximately, the same vertical stress near the surface of the subgrade as before, the choice being based on a rough calculation using layered system theory.[22] (This same procedure had been used originally by Tory.[11] Starting with a 5 ton wheel load, he calculated the vertical stress at the top of the subgrade. This was, however, considered too small to give useful readings from the transducers and larger values were consequently adopted.) The values chosen were 30 lb/sq.in. and 17 lb/sq.in. and the rates of loading were taken as before. Intermediate values were not used, since it was intended that an investigation into the effects of contact pressure and rate of loading should

TABLE 5.2 DETAILS OF TESTS ON TWO LAYER SYSTEM

Test No.	Symbol for plots	Contact pressure (lb/sq.in.)		Assumed contact area / Actual contact area (%)	Nominal loading time (sec.)	Radius of loaded area (in.)
		Nominal	Mean			
D/A	O	30	27.7	90	2.0	6
D/B	Δ	30	29.6	89	0.1	6
D/C	□	17	17.9	85	0.1	6
D/D	∇	17	16.1	84	2.0	6
D 18/A	O	30	27.9	97	2.0	9
D 18/B	Δ	30	29.5	97	0.1	9
D 18/C	□	17	15.5	95	0.1	9
D 18/D	∇	17	15.9	96	2.0	9

be conducted at a later stage using fewer measurements. Any trends, however, would emerge from the present experiments. Eight test runs were carried out on the two layer system and details are shown in Table 5.2.

Readings of both the soil tensiometers were recorded during tests, so that any changes in moisture content could be detected. By referring to the soil suction/ moisture content curves (figs. 2.10 and 2.11) for the two materials it was concluded that the change in moisture content was of the order of 0.2% and therefore insignificant.

CHAPTER 6 METHOD OF PRESENTATION AND CALCULATION OF THE EXPERIMENTAL RESULTS

6.1 Stress

All plots of stress distribution show stresses expressed as a percentage of the contact pressure and these are termed "normalised" stresses. This approach allows stress distributions resulting from the application of different contact pressures to be plotted on the same graph. Contact pressure varied in two ways. During a test run on the pit at one nominal contact pressure, there were slight variations between load applications, and for different test runs there were much larger and intentional differences.

For this method of plotting to be strictly correct, stress should be proportional to contact pressure. Conversely, if normalised stress varies with contact pressure, lack of proportionality is indicated. Hence by plotting normalised stress, results from different load applications on one test, and results from different tests can be combined to study distribution and check whether stress is proportional to contact pressure.

6.2 Strain

It was considered desirable to plot strain measurements in much the same way as those of stress, but this was less straightforward. Strain could not be expressed as a percentage of the contact pressure but normalised strain was obtained by dividing the strain measurement by the contact pressure, the units being microstrain per lb/sq.in.

For strain to be proportional to contact pressure, the material would have to be linear elastic and, hence, any change in normalised strain with contact pressure would indicate non-linearity, and this trend was studied for the experimental results. A similar, though less marked, effect would result if the material were not homogeneous, since results are taken from different locations in the test pit.

Normalised strain as defined herein differs from that used by Tory by a factor of 100, which produced needlessly large numbers and did not perform the same function as for stress, which by including the 100 could be expressed as a percentage of the contact pressure.

6.3 Deflection

Measurements of vertical surface deflection were

only taken for the single layer system and they have also been expressed in normalised form for the same reasons as stress and strain.

Normalised deflection is the deflection in thousandths of an inch divided by contact pressure, the resulting units being thou. per lb/sq.in. This differs from the definition used by Tory in the same way as strain and for the same reason.

6.4 Equilibrium and Compatibility Corrections

In addition to the stresses, strains and deflections which were directly measured in the test pit, various other quantities such as principal stresses have been calculated using combinations of the measured effects. This process involved superimposing results measured in different parts of the test pit and, clearly, equilibrium of stresses and compatibility of strains at a point had first to be established, before calculations could proceed.

By superimposing results, stresses on five different planes were obtained at a point (fig. 6.1). These stresses were: p_z = Vertical stress, p_r = Radial stress, p_θ = Tangential stress, p_{45} = 45° stress, p_{135} = 135° stress. They form two sets of three orthogonal stresses with the

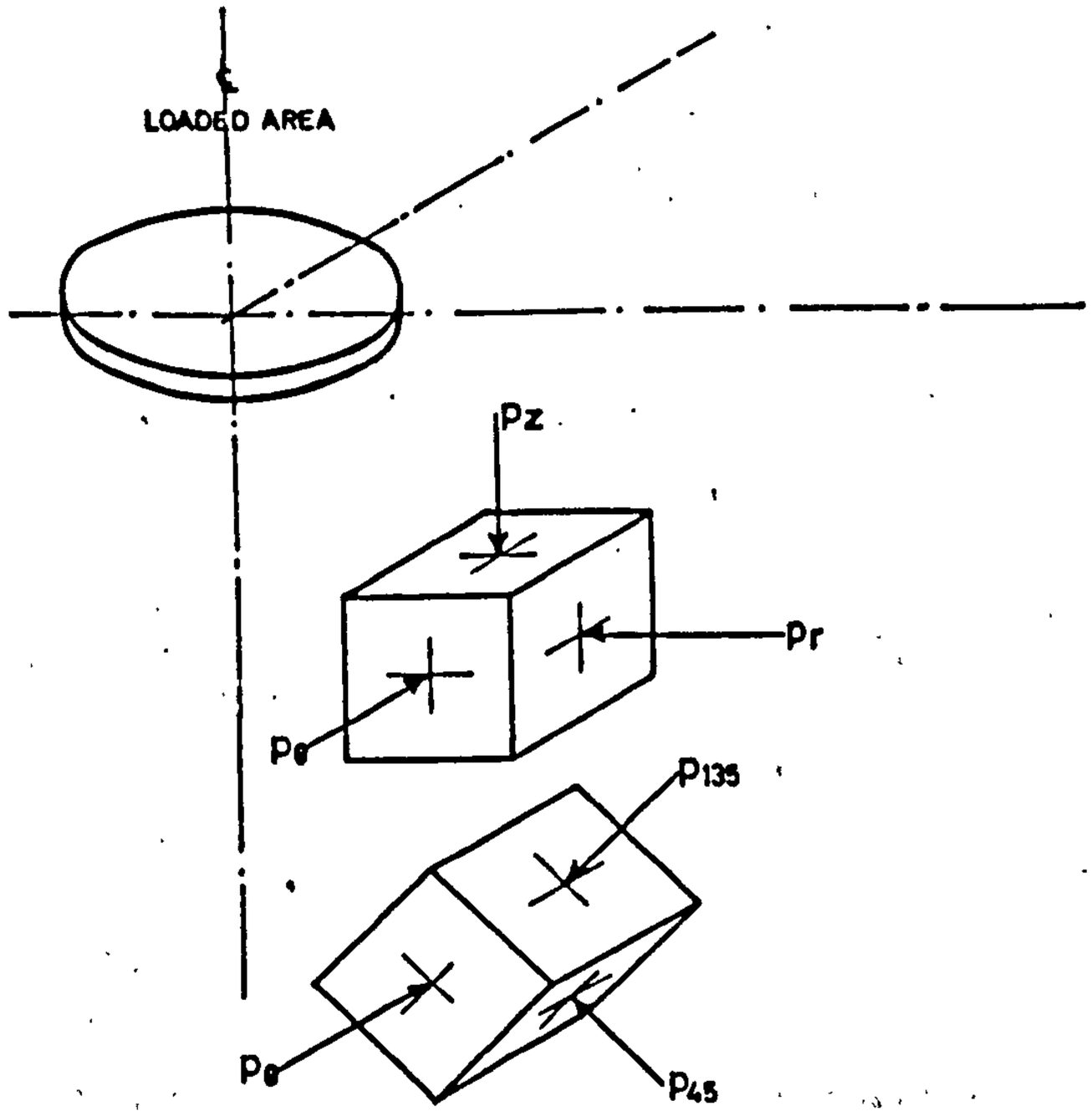

FIG. 6.1 PLANES ON WHICH MEASUREMENTS WERE TAKEN

tangential stress (p_θ) common to both. For equilibrium, the sum of any three orthogonal stresses at a point should be an invariant. Since one stress is common to both sets, the problem is reduced to a two dimensional one in this case, and the resulting equilibrium equation is:

$$p_z + p_r = p_{45} + p_{135} \qquad \ldots (1)$$

Because of the inevitable introduction of errors in the stress measurements, this equilibrium condition is

unlikely to be fulfilled everywhere, and the error has been expressed in the form

$$x = (p_z + p_r) - (p_{45} + p_{135}) \quad \ldots (2)$$

where x = equilibrium error.

The above remarks apply equally for strains which have been measured on the same planes, the compatibility error (y) being:-

$$y = (e_z + e_r) - (e_{45} + e_{135}) \quad \ldots (3)$$

in which e = strain with the suffices indicating the same planes as for stress.

The various factors likely to cause these errors are discussed in Chapters 7 and 8. In order to use stress and strain measurements to calculate other functions such as principal stresses and elastic constants, it was necessary to apply corrections to them so as to satisfy the equilibrium and compatibility conditions at a point. These corrections were arrived at by estimating the reliability of the various measurements based on the fact that some results were the mean of several readings from different parts of the pit, while others were single readings. Full details appear in Chapters 7 and 8.

6.5 Derived Stresses and Strains

The following quantities were derived from corrected

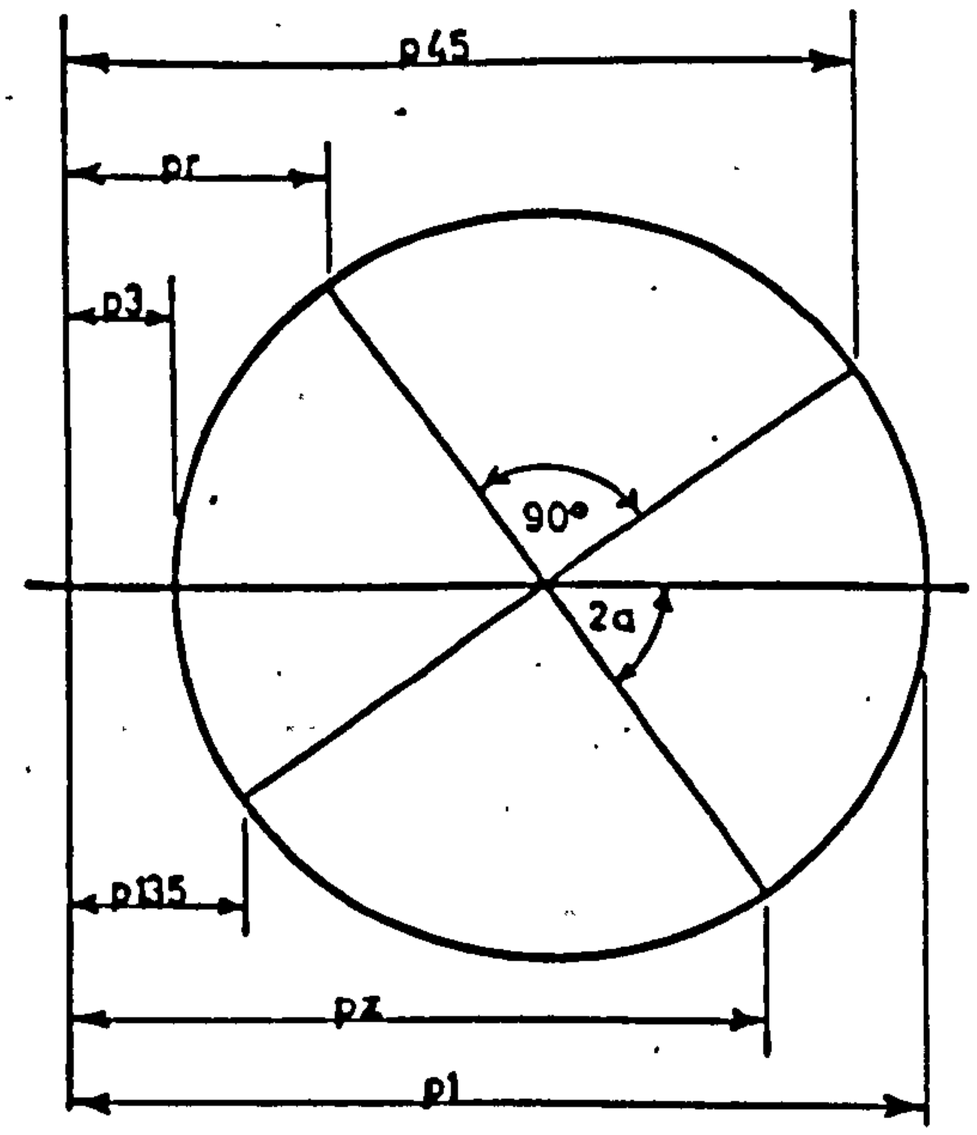

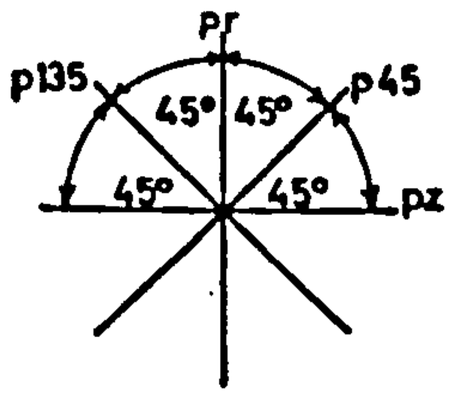

RELATIVE POSITIONS OF PLANES.

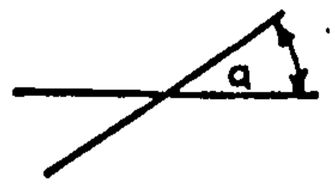

ELEVATION OF MAJOR PRINCIPAL PLANE.

FIG. 6.2 MOHR'S CIRCLE

stresses and strains as indicated below, the Mohr's circle of fig. 6.2 clarifying the definitions.

1. <u>Major principal stress</u> (p_1):

$$p_1 = \tfrac{1}{2}[(p_z+p_r) + \sqrt{\{(2p_{45}- p_z-p_r)^2 + (p_z- p_r)^2\}}] \quad \ldots (4)$$

2. <u>Minor principal stress</u> (p_3):

$$p_3 = \tfrac{1}{2}[(p_z+ p_r) - \sqrt{\{(2p_{45}- p_z-p_r)^2 + (p_z- p_r)^2\}}] \quad \ldots (5)$$

3. Positions of principal planes: The angle between the major principal plane of stress and the horizontal (α) was calculated as follows:

$$\alpha = \tfrac{1}{2} \tan^{-1} \left[\frac{2p_{45} - p_z - p_r}{p_z - p_r} \right] \qquad \ldots (6)$$

A similar expression was used to obtain the positions of principal planes of strain.

4. Maximum shear stress (τ max):

$$\tau \text{ max} = \tfrac{1}{2} (p_1 - p_3) \qquad \ldots (7)$$

5. Major and Minor principal strains: These quantities were obtained from expressions similar to those used for principal stresses.

6. Maximum shear strain (γ max):

$$\gamma \text{ max} = (e_1 - e_3) \qquad \ldots (8)$$

6.6 Modulus and Poisson's Ratio

The following method for calculation of modulus and Poisson's ratio assumes that the materials are linear elastic. A more accurate analysis is outlined in Appendix II. The stresses and strains measured in the test pit are such that they form two sets of three orthogonal values. By applying the elastic equations for each set, five equations in two unknowns, E (modulus) and ν (Poisson's ratio), result.

The first set of measurements consists of

p_z, p_r, p_θ, e_z, e_r, and e_θ

and the elastic equations are

$$E.\ e_z = p_z - \nu\ (p_r + p_\theta) \qquad \ldots (9)$$

$$E.\ e_r = p_r - \nu\ (p_z + p_\theta) \qquad \ldots (10)$$

$$E.\ e_\theta = p_\theta - \nu\ (p_z + p_r) \qquad \ldots (11)$$

The second set of measurements is

p_{45}, p_{135}, p_θ, e_{45}, e_{135} and e_θ

from which a similar set of three elastic equations results. Because of the equilibrium condition one equation is identical in each group, and hence there are only five independent equations.

A method of least squares was used to find the "best" values of E and ν from the five equations above.

Each equation was written in the following form:

$$E - \frac{p_z}{e_z} + \nu\ \frac{(p_r + p_\theta)}{e_z} = 0$$

This equation and the other four like it, are analogous to the standard straight line $y = mx + c$, where in the case of the above equation

$$y = \frac{p_z}{e_z},\quad x = \frac{(p_r + p_\theta)}{e_z},\quad m = \nu,\ \text{and}\ c = E.$$

For the other four equations x and y will assume

similar functions of $\frac{\text{stress}}{\text{strain}}$.

The procedure for obtaining a best fit value for E and for ν from these equations is to perform the standard y regression on x and also the x regression on y. This yields two values for E (the intercept on the y-axis in each case) and two values for ν (the slope in each case). The best fit value has been taken as the mean of the two values thus obtained. In the ideal case of all values of x and y falling on a straight line the two regression lines would coincide and a single value of E and of ν would emerge. The amount by which these lines differ and consequently the difference between the E and ν values which they produce is a measure, though not a statistically correct one, of the accuracy of the best fit values obtained by this method.

The form chosen for the elastic equations is one of many ways in which they can be written. It was chosen so as to arrange for the x and y functions to be of the same order of magnitude, making for more accurate solutions for E and ν.

6.7 Theoretical Results

One of the main objects of this work has been to compare measured values of stress, strain and deflection

with those predicted by linear elastic theory. Thus on all plots of stress, strain and deflection, one or more theoretical lines have been superimposed for comparison with the plotted points.

For the single layer system, all the theoretical solutions were computed from the tables of Ahlvin and Ulery.[27] These tables were also used to produce the Boussinesq distributions shown on some of the two layer plots.

Two layer theoretical results were computed using the multi-layer programme developed by Jones.[28] This was run with appropriate data in order to give specific results for the systems which were tested in the laboratory.

Further details of how theoretical results were calculated are given in Chapters 7 and 8.

6.8 Visco-Elastic effects

Two effects, both previously pointed out by Tory[11] for Keuper Marl, indicate that the materials in both layers behave in a visco-elastic manner. A study of strain pulses obtained during test runs on the pit, shows that there is a time lag between stress and strain and, since stress follows the applied load without any lag, between contact pressure and strain also. The second effect is that each strain pulse consists of an apparently

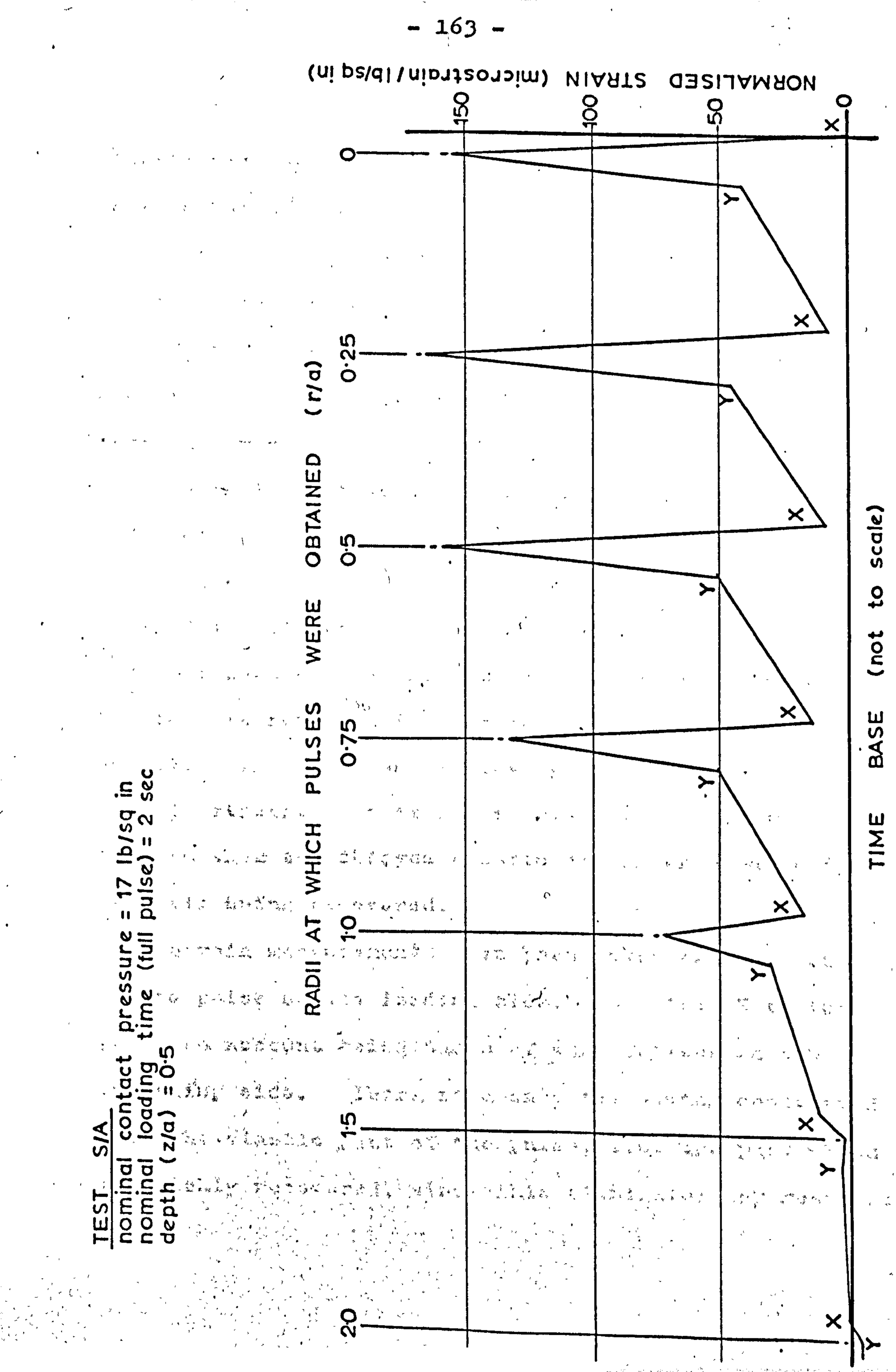

TEST S/A
nominal contact pressure = 17 lb/sq in
nominal loading time (full pulse) = 2 sec
depth (z/a) = 0·5

FIG. 6.3 SUCCESSIVE VERTICAL STRAIN PULSES

elastic portion, quickly recovered and a delayed elastic portion which is recovered much more slowly.

Fig. 6.3 shows a succession of pulses of vertical strain in the Keuper Marl taken with the load moving away from the cell for successive pulses. Where there was difficulty in locating the exact end of the elastic portion marked Y, the length of the pulse was made equal in time to that of the applied load. The horizontal time scale is not drawn to scale, but the strain, measured vertically, is. It can be seen that the delayed elastic portion does not quite return to the original zero before application of the second pulse and this is repeated for the third, fourth and fifth pulses. The sixth and seventh pulses represent small tensile strains, but it is of interest to note that between them the delayed elastic strain from pulse five is still being recovered.

Strain measurements have been taken as the height of the pulse on its loading side, i.e., from X to the peak, no account being taken of what follows on the unloading side. There is a case for having considered only the elastic part of the pulse, i.e. the part which is quickly recovered, since this eliminates any residual

strains. The peak value has been taken in all cases despite the time lag, since it was considered that the maximum values of strain are the ones that matter in a pavement.

The magnitudes of the peak values which have been used, and also possibly those of the elastic portions of these strains, depend on the time interval between successive load pulses, If sufficient time is allowed, the delayed elastic portion may be fully recovered, while at the other extreme if cyclical loading is applied, none of the delayed elastic portion is recovered and the material will behave in a non-viscous manner.

The time interval between pulses on the test pit was not constant, its mean value being about 3 minutes. This meant different amounts of delayed elasticity were recovered, but in no case was the interval long enough for complete recovery. This could not have really been catered for, because of the length of time needed in this case for each test run.

The situation under a real pavement is likely to be even more variable than that in the test pit, although many more "preloading" cycles will have been applied in the case of an actual pavement. Neither the peak value nor just the elastic part of the pulse is the reading

which should ideally be taken, but since peak values were measured before this detailed analysis took place they are the strains reported herein. An analysis of some typical results has, however, indicated that the elastic portion is of the order of 25% smaller than the peak value and hence yields values of modulus 25% larger than those reported in later chapters.

CHAPTER 7 DISCUSSION OF RESULTS FOR THE SINGLE LAYER SYSTEM

7.1 Modulus and Poisson's ratio

Values of in-situ modulus and Poisson's ratio were calculated for both layers as described earlier. Fig. 7.1 shows the variation of modulus in the subgrade clay with major principal stress and demonstrates clearly the non-linear nature of the soil, the modulus increasing sharply at low stress levels. The superimposed line represents the results of several unconfined compression tests on 9 in. dia. x 18 in. long remoulded specimens of clay. Considering the different conditions under which the results were obtained the correlation is considered satisfactory.

Since the problem is a three dimensional one, it was thought that the variation of modulus should be plotted against a more appropriate stress function. In fig. 7.2 modulus is plotted against the 1st stress invariant J_1 which is the sum of the three principal stresses, and in fig. 7.3 it is plotted against the 2nd deviator stress invariant I_2 which is defined as:

$$I_2 = \tfrac{1}{2}[(p_1 - s)^2 + (p_2 - s)^2 + (p_3 - s)^2].$$

where $s = J_1/3$ and $J_1 = p_1 + p_2 + p_3 = p_1 + p_\theta + p_3$

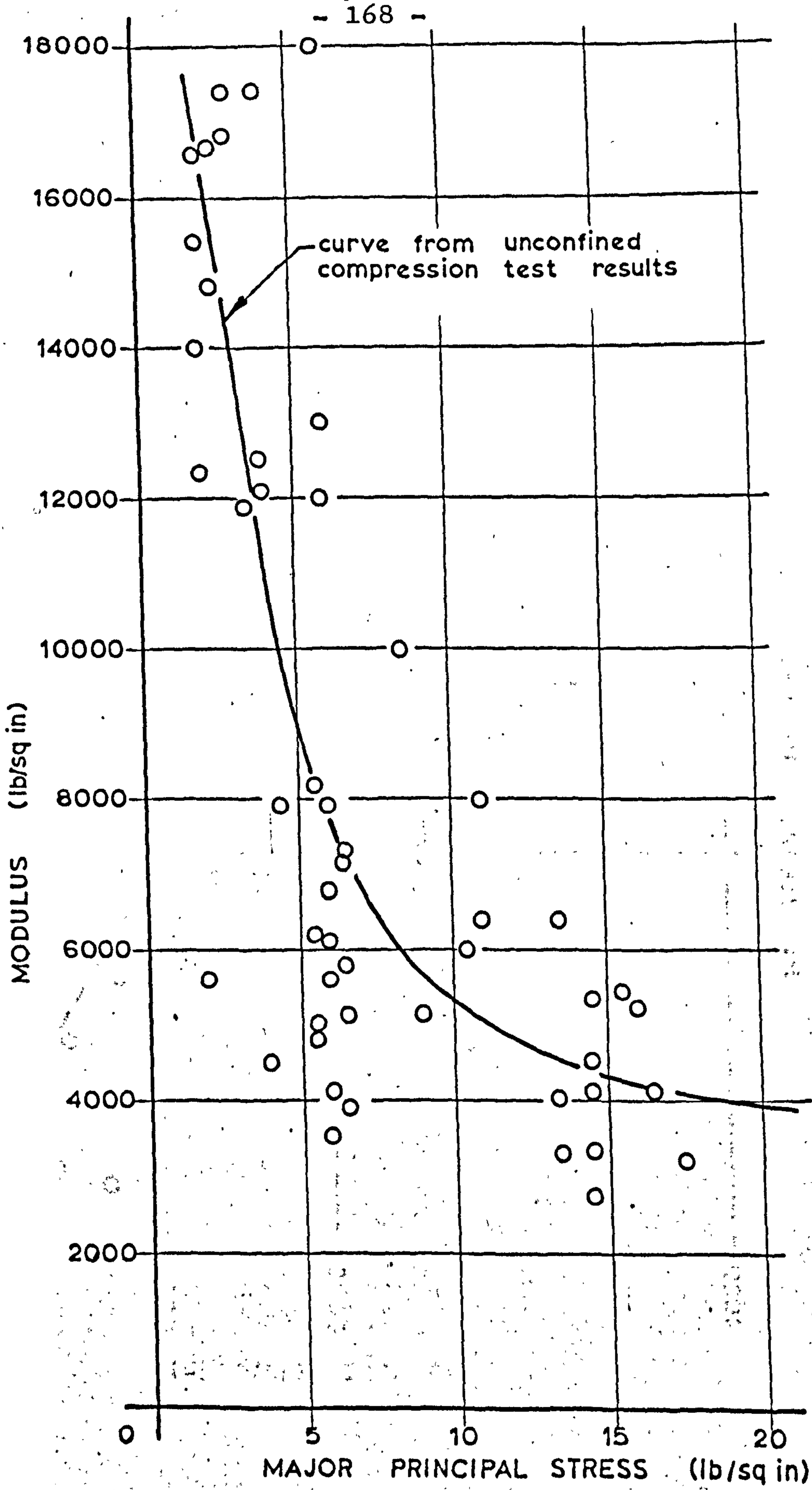

FIG. 7.1 MODULUS AGAINST MAJOR PRINCIPAL STRESS - KEUPER MARL

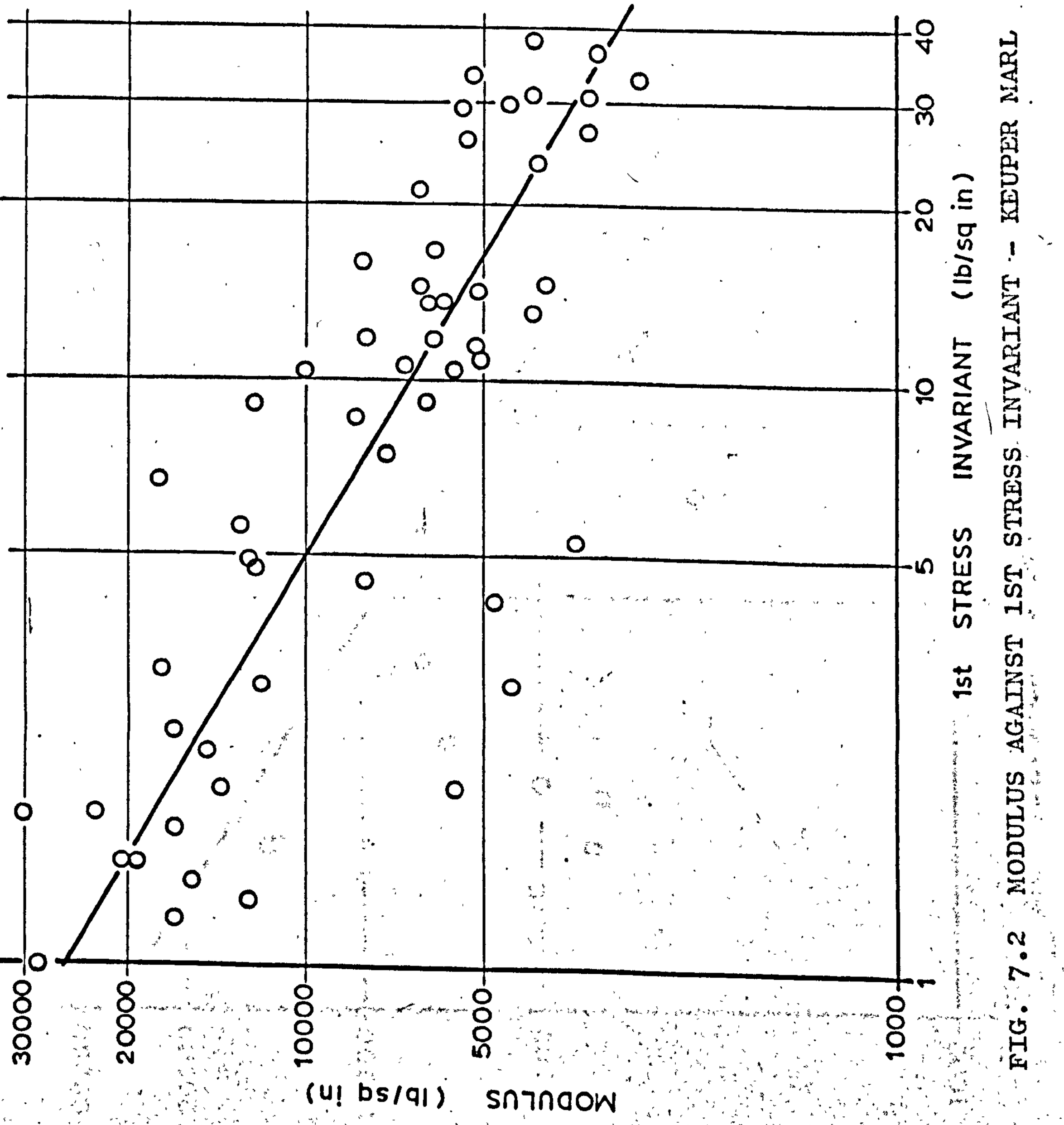
MODULUS (lb/sq in)
30000
20000
10000
5000
1000
0
1
5
10
20
30
40
1st STRESS INVARIANT (lb/sq in)
I2 MODULUS AGAINST 1ST STRESS INVARIANT - KEUPER MARL

FIG. 7.2

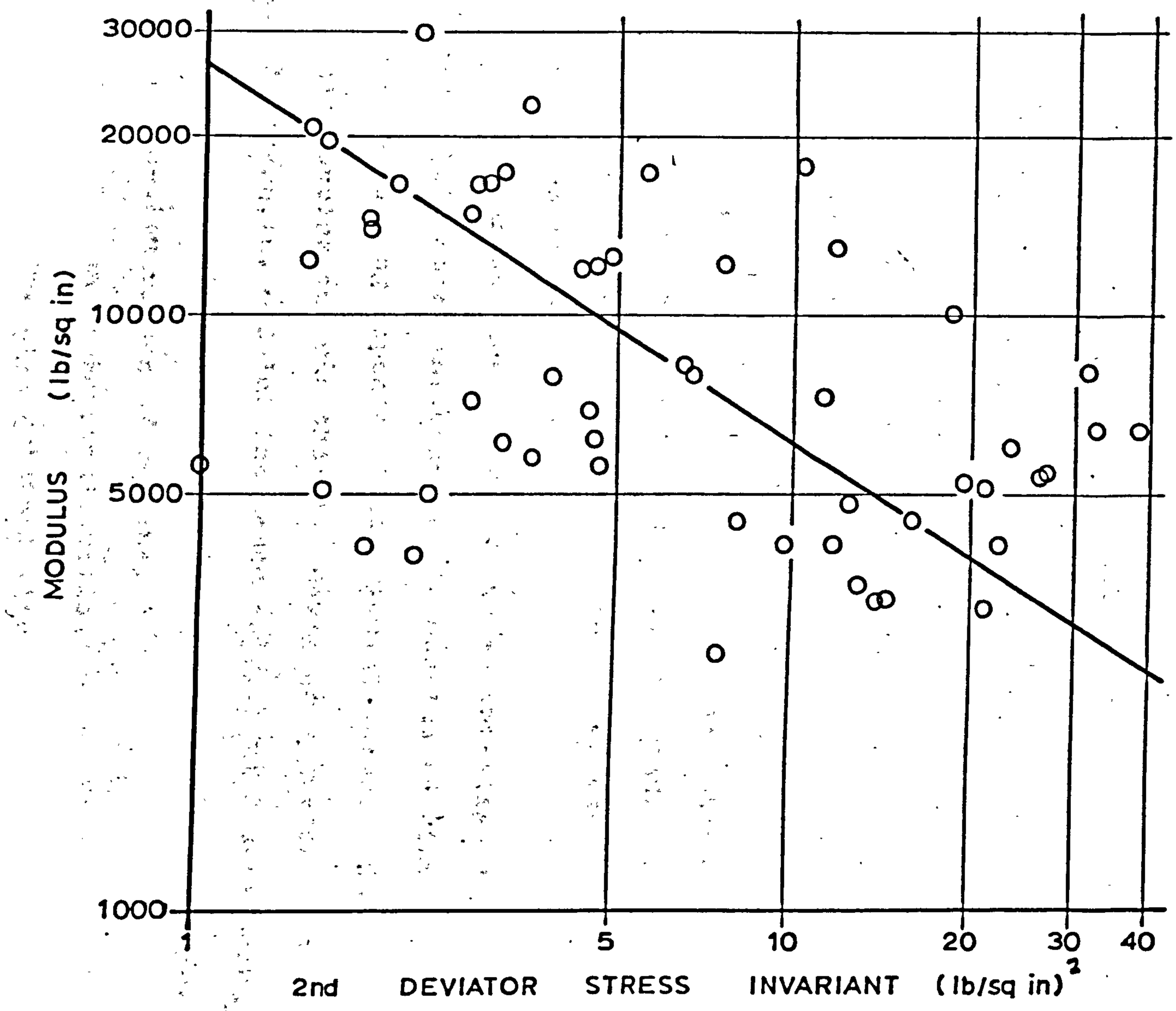

FIG. 7.3 - MODULUS AGAINST 2nd DEVIATORIC STRESS INVARIANT - KEUPER MARL

This function is analogous to deviator stress in three dimensions. Both figs. 7.2 and 7.3 are on a log-log basis and incorporate a "best fit" straight line through the experimental points. Despite the scatter on fig. 7.2 it is clear that modulus decreases with increasing stress level.

Variation of modulus for a clay is more commonly referred to deviator stress, but in fig. 7.2 there is less scatter of points that fig. 7.3 where 2nd deviator stress invariant is the parameter.

Although strain and to some extent stress measurements were influenced by the rate of loading, there is no conclusive evidence that modulus is affected. Any trend that may have emerged is swamped by the dependence of modulus on stress level.

Seed, Chan and Lee[34] carried out an investigation to study the factors influencing the modulus of clay as measured during repeated load triaxial tests. One of their conclusions was that for deviator stresses less than 10 lb/sq.in. modulus increased sharply with decreasing stress. This result is in line with the findings herein, based on in-situ values of modulus.

The variation of Poisson's ratio for the clay appears to be quite random, most values falling between 0.2 and

0.6 with a mean of 0.41. The values greater than 0.5 are of interest and since there are several of them, they cannot be dismissed as freak results. The indications are that the soil is dilating and hence bulk volumetric strain should be negative at the points concerned. In fact this is not conclusively the case, and the reason is probably found in the error introduced by superimposing results from different parts of the test pit, since the soil is not perfectly homogeneous.

7.2 Theoretical Results

In using the tables prepared by Ahlvin and Ulery[27] to calculate theoretical stresses, strains and deflections, appropriate values of modulus of elasticity and Poisson's ratio need to be chosen. However, for vertical stresses neither of these quantities is required and for horizontal stresses only Poisson's ratio is needed.

It was clear from a study of the values of the elastic "constants" calculated from experimental measurements that the soil was non-linear and therefore a unique value of modulus did not exist. Poisson's ratio also varied and in a somewhat irregular manner.

Most single layer results have been plotted to show variations of the measured, or derived effect with radius.

To superimpose a theoretical line, it was desirable to have one value of modulus and of Poisson's ratio for a particular plot. This meant that while variations of modulus with depth could be catered for, variations with radius would have to be compromised. The procedure adopted was to take the mean values of modulus and Poisson's ratio obtained from experimental results at a particular effective depth ($^{z}/_{a}$) and use these to calculate theoretical results at that depth. The values adopted are shown in Table 7.1, and it should be noted that those for $^{z}/_{a}$ = 1.0, 1.33 and 2.0 are based on calculations carried out before the error in position of vertical strain cell 13 was discovered. This error meant that vertical strains at a radius of 12 in. were the only useful ones at these depths. Consequently instead of a number of values of modulus and Poisson's ratio, at various radii, only one result was obtainable for each test. By comparing correct calculations with those carried out originally, it appears that the values quoted in Table 7.1 for the lower three depths are correct to within 20%, and they have, therefore, been retained.

The calculation of theoretical surface deflections could not be carried out on the lines indicated for stresses and strains, since representative values for the elastic

"constants" could not be calculated from experimental results. As the soil modulus varied considerably, it was difficult to specify a value representative of the soil mass as a whole, so the procedure adopted by Sparrow and Tory[11,17] was used. This involved calculating that value of modulus which produced a theoretical deflection on the axis equal to the mean of the measured ones.

Poisson's ratio did not vary so much or so rationally as modulus and was thus taken as 0.41, the mean of the values used to calculate theoretical strains at various depths. The elastic constants used for theoretical surface deflection calculations are shown in Table 7.2.

7.3 Equilibrium and Compatibility Errors

The equilibrium error (x) defined in section 6.4 as: $x = (p_z + p_r) - (p_{45} + p_{135})$ was found to be exclusively positive, i.e., $(p_z + p_r) > (p_{45} + p_{135})$. This seemed rather remarkable and an investigation of the factors likely to influence this error was conducted.

An estimate of the magnitude of the various errors which were possibly incurred during the experimentation and interpretation of individual results is as follows:

1. Position of transducer in plan and elevation $\pm \frac{1}{4}$ in.
2. Orientation of transducer $\pm 5^{\circ}$

TABLE 7.1 VALUES OF MODULUS AND POISSON'S RATIO USED FOR THEORETICAL CALCULATIONS (SINGLE LAYER SYSTEM)

Effective Depth ($^{z}/_{a}$)	Modulus (lb/sq.in.)	Poisson's Ratio
0.25	5700	0.35
0.33	7600	0.40
0.50	8500	0.41
1.00	9700	0.43
1.33	12100	0.44
2.00	18000	0.44

TABLE 7.2 VALUES OF MODULUS USED FOR THEORETICAL SURFACE DEFLECTION CALCULATIONS (SINGLE LAYER SYSTEM)

Radius of loaded area (a) (in.)	Modulus (lb/sq.in.)
6	3600
9	4000
12	5200

3. Position of loaded area in plan $\pm \frac{1}{4}$ in.

4. Trace reader errors $\pm$ 2%

5. Transducer calibration errors $\pm$ 5%

The percentage errors caused by wrong positioning of the load and the transducers will depend on their relative positions. In particular for vertical stresses under the edge of the loaded area where the stress gradient is steep, the errors incurred are likely to be higher than elsewhere.

To assess the contribution of pressure cell cross-sensitivity, an analysis similar to those carried out in Chapter 3 can be used.

$$x = (p_z + p_r) - (p_{45} + p_{135}).$$

Denoting corrected stresses by a prime.

Corrected

$$x = p_z + 0.05\,(J_1 - p_z') + p_r + 0.05\,(J_1 - p_r')$$
$$- p_{45} - 0.05\,(J_1 - p_{45}') - p_{135} - 0.05\,(J_1 - p_{135}')$$
$$= p_z + p_r - p_{45} - p_{135} - 0.05\,(p_z' + p_r' - p_{45}' - p_{135}')$$
$$= x$$

$\therefore$ Pressure cell cross-sensitivity has no influence on equilibrium error.

Items 1 to 5 above could possibly introduce an error of $\pm$ 10%, bearing in mind that values of vertical and

radial stress were taken as a mean of four and three measurements respectively, thus reducing the errors due to bad positioning of load and cell.

The errors discussed so far could provide only a relatively small contribution to the equilibrium error (x), particularly in view of the fact that they are "plus or minus" errors. There are two other important factors which need to be considered before an explanation of the nature of the equilibrium error can be provided.

Errors in orientation of the pressure cells measuring vertical and radial stresses were largely eliminated by loading either side of the cells and taking mean values. 45° and 135° stresses, however, resulted from single readings on one cell and both these stresses were measured by the same cell, loading on either side of it.

If there was an error in the orientation of this 45° cell so that it made an angle of $(45 + \theta)^\circ$ with the horizontal, the resulting Mohr's circle for the four measured stresses at a point would be as shown in fig. 7.4. It can be seen that the error is magnified because 45° and 135° stresses were measured from the same cell and that if $p_z > p_r$ then

$$(p_z + p_r) > (p_{45} + p_{135})$$

i.e., $x > 0$

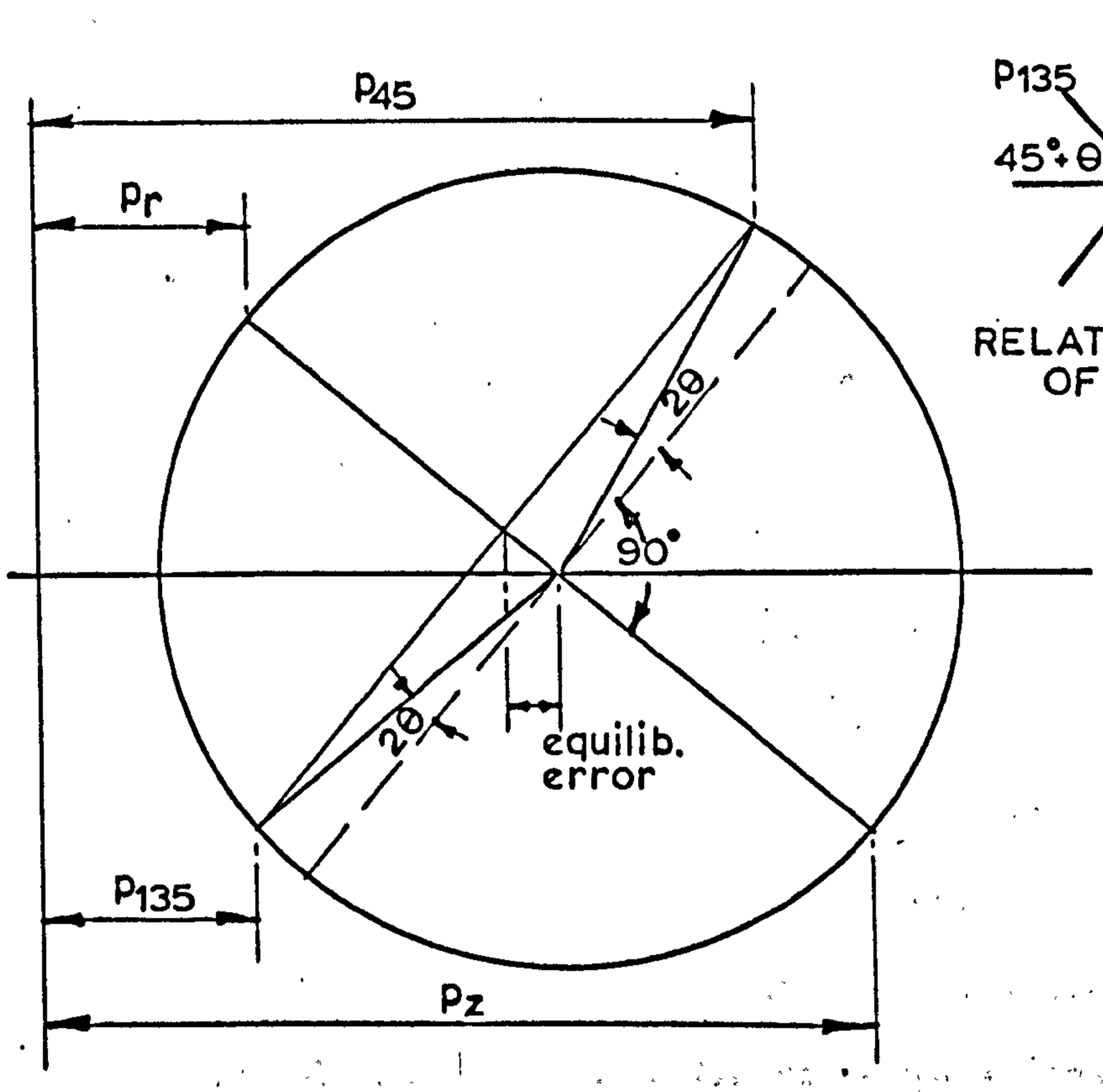

FIG. 7.4 MOHR'S CIRCLE SHOWING EFFECT OF ERROR IN POSITION OF 45° CELL

This cannot fully explain the exclusively positive equilibrium error, since by this analysis it only occurs when vertical stress is larger than radial stress, but it may well contribute to it.

The real reason for the positive equilibrium error

can probably be explained by studying the distribution of pressure cells in the test pit. As explained above, the chief difference between p_z and p_r measurements and those for p_{45} and p_{135} is that the former have, by taking means, had some superposition errors removed. The largest superposition error is likely to be caused by the variable nature of the soil in different parts of the pit. The portion of the pit used to obtain 45° and 135° stresses is remote from that used to measure the other stresses (fig. 2.2) so it is thought reasonable to assume that the soil around the 45° cells is likely to yield consistently lower (or higher) stresses than elsewhere. It should be born in mind here that there are two layers of cells at the 3" and 12" depths and that the equilibrium problem is the same in both cases.

Before the four stresses at a point can be used to derive other stress functions, the equilibrium error has to be eliminated by correcting each stress by some appropriate amount. Since vertical and radial stresses are more reliable than those at 45° and 135°, any corrections should be suitably weighted. This has been done in Table 7.3, by an approximate method based on the number of cells and the number of readings of each effect. Corrections have been weighted in inverse proportion to

TABLE 7.3 EQUILIBRIUM AND COMPATIBILITY CORRECTIONS (SINGLE LAYER SYSTEM)

Measurement		Correction
p_z	p_r	- 0.1x
p_{45}	p_{135}	+ 0.4x
e_z	e_r	- 0.17y
e_{45}	e_{135}	+ 0.33y

the sum of these factors. No positive information exists to suggest any substantial error in the orientation of cells in the test pit, so the angles of 45° and 90° between cells have been assumed correct, resulting in an equal correction for vertical and radial stresses on the one hand and 45° and 135° on the other.

No mention has yet been made of the magnitude of the equilibrium errors, discussion having revolved around their sign. To give some idea of the magnitude, each error has been expressed as a percentage of the sum of the major and minor principal stresses. This sum is

equal to that of vertical and radial stresses and also of 45° and 135° stresses after correction. Taking the mean value,

$$\frac{x}{(p_1 + p_3)} \times 100 = 31\%$$

A study of the compatibility error, y, for strains at a point shows almost exclusively negative values. The magnitude of the errors has been expressed in the same way as for stress and again taking the mean value,

$$\frac{y}{(e_1 + e_3)} \times 100 = -30\%$$

which is comparable with the stress error, though of opposite sign.

The distribution of strain cells in the test pit (fig. 2.2) shows, as for stress, that the 45° cell is remote from those reading radial and vertical strains. Since the soil is almost certainly not homogeneous, it is reasonable to suppose that the soil around the 45° cell will be less stiff than around the others, thus producing higher strains for the same applied stress.

The difference in reliability between vertical and radial strains and the diagonal ones is not so marked as for stress. Vertical strain results from 2 readings on one cell, radial strain is a single reading and, as

for stress, 45° and 135° strains result from single readings either side of the same cell. Weighted corrections have been applied as shown in Table 7.3.

7.4 Stresses (Figs. 7.5 to 7.13)

Normalised stress has been plotted against radius at various depths. The symbols used to indicate experimental results follow the code shown in Table 5.1. A theoretical line has been superimposed for comparison, its derivation having been explained in section 7.2.

Stress distribution plots in general show close agreement with the theoretical Boussinesq calculations. In particular, vertical and 45° stresses, of those directly measured, are close to theory. The horizontal stresses agree less well, radial stress being everywhere higher than theory, though showing a similar variation with radius. Tangential stress, while agreeing with theory well under the loaded area shows tensile values at greater radii which are not predicted by theory. It should be pointed out that the pressure cell is not designed to measure tensile stresses, but because of an initial pre-stress caused by overburden pressure, some tensile

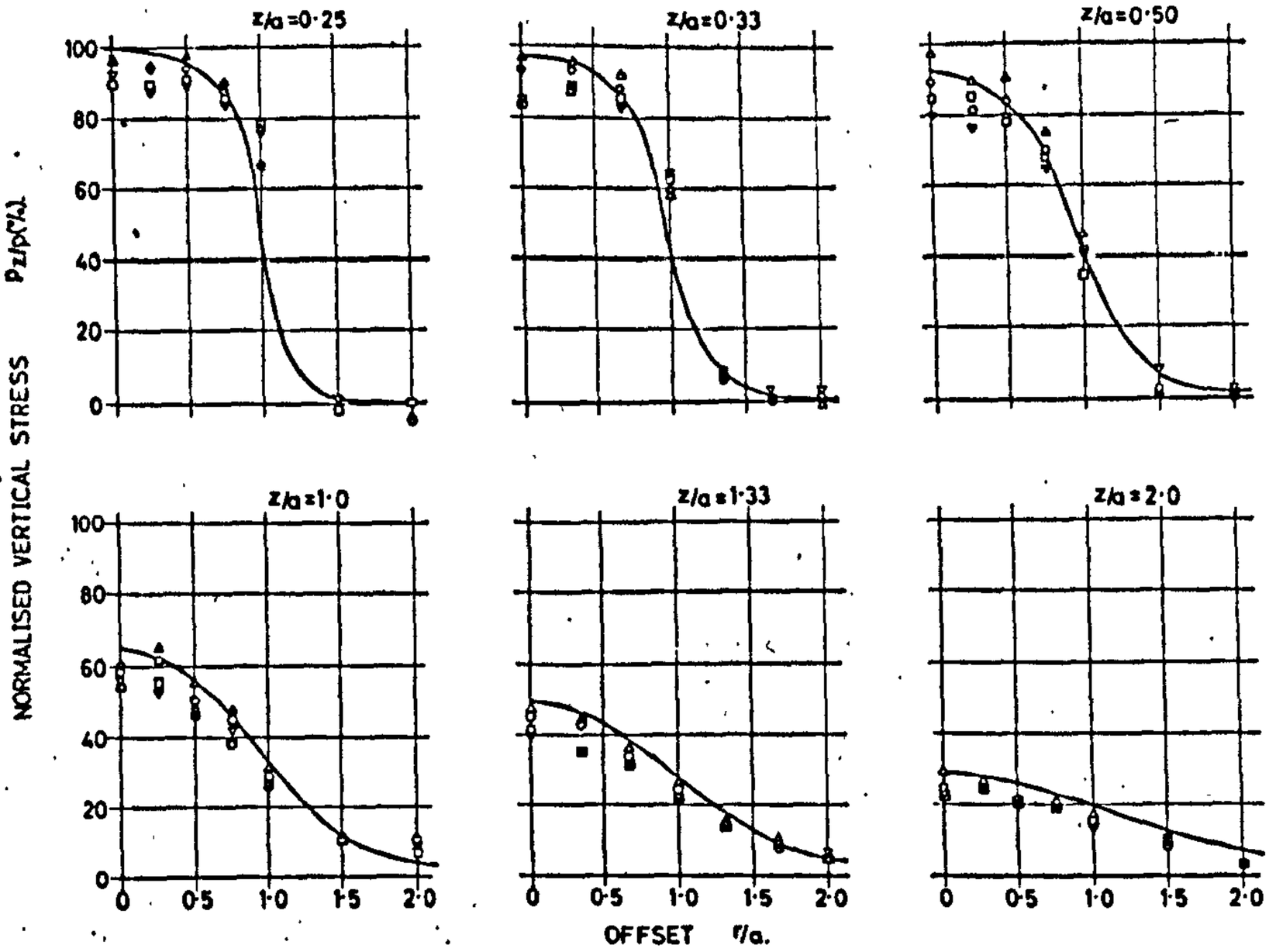

FIG. 7.5 VERTICAL STRESS WITH RADIUS - SINGLE LAYER SYSTEM

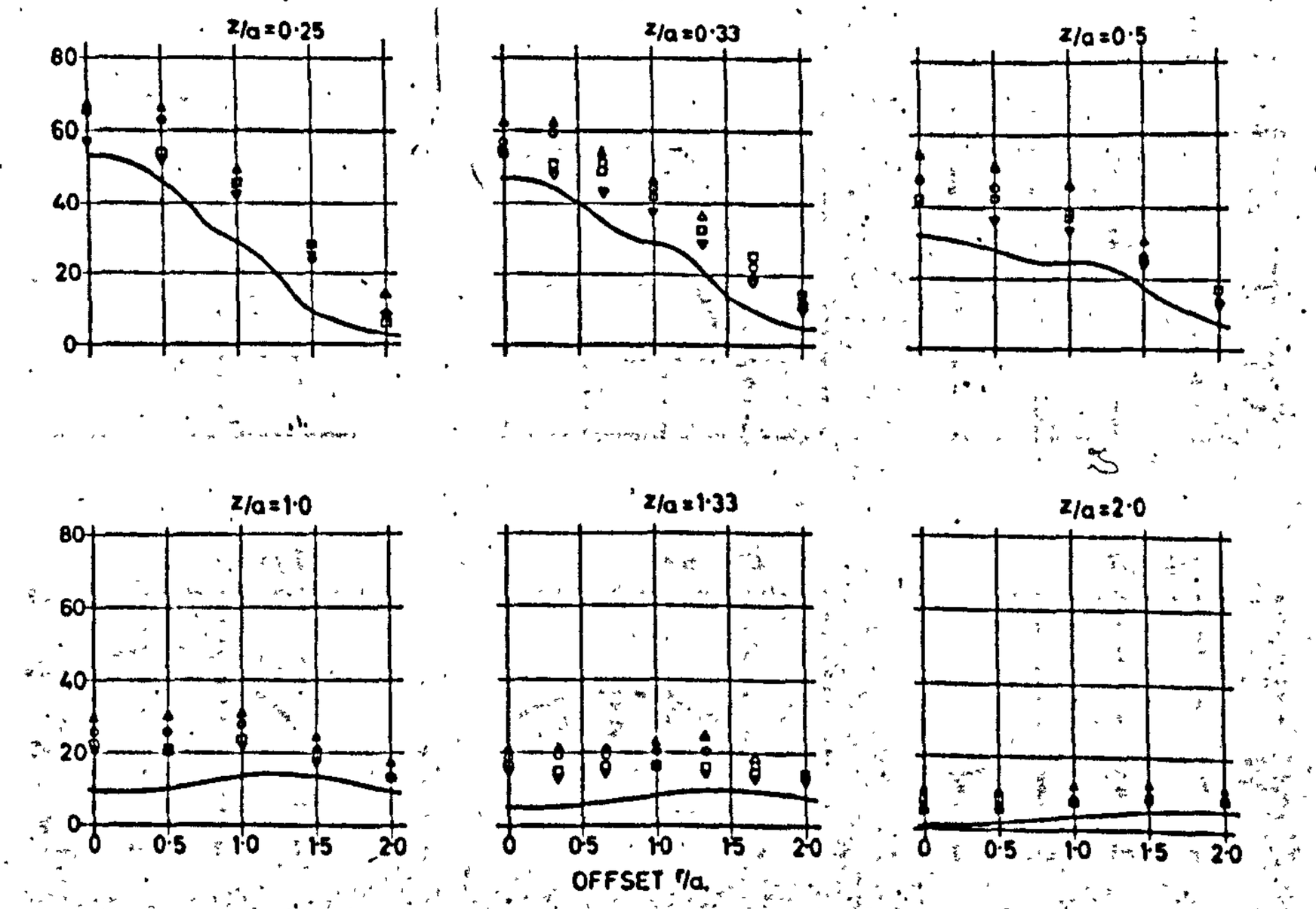

FIG. 7.6 RADIAL STRESS WITH RADIUS - SINGLE LAYER SYSTEM

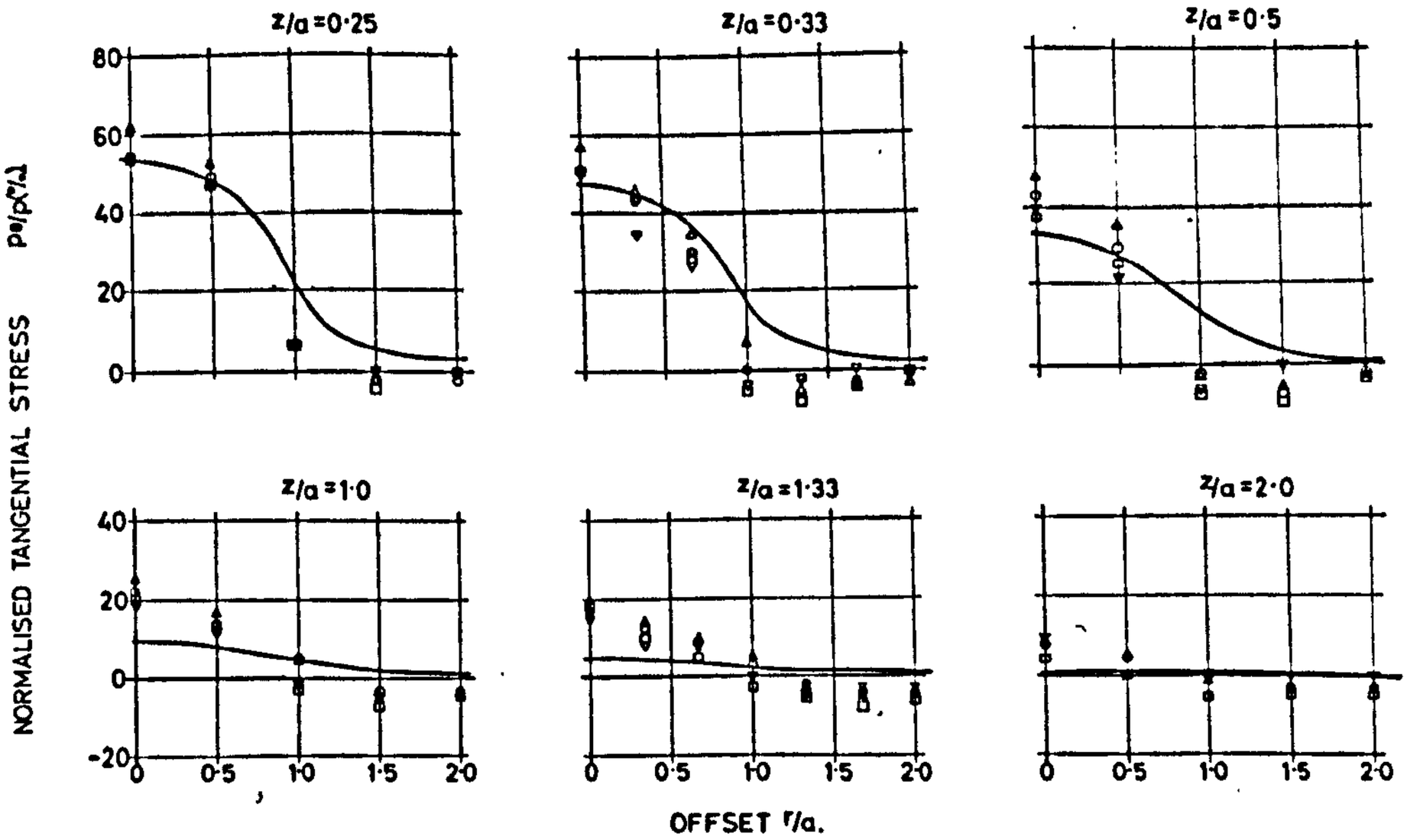

FIG. 7.7 TANGENTIAL STRESS WITH RADIUS - SINGLE LAYER SYSTEM

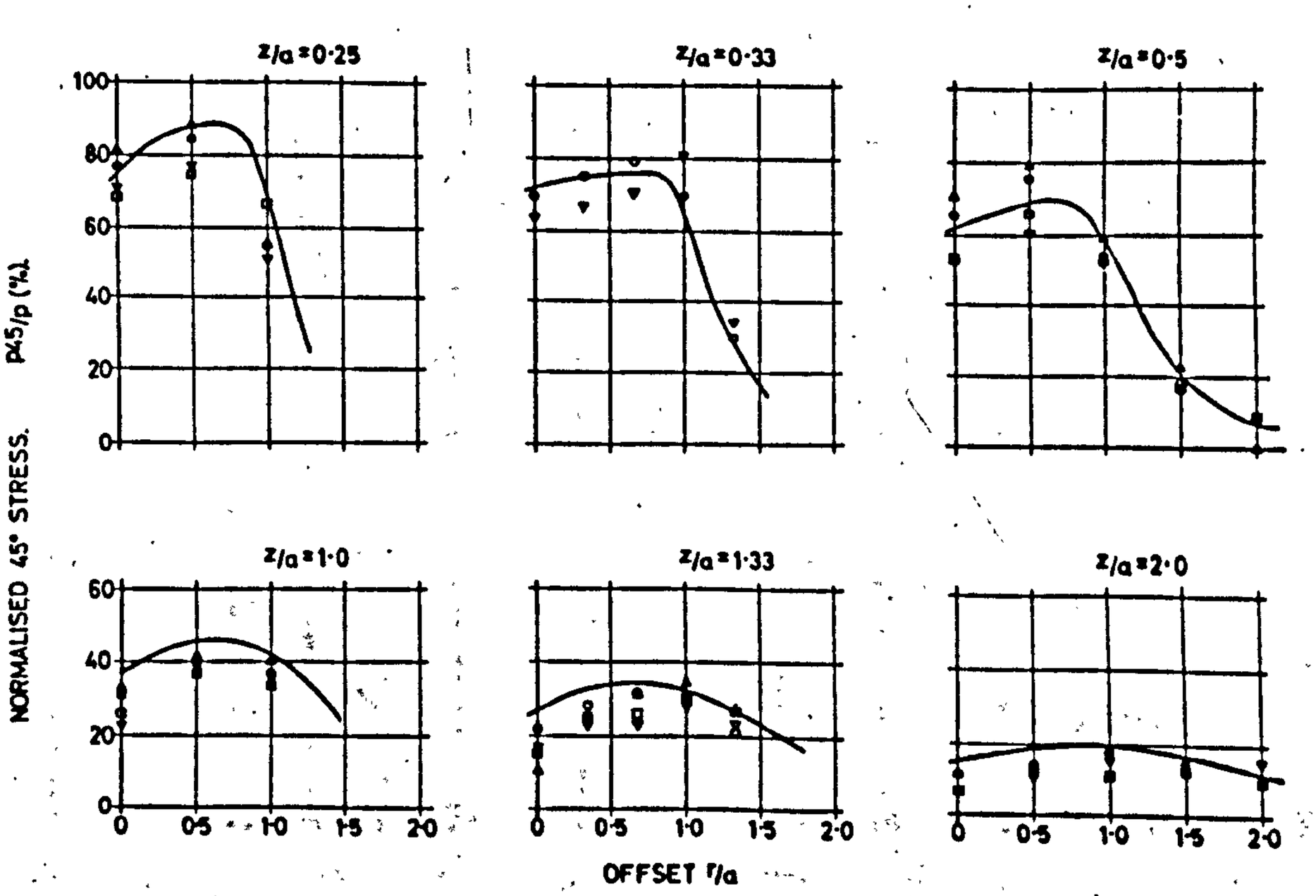

FIG. 7.8 45° STRESS WITH RADIUS - SINGLE LAYER SYSTEM

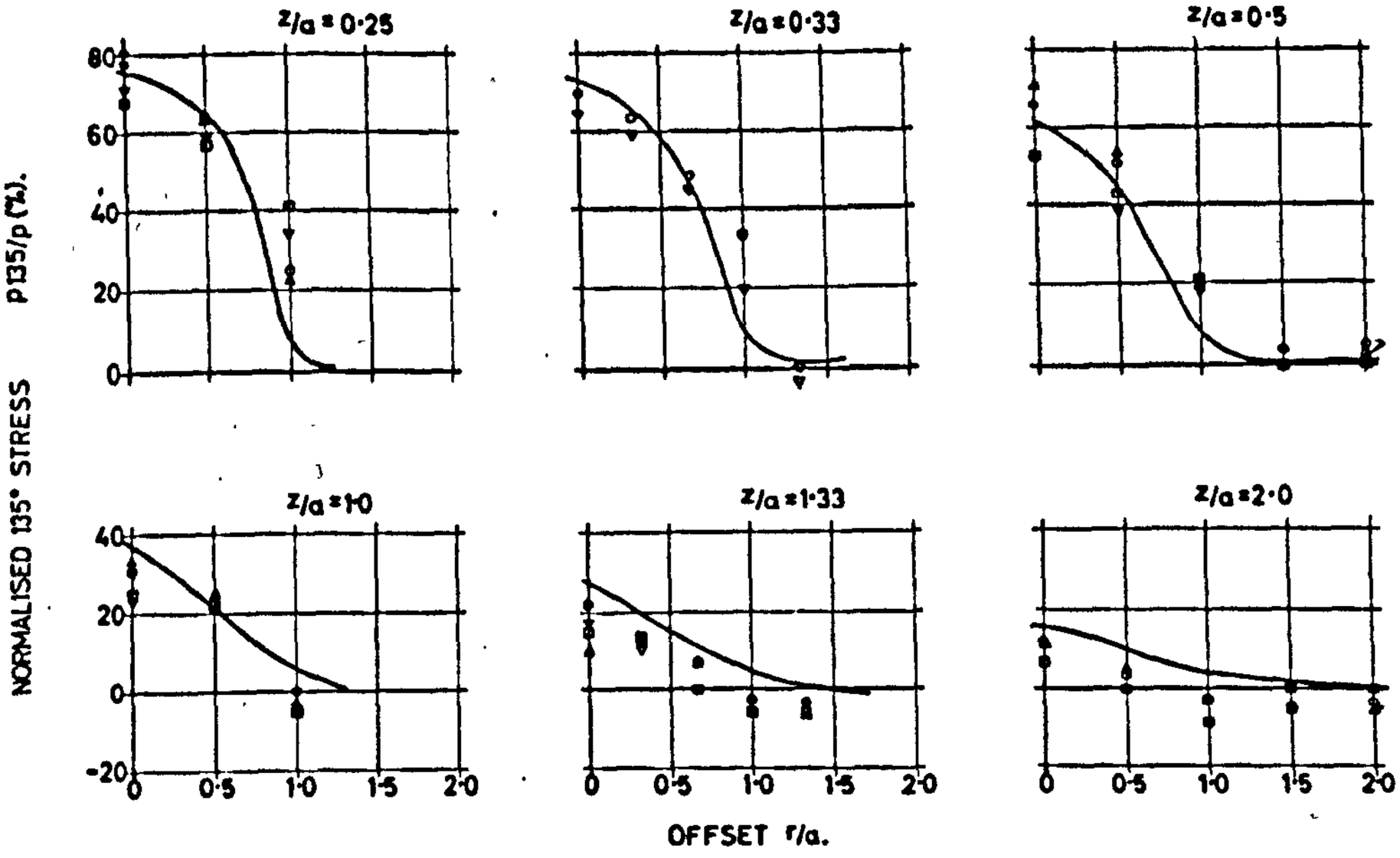

FIG. 7.9 135° STRESS WITH RADIUS - SINGLE LAYER SYSTEM

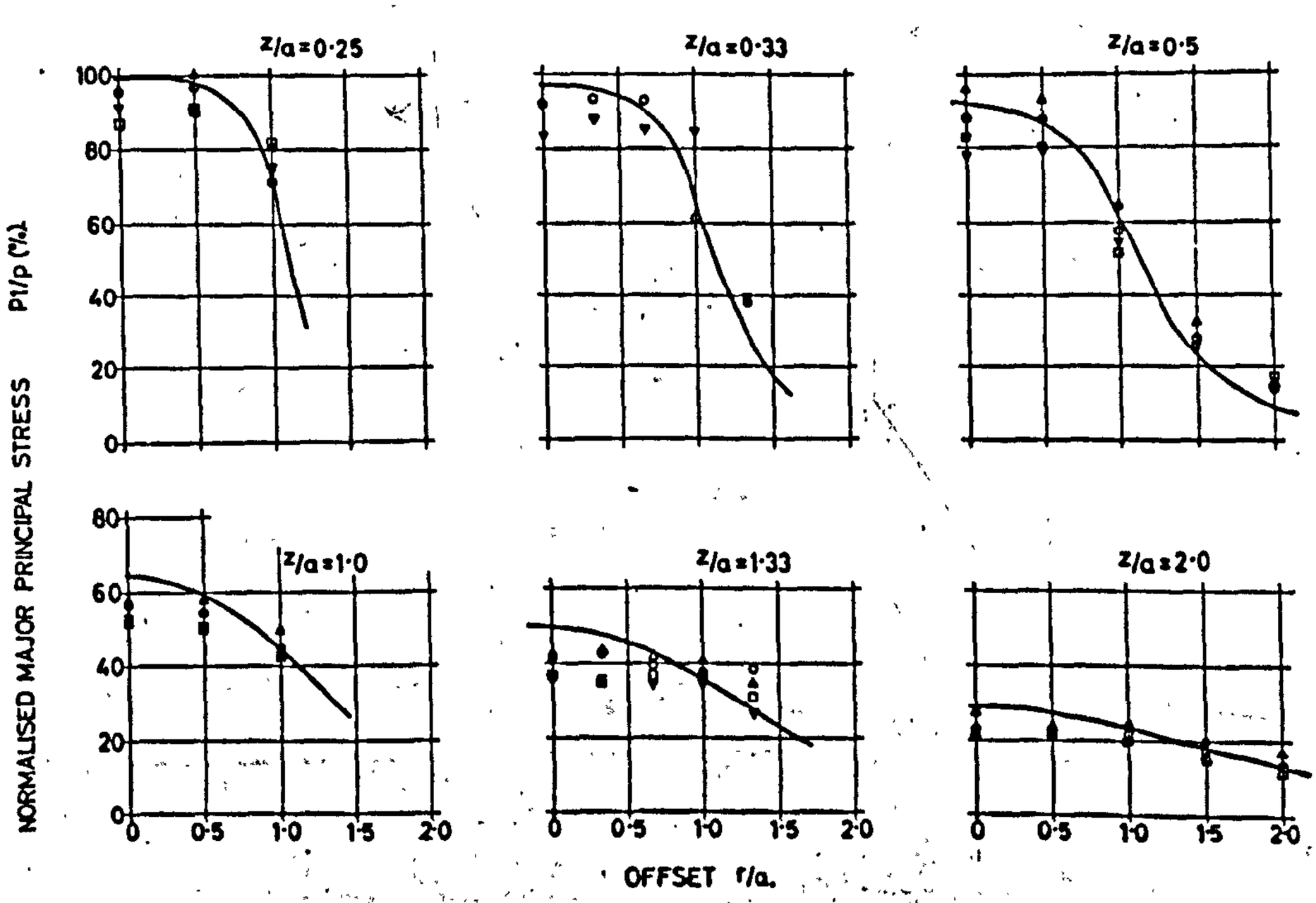

FIG. 7.10 MAJOR PRINCIPAL STRESS WITH RADIUS - SINGLE LAYER SYSTEM

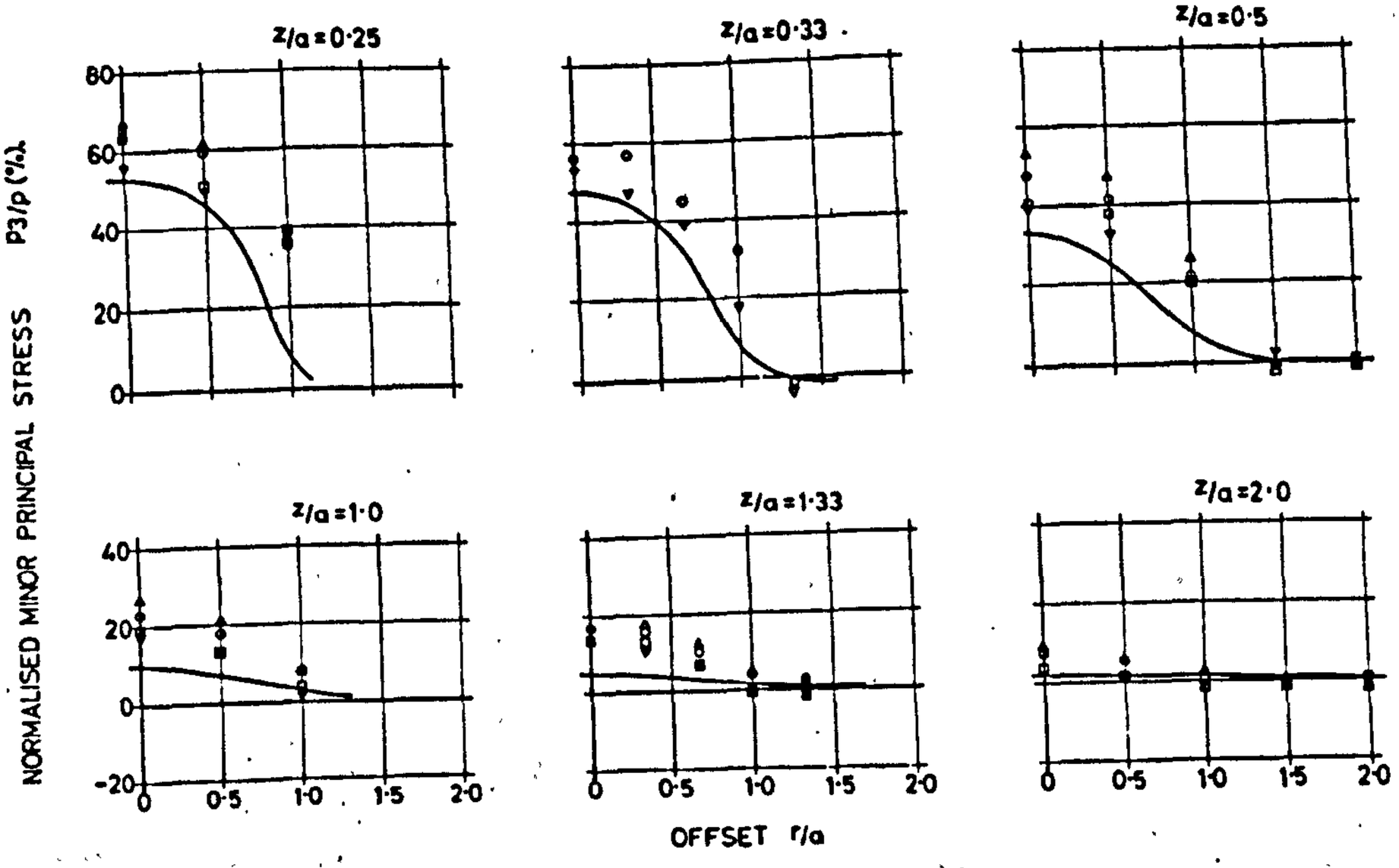

FIG. 7.11 MINOR PRINCIPAL STRESS WITH RADIUS - SINGLE LAYER SYSTEM

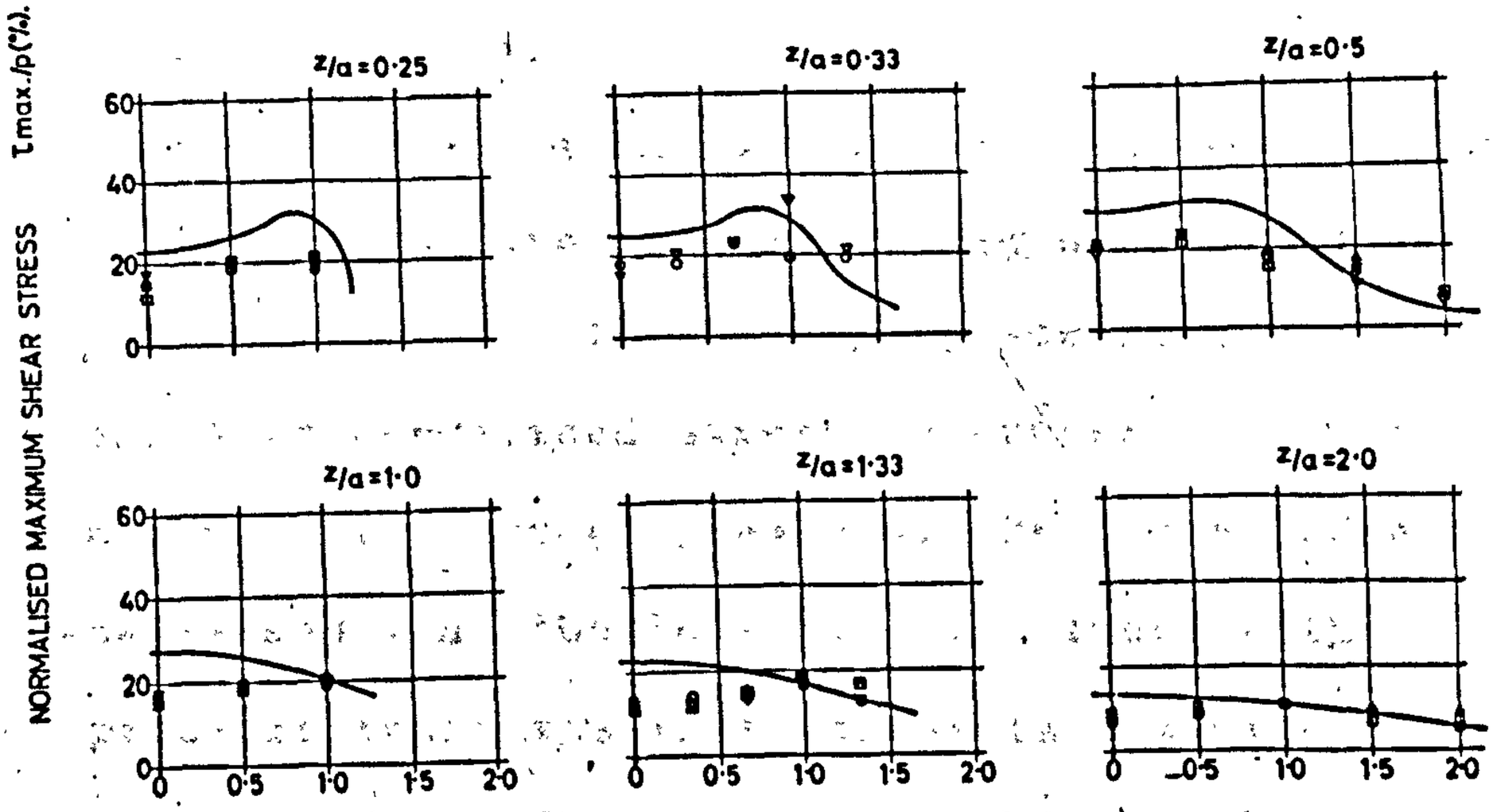

FIG. 7.12 MAXIMUM SHEAR STRESS WITH RADIUS - SINGLE LAYER SYSTEM

transient stress can be recorded. The quantitative value of tensile stress measurements is therefore unlikely to be accurate. The remarks for tangential stresses apply similarly to those at 135°.

Of the derived results, major principal stress agrees well with theory while minor principal stresses, where they are influenced by radial values are higher than theory, i.e., beneath the loaded area. Maximum shear stress which is of importance from a design point of view, does not show very close agreement with the theoretical line, though the discrepancy is on the safe side. The maximum shear stresses occur beneath the edge of the loaded area.

By plotting stresses in normalised form, trends with contact pressure and rate of loading can be studied as outlined in Chapter 6. In the highly stressed regions it is clear that normalised stress increases with rate of loading and with contact pressure, the former effect being less marked than the latter. The trend with contact pressure indicates that stress is not directly proportional to it and the reason for this is the non-linear nature of the soil.

The variation of stress with contact pressure is analogous to that produced in layered systems when the

modular ratio changes. Since modulus is stress dependent, the variation of modulus with position in the soil will vary with contact pressure and hence stress would be expected to vary also. The trend with rate of loading is more difficult to explain. Pressure cells measure total stress. For a fast rate of loading high pore pressures are produced, while for slower conditions when pore pressures are able to dissipate, more of the stress is transferred to the soil structure in the form of effective stress. The total stress in each case, however, should be the same for equilibrium, unless a different distribution with radius occurs. For vertical equilibrium, vertical stresses at a particular depth can be summed to equal the applied load. If, for a slow rate of loading the stress is lower near the axis as appears to be the case, there should be an opposite effect at greater radii so as to produce equilibrium. Trends outside the loaded area are, however, not apparent, where the stresses are very small.

Fig. 7.13 shows vertical stresses on the axis of the load. The results of earlier tests on the same layout and from Tory's installation are included. The indications are that repeatable results can be obtained for vertical stress at least.

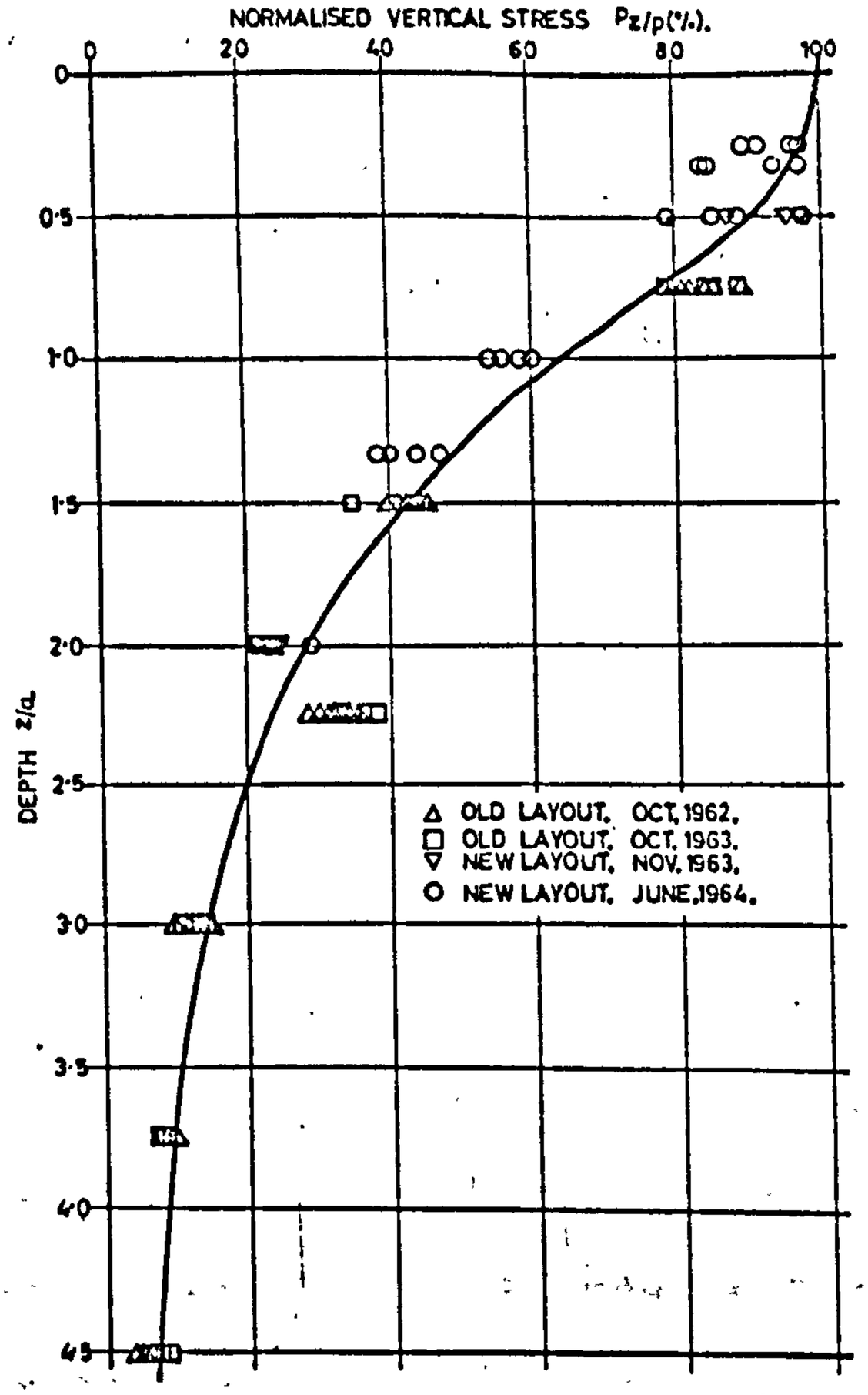

FIG. 7.13 VERTICAL STRESS ON ℄ WITH DEPTH - SINGLE LAYER SYSTEM

Several workers have obtained similar agreement for stress measurements, notably the W.E.S. in their homogeneous test sections,[12,13] although in their tests static loading was applied.

The results of Sparrow and Tory[11,17] showed similar

agreement for vertical and 45° stresses, but their horizontal stresses were far more at variance with the theoretical lines and they showed stress to be independent of contact pressure. In the tests reported here the range of contact pressure was slightly larger and although there are no plots of contact pressure against stress, because only two nominal contact pressures were used, a study of the stress distribution plots clearly shows the trend in the areas of high stress.

Sparrow and Tory showed that stress was independent of rate of loading within the range studied. The current results show a slight increase of stress with rate of loading, although this trend is less pronounced than that for contact pressure.

7.5 Strains (Figs. 7.14 to 7.21)

Normalised strains have also been plotted with radius, the experimental points being represented by the symbols of Table 5.1 and the theoretical line on each plot having been derived in the manner described in section 7.2.

The most striking thing about the strain distribution plots is the large scatter of experimental results. This scatter does, however, form some logical pattern and can be explained in terms of trends with contact pressure and

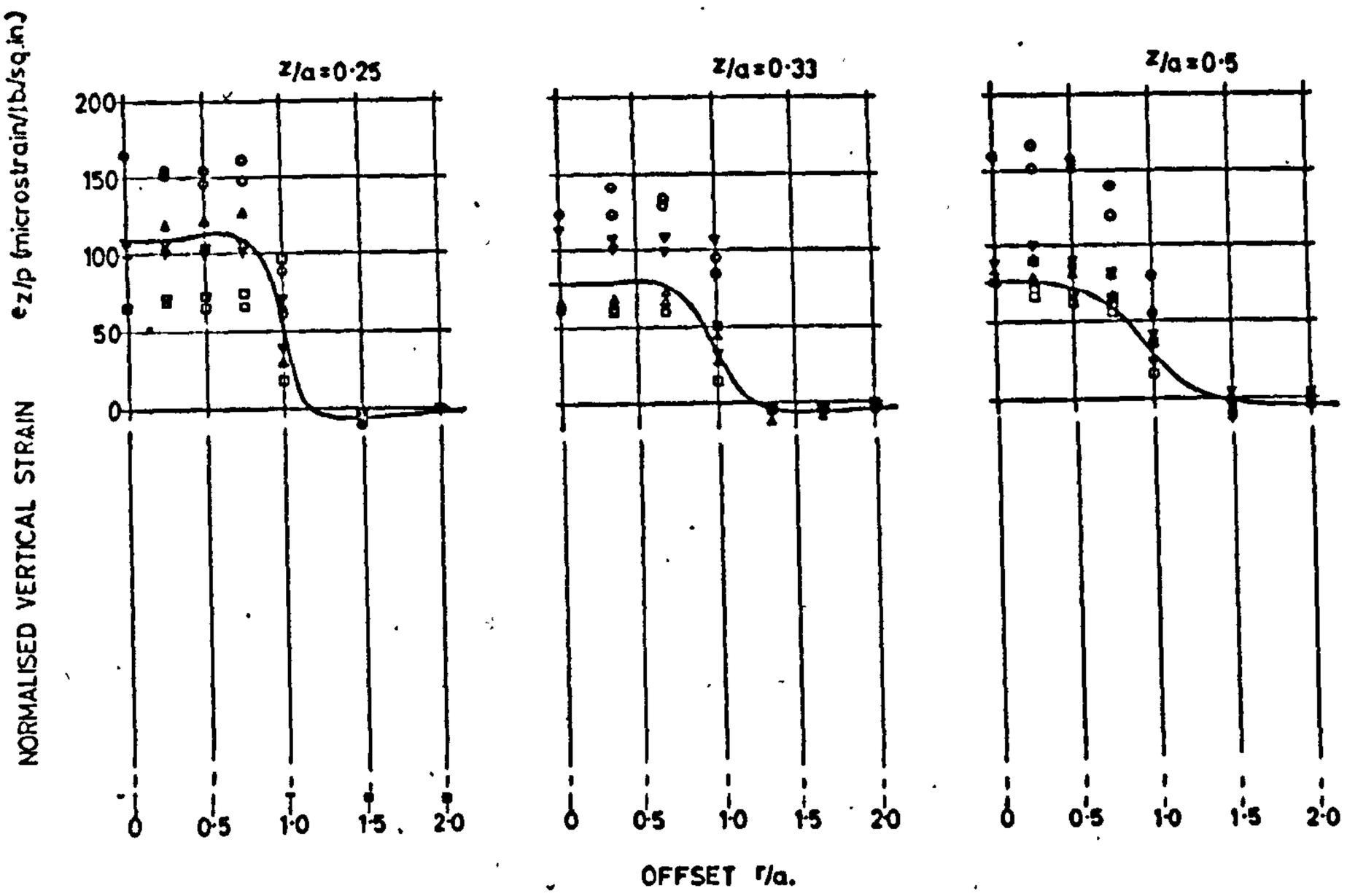

FIG. 7.14 VERTICAL STRAIN WITH RADIUS - SINGLE LAYER SYSTEM

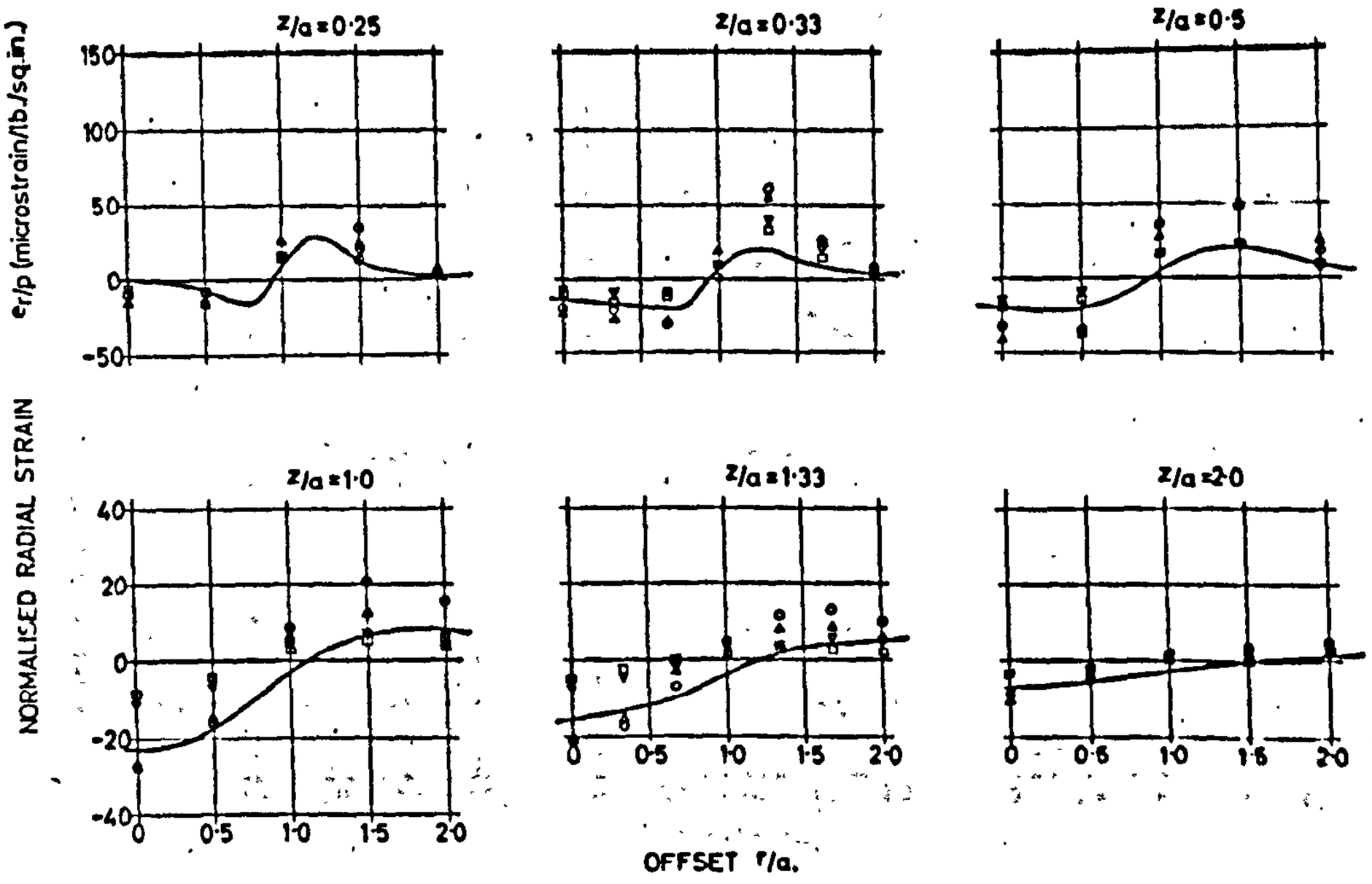

FIG. 7.15 RADIAL STRAIN WITH RADIUS - SINGLE LAYER SYSTEM

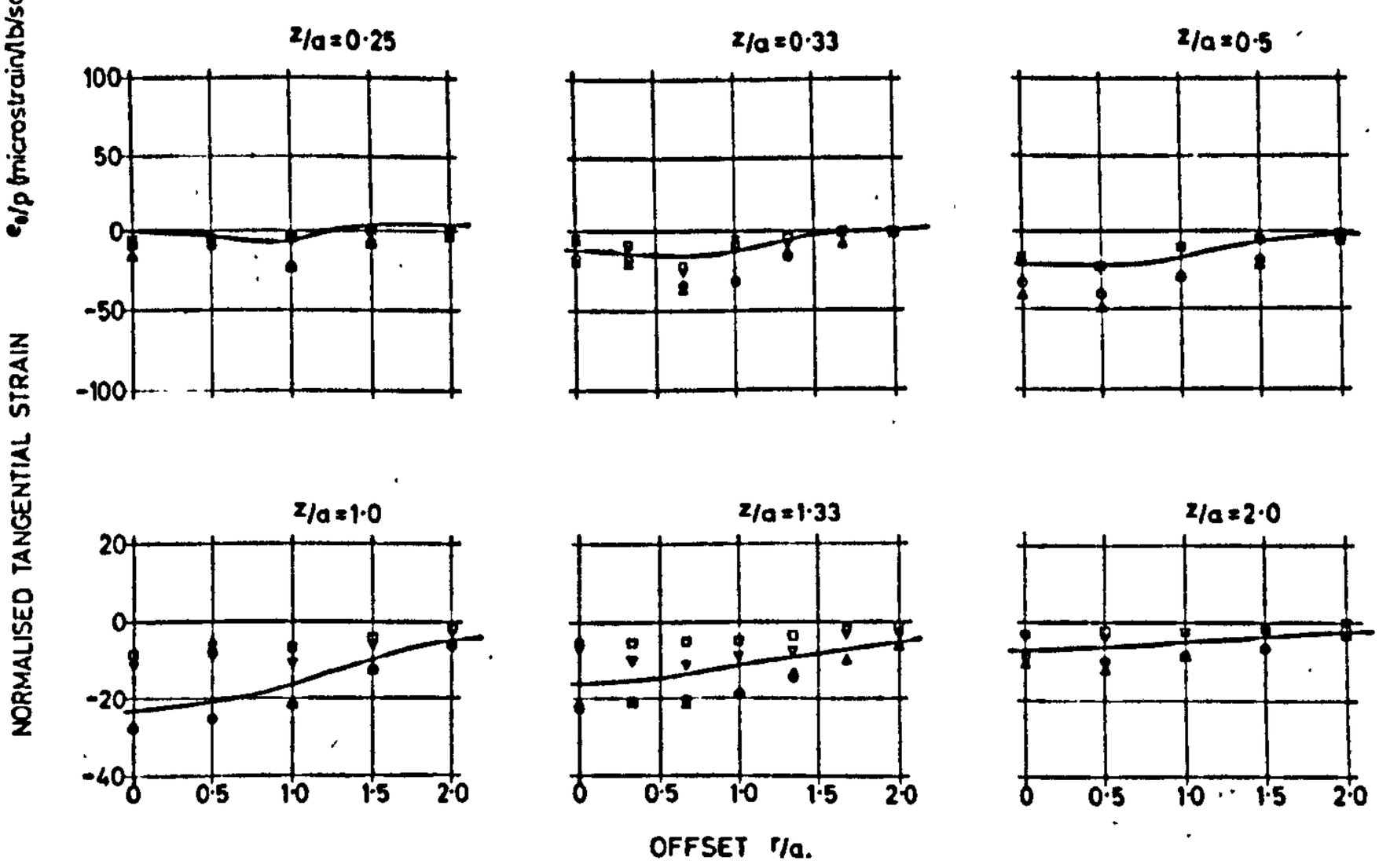

FIG. 7.16 TANGENTIAL STRAIN WITH RADIUS - SINGLE LAYER SYSTEM

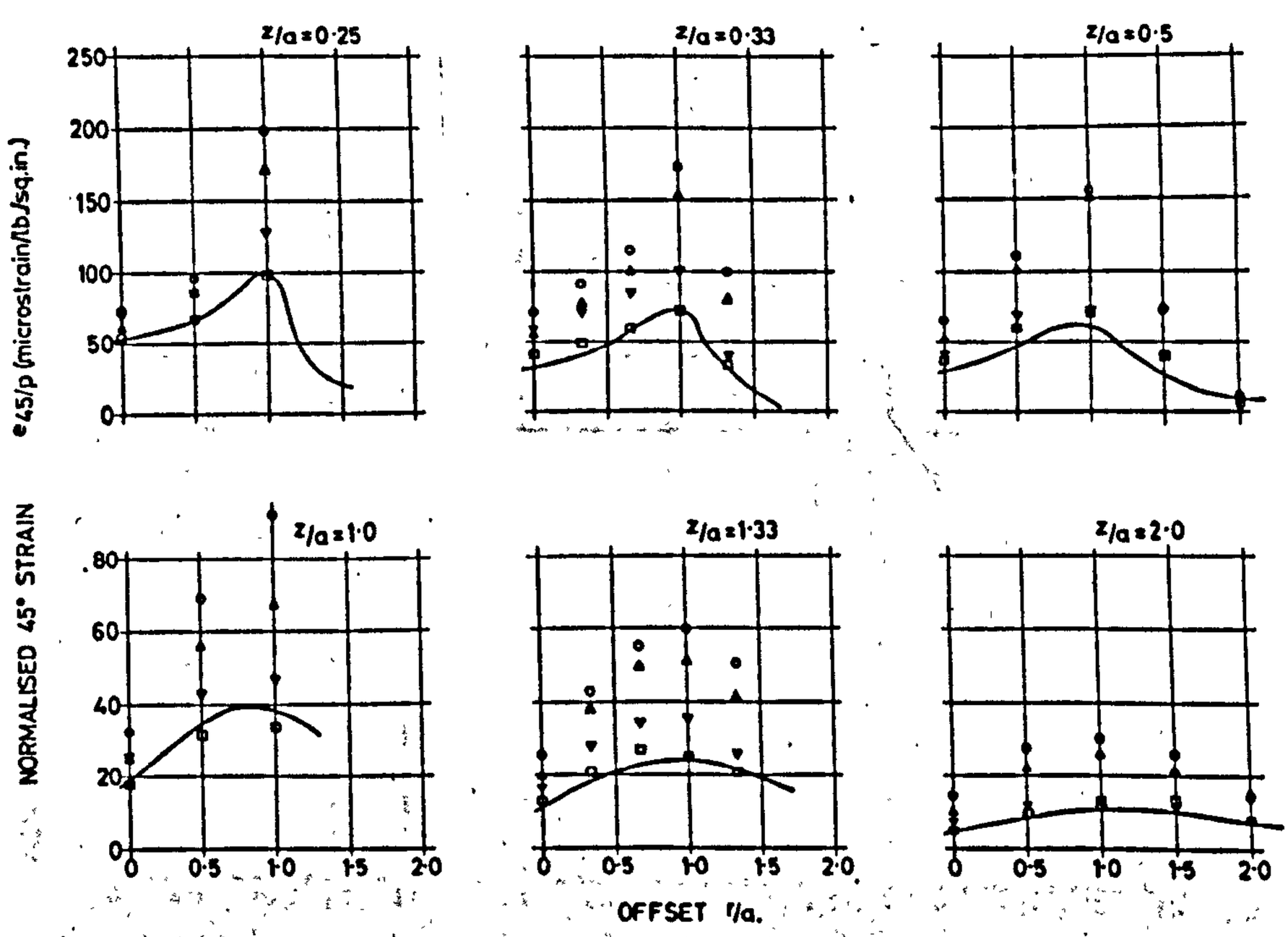

FIG. 7.17 45° STRAIN WITH RADIUS - SINGLE LAYER SYSTEM

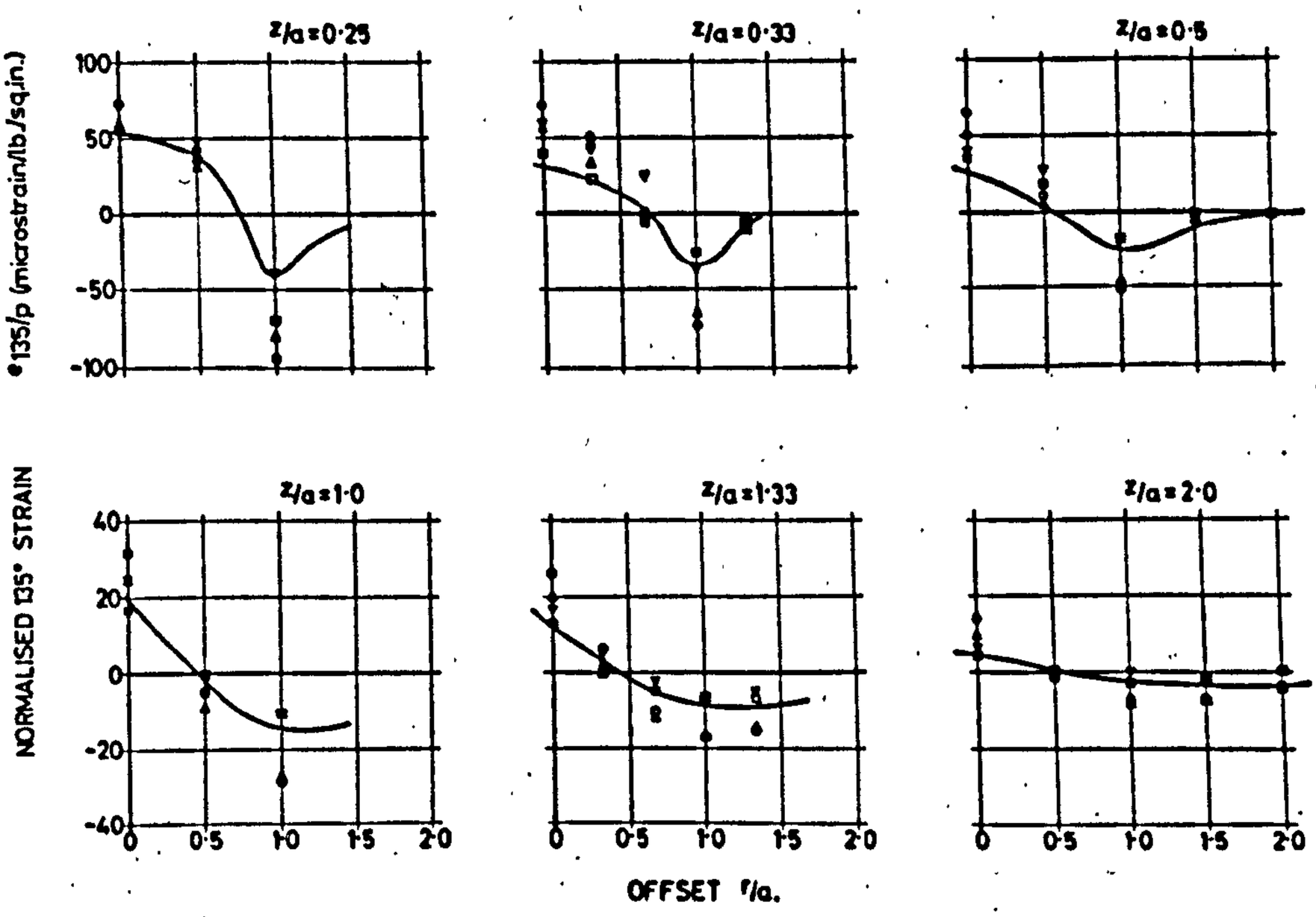

FIG. 7.18 135° STRAIN WITH RADIUS - SINGLE LAYER SYSTEM

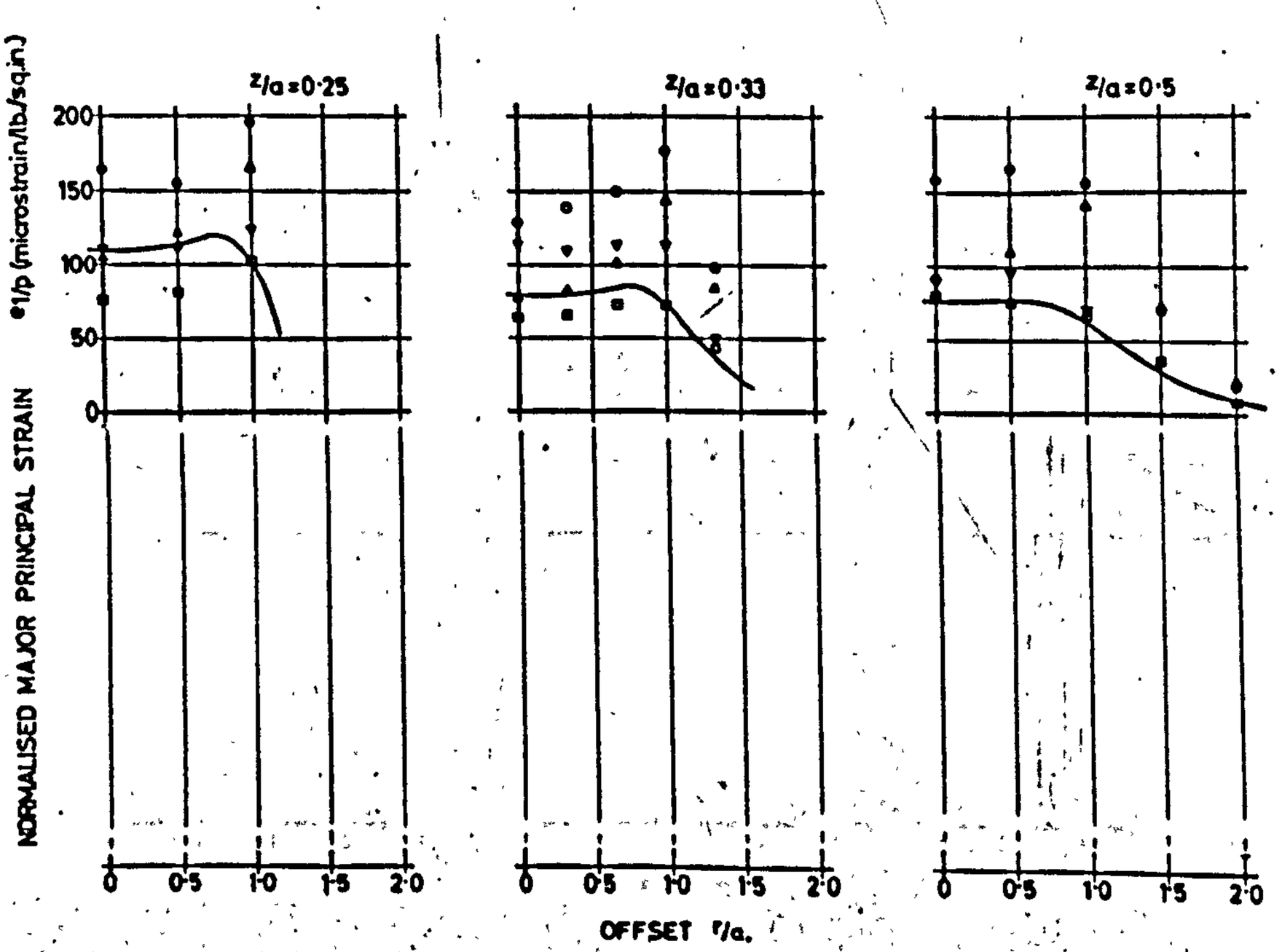

FIG. 7.19 MAJOR PRINCIPAL STRAIN WITH RADIUS - SINGLE LAYER SYSTEM

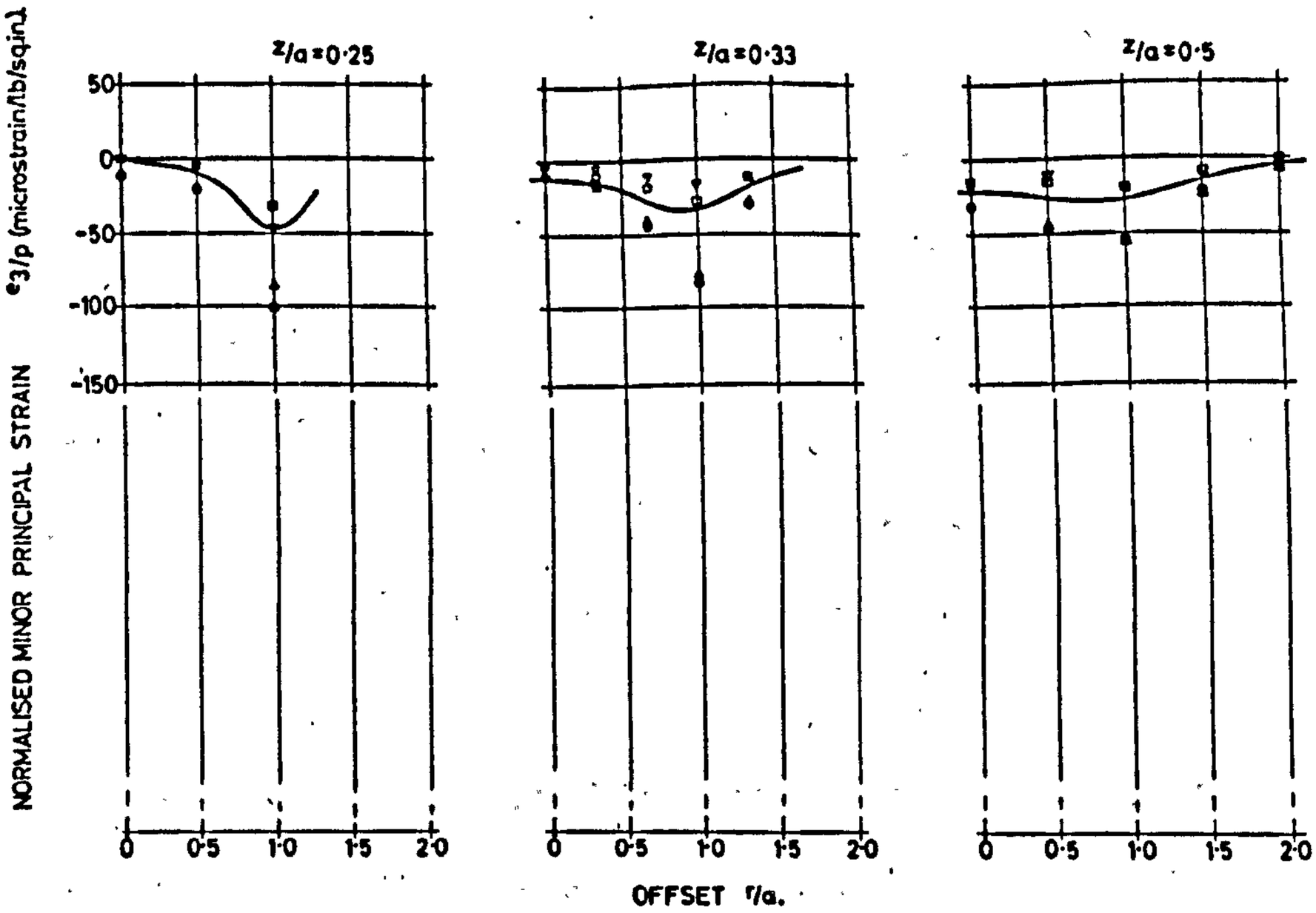

FIG. 7.20 MINOR PRINCIPAL STRAIN WITH RADIUS - SINGLE LAYER SYSTEM

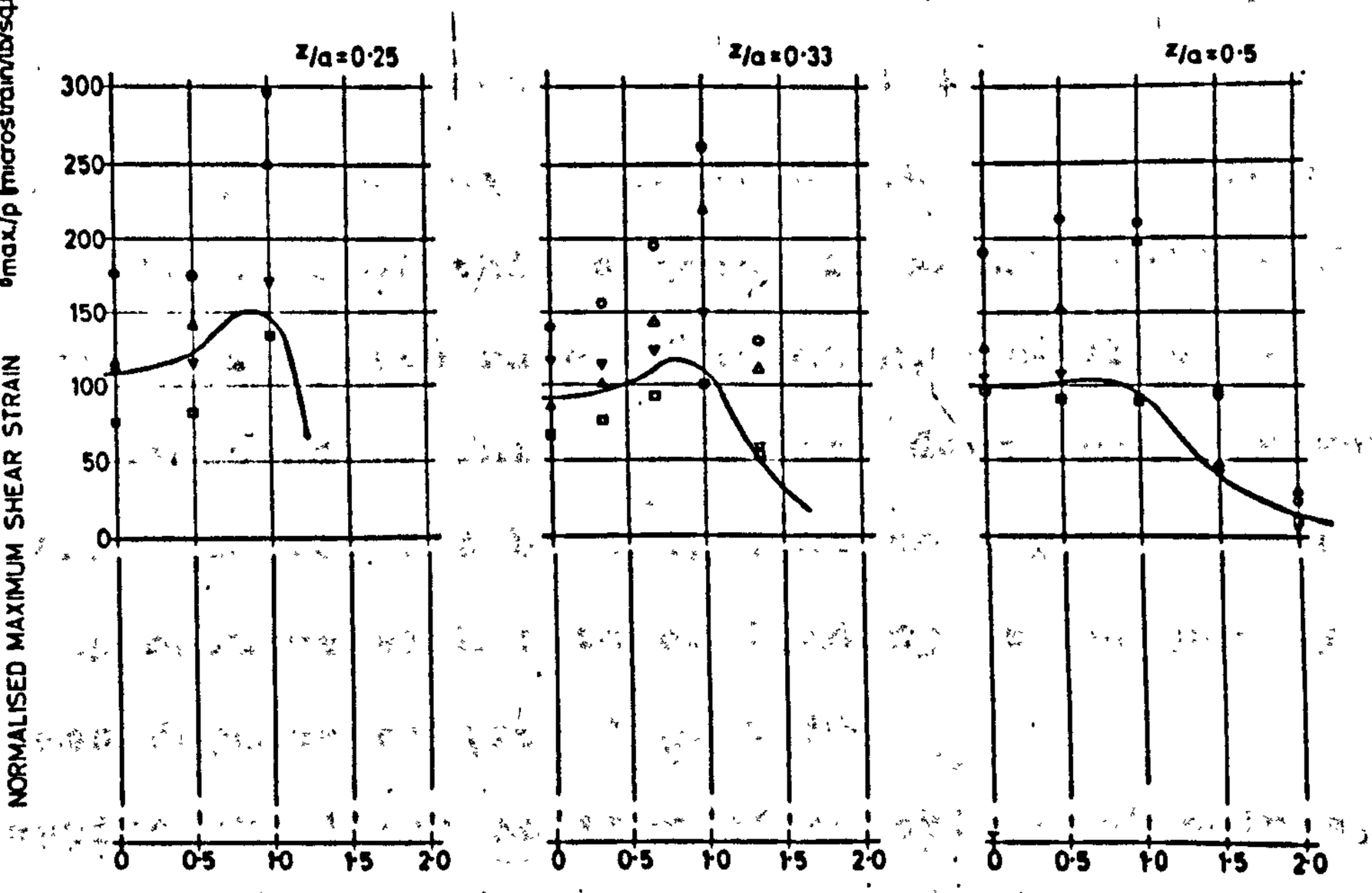

FIG. 7.21 MAXIMUM SHEAR STRAIN WITH RADIUS - SINGLE LAYER SYSTEM

rate of loading. Because of the non-linear stress/ strain relationship for the soil, a high contact pressure producing a high stress level, and hence a low modulus, will cause a high strain. The converse will be true for a low contact pressure. This trend of increasing strains with contact pressure can be easily seen on most plots.

The trend with rate of loading is for strain to decrease as the rate increases. This trend is the converse of that for stress and is considered to be caused by pore pressure dissipation. At fast rates of loading little pore pressure dissipation has time to take place and hence low strains result, while at slow rates of loading, a larger amount of dissipation causes higher strains. Because of this affect, it should follow that modulus increases with rate of loading, and this is generally accepted. This conclusion does not, however, emerge from the results herein, because any trend for increasing modulus with rate of loading is swamped by its stress dependence (see fig. 7.1).

Despite the large scatter of experimental points, there is tollerably good agreement with the theoretical lines, particularly if a mean experimental line is imagined on the plots. This has in fact not been included

so as to avoid crowding. 45° Strains are higher than theory and show a large amount of scatter under the edge of the loaded area. At this radius ($^{r}/_{a} = 1$) the 45° strain is approximately equal to the major principal strain, and hence is large. The trend with contact pressure also happens to be particularly marked at this radius, as the stress level has fallen to the steep part of the modulus/stress curve (fig. 7.1) i.e., $p_1 \leq 10$ lb/sq.in.

The derived results show poorer agreement with theory than those directly measured. The plots of major and minor principal strains show that maximum compressive and tensile strains at each of the depths investigated occur under the edge of the loaded area. The maximum compressive strain measured in the soil was about 3,000 micro-strain and the maximum tensile strain, 1500 micro-strain. These values were 45° and 135° strains at $^{r}/_{a} = 1$ and the shallowest depth ($^{z}/_{a} = 0.25$) and they were equal to the major and minor principal strains at this point.

The derived values for maximum shear strain show considerable scatter, again with the maximum value occuring under the edge of the loaded area at all depths. The increased scatter occurs because maximum shear strain is the sum of the major and minor principal strains

(see equ. 8) since these were always of opposite sign while showing an increased magnitude with increasing contact pressure.

With the exception of Sparrow and Tory[11,17] there has been little or no useful information published on the subject of "in-situ" strain measurements. The W.E.S.[12] used a rather large strain cell in their sand-test section without very much success.

Sparrow and Tory produced a limited number of strain measurements, which showed good agreement with theory, based on values of modulus arrived at by different means from those adopted in the present work. The values of strain measured by Sparrow and Tory are approximately twice as large as those reported herein, at corresponding depths. The same discrepancy is also evident in deflection measurements. Their theoretical lines are, therefore based on correspondingly lower values of modulus.

This large discrepancy is presumably a function of the difference in the two installations and indicates that repeatable strain results are not so easily obtainable as those for stress. The smaller values of strain reported herein indicate a stiffer soil, resulting from a combination of slightly lower moisture content and, possibly, better compaction. Sparrow and Tory's con-

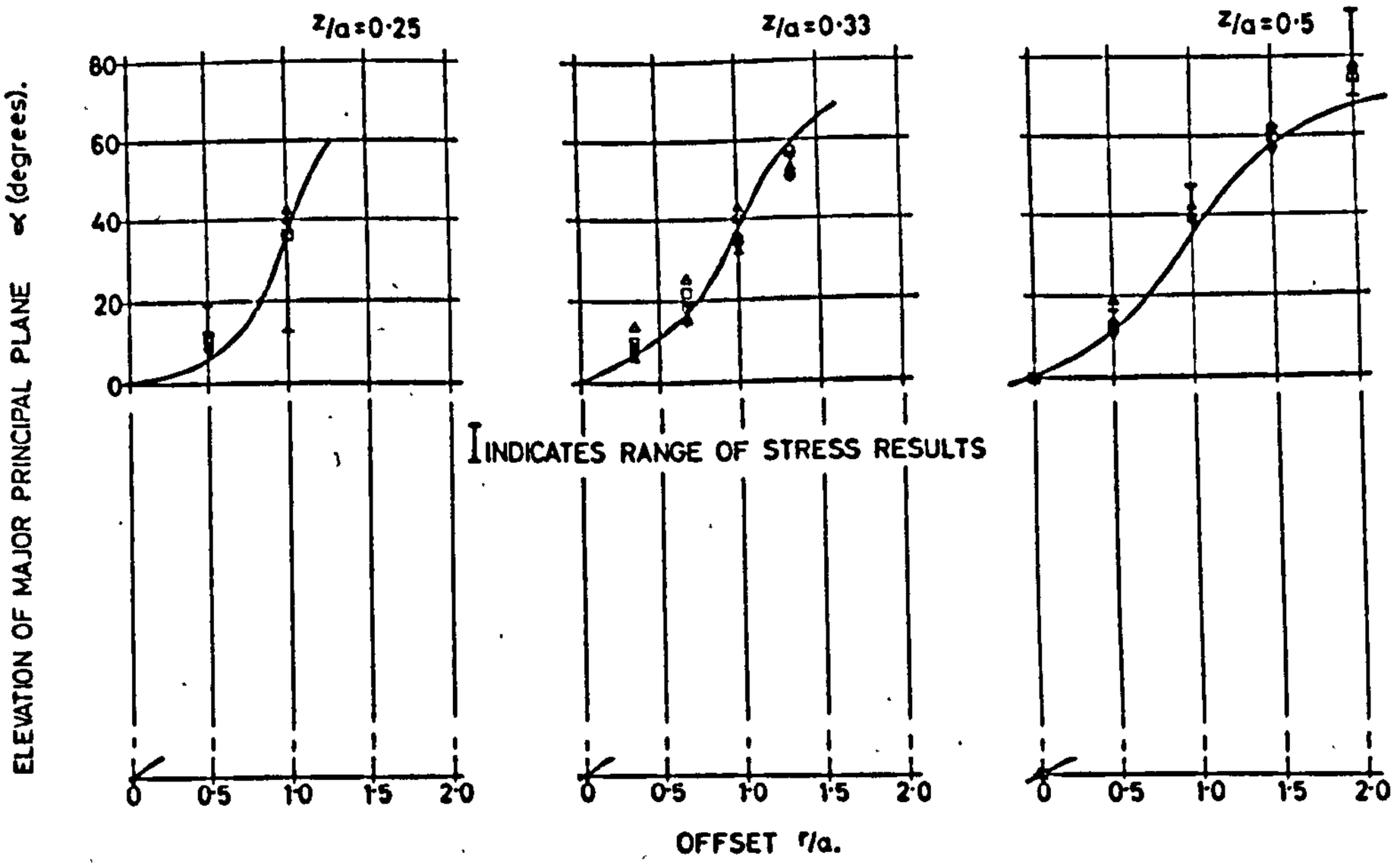

FIG. 7.22 ELEVATION OF MAJOR PRINCIPAL PLANE WITH RADIUS - SINGLE LAYER SYSTEM

clusions regarding dependence of strain on contact pressure and rate of loading are the same as those of the Author.

7.6 Principal planes

The elevation of the major principal plane from the horizontal was calculated from stress measurements and, independently, from strains. The individual results from strain measurements are shown in fig. 7.22, with

the range of stress results superimposed, and they are compared with appropriate theoretical lines. The two sets of results show very good mutual agreement, although results based on stress measurements show more scatter. Agreement with theory is good, and the fact that principal planes of stress and strain are coincident indicates that the soil is isotropic.

There is a noticeable lack of scatter of principal plane positions for strain in view of the large scatter found generally on strain distribution plots. The reason for this is that the angle of elevation is independent of modulus (see equ. 6)

7.7 Surface deflection

Variation of vertical surface deflection with radius is shown in fig. 7.23 for each of the three sizes of loaded area used. The theoretical lines have been derived so as to provide agreement with measurements on the axis as described in section 7.2. Table 7.2 shows the values of modulus which were used, all being less than those of Table 7.1 for calculating theoretical strains at the 3 in. depth. Vertical deflection must be a summation of vertical strains at various depths, or if vertical strain is plotted against depth, the area

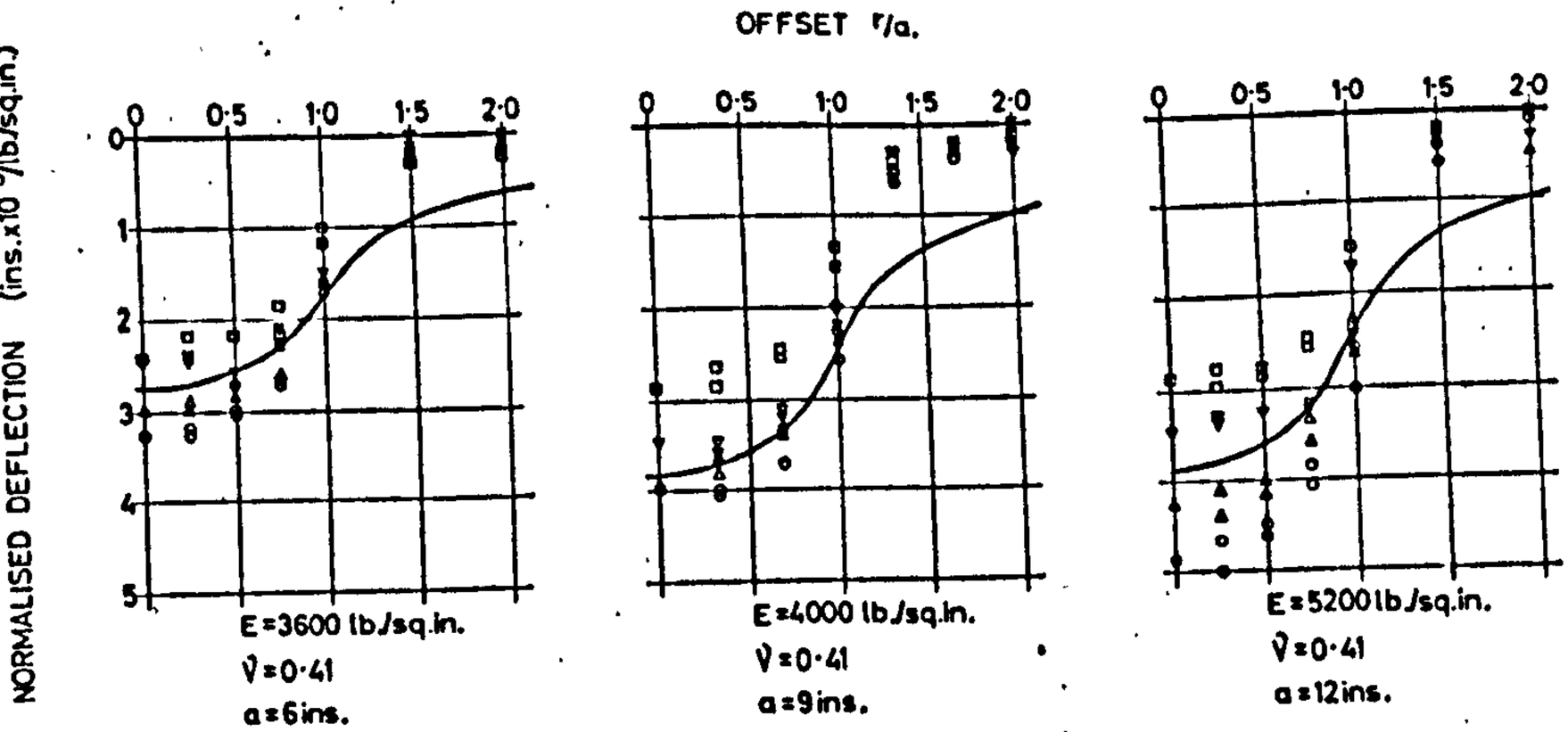

FIG. 7.23 VERTICAL SURFACE DEFLECTION WITH RADIUS - SINGLE LAYER SYSTEM

under the resulting curve. The low values of modulus needed to predict deflections on the axis indicate that these deflections are mostly caused by vertical strains at, and just below, the surface, where the stress level is high.

A check was made to see whether measured vertical strains when summed, agreed with measured vertical surface deflection. Fig. 7.24 shows the variation of vertical strain with depth for a = 6 in. This is obtained by superimposing all six effective depths and the values of strain are taken as the mean beneath the loaded area,

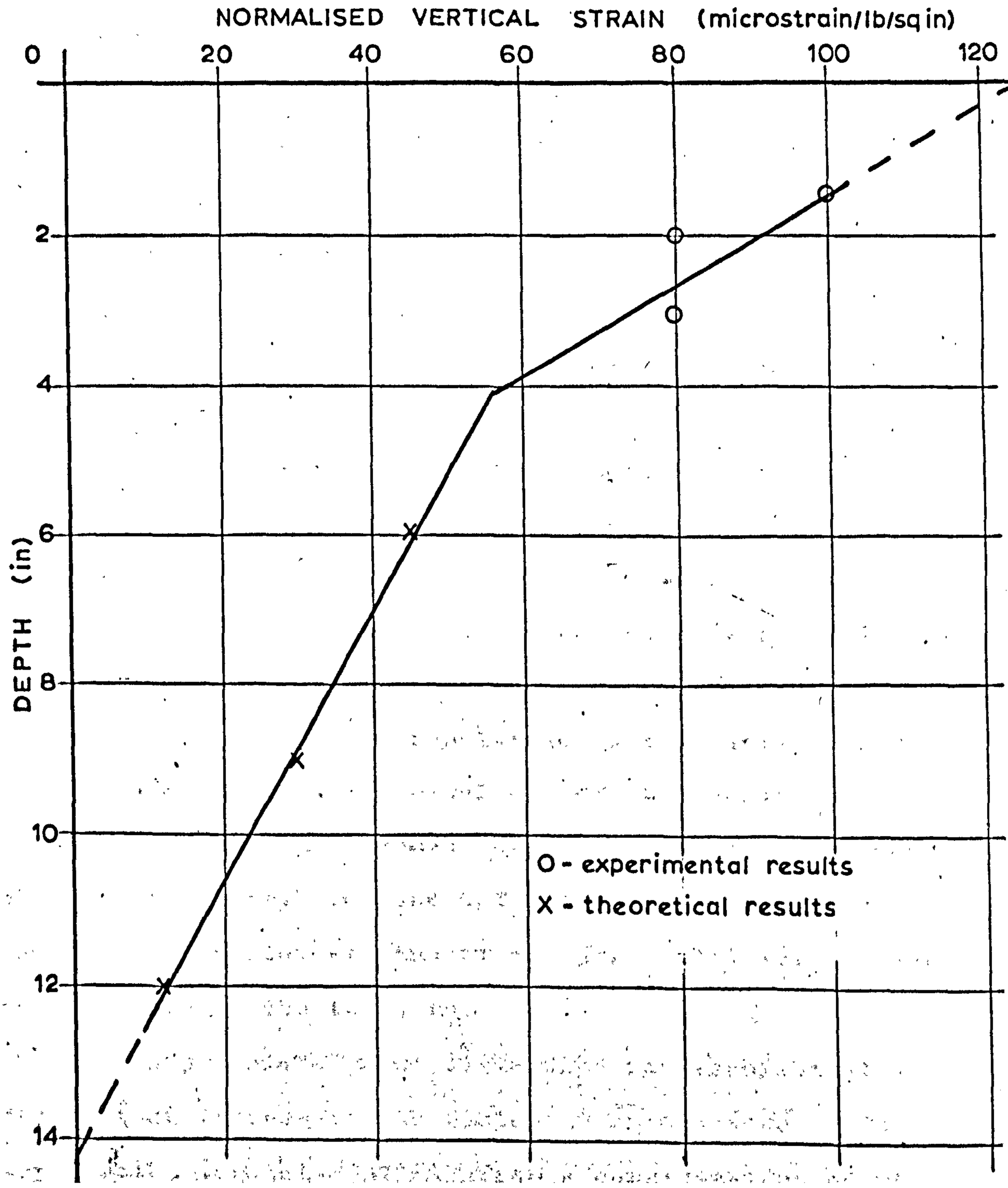

FIG. 7.24 VERTICAL STRAIN WITH DEPTH. a = 6 in.,

i.e., the mean of all values for $0 \leq \frac{r}{a} \leq 1$. The lower three values are theoretical strains, because no experimental ones were available. It was clear from this plot that strain increased rapidly near the surface, but for an initial calculation the dotted line extrapolations were added to a straight line approximation of the actual strain variation. The area under the resulting figure gave a value of 0.7 for the mean normalised deflection beneath the loaded area. This was much smaller than the measured value of about 2.3. There are two possible explanations for this discrepancy. Firstly the deflection gauge, being less accurate than the strain cell could have been over-registering vertical deflections. Secondly, the assumed extrapolation to the surface, very much under-estimated the magnitude of strains at this level. This second argument supports the idea mentioned above that vertical surface deflection is caused very largely by vertical strains at and just below the surface, in this case in the top 3 in.

The appropriate value of modulus for theoretical deflections increased with radius of loaded area. An explanation for this follows from a consideration of the theoretical expression for vertical surface deflection, i.e.,

$$w_z = \text{Const.}\ x(1 - \nu^2)\ .\ p\ .\ {}^{a}/_{E}$$

where p = contact pressure, a = radius of loaded area.

$\therefore$ Normalised deflection $\frac{w_z}{p} \propto \frac{a}{E}$ for p = constant.

$$\therefore E \propto \frac{a}{\left(\frac{w_z}{p}\right)}$$

The values of the function $a/\left(\frac{w_z}{p}\right)$ increase with increasing a, indicating an increase in E also. If there were a unique value of E for the soil this function would remain constant.

The trends with contact pressure and rate of loading are the same as for strains and occur for the same reasons. Duplicate readings taken at the same radii but on different sides of the transducer (see fig. 7.23) show close agreement and a mean line through all experimental points would agree with the theoretical lines beneath the loaded area. At greater radii the measured deflections are much smaller than theory, indicating possibly, a higher value of modulus to be relevant in these areas having lower stress levels. This illustrates better than the strain distribution plots, the difficulty in taking one value of modulus for a particular depth, since modulus, being stress dependent, increases with radius as well as depth. It also indicates that to assume a variation of modulus with depth beneath the loaded area may be valid

i.e., for $^{r}/_{a} \leq 1$, this matter being dealt with in the next section.

The pattern of comparison with theory shown here agrees with that obtained by Tory[11] and the W.E.S.[13] who also showed the same trends with contact pressure.

7.8 Multilayer approach

The following analysis is based on the original calculations for modulus, but actual values are not likely to be very different as indicated in section 7.2. From the foregoing discussion it is clear that modulus varies with stress level. In obtaining theoretical solutions for strains using Ahlvin and Ulery's tables,[27] one value of modulus has been chosen for calculating strains at each depth. This implies that the soil mass as a whole adopts the chosen value of modulus, whereas in fact the modulus varies with location for a particular stress distribution.

If the variation of modulus is thought of in terms of position rather than stress level, it is apparent that it varies both with depth and radius since stress levels generally decrease with distance from the applied load. If the radius is restricted to that of the loaded area, the modulus may be considered to vary with depth alone.

In fig. 7.25 an approximate set of contours of modulus have been shown within this range of radius to indicate that the change in modulus with radius at a particular depth is not too great. This approach could be made more accurate by further restriction of the radius.

Although the system resulting from this approach has modulus varying continuously with depth, the curve may be approximated to a series of steps. If this is done, Jones' multilayer computer programme[28] can be used to analyse the system by considering it as a number of layers, each layer having a different constant value of modulus.

Different contact pressures give rise to different stress levels at a particular point and hence two separate systems have been considered for the two nominal contact pressures which were used. For each system the variation of modulus with depth has been determined taking mean values of modulus at $^{r}/_{a} \leq 1$ for each depth. Six effective depths resulted from measurements using three different sizes of loaded area. These were superimposed, so as to convert them to absolute depths by considering one value of radius of loaded area. This was taken as 12 in. and the resulting depths at which measurements were taken are 3, 4, 6, 12, 16 and 24 in.

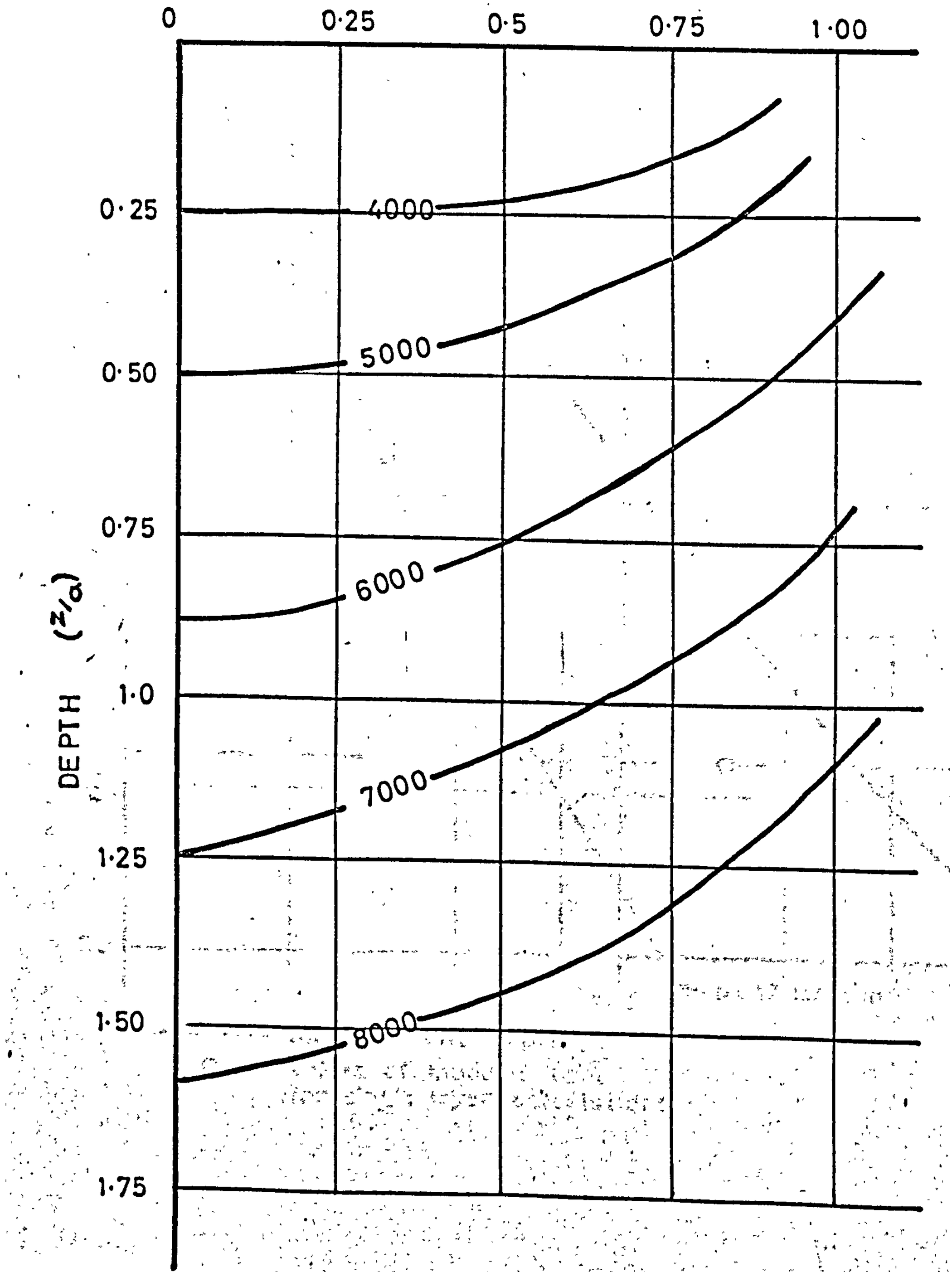

FIG. 7.25 CONTOURS OF EQUAL MODULUS

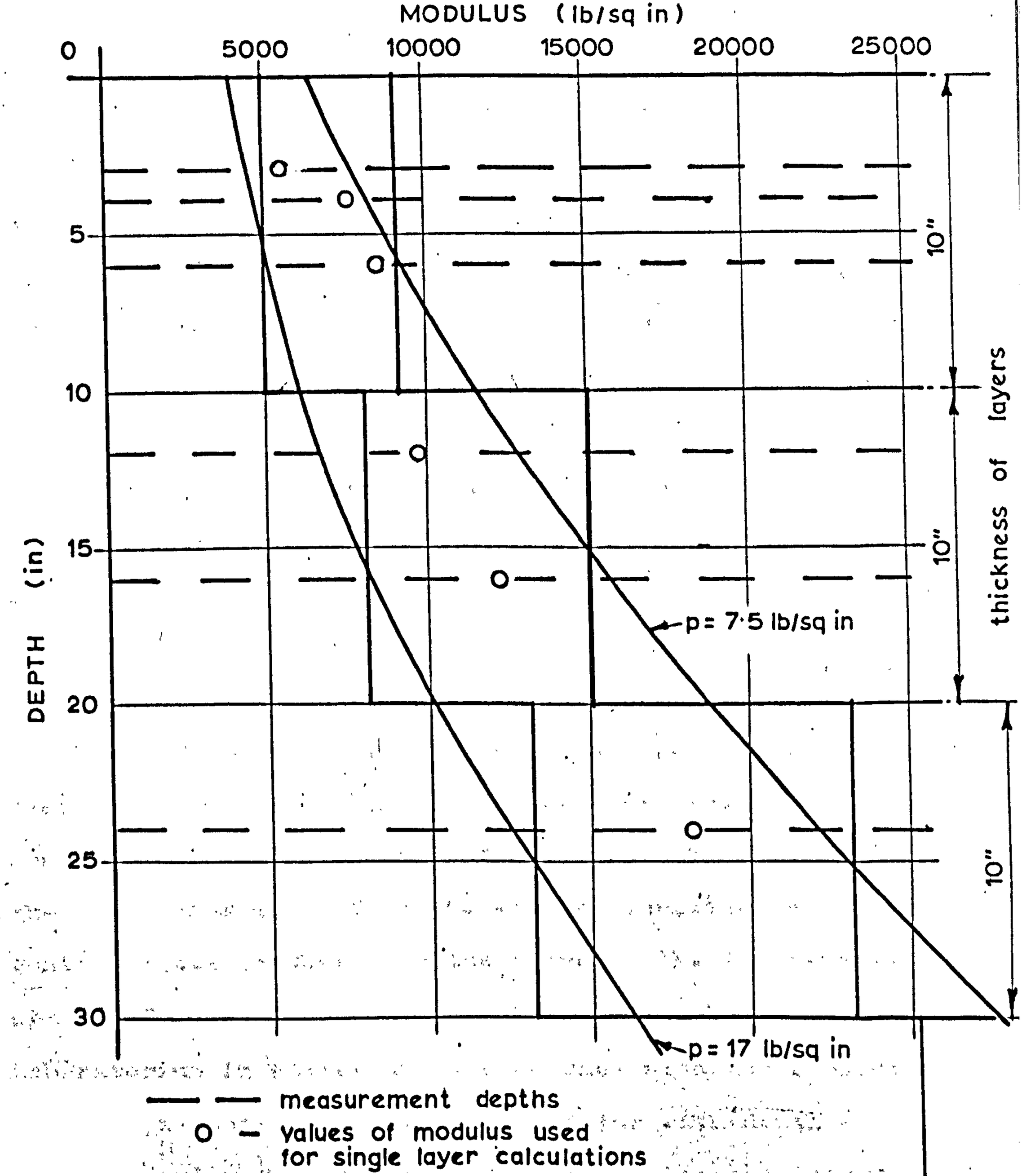

FIG. 7.26 VARIATION OF MODULUS WITH DEPTH

Fig. 7.26 shows the variation of modulus with depth for both systems. The lower contact pressure producing low stress levels results in higher values of modulus.

By treating a homogeneous soil mass as a series of layers, discontinuities are introduced at the assumed interfaces. It was therefore arranged that the interfaces should be away from the depths at which strains were required. The discontinuities can be reduced, and the stepped system can better approximate to the curve if more layers are taken. However, with a large number of layers the computing time was prohibitive and so the systems were each divided into four layers, the top three being 10 in. thick in each case. It can be seen from fig. 7.26 that the depths at which strains were required fall approximately in the centre of a layer. This means that the value of modulus from the stepped function is approximately equal to that from the curve. The future development of Jones' programme at the Koninklijke-Shell Laboratorium in Amsterdam is concerned with the consideration of a continuously varying modulus with depth. If the particular function can be matched with the actual variation, then a very significant step forward will have been achieved. The present programme has only been recently developed, however, and is itself a big advance

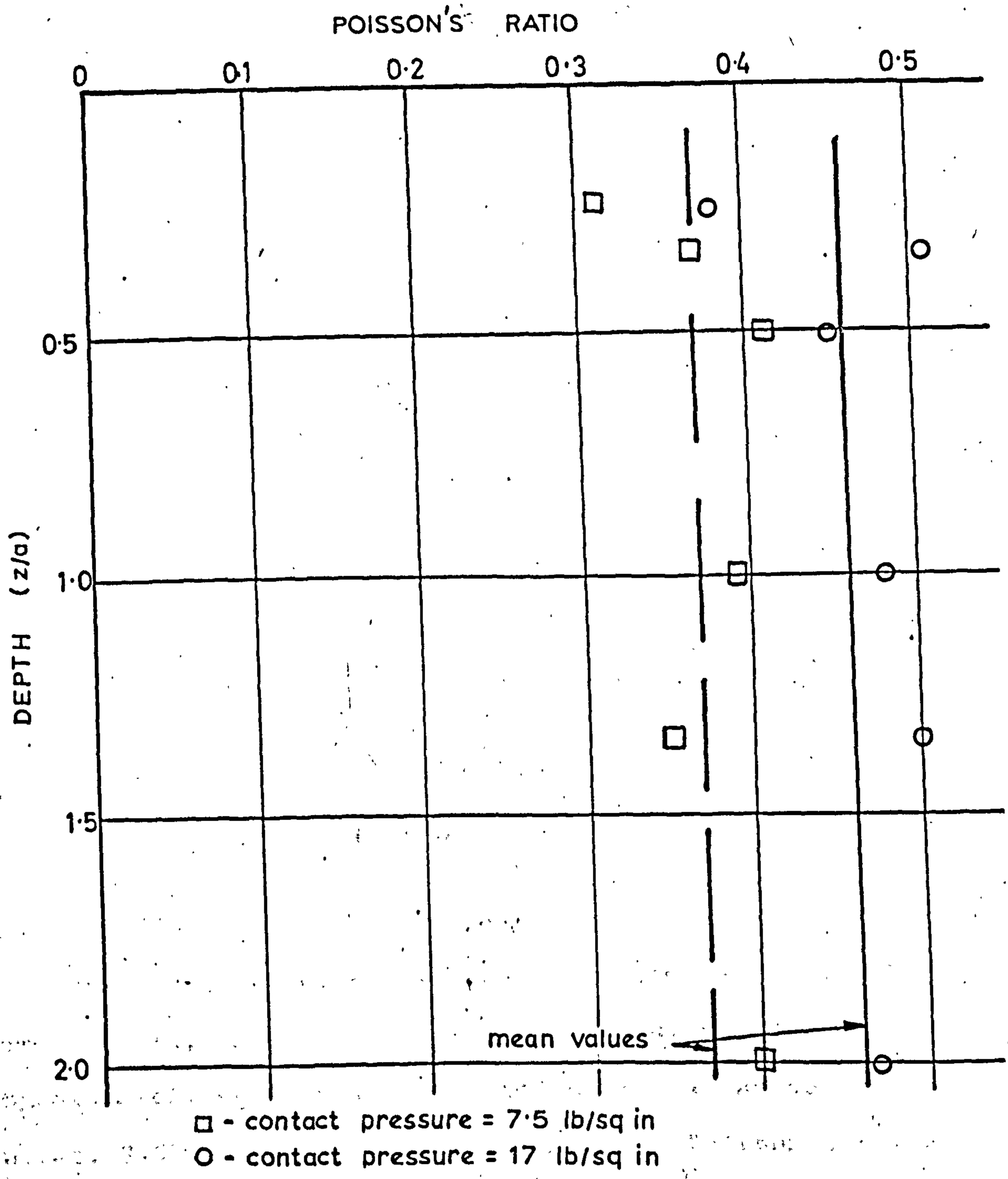

FIG. 7.27 VARIATION OF POISSON'S RATIO WITH DEPTH

TABLE 7.4 MULTILAYER SYSTEMS FOR CALCULATION OF THEORETICAL SINGLE LAYER SYSTEM RESULTS

Layer No.	Layer Thickness (in.)	Modulus (lb/sq.in.)	
		System 1	System 2
1	10	5000	9000
2	10	8000	15000
3	10	13000	23000
4	$\infty/2$	25000	40000
Poisson' ratio		0.46	0.35
Nominal contact Pressure (lb/sq.in.)		17.0	7.5

$a = 12$ in.

on previous theoretical solutions.

The variation of Poisson's ratio with depth was also investigated, and the two systems had a different, but approximately constant, value with depth as can be seen in fig. 7.27. The values of modulus and Poisson's ratio used in both systems are shown in Table 7.4.

The computer programme was run with this data to produce a complete description of stress and strain at the

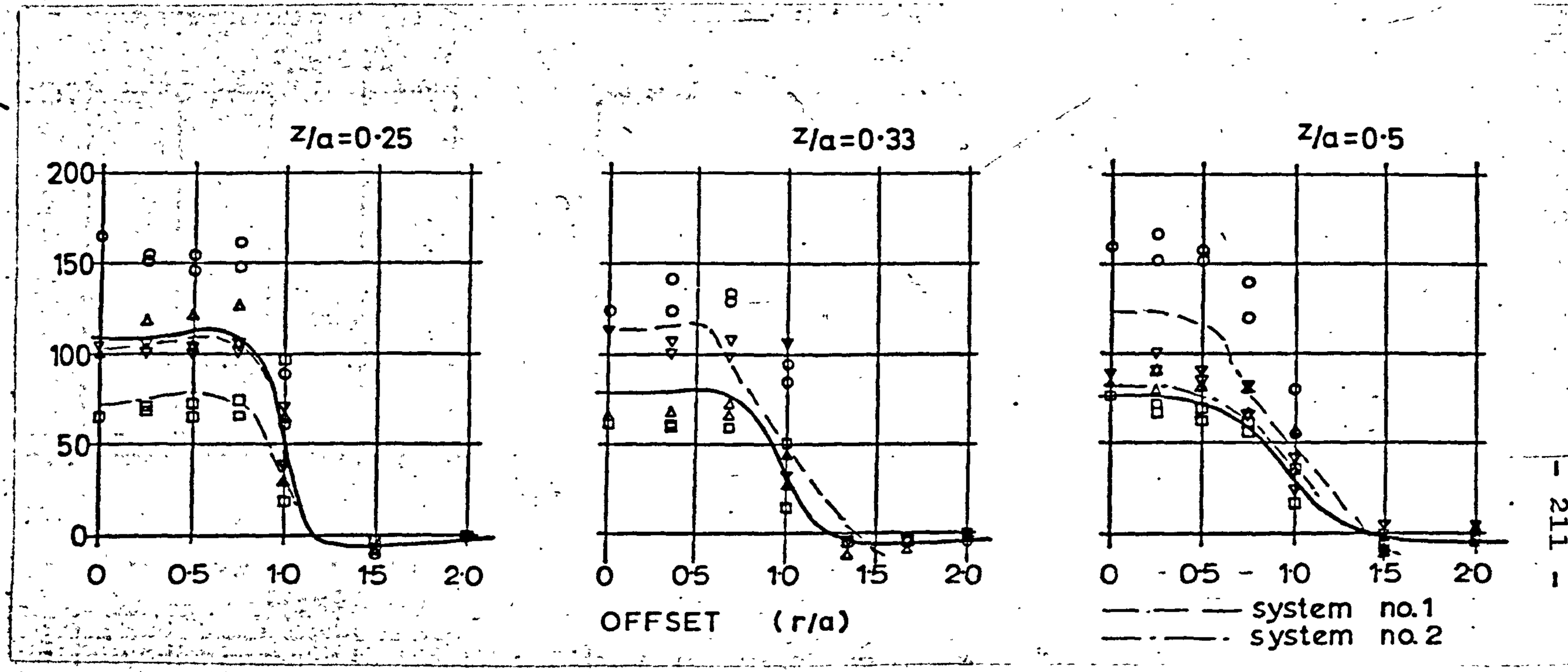

FIG. 7.28 VERTICAL STRAIN WITH RADIUS - MULTILAYER THEORY

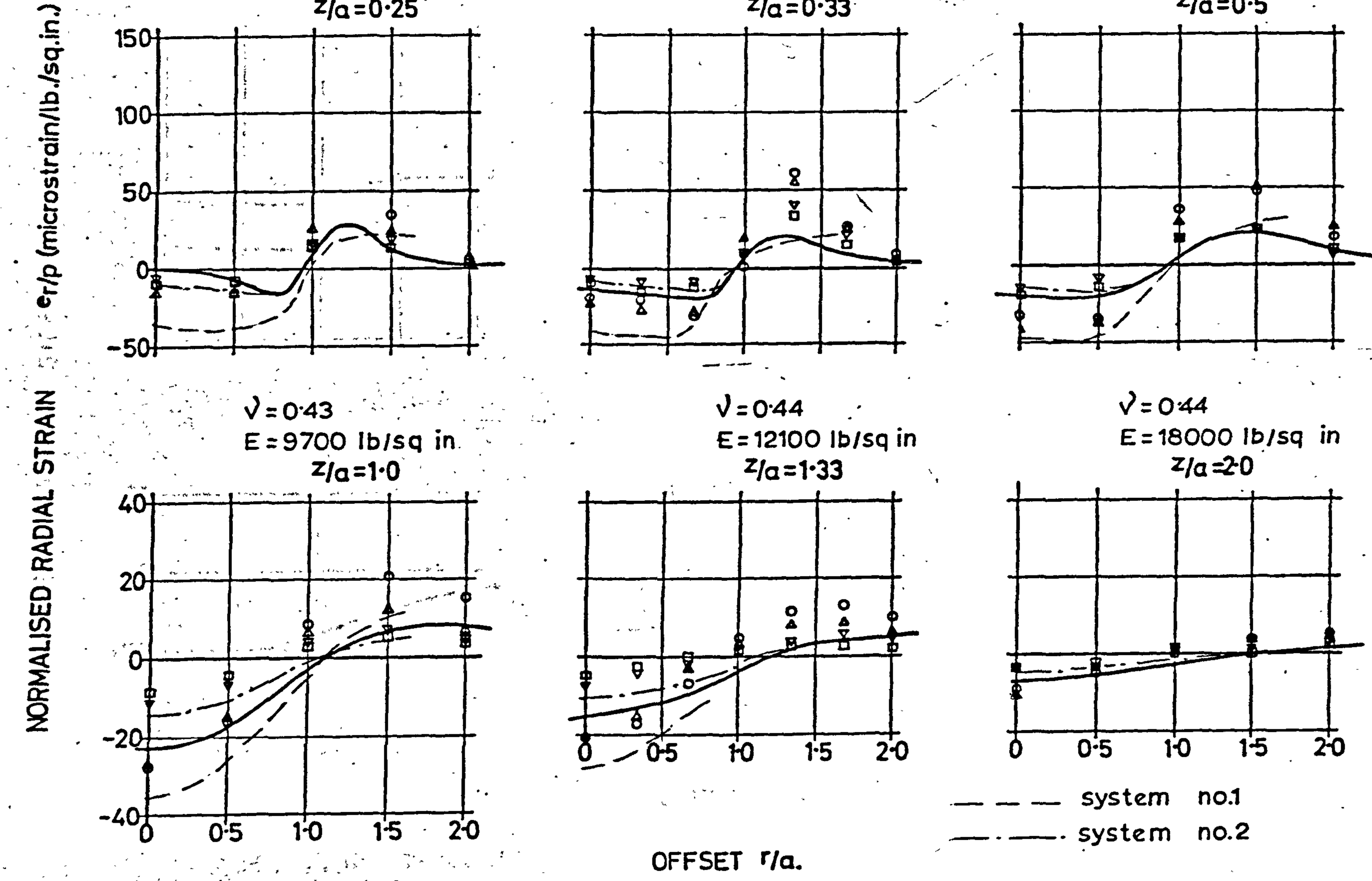

FIG. 7.29 RADIAL STRAIN WITH RADIUS - MULTILAYER THEORY

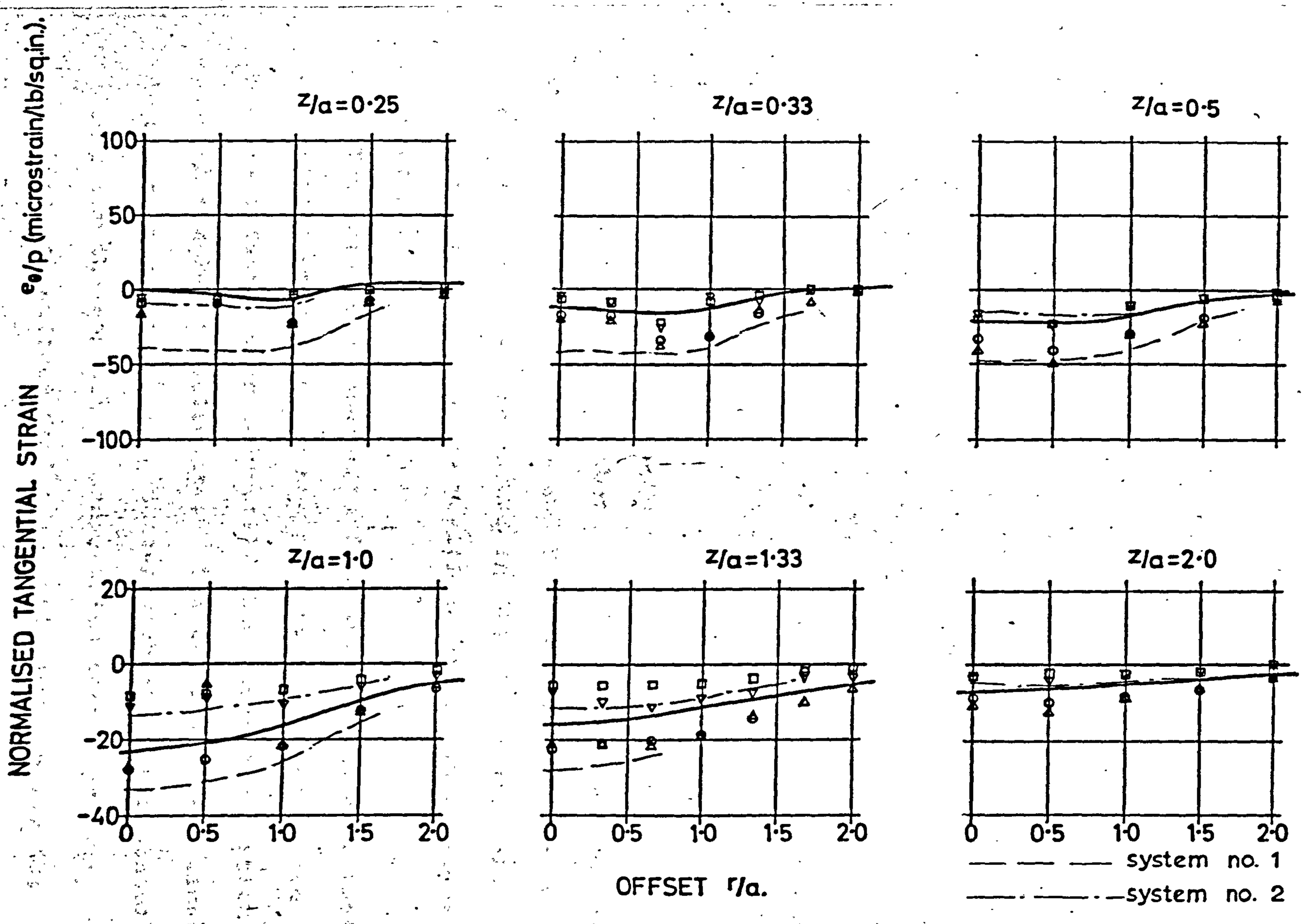

FIG. 7.30 TANGENTIAL STRAIN WITH RADIUS - MULTILAYER THEORY

required depths and radii and also values of vertical surface deflection. The values of stress were almost identical to those predicted by Boussinesq using Ahlvin and Ulery,[27] since they only depend on modular ratios which in this case were relatively near to and less than unity, which is the Boussinesq case.

Strain distributions have been plotted in figs. 7.28 to 7.30 for vertical, radial and tangential directions and they are superimposed on the experimental points and also the Boussinesq line. The dotted line for system no. 1 representing the high contact pressure should be compared with the appropriate experimental points (see Table 5.1) as should the chain dotted line of system no. 2. The values of modulus and Poisson's ratio used in the Boussinesq case are marked in fig. 7.29 as a guide to explaining the relative positions of the three lines on each plot.

The immediate conclusion from this exercise is that the multilayer results do not predict stress or strain measurements any more accurately than Boussinesq, which is much simpler to calculate. The two multilayer lines do not consistently agree better with the experimental points for the contact pressure which they represent.

Vertical surface deflection calculations for the

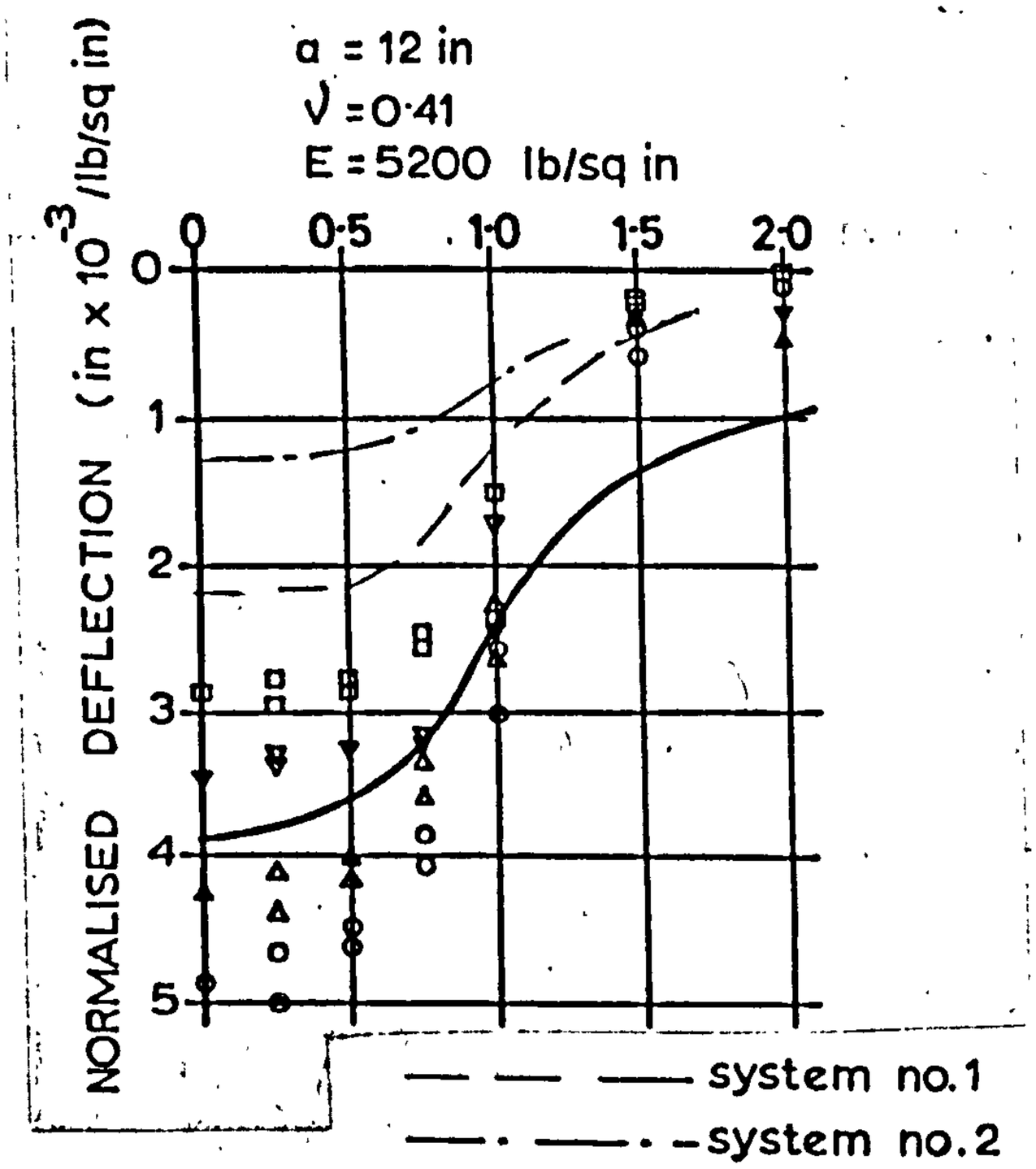

FIG. 7.31 VERTICAL SURFACE DEFLECTION WITH RADIUS - MULTILAYER THEORY

multilayer programme indicate lower values than those measured (fig. 7.31). The difference between the two lines is, however, about the same as that between experimental points for the two contact pressures. This low prediction may be caused by assuming too high a modulus near the surface. In section 7.7 a low value of deflection was also obtained by summation of strains.

In both cases extrapolation was relied on to predict behaviour in the top 3 in. of soil. The variation of modulus near the surface was, however, based on stress level and is thought to be the more reliable.

If the variation of modulus with depth is not so steep as to cause discrepancies between Boussinesq and multilayer stress predictions, then the following procedure may be adopted to calculate strains in the single layer system.

1. Assume a value of Poisson's ratio.
2. Calculate the first stress invariant, which is the sum of three orthogonal stresses, at the required point using Ahlvin and Ulery.[27]
3. Read off the value of modulus at that point from fig. 7.2.
4. Calculate strains from Ahlvin and Ulery using this modulus and the assumed Poisson's ratio.

If a reliable relationship between modulus and stress level such as fig. 7.2, can be obtained from triaxial tests for a particular soil, then this procedure could be extended to cater for any homogeneous soil mass.

CHAPTER 8 DISCUSSION OF RESULTS FOR THE TWO-LAYER SYSTEM

8.1 Modulus and Poisson's ratio

Values of modulus and Poisson's ratio were calculated from stress and strain measurements in the two layer system in the same way as for the single layer. In this case there were two materials to consider, since computations were again performed on results taken in the Keuper Marl, now forming the subgrade layer.

Because of the failure of a 45° pressure cell the complete set of stresses could not be obtained 3 in. below the interface. Results in the Keuper Marl were, therefore, originally confined to the lower depth, i.e., 12 in. below the interface, but these had to be abandoned because of the vertical strain cell error (see section 2.2). The few values of modulus correctly calculated at this depth are comparable to those from the single layer system and in fig. 7.2 they have been included in the plot of modulus against 1st stress invariant. It would have been possible with the available information to calculate values of elastic constants 3 in. below the interface, but they would not have been consistent with those obtained elsewhere. This is because the

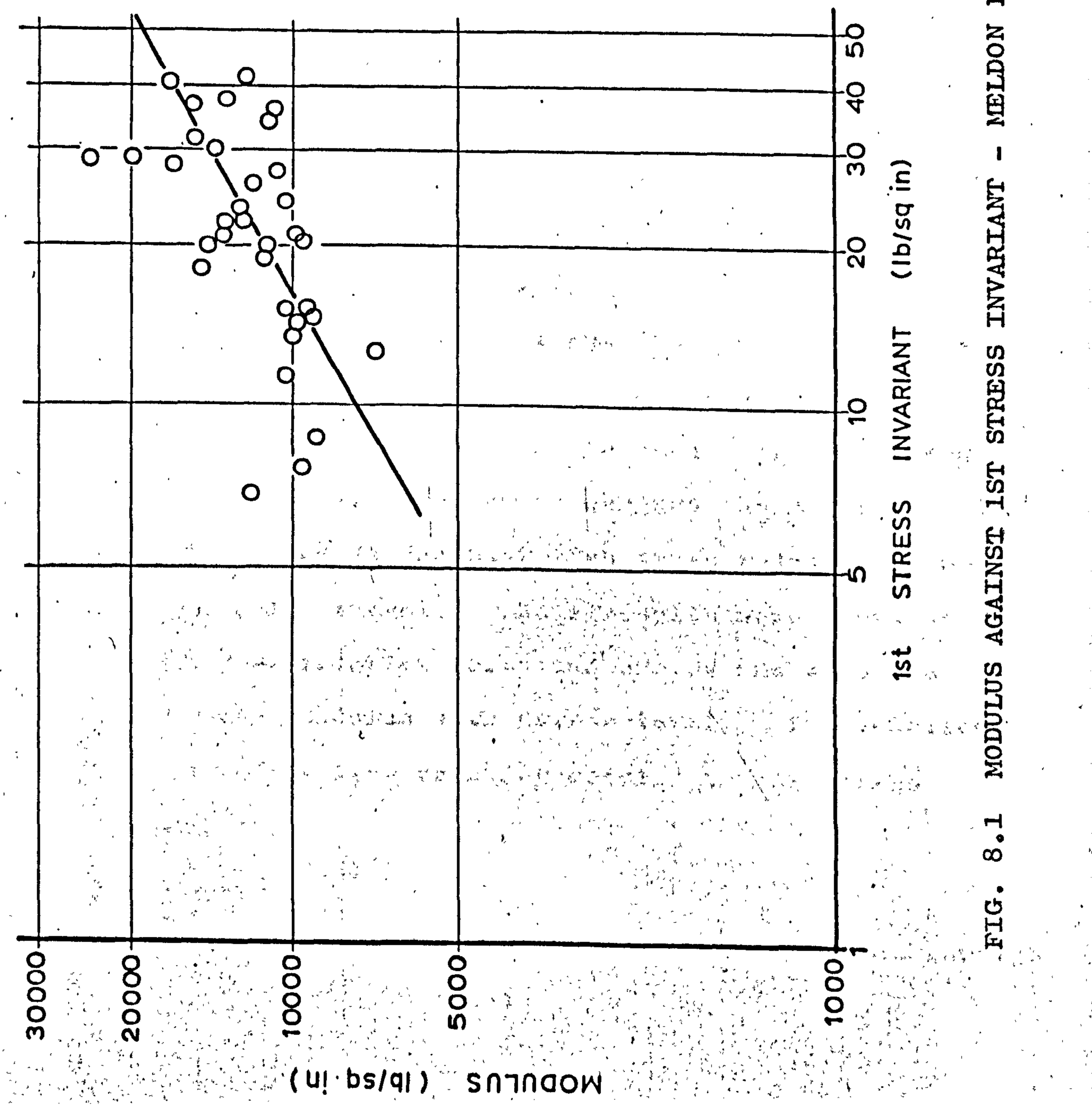
MODULUS AGAINST 1ST STRESS INVARIANT - MELDON DUST
1st STRESS INVARIANT (lb/sq in)
MODULUS (lb/sq in)
1
5
10
20
30
40
50
1000
5000
10000
20000
30000

FIG. 8.1

equilibrium check could not be carried out as a result of the lack of 45° and 135° stresses.

The variation of modulus with stress level in the upper layer of granular material is shown in fig. 8.1. Although the range of stress is somewhat limited, it is clear that the modulus increases with increasing stress level, which is the opposite effect to that observed for the Keuper Marl (fig. 7.2).

The stress dependence of modulus for clay and also for granular materials has been indicated by others and particularly in the context of pavement design by Seed et al.[6] It is of interest to compare the results obtained for the Meldon Dust with those reported by Seed et al for a dry gravel. Their results were based on repeated load triaxial tests and showed the same trend of increasing modulus with stress level. The equation of the straight line relating modulus to 1st stress invariant was:

$$E = 1900\ J_1^{0.61}$$

while the equation of the "best fit" straight line through the results in fig. 8.1 is:

$$E = 2040\ J_1^{0.57}$$

This correlation is remarkably close especially when considering how the results were obtained. The Meldon

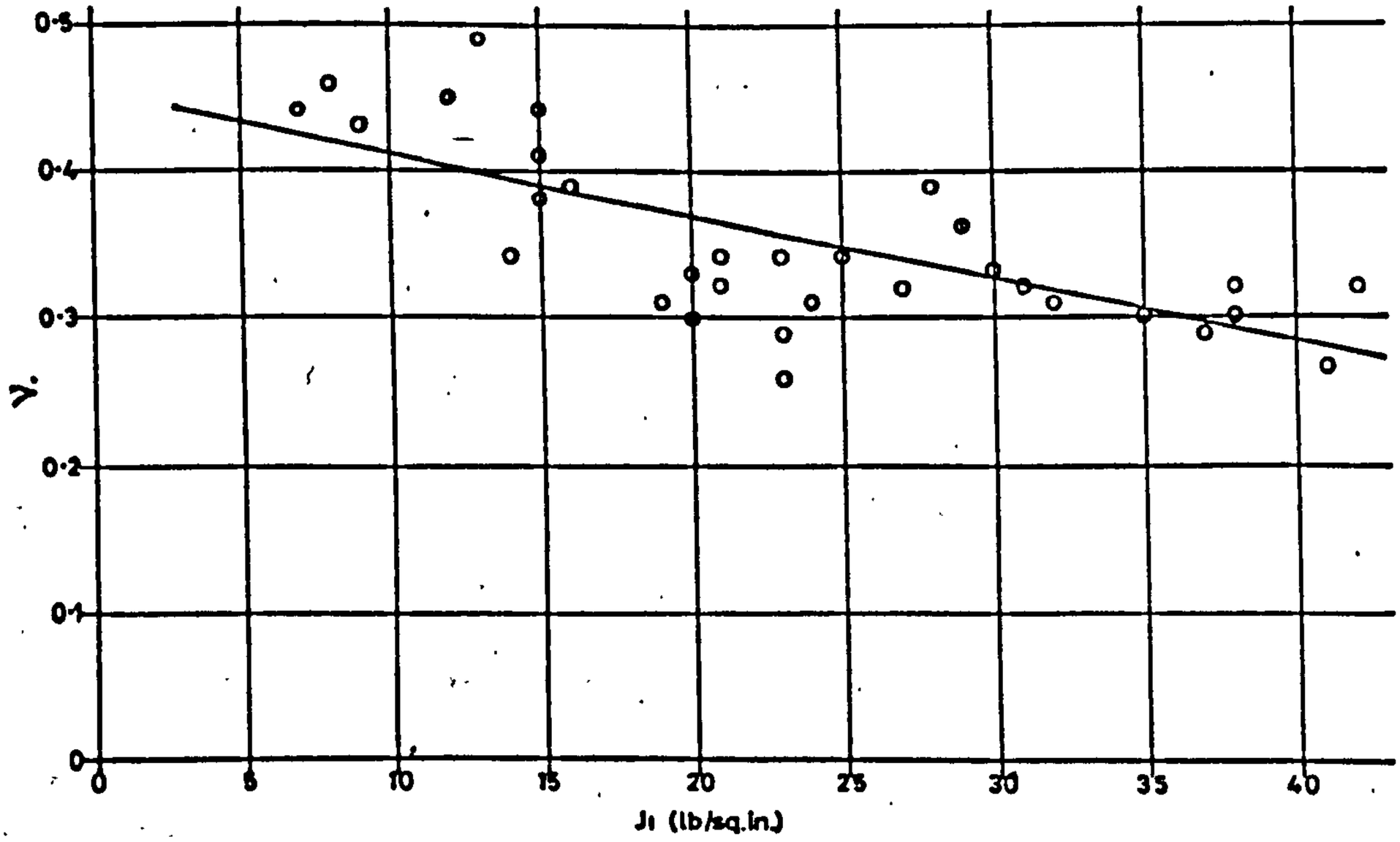

FIG. 8.2 POISSON'S RATIO WITH 1st STRESS INVARIANT - MELDON DUST

dust had a smaller particle size ($\frac{3}{8}$ in. maximum), and total stress as opposed to effective stress was used in the calculations of moduli. Understandably, scatter of results from in-situ tests was considerably greater than for the controlled laboratory specimens.

Poisson's ratio for the Meldon Dust appeared to vary with stress level. In fig. 8.2 it is plotted against 1st stress invariant and clearly decreases with increasing stress, whereas no noticeable trends were evident for Poisson's ratio of the Keuper Marl in the

single layer system.

8.2 Theoretical results

Theoretical results for the two layer systems were obtained in two ways. Firstly, Boussinesq solutions were calculated with the aid of Ahlvin and Ulery's tables[27] in exactly the same way as for the single layer system and secondly, Jones' multilayer computer programme[28] was used to compute various two-layer systems.

The values of modulus and Poisson's ratio used for these theoretical solutions are those originally calculated before the error in vertical strain 12 in. below the interface was discovered. Corrected calculations, which were less complete, indicated values of modulus within 30% of those used.

The problem in using Jones' programme was that of choosing the appropriate values of modulus and Poisson's ratio to use for each layer. This was resolved in almost the same way as for the single layer system. For the upper layer, the mean value of modulus calculated from experimental results in the centre of the layer was taken. In the lower layer, two values of modulus were used, one resulting from stresses and strains 12 in.

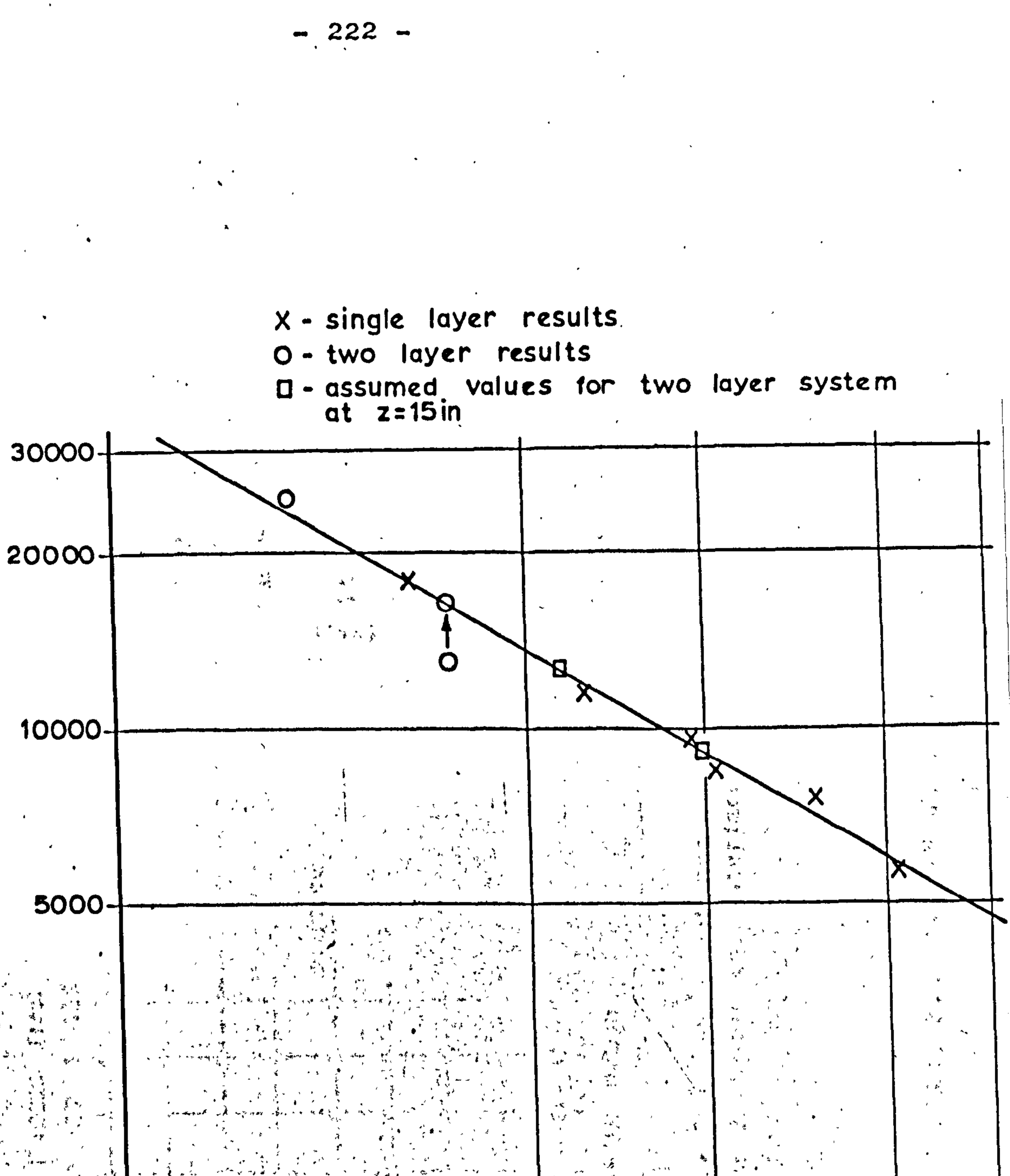

FIG. 8.3 MEAN MODULUS AGAINST 1ST STRESS INVARIANT - KEUPER MARL

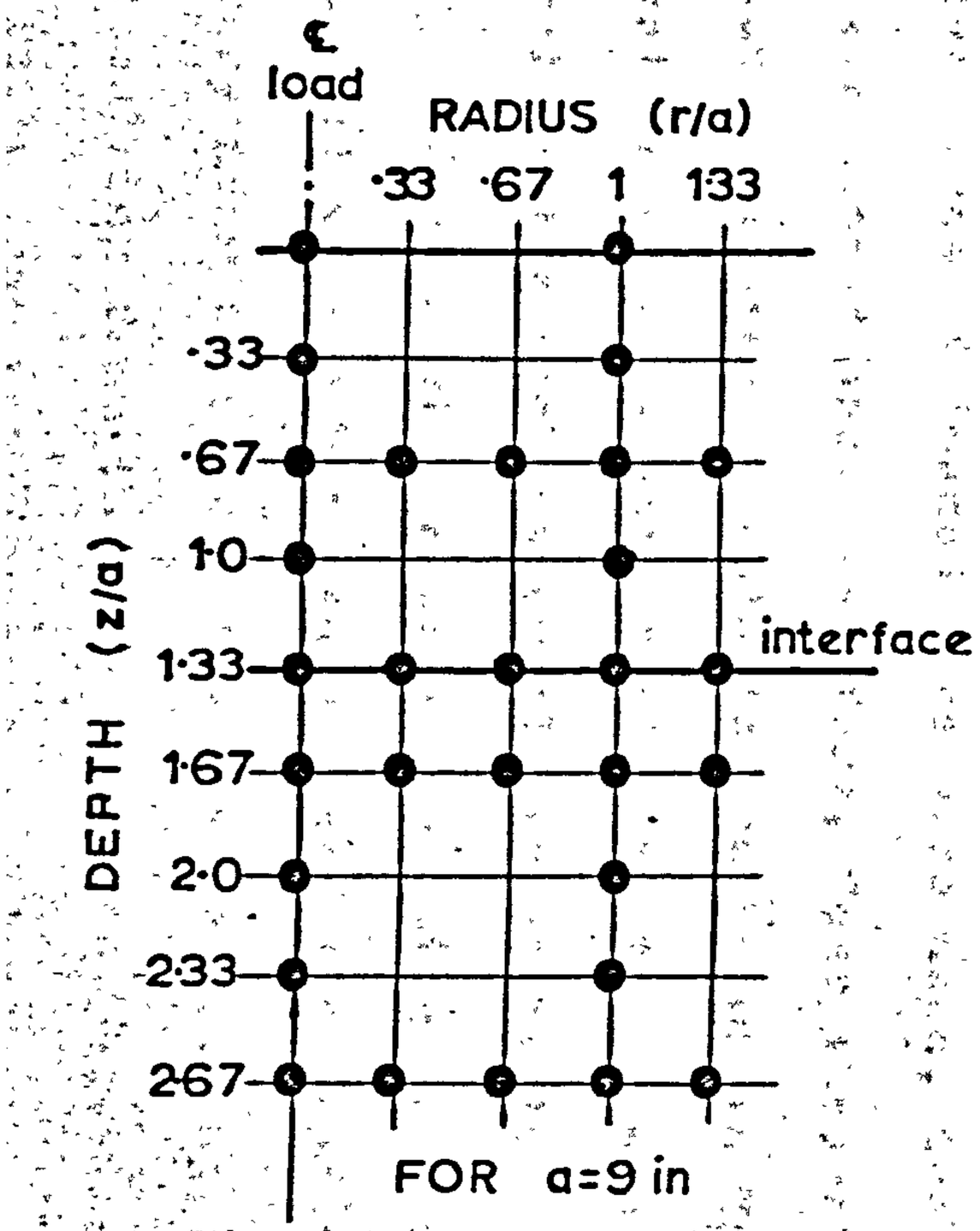

NOTE interfacial values obtained just above & below the interface.

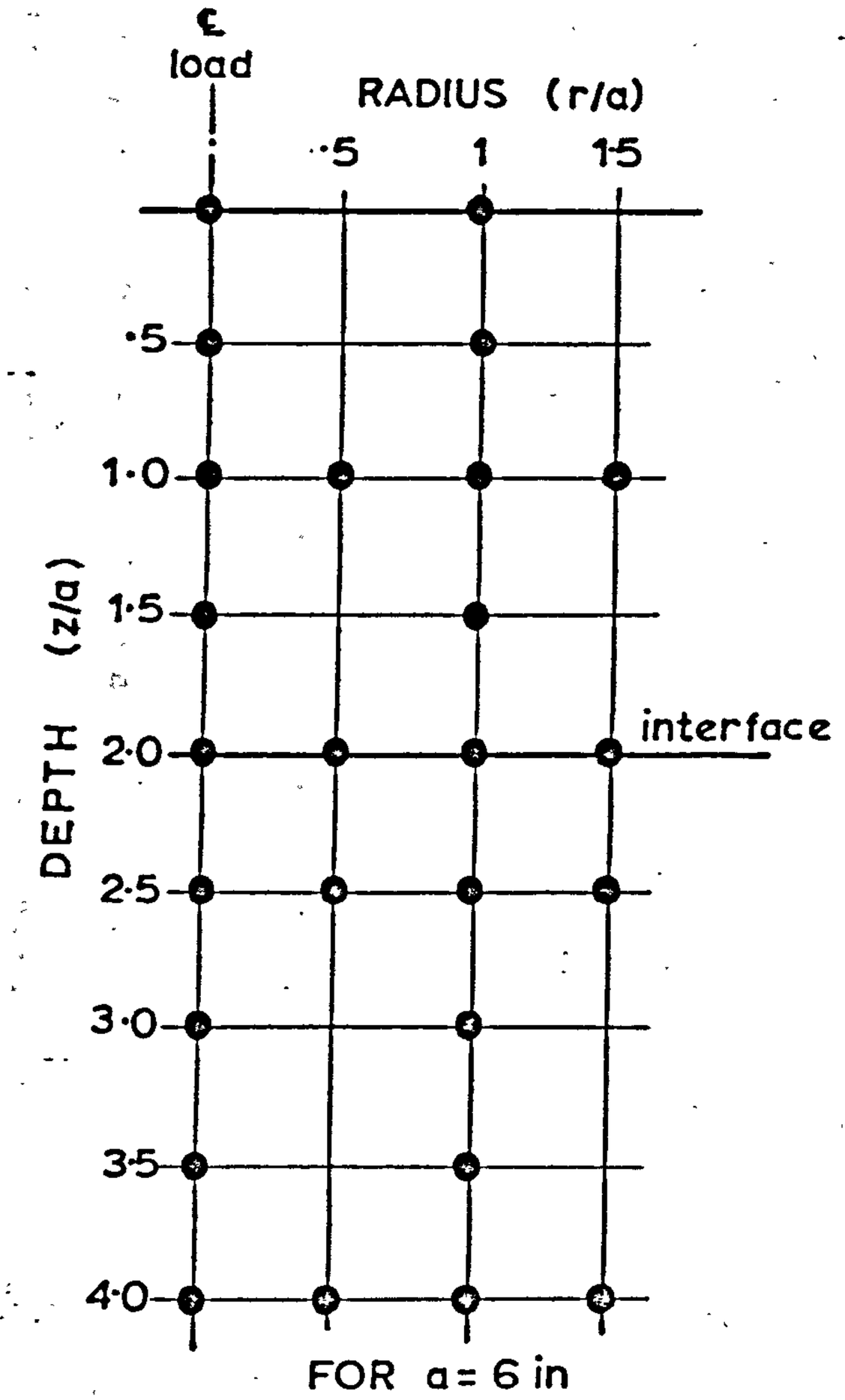

FIG. 8.4 POINTS WHERE TWO LAYER THEORETICAL RESULTS WERE COMPUTED

below the interface and the other was obtained indirectly from measurements 3 in. below the interface. An indirect approach had to be used here because, as explained in section 8.1, values of modulus were not calculated at this depth owing to a pressure cell failure. This approach was based on fig. 8.3 relating mean modulus at each depth with 1st stress invariant. All the values used for the single layer system fell on the straight line, so the two layer results were correlated on this plot. This meant that for one two-layer system, two theoretical two-layer systems were computed, one with a value of E_2 appropriate to measurements 3 in. below the interface, and the other to those 12 in. below. As two sizes of loaded area were used, two actual systems were tested and, therefore, four theoretical systems were computed. Details are shown in Table 8.1. The values of Poisson's ratio are the means of all calculated values for each material respectively.

The modular ratios resulting from these choices of moduli varied between 0.5 and 1.3 and since they were very near to unity, the theoretical stresses and strains resulting from the two layer computations differed very little from the Boussinesq calculations. None the less, on most plots, two lines calculated by two-layer theory

TABLE 8.1 DETAILS OF TWO-LAYER SYSTEMS USED FOR COMPUTING THEORETICAL RESULTS

System No.	Upper layer		Lower layer		Modular ratio E_1/E_2	Radius of loaded area (a) (in.)
	E_1 (lb/sq.in.)	ν_1	E_2 (lb/sq.in.)	ν_2		
1	13,500	0.35	12,700	0.41	1.1	6
2	13,500	0.35	25,000	0.41	0.5	6
3	11,500	0.35	9,100	0.41	1.3	9
4	11,500	0.35	16,500	0.41	0.7	9
Rough Interface			Thickness of upper layer = 12 in.			

and a Boussinesq distribution have been included for comparison with each other as well as with experimental points.

Fig. 8.4 shows the positions at which theoretical results were calculated. To facilitate plots with depth, additional results were computed at $^{r}/_{a}$ = 0 and 1. The number of positions was kept to a minimum so as to reduce the computing time which for the four systems amounted to 51 minutes on the IBM 7090 machine.

8.3 Equilibrium and Compatibility errors

The equilibrium and compatibility errors for measurements in the upper layer, consisting of Meldon Dust, were much smaller than those obtained in the single layer system of Keuper Marl. These errors are expressed in the same way as for the single layer system (section 7.3) to give an idea of magnitudes.

$$\frac{x}{(p_1 + p_3)} \times 100 = -1.7\%$$

and

$$\frac{y}{(e_1 + e_3)} \times 100 = -25.2\%$$

The values of x were not exclusively positive as was the case for the single layer results, neither were the

values of y exclusively negative. Following the argument presented in section 7.3, this indicates that the Meldon Dust was more homogeneous than the Keuper Marl.

If strain readings beneath the loaded area are considered alone the magnitude of the mean compatibility error is greatly reduced, viz.

$$\frac{y}{(e_1 + e_3)} \times 100 = -2.5\%$$

which is considerably better than for the Keuper Marl. The Keuper Marl results were not improved particularly by confining attention to points beneath the loaded area.

Results in both layers were corrected in the manner described for the single layer system (section 7.3), before proceeding to calculate derived results.

8.4 Stresses (Figs. 8.5 to 8.11)

Stresses have been plotted in normalised form against radius, and in some cases, depth. Fewer results are presented here than was the case for the single layer system; the trends and comparison with theory not suffering in any way as a result.

Experimental points have again been represented according to a code as shown in Table 5.2 which allows

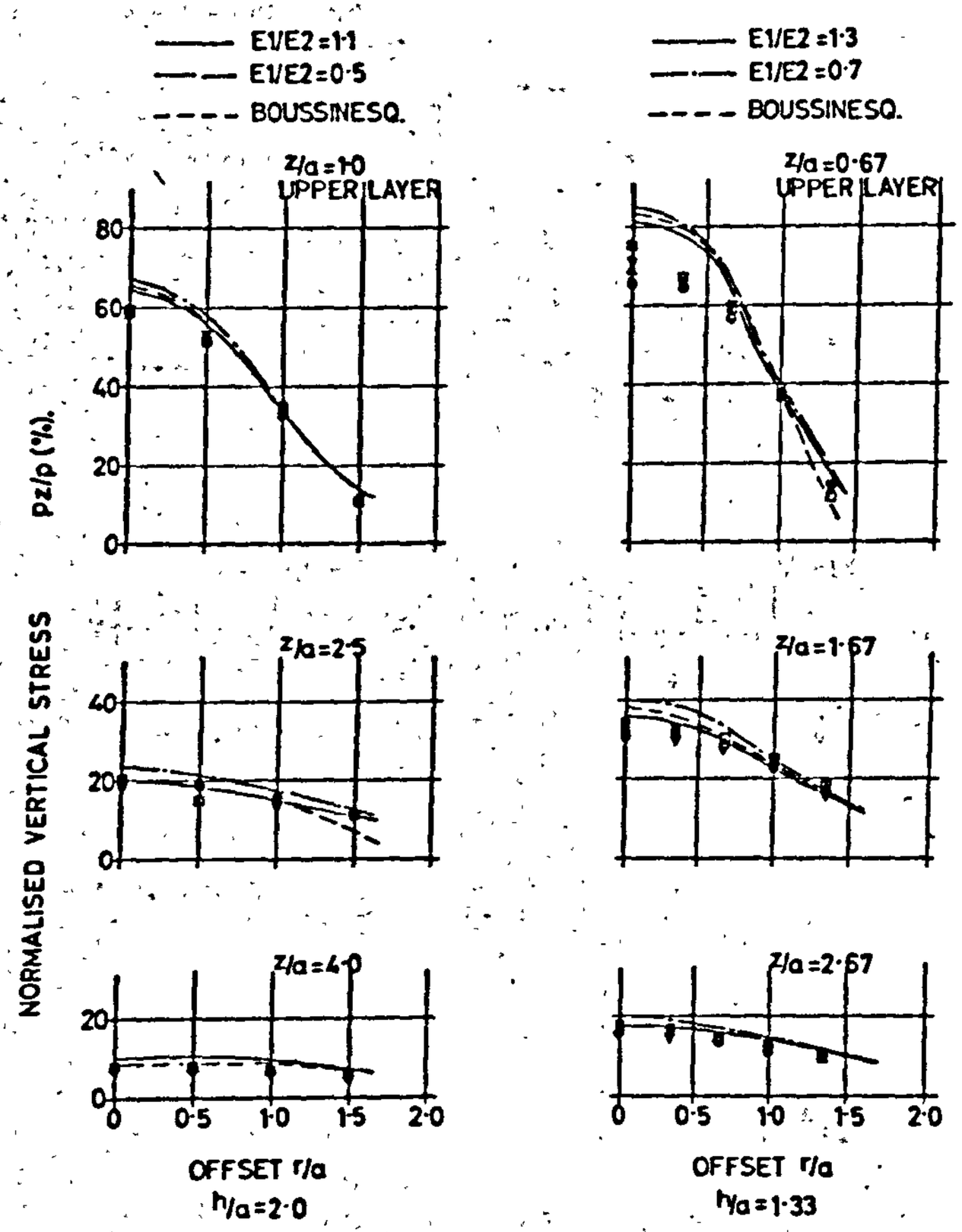

FIG. 8.5 VERTICAL STRESS WITH RADIUS - TWO LAYER SYSTEM

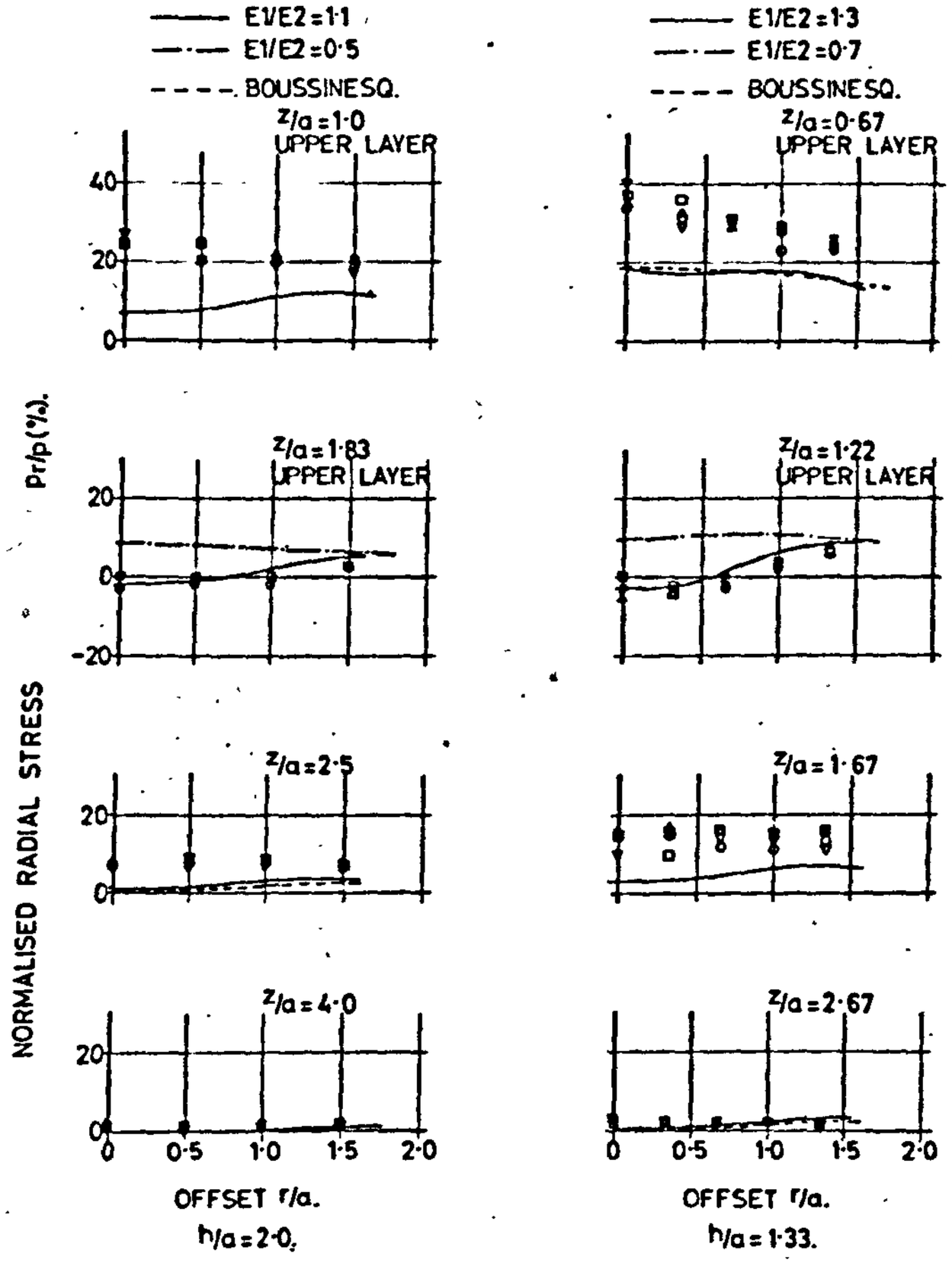

FIG. 8.6 RADIAL STRESS WITH RADIUS - TWO LAYER SYSTEM

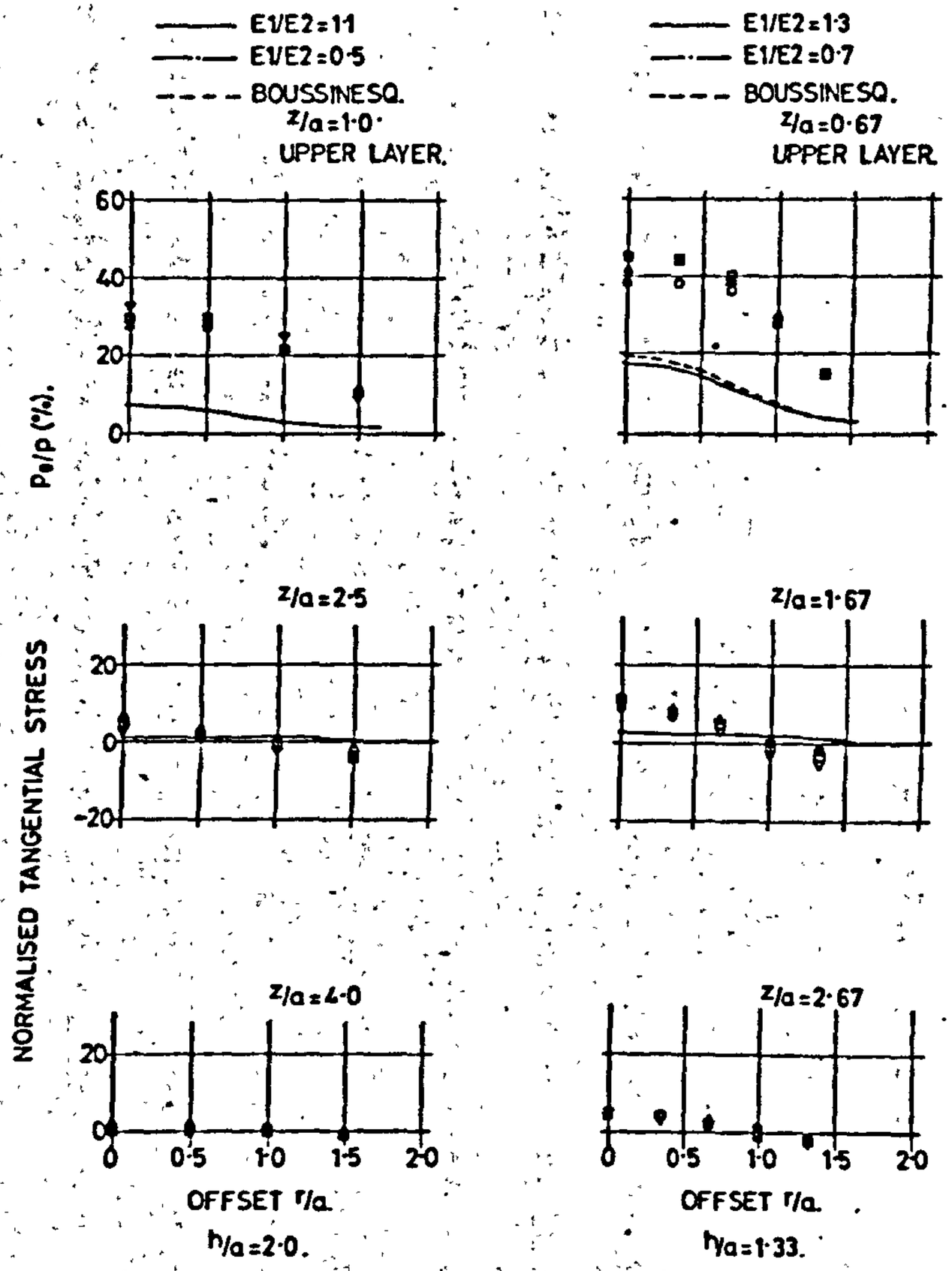

FIG. 8.7 TANGENTIAL STRESS WITH RADIUS - TWO LAYER SYSTEM

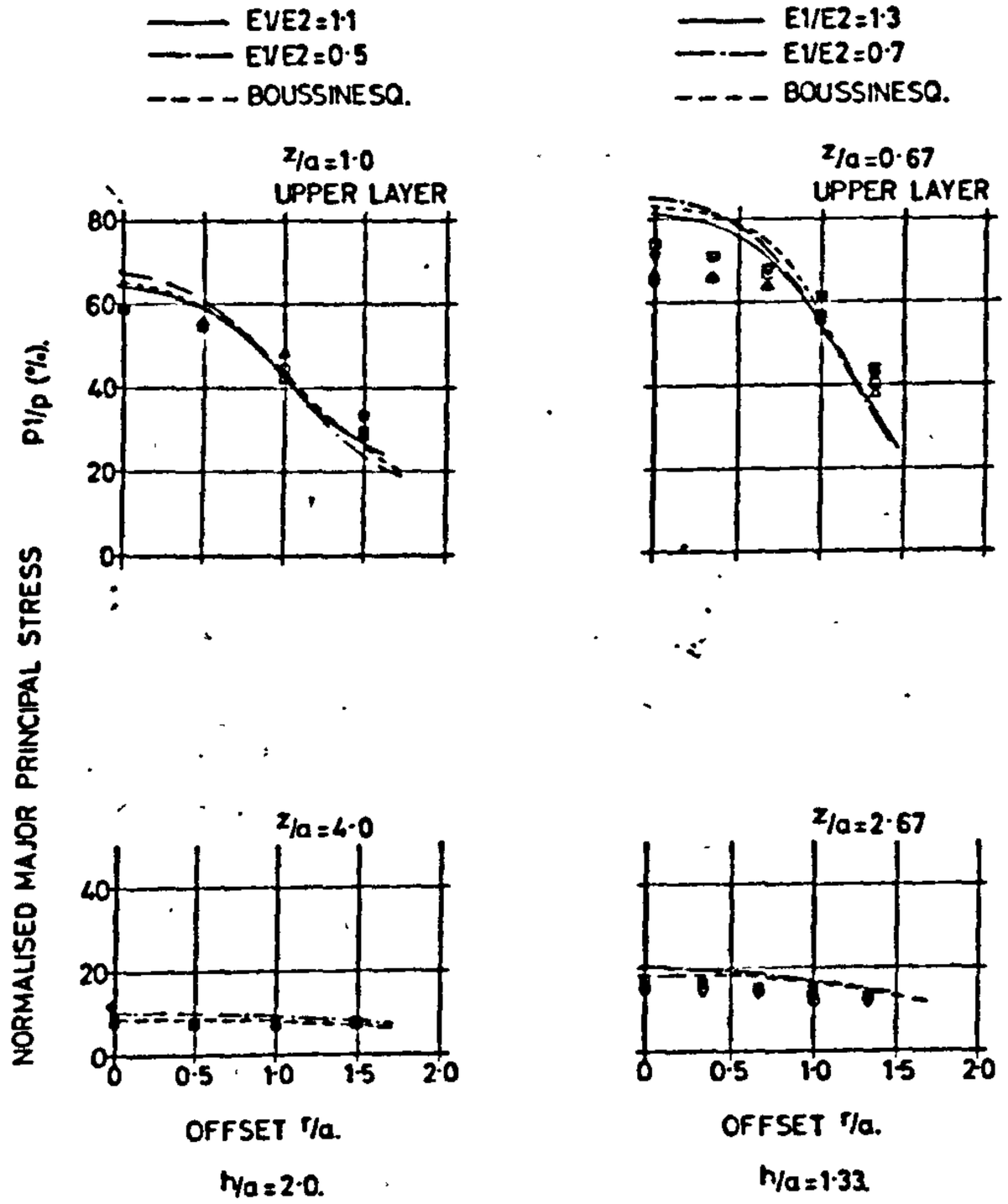

FIG. 8.8 MAJOR PRINCIPAL STRESS WITH RADIUS - TWO LAYER SYSTEM

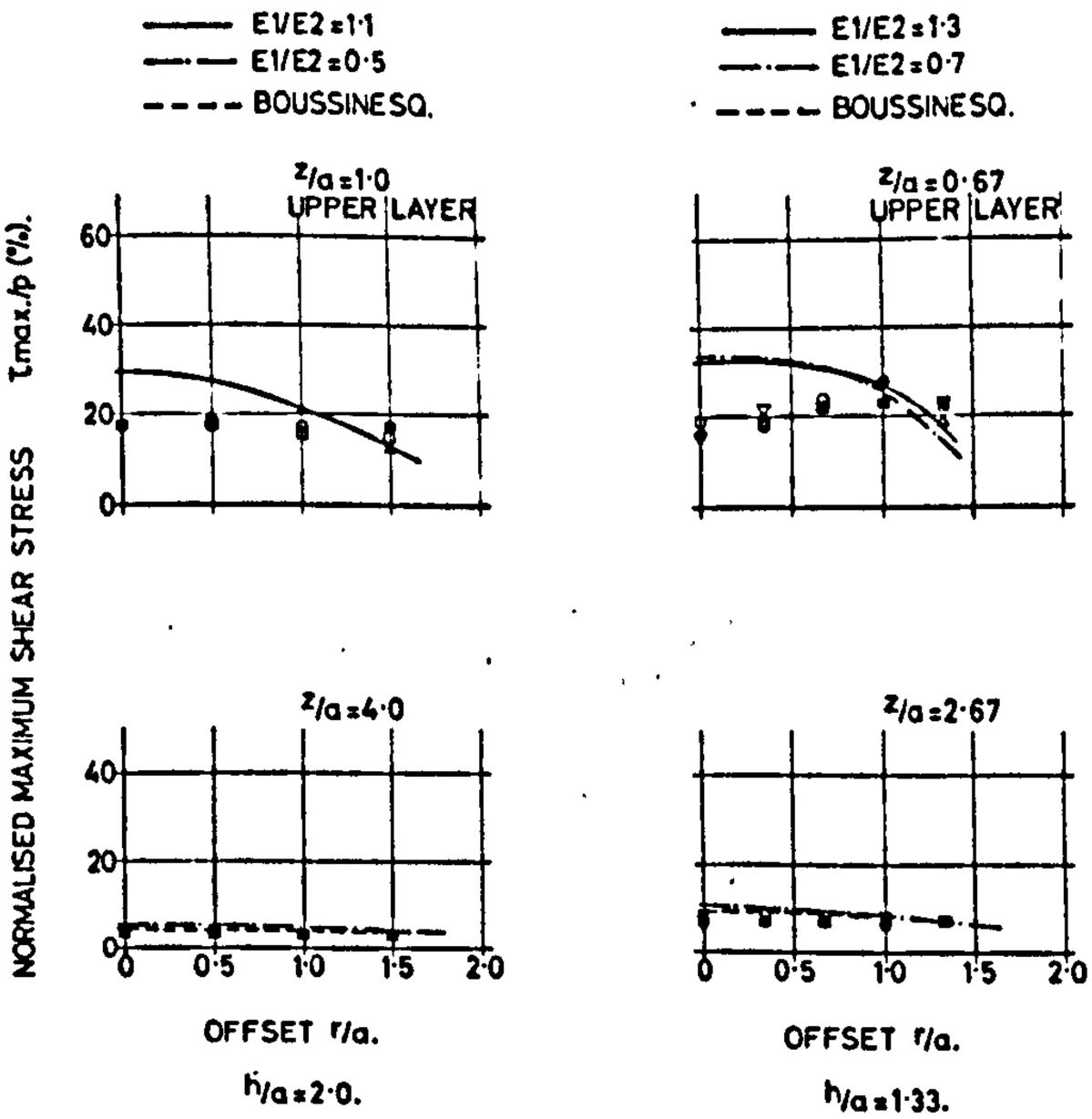

FIG. 8.9 MAXIMUM SHEAR STRESS WITH RADIUS - TWO-LAYER SYSTEM

for any trends with rate of loading and contact pressure to be identified. On most plots three theoretical lines are superimposed, one being a Boussinesq distribution and the other two are based on two-layer theory as explained in section 8.2. There is hardly any difference between these theoretical lines, except for radial stress near the interface which would appear to be very sensitive to modular ratio changes.

There is good agreement between theory and experi-

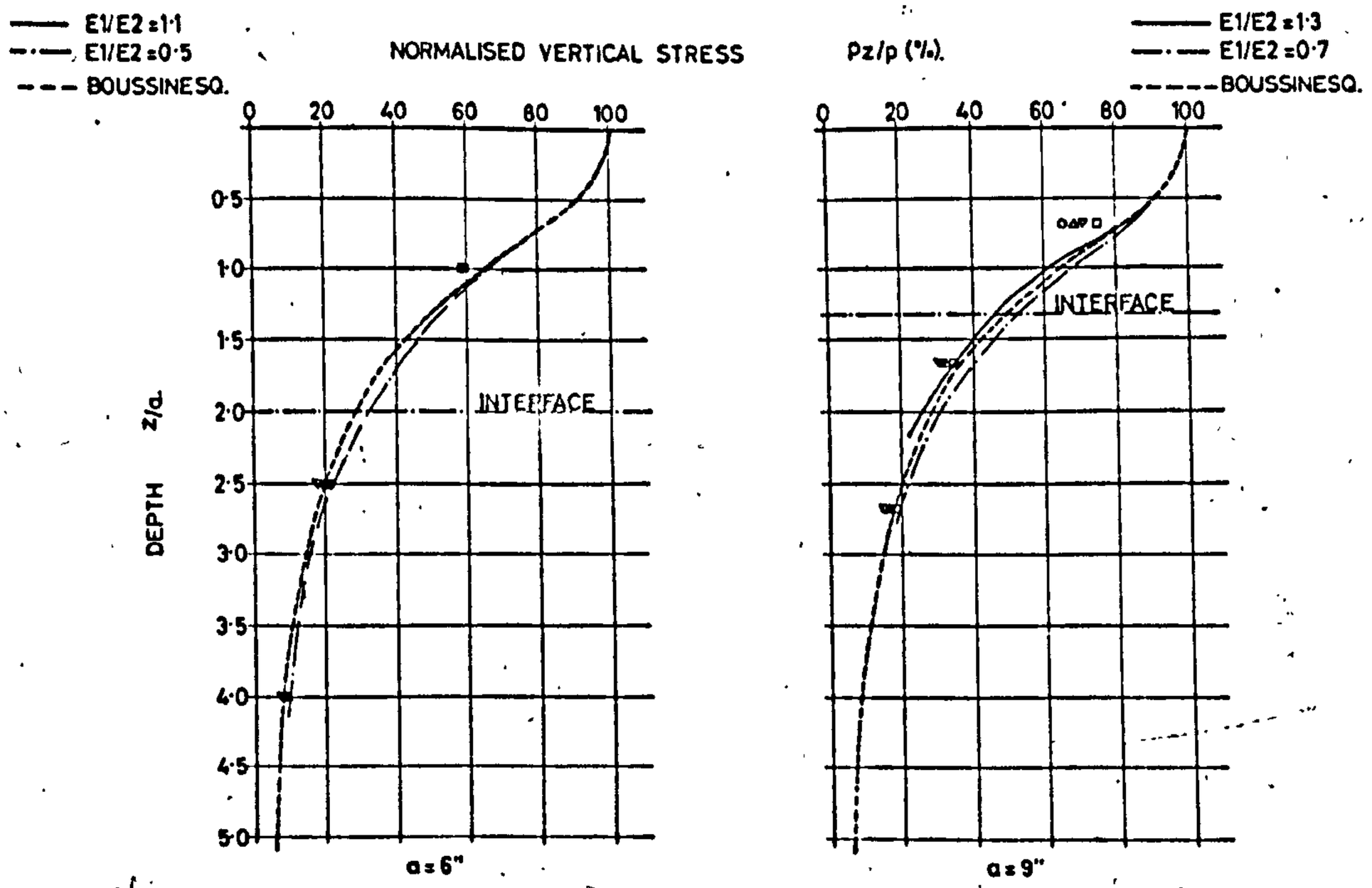

(c.f. Fig 7.13. Also note Boussinesq less adequate.)

FIG. 8.10 VERTICAL STRESS WITH DEPTH - TWO-LAYER SYSTEM

mental points in the lower layer for all stresses. The comparison is very similar to that observed in the single layer tests, although there are no depths common to both sets of results for direct comparison. The trend for radial stress to be higher than theory is noticeable again, as is that for tangential stresses to be tensile at, and outside the loaded area.

Stress measurements in the upper layer show poorer agreement with theory than those down below. Vertical

stress in the centre of the upper layer is slightly low beneath the loaded area, and radial stress is everywhere higher than theoretical predictions. Tangential stress is considerably higher than theory at all radii and this comparison is significantly different from that observed in the single layer system at a comparable depth (fig. 7.7). Major principal stress shows generally good agreement with theory although it does reflect the influence of vertical and radial stress comparisons beneath and outside the loaded area respectively. The variation of maximum shear stress with radius is similar to that for the single layer system, showing a maximum beneath the edge of the loaded area in contrast to the theoretical line which shows the maximum to occur on the axis of the load.

The variation of radial stress with depth is of interest, particularly since this indicates values at the interface. Slight tensile stresses were measured just above the interface indicating qualitatively rather than quantitatively, the presence of such stresses at a point considered critical for design purposes. Despite the fact that the pressure cell cannot measure tensile stresses larger than the prestress caused by overburden pressure, comparison with one of the theoretical two-

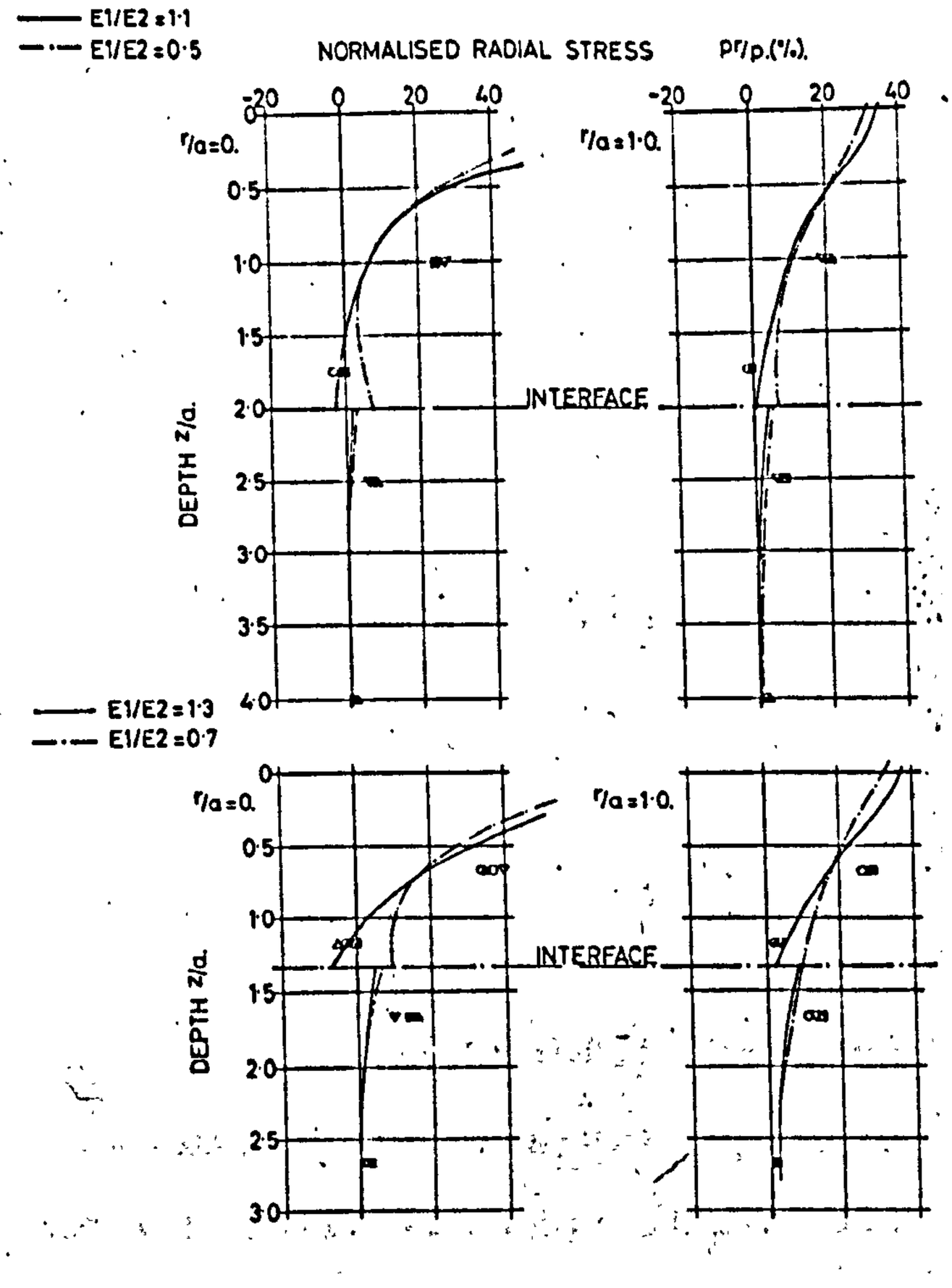

FIG. 8.11 RADIAL STRESS WITH DEPTH - TWO LAYER SYSTEM

layer lines is very close, particularly on the axis of the load. The relevant line was calculated for E_1/E_2 = 1.1 (1.3 in the lower plot) which is based on E_2 at a depth of 3 in. below the interface.

There is less scatter of experimental results than at similar depths in the single layer system, consequently no consistent trends emerge to show variations with either contact pressure or rate of loading. The former effect is caused by smaller changes in modulus, as a result of applying the two contact pressures used in these tests, than occurred in the single layer system. If the mean values of 1st stress invariant (J_1) are taken beneath the loaded area at the shallowest depths for tests first with the high contact pressure, and then with the low one, the corresponding variation of modulus can be read off figs. 7.2 and 8.1 for each material respectively. For the Keuper Marl in the single layer system, the change in modulus is 76% of the lower value, while for Meldon Dust in the two-layer system, the change is only 39%. In the first case it is a decrease and in the second case an increase with increasing contact pressure. Details are shown in Table 8.2.

Comparison with results obtained by other workers is difficult because only vertical stresses in the subgrade

TABLE 8.2 VARIATION OF MODULUS WITH CONTACT PRESSURE

Material	Contact Pressure (lb/sq.in.)	1st stress invariant (lb/sq.in.)	Modulus (E) (lb/sq.in.)	Change in E as % of lower value
Keuper Marl	17.0	26.3	3,800	76%
	7.5	10.5	6,700	
Meldon Dust	30	32.2	16,800	39%
	17	19.8	12,100	

have been previously measured in comparable experiments. Under static loading conditions Sowers and Vesic[16] have shown that the Boussinesq distribution predicts subgrade stresses better than layered system theory if the base layer consists of unbound material. Since the results obtained by the Author indicated modular ratios very near to unity, there has been no real check on these findings. This very fact may have some bearing on the poor comparison with two-layer theory which Sowers and Vesic report, since they used a modular ratio of four, this figure being based on tests conducted on specimens

of the pavement materials. The same argument applies against the modular ratio of ten used by McMahon and Yoder.[14] This was arrived at by plate bearing tests and calculations using Burmister two-layer theory. Heukelom and Klomp[41] report low modular ratios between unbound bases and subgrades under dynamic conditions. This is in keeping with the findings herein since they explain the low values in terms of tension developed at the bottom of the base layer, a fact measured and discussed above. If the contact pressure was increased, it may be possible to obtain higher modular ratios. This follows from a study of the opposite stress dependence of modulus in the granular and clay type materials. An increase in stress level generally would increase the base layer modulus and decrease that of the subgrade. It remains to be seen whether the maximum value of 2.3 or theoretically 3, suggested by Heukelom and Klomp can be realised with this apparatus.

The stress results obtained in the two-layer system agreed with Boussinesq equally as well as with two-layer theory, which is not to say that agreement was particularly good in either case. There was, however, one important exception. Tensile radial stresses just above the interface could never be predicted by Boussinesq, and

since their magnitude is important from a design point of view, two-layer theory should be used to predict stresses at the interface. This theory is only as good as the value of modular ratio allows it, for stress determination. The higher the modular ratio, the greater the tensile radial stresses above the interface, so if the suggested limiting value of between two and three can be confirmed then this would be the proper value to use. Further work at Nottingham is likely to clear this point up. It should be emphasised that, because of the stress dependence of modulus in the pavement no unique value of modular ratio exists. The idea of a constant value of modulus for each layer may disappear as theoretical solutions based on a variable modulus are developed. In the meantime, the required value should be the one which predicts critical design stresses most accurately.

8.5 Strains (Figs. 8.12 to 8.18)

All strains have been plotted in normalised form as defined in section 6.2. On most plots with radius three theoretical lines are shown, one Boussinesq and two calculated by two-layer theory. Plots with depth just show the layered theory lines since it would be necessary

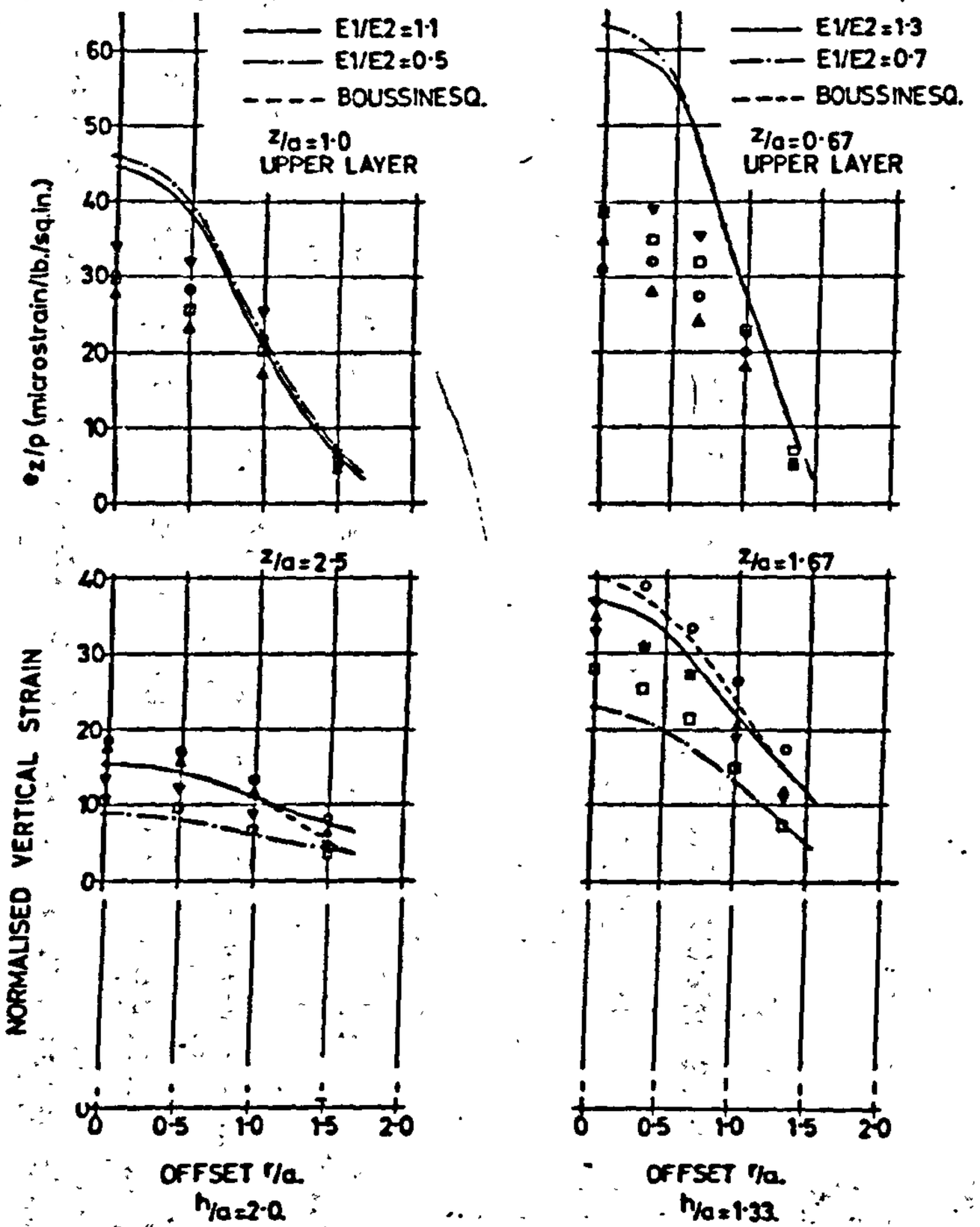

FIG. 8.12 VERTICAL STRAIN WITH RADIUS - TWO LAYER SYSTEM

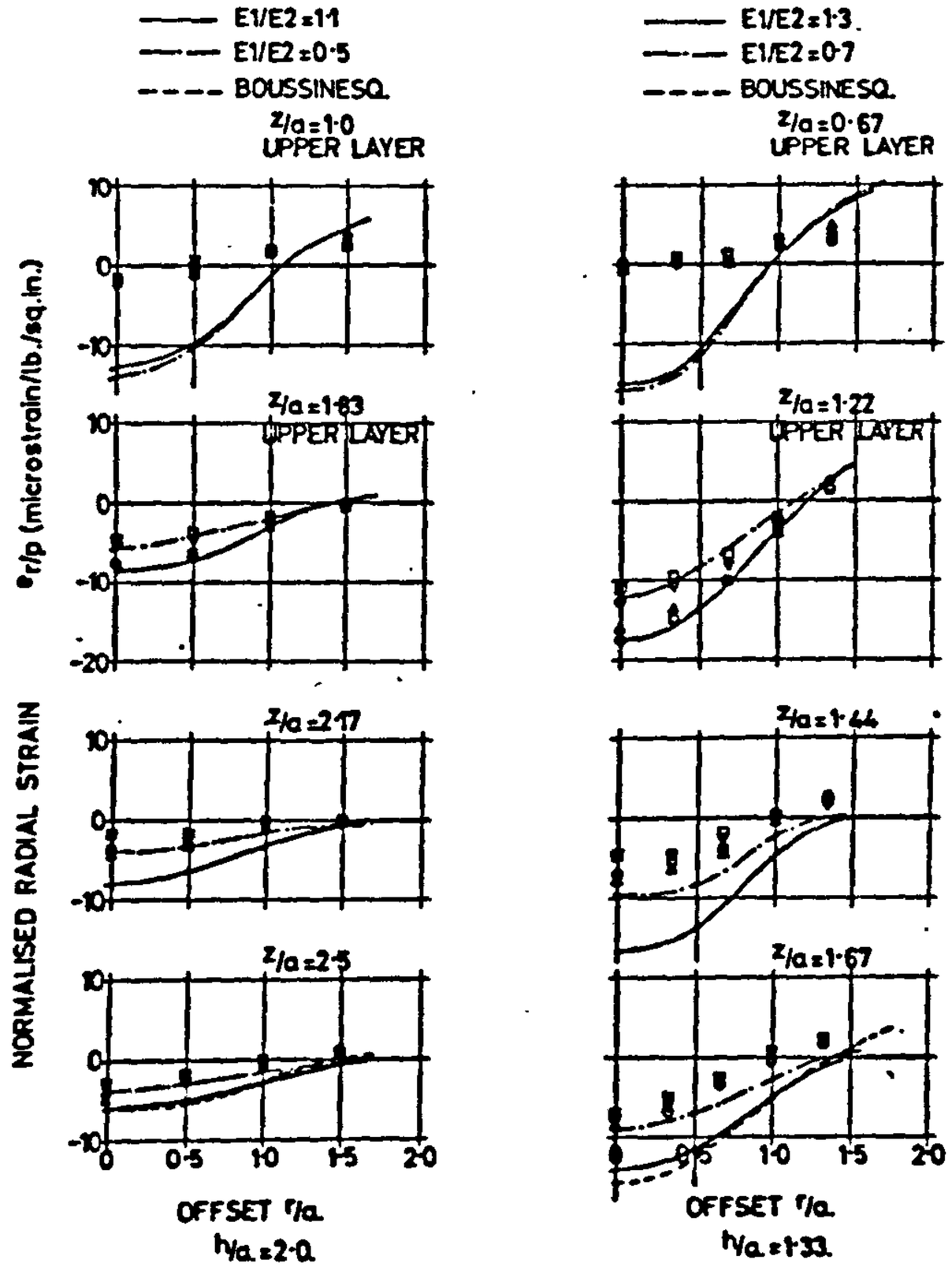

FIG. 8.13 RADIAL STRAIN WITH RADIUS - TWO LAYER SYSTEM

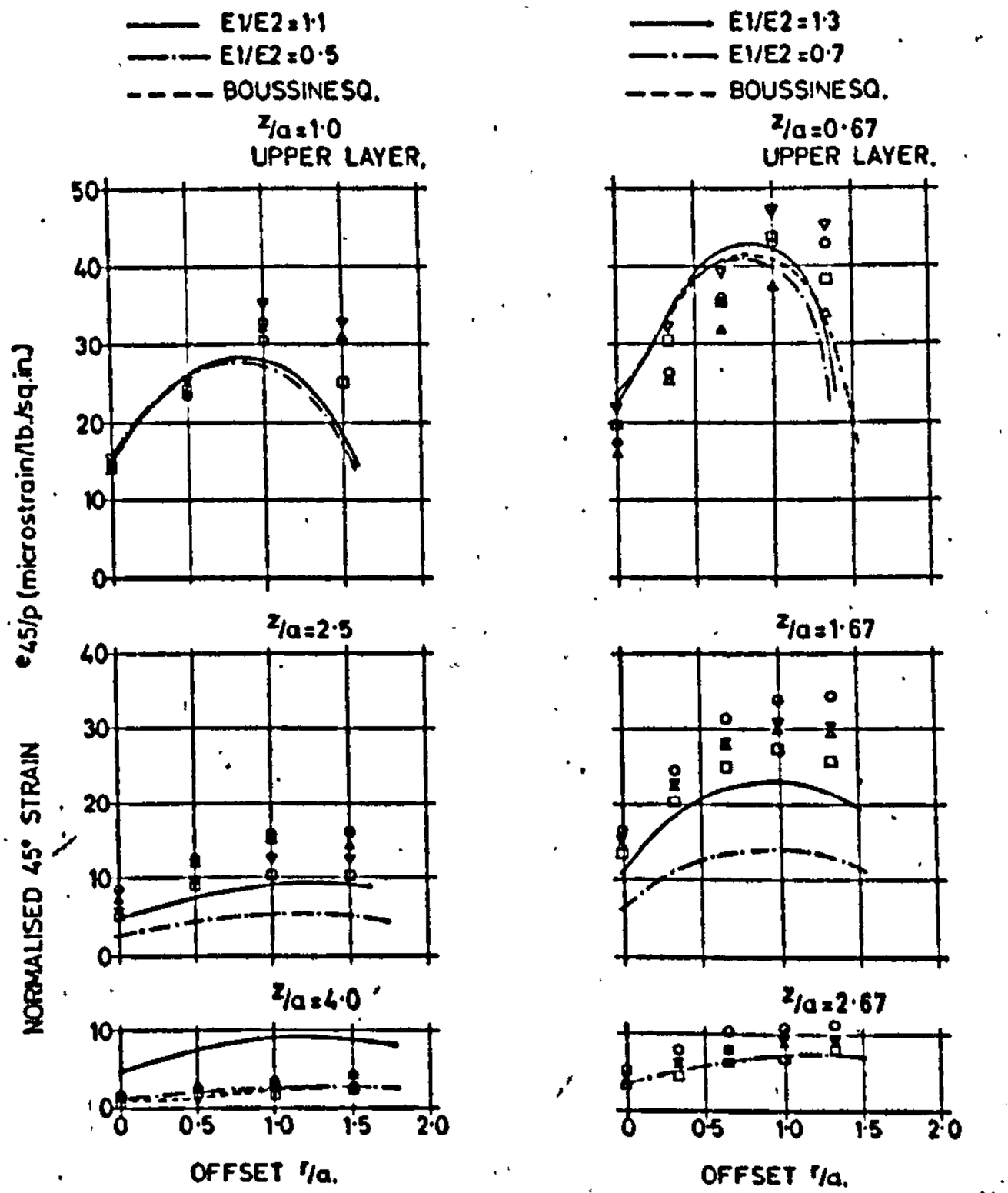

FIG. 8.14 45° STRAIN WITH RADIUS

TWO LAYER SYSTEM

to show three Boussinesq lines for the different values of modulus adopted at the three depths at which full sets of measurements were made (see section 8.2).

The scatter of results is less on these plots than on single layer strain distributions, but is again caused by difference in contact pressure and rate of loading

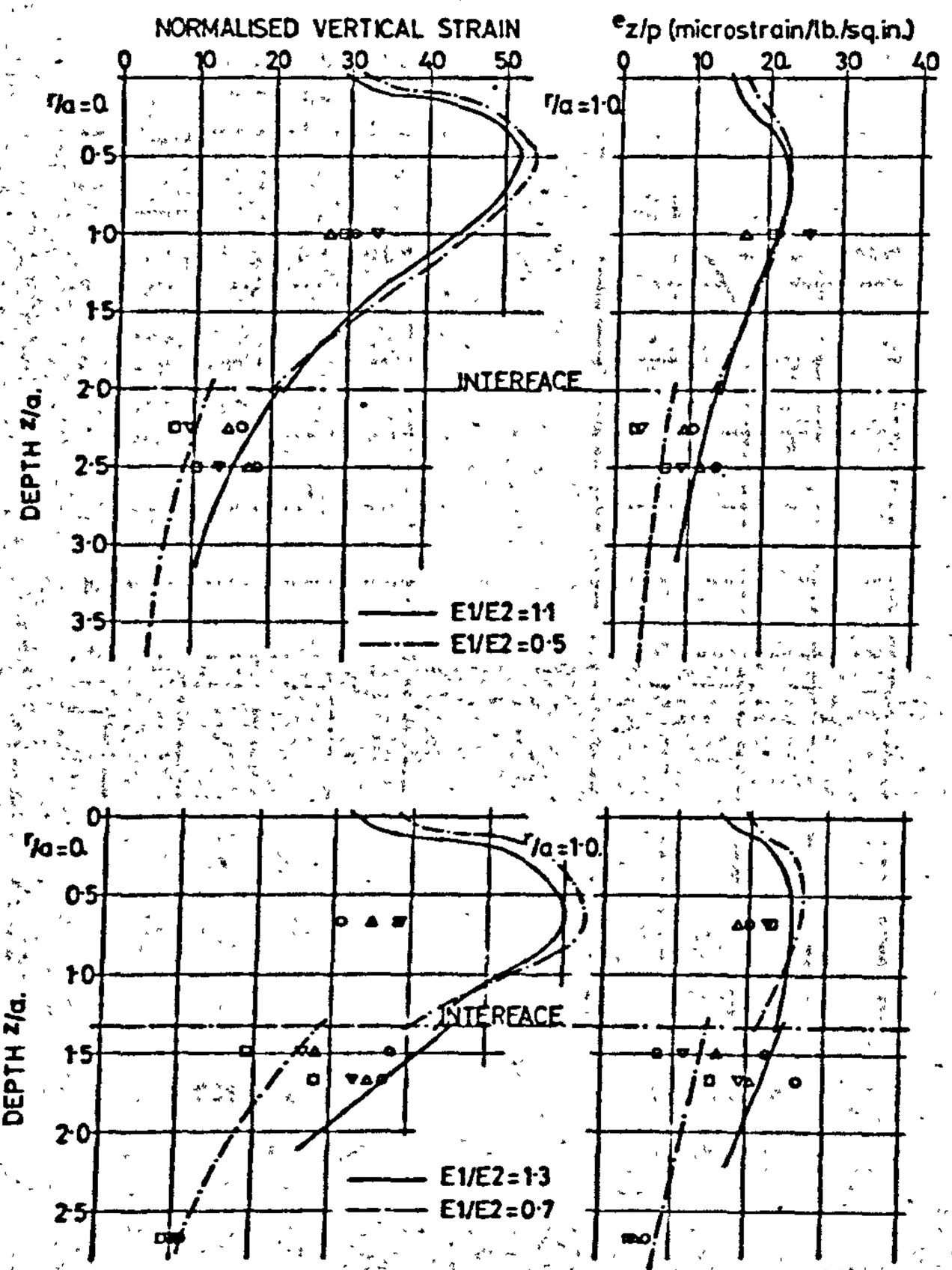

FIG. 8.15 VERTICAL STRAIN WITH DEPTH - TWO LAYER SYSTEM

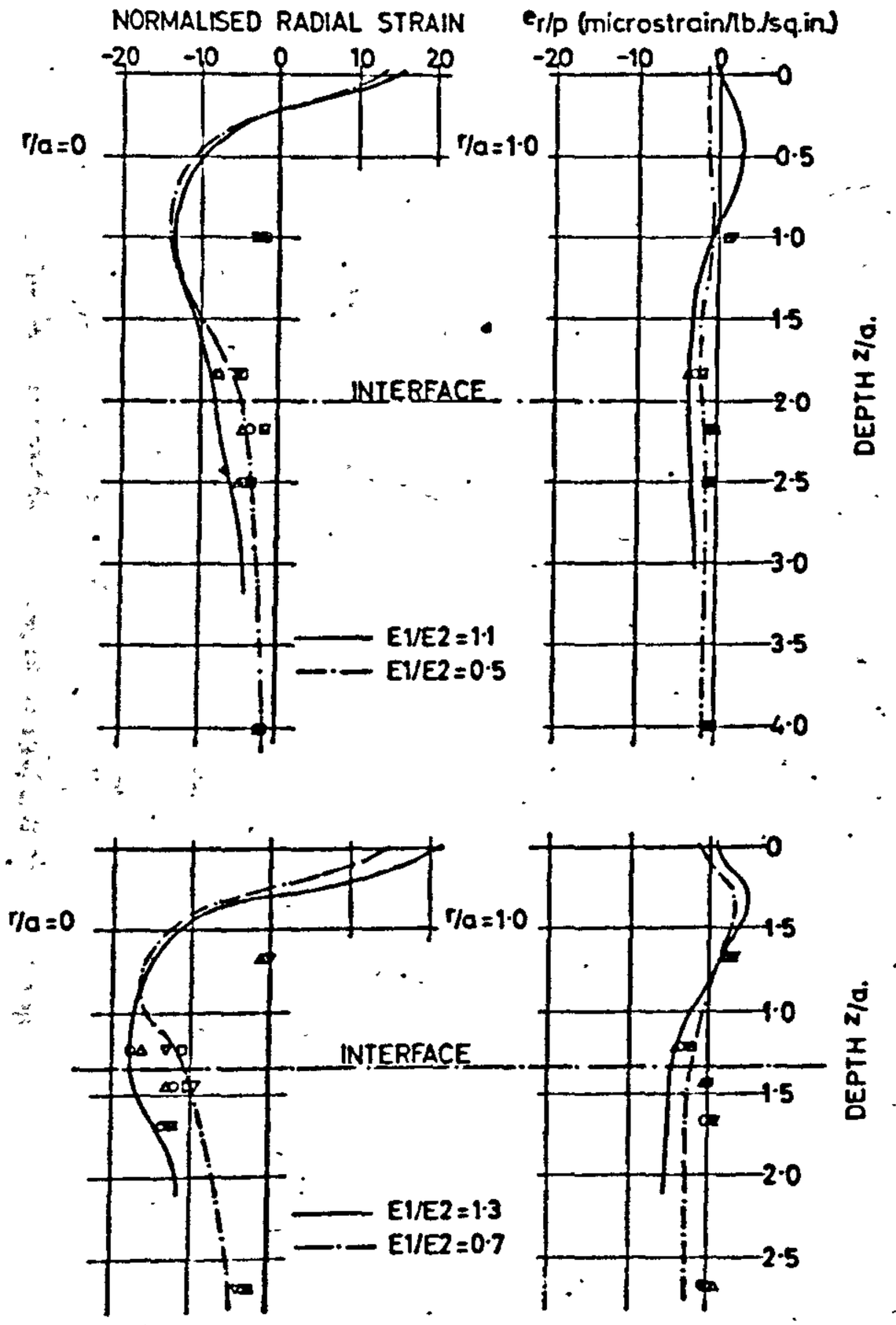

FIG. 8.16 RADIAL STRAIN WITH DEPTH - TWO LAYER SYSTEM

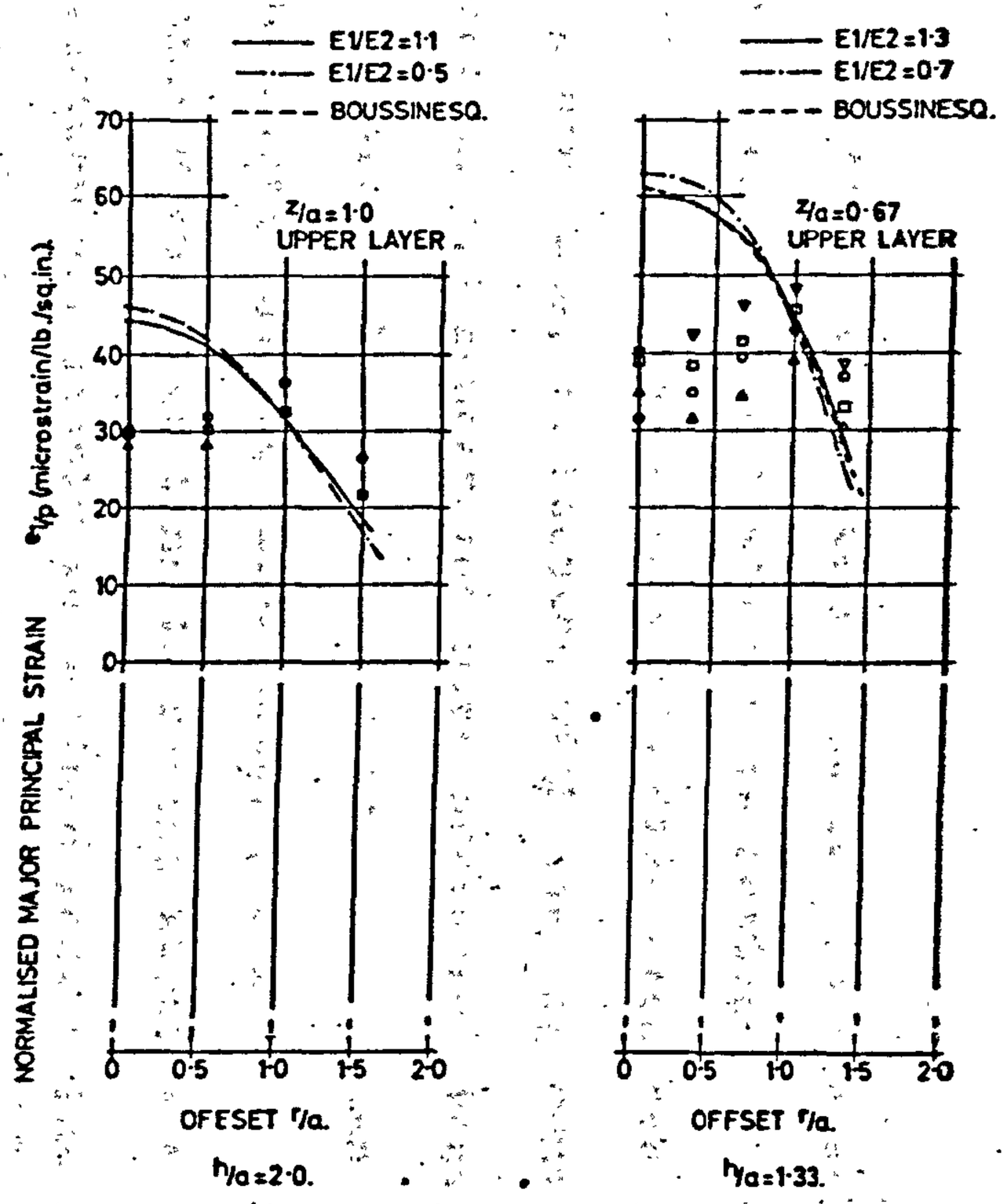

FIG. 8.17 MAJOR PRINCIPAL STRAIN WITH - RADIUS - TWO LAYER SYSTEM

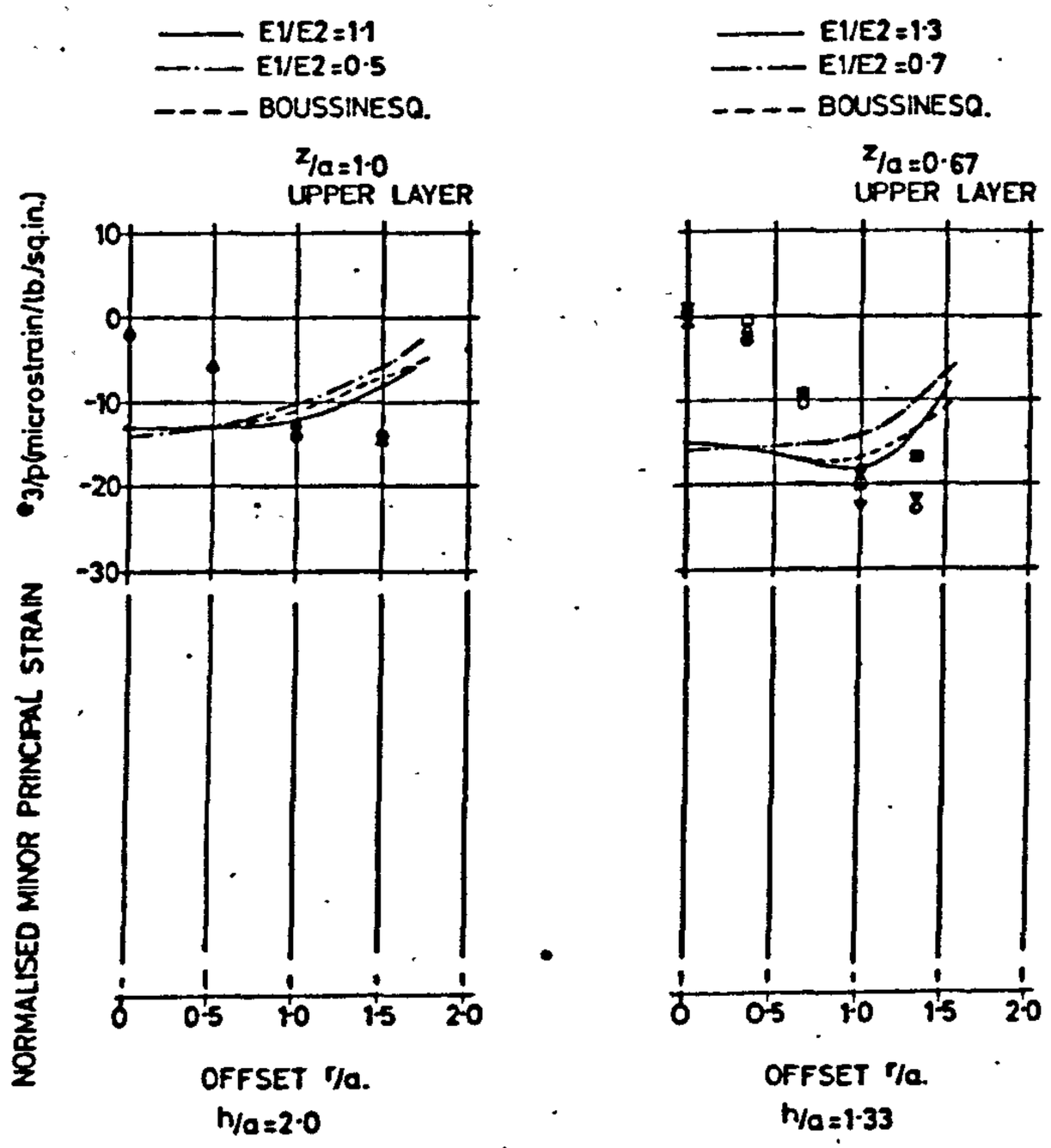

FIG. 8.18 MINOR PRINCIPAL STRAIN WITH RADIUS - TWO LAYER SYSTEM

between tests. As can be seen from fig. 8.1 modulus increases with stress level in the Meldon Dust, and hence normalised strain would be expected to decrease with increasing contact pressure. This is in fact the case and the trend is noticeable on the plots of vertical and 45° strains. This effect is reversed in the Keuper Marl subgrade, where normalised strain increases with contact pressure in the same way as it did for the single layer system. The smaller amount of scatter for results in the Meldon Dust indicates that the modulus is changed less by differing contact pressures than was the case for the Keuper Marl. This effect is discussed in section 8.4 when dealing with stresses.

The trend with rate of loading is the same as noted in the single layer tests and is noticeable here for both materials. A fast rate of loading produces lower strains than a slow one, in keeping with the argument put forward in section 7.5 concerning pore pressure dissipation.

Before analysing the comparison between two-layer measurements and the theoretical predictions it should be pointed out that tensile radial strains 6 in. below the surface are likely to be in error. The instrument recording this effect was not working properly in tension although compression results were considered satisfactory.

The error became apparent when using the same instrument to measure tangential strains which were exclusively negative, but clearly not of sufficient magnitude. A study of the traces produced by this cell when subjected to tensile strain indicated that the maximum reading was not being reached. This conclusion was based on the time lag between strain pulses from deeper cells, and the offending one when attempting to measure tensile strains. The time lag, if present, should have been the other way round with the shallow cell responding first, and this was in fact the case when measuring compressive strains. This failure to record tensile strains accurately may have been caused by the instrument being at the end of its travel. During installation care was taken to keep the instrument about at its mid-travel position, but subsequent compaction may have "opened it out". Another possibility is that this strain cell may have had a large zero error in tension, but this is unlikely to have been the sole cause of the very small readings.

The plots of strain with radius show, for the upper layer, vertical strains to be lower than theory beneath the loaded area, but in agreement elsewhere, the reverse to be true of 45° strains and radial strains to be in acceptable agreement with either of the theoretical lines. Where the Boussinesq

line is not apparently shown on these plots it can be taken as coincident with the line for a modular ratio of 1.1 or 1.3. The divergence of vertical strains from the theoretical values near the axis appears to get larger at lower effective depths. The tensile radial strains which are in error are those at $^{z}/_{a}$ = 1.0 and 0.67. Just above the interface, the predominantly tensile radial strains show good agreement with theory.

In the subgrade, vertical and 45° strains agree best with the appropriate theoretical line i.e. the full line at the shallow depth and the chain dotted one lower down. Vertical strains are in good agreement, but 45° strains are higher than theory 3 in. below the interface, as was the case in the single layer system at a comparable effective depth. (cf $^{z}/_{a}$ = 1.67 fig. 8.14, and $^{z}/_{a}$ = 1.33 fig. 7.17). Radial strains in the subgrade compare well with the theoretical line based on the lower modular ratio at both the depths shown. These are just below the interface and 3 in. below, compared with 3 in. and 12 in. below in other plots. Looked at another way, radial strains are lower than theory since, to be consistent, the appropriate line at $^{z}/_{a}$ = 2.5 and 1.67 is based on the higher modular ratios of 1.1 and 1.3 respectively, arrived at by calculation of moduli at these depths.

The plots of vertical strain with depth (fig. 8.15) show, what is not always obvious, that there is theoretically a discontinuity of vertical strain at the interface. This is apparent when it is realised that there must be equilibrium of vertical stress across the interface and because of the change in modulus, a discontinuity of vertical strain.

The two sets of vertical strain measurements just below the interface are not mutually consistent, the indication being that there is a slight increase in strain with depth. This may have been caused by the non-homogeneous nature of the soil, since results immediately below the interface were obtained from a different location in the test pit from the others. The main object of measurements just below the interface was to determine the maximum subgrade strain, a factor considered critical in design. The inconsistency of results in this area makes a definite conclusion difficult, but from a design point of view the maximum strains appear to be predicted by the larger modular ratios based on local values of E_3 viz. the full line in fig. 8.15.

Fig. 8.16 shows radial strain with depth and its main purpose is to investigate whether the assumed condition of perfect roughness at the interface is valid.

This is proven if the plot is continuous across the interface. In general, experimental points show better agreement with the chain dotted lines i.e., those for the lower modular ratios. In particular the experimental points agree well with these lines just above and below the interface, indicating continuity. A further indication that the interface is perfectly rough is that the trend with contact pressure just below the interface is repeated just above, whereas it should characteristically be reversed. This indicates that the subgrade is influencing the magnitude of the radial strains in the base at the interface, and this could only be possible if there were continuity.

Major principal strain in the upper layer compares poorly with theory, especially beneath the loaded area where the influence of vertical strain is greatest. Measurements indicate a maximum value of compressive strain beneath the edge of the loaded area. Minor principal strain suffers, near the axis, from the unreliable tensile radial strain readings reported above. Again the maximum value of strain, this time tensile, appears to be at $r/a = 1$.

The problem over theoretical calculation of strains in the two-layer system is the same as for the single layer, namely the appropriate choice of modulus. Strains depend,

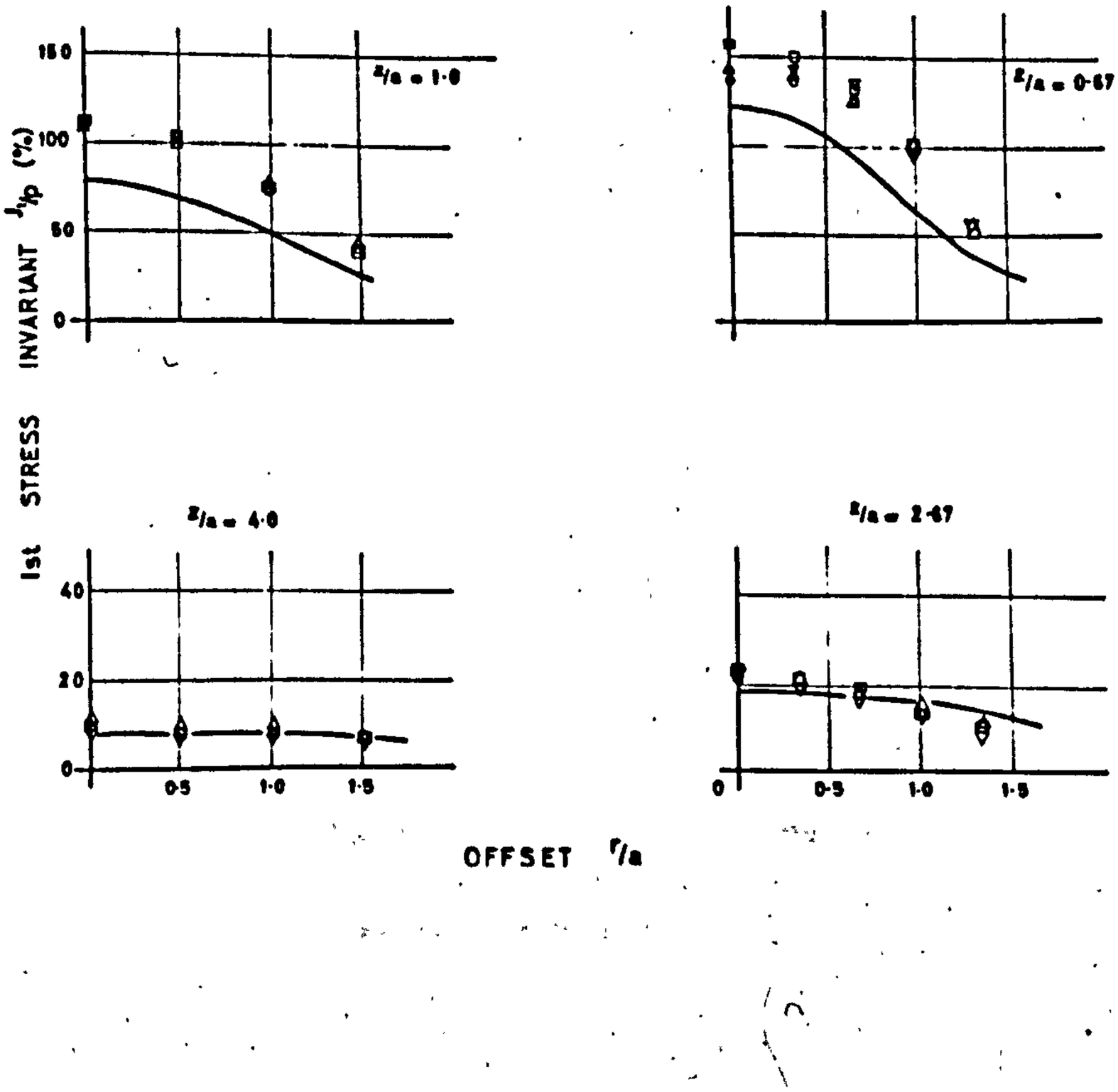

FIG. 8.19 1st STRESS INVARIANT WITH RADIUS - TWO LAYER SYSTEM

in particular, on the value of modulus at the point concerned. This can be determined, if the stress level is known, from fig. 7.2 or 8.1 relating modulus to 1st stress invariant. On the evidence presented in section 8.4 it appears that neither Boussinesq nor two-layer theory can be used for accurate prediction of stresses, at all locations. Fig. 8.19 shows plots of 1st stress invariant with radius at the two depths where full sets

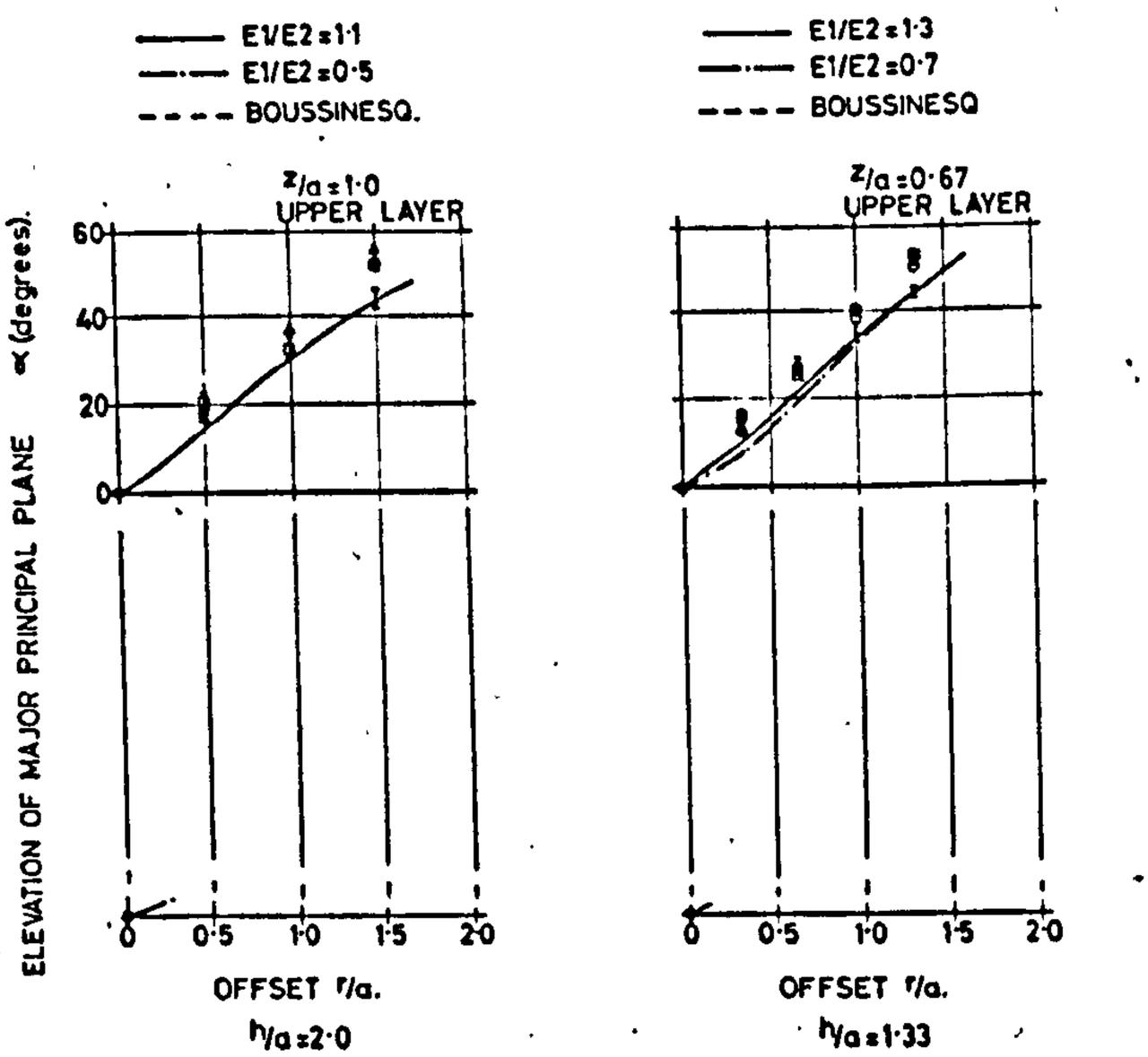

FIG. 8.20 ELEVATION OF MAJOR PRINCIPAL PLANE - TWO LAYER SYSTEM

of measurements were taken. The superimposed line represents the Boussinesq theoretical distribution which is much the same as layered theory in this case. In the upper layer the comparison is not good, experimental points lying above the theoretical line but in the subgrade agreement is close. If the theoretical values of 1st stress invariant were used to obtain modulus, the correct values would emerge for the subgrade, while lower values would result in the base. This would be on the

safe side for design purposes, since higher strains would result.

8.6 Principal planes

Fig. 8.20 shows the elevation of the major principal plane above the horizontal, calculated from stress and from strain measurements independently. The range of stress results have been superimposed on a plot showing individual strain results and comparison between them is quite good. The Boussinesq theoretical line coincides with the two-layer one on both of these plots.

CHAPTER 9 CONCLUSIONS AND CONCLUDING REMARKS

9.1 Validity of Elastic Theory

The main object of the work described in this thesis is to assess, by experimentation, the validity of the theory of elasticity solution for multilayer pavement systems, or in this case more specifically, the single and two layer problems. The Boussinesq theory and the multilayer approach both assume that the materials are homogeneous, isotropic and linear elastic. These assumptions are not generally true for road making materials and the experimental results confirm this. While the inaccuracy of these assumptions was well known at the outset, there was the possibility that under dynamic loading conditions, theory of elasticity calculations would provide solutions which were sufficiently accurate for design purposes. In addition, since a great deal of time and effort by other workers had gone into the development of rational design methods based on the theory of elasticity, it was considered important to check the validity of this theory by experimentation.

An important variable in pavement design is that of moisture content, particularly in the subgrade. This has been intentionally kept constant in this project, so as to elliminate one of the many variables involved. Conclusions from these tests, therefore, may only be valid for the particular materials which were used. Extrapolation to other materials under other conditions must only be performed with caution at this stage.

Two materials were included in the model pavement, a clay subgrade of Keuper marl and a granular base layer of Meldon dust. The following conclusions can be drawn about the behaviour of these materials:-

1. The in-situ secant modulus of the clay increased with decreasing stress level, particularly at the low stress levels expected in subgrades.
2. The in-situ secant modulus of the granular material increased with increasing stress level.
3. For the Keuper marl, stress increased and strain decreased with increasing rate of loading, the effect being more marked for strains. In the Meldon dust the trend was observed with strain only.

These conclusions show behaviour at variance with the theoretical assumptions, and explain a good deal of what follows. Stresses and strains were affected to the extent that the following conclusions were drawn:-

4. Strain was not proportional to contact pressure in either material.

5. Stress was not proportional to contact pressure in the clay, where there was a greater stress dependence of modulus.

Triaxial tests were carried out on large samples of the clay during strain cell calibration tests resulting in the following conclusion:-

6. Realistic values of modulus, applicable to the soil mass in the subgrade, appear to be predicted from triaxial tests.

This conclusion is somewhat tentative, since a thorough investigation of triaxial specimens is needed to form a proper conclusion. Also see Appendix II.

Other conclusions regarding the validity of the theory of elasticity are:-

7. The materials appeared to be isotropic but not homogeneous. In this latter respect the granular material was better than the clay.
8. Stresses in the subgrade and the single layer were predicted well by theory.
9. Vertical and maximum shear stresses were predicted adequately for design purposes. The maximum shear stresses occurred under the edge of the loaded area, not on the axis as predicted by theory.
10. Strains in the subgrade and the single layer were predicted quite well provided that the appropriate value of modulus was used.
11. The appropriate value of modulus for strain calculations is the value existing at the required location.
12. Maximum values of surface deflection are predicted adequately provided the appropriate value of modulus is used, in this case the value near the surface.
13. Tensile stresses were measured at the bottom of the base layer in the radial direction, and also

tangentially in the single layer system, but their magnitudes were of doubtful reliability, since the pressure cells were only designed to measure compression.

14. The tensile horizontal stresses at the bottom of the base layer were well predicted by two layer theory, although the remarks in conclusion 13 should be noted.

15. The two layer system modular ratios were all near to unity so that Boussinesq theory predicted most stresses equally as well as layered theory.

16. Further tests on the two layer system with higher contact pressures are required to see whether there is an upper limit to modular ratio for an unbound base as predicted elsewhere[41].

17. Measurements of radial strain either side of the interface indicated that the theoretical assumption of perfect roughness at the interface is valid.

18. Provided a reliable relationship exists between stress level and modulus for a single layer system strains can be predicted by Boussinesq theory using an assumed value of Poisson's ratio.

19. Poisson's ratio for the Keuper marl varied in an irregular manner showing no relationship to stress or strain. The mean value was 0.41.

20. Poisson's ratio for the Meldon dust decreased with increasing stress level. The mean value was 0.35.

From the work done with instrumentation, the following two conclusions emerge:-

21. Strain can be successfully measured in a soil mass.

22. Diaphragm type pressure cells are liable to be cross-sensitive, and should thus be carefully designed and calibrated to ensure that this defect is not present.

9.2 Summary of the main findings

In many respects, experimental work is lagging behind theoretical developments in the evolution of a rational structural design approach to the design of flexible pavements. The work described in this thesis is part of an attempt to fill the gap on the experimental side.

The ability to measure in-situ strains in the pavement structure was of primary importance in this work, not only for the actual strain values, but because in conjunction with stress measurements, values of in-situ modulus and Poisson's ratio could be calculated. Previous attempts to assess the moduli of the various layers in a pavement had been carried out by indirect methods as outlined in Section 1.3, and some of these seem to have indicated reliable values for the calculation of surface deflections.

The method of calculating modulus and Poisson's ratio outlined in Section 6.6, while using actual stress and strain measurements, is based on the assumptions of linearity. This was necessary if the material was to be described in terms of a Young's modulus of elasticity (effectively a secant modulus) and a Poisson's ratio. This assumption did not affect the results qualitatively and even quantitatively, average values of modulus at average stress levels were probably as close as was possible with a quasi-linear approach, i.e. using only two elastic constants. A more refined method for analysing the stress/strain

relationships for the two materials which were used, is presented in a preliminary way in Appendix II. This analysis indicates that the soils cannot be described simply in terms of a "modulus" and Poisson's ratio if a rigorous solution is required. However, a first step would appear to be the assumption of a "modulus" which varies with position, followed perhaps by a successive approximation method taking account of the stress dependence of the modulus.

The stress dependence of modulus for both materials was an important confirmation of other work, since the values herein were genuine in-situ results. This emphasised the problem of applying layered system theory, which assumes a constant modulus for each layer, to a structure, where within certain limits, the modulus varies approximately with depth. Moreover, for a two layer system of granular and clay type materials, the variation with depth shows a decrease down to the interface followed by an increase in the subgrade. There will usually be some discontinuity at the interface, but under certain circumstances the modular ratio at this depth could be unity or less.

The main problem in applying linear elastic theory is the choice of appropriate values of modulus for each layer. The conclusion from the present work is that this appropriate value depends on what is being calculated, and where. Stresses depend only on the modular ratios between layers, but strains depend on the actual value of modulus at the point concerned. The best solution, therefore, would appear to be to take values of modulus in each layer at what may be considered the critical points. The interfacial values suggest themselves in this context, although no results were calculated on this basis since only a few measurements were taken at the interface.

Further work is required to establish the "best" values of modulus for each layer and also to investigate whether an upper limit for modular ratio exists when using an unbound base. Seed et al[6] and Trollope et al[15] have pointed out that the linear log-log relationship between modulus and confining stress only exists when failure is not imminent. It may well be that as the modular ratio approaches 2 or 3, the limit suggested by Heukelom and Klomp[41] failure does occur, presumably

at the bottom of the base layer, thereby upsetting the modulus/stress relationship. A computer programme is at present being developed at the Koninklijke-Shell Laboratorium, Amsterdam to deal theoretically with a multilayer system in which modulus varies with depth. If the chosen variation with depth is realistic, then this program comes closer to the experimental findings than past efforts, although it must be remembered that the variation with depth is itself an approximation which is only valid for a restricted distance from the axis of the load. The problem will be better solved if modulus could be expressed as a function of stress, but this involves complications, since stresses themselves in a multilayer system are functions of modular ratios. A successive approximation solution may be possible here. A variation of modulus with radius as well as depth would be a further step towards stress dependence, but this could only apply for a particular contact pressure, producing a unique variation of modulus with position as well as with stress.

From the point of view of supporting existing

rational design suggestions, this thesis alone, probably does not contribute greatly, since further work on the main project is likely to deal more rigorously with layered systems and in particular the three layer system, not dealt with herein. Evidence collected so far suggests that the theory of elasticity is probably adequate, provided some knowledge of the stress/ modulus relationship for the pavement materials exists. There is some doubt, however, as to whether with an unbound base, the elaborate multilayer theory is necessary, since Boussinesq solutions appear adequate as a result of the very low tensile strength of the base layer. One important exception to this occurs either side of the interface, where Boussinesq values are not accurate.

Much of the project to date has been concerned with instrumentation as discussed in Chapters 3 and 4. Several problems have been overcome, in particular that of pressure cell cross-sensitivity, while others such as the strain cell zero error have been unearthed, but not yet solved. A number of pressure cells failed relatively soon after installation and others after

longer service. This is still being investigated, as is the failure of the deflection gauges. Until the instruments are made rather more reliable, they must be regarded as still in the experimental stage, but the work described herein indicates that they can give satisfactory results.

NOTE ON AUTHOR'S PUBLICATIONS

Some of the content of this thesis has already been published, or is due for publication.

A paper dealing with instrumentation and tests on the single layer system can be found under the following reference:-

Brown, S.F. and Pell, P.S., "Subgrade stress and deformation under dynamic load", Journal of the Soil Mechanics and Foundation Division, A.S.C.E., Vol. 93, No. S.M.1., Jan. 1967, pp 17-46.

A paper presenting both single and two layer results is to be presented at the Second International Conference on the Structural Design of Asphalt Pavements to be held at Ann Arbor, Michigan in August 1967. This reference at the time of writing is:

Brown, S.F. and Pell, P.S., "An experimental investigation of the Stresses, Strains and Deflections in a Layered Pavement Structure Subjected to Dynamic Loads", Preprint Vol. of 2nd Int. Conf. on Struct. Des. of Asph. Pavements, 1967, pp. 384-403.

NOTATION

a = Radius of loaded area

e = Strain with suffices having the same meaning as for stress

E = Secant modulus

E_1 = Secant modulus of upper layer

E_2 = Secant modulus of lower layer

h = Thickness of upper layer

I_2 = Second deviator stress invariant

J_1 = First stress invariant

p = Contact pressure

p_1 = Major principal stress

p_3 = Minor principal stress

p_z = Vertical Stress (see fig. 6.1)

p_r = Radial stress (see fig. 6.1)

p_θ = Tangential stress (see fig. 6.1)

p_{45} = 45° stress (see fig. 6.1)

p_{135} = 135° stress (see fig. 6.1)

r = Radius

z = Depth

α = Angle between major principal plane and horizontal

γ = Shear strain

ν = Poisson's ratio

τ = Shear stress

ACKNOWLEDGEMENTS

The work described in this thesis is part of a research project sponsored by the Koninklijke-Shell Laboratorium, Amsterdam. The Author would like to express his thanks to Shell and particularly to Dr. W. Heukelom. He is also indebted to Professor R. C. Coates who, as Head of the Civil Engineering Department, provided all necessary facilities for conducting the work, as well as showing a helpful interest in its progress.

Thanks are also due to many other people especially Dr.'s P.S. Pell and R. W. Sparrow for their general supervision and guidance at different times over a period of nearly four years.

A special word of gratitude is due to Miss C.A. Smith for typing the final version of the thesis, and to Mrs. S.A. Howett for her assistance. A lot of the draughting work was undertaken by Mr. D. Bowen and Miss H. Scarborough, to whom thanks are also due.

The Author would like to acknowledge the computing facilities provided by the Cripps Computing

Centre at the University, and by the Computer Unit at Imperial College, London. A word of thanks is also due to Mr. A. Jones of Shell's Thornton Research Centre for guidance in the use of his multilayer computer program and to the staff of Players's data processing department, particularly Mrs. J. Hills, for doing all the card punching.

For providing a measure of continuity at the beginning and end of the work, thanks are due to Dr. A.C. Tory and Mr. D.I. Bush respectively.

The Author also wishes to record his thanks to the technical staff of the Department of Civil Engineering under Mr. W.H. Peskett and later Mr. J.G. Redfern, for assistance in a variety of ways.

Finally to various other colleagues, particularly Mr. C. Snell for useful suggestions on stress analysis problems, the Author is grateful for assistance.

REFERENCES

1. 'Guide to the structural design of flexible and rigid pavements in the construction of new roads,' D.S.I.R. Road Research Laboratory, Road Note No. 29, H.M.S.O., 1960.

2. Thenn de Barros, S., 'A critical review of present knowledge of the problem of rational thickness design of flexible pavements,' H.R.R. No. 71, 1965, pp 105-128.

3. Burmister, D.M., 'Theory of stresses and displacements in layered systems and application to the design of airport runaways,' Proc. H.R.B., Vol. 23, 1943, pp 126-148.

4. Peattie, K.R., 'A fundamental approach to the design of flexible pavements,' Proc. Int. Conf. on Struct. Des. of Asphalt Pavements, 1962, pp 403-411.

5. Monismith, C.L. and Secor, K.E., 'Viscoelastic behaviour of asphalt concrete pavements,' Proc. Int. Conf. on Struct. Des. of Asphalt Pavements, 1962, pp 476-498.

6. Seed, H.B., Mitry, F.G., Monismith, C.L. and Chan, C.K., 'Prediction of pavement deflections from laboratory repeated load tests', Report No. TE-65-6, Soil mechanics and Bituminous Materials Research Laboratory, University of California, 1965.

7. Whiffin, A.C. and Lister, N.W., 'The application of elastic theory to flexible pavements,' Proc. Int.Conf. on Struct. Des. of Asphalt Pavements, 1962 pp 499-521.

8. Programme for the Second Int. Conf. on Structural Design of Asphalt Pavements, 1967.

9. Peattie, K.R., 'Surface deflection on road structures: 1. The significance of the surface deflection of pavements', Symposium on Road Tests for Pavement Design, Lisbon 1962.

10. Whiffin, A.C. and Morris, S.A.H., 'Piezoelectric gauge for measuring dynamic stresses under roads,' The Engineer, Vol. 213, April 1962, pp 741-746.

11. Tory, A.C., 'Stress and deformation in a semi-infinite soil mass subjected to dynamic loading' Ph.D. Thesis, University of Nottingham, 1964.

12. 'Investigations of pressure and deflections for flexible pavements; homogeneous sand test section;' Report No. 2, U.S. Corps of Engineers, Waterways Experiment Station, Vicksburg, Miss., 1954.

13. 'Investigations of pressure and deflections for flexible pavements: homogeneous clayey-silt test section.' Report No. 1, U.S. Corps of Engineers, W.E.S., Vicksburg, Miss., 1951.

14. McMahon. T.F. and Yoder, E.J., 'Design of pressure sensitive cell and model studies of pressures in a flexible pavement subgrade,' Proc. H.R.B. Vol. 39, 1960, pp 650-682.

15. Trollope, D.H., Lee, I.K. and Morris, J., 'Stresses and deformation in two layer pavement structures under slow repeated loading,' Proc. Australian Road Research Board, Vol. 1, Pt.2, 1962, pp 693-721.

16. Sowers, G.F, and Vesic, A.B., 'Vertical stresses in subgrades beneath statically loaded flexible pavements.' Bulletin 342, H.R.B, 1962, pp 90-123.

17. Sparrow, R.W. and Tory, A.C., 'Behaviour of a soil mass under dynamic loading,' Journal of the soil Mech. and Found. Div., A.S.C.E., Vol.92, No. S.M.3., May 1966, pp 59-83.

18. Burmister, D.M., 'The general theory of stresses and displacements in layered systems,' Journal of Applied Physics, Vol.16, Nos.2,3 and 5, 1945, pp 89-94, 126-127 and 296-302.

19. Fox, L. 'Computation of traffic stresses in a simple road structure,'Road Research Tech. Paper No.9, D.S.I.R., H.M.S.O., 1948.

20. Hank, R.J. and Scrivner, F.H., 'Some numerical solutions of stresses in two and three layered systems,' Proc. H.R.B., Vol.28, 1948, pp 457-468.

21. Acum, W.E.A. and Fox, L., 'Computation of load stresses in a three layer elastic system,' Geotechnique, Vol.2, 1951, pp 293-300.

22. Jones, A., 'Tables of stresses in three-layer elastic systems,' Bulletin 342, H.R.B., 1962, pp 176-214.

23. Mehta, M.R. and Veletsos, A.S., 'Stresses and displacements in layered systems,' Civil Eng. Studies. Struct. Res. Series No. 178, University of Illinois, 1959.

24. Jones, A., 'Surface deflection on road structures: 2. The calculation of surface deflection for three layer elastic systems,' Symposium on Road Tests for Pavement Design, Lisbon, 1962.

25. Boussinesq, J., 'Application des potentials a l'etude de l'equilibre et du mouvements des solids elastiques,' Gauthier-Villars, Paris, 1885.

26. Frölich, O.K., 'Drukverteilung im baugrunde,' De Ingenieur, April, 1932.

27. Ahlvin, R.G. and Ulery, H.H., 'Tabulated values for determining the complete pattern of stresses, strains and deflections beneath a uniform circular load on a homogeneous half space,' Bulletin 342, H.R.B. 1962, pp 1-13.

28. Jones, A., Private communication; paper to be presented at Ann Arbor, 1967.

29. Private communication from Shell.

30. Cumming, D.A. and Gerrard, C.M., 'Computation of stresses on pavements,' Proc. Australian Road Research

Board, Vol. 2, Pt. 2, 1964, pp 729-743.

31. Allwood, R.J., 'An experimental investigation of the distribution of pressure in sand,' Ph.D. Thesis, University of Birmingham, 1956.

32. Hu, G.C-Y., 'An experimental investigation of the distribution of pressure in a homogeneous sand test section and two layer system,' Ph.D. Thesis, University of Birmingham, 1961.

33. Buck, G.F., 'An investigation of earth pressure cell response and the stress distribution in test pavement subgrades,' Ph.D. Thesis, University of Birmingham, 1963.

34. Seed, H.B., Chan, C.K. and Lee, C.E, 'Resiliance characteristics of subgrade soils and their relation to fatigue failures in asphalt pavements,' Proc. Int. Conf. on the Struct. Des. of Asphalt Pavements, 1962, pp 611-636.

35. Sparrow, R.W., 'A direct shear apparatus for repeated loading on cohesive soils,' Civil Eng. and Pub. Works Review, Vol. 60, April 1965, pp 531-533.

36. van der Poel, C.J., 'Time and temperature effects on the deformation of bitumens and bitumen-mineral mixes,' Soc. of Plastic Engineers Journal, Vol. 11, 1955, pp 47-64.

37. Burmister, D.M., 'Application of layered system concepts to interpretations and evaluations of asphalt

pavement performances and to design and construction,' Proc. Int. Conf. on Struct. Des. of Asphalt Pavements, 1962, pp 441-453.

38. Heukelom, W., 'Analysis of dynamic deflections of soils and pavements,' Geotechnique, Vol. 2, 1961, pp 224-243.

39. Heukelom, W. and Foster, C.R., 'Dynamic testing of pavements,' Journal of the soil Mech. and Found. Div., A.S.C.E., Vol. 86, No. S.M.1., 1960, pp 1-28.

40. Heukelom, W. and Klomp, A.J.G., 'Road design and dynamic loading,' Proc. A.A.P.T., 1964, pp 92-105.

41. Heukelom, W. and Klomp, A.J.G., 'Dynamic testing as a means of controlling pavements during and after testing,' Proc. Int. Conf. on Struct. Des. of Asphalt Pavements, 1962, pp 667-679.

42. Jones, R., 'In-situ measurement of the dynamic properties of soils by vibration methods,' Geotechnique, Vol. 8, No.1, 1958, pp 1-21.

43. Jones, R., 'Measurement and interpretation of surface vibrations on soil and roads,' Bulletin No. 277, H.R.B., 1960, pp 8-29.

44. Jones, R., 'Surface wave technique for measuring the elastic properties and thicknesses of roads: theoretical developments,' Brit. Jour. of App. Phys., Vol. 13, 1962, pp 21-29.

45. Jones, R., 'Following changes in the properties of road bases and sub-bases by the surface wave propagation method,' Civil Eng. and Pub. Wks. Review, May and June 1963.

46. Jones, R and Mayhew, H.C., 'Thickness and quality of cemented surfacings and bases - measuring by a non-dist±u/^ctive surface wave method,' Civ. Eng and Pub. Wks. Review, Vol. 60, 1965, pp 523-529.

47. Dehlen, G.L., 'An investigation of flexure cracking on a major highway,' Proc. Int. Conf. on Struct. Des. of Asphalt Pavements, 1962, pp 812-820.

48. Dorman, G.M., 'The extension to practice of a fundamental procedure for the design of flexible pavements,' Proc. Int. Conf. on Struct. Des. of Asphalt Pavements, 1962, pp 785-793.

49. Dorman, G,M. and Metcalf, C.T., 'Design curves for flexible pavements based on layered system theory,' H.R.R. No. 71, 1965, pp 69-84.

50. Klomp, A.J.G. and Dorman, G.M., 'Stress distribution and dynamic testing in relation to road design,' Proc. 2nd Conf. Australian Road Res. Board, 1964.

51. Dorman, G.M., Edwards, J.M. and Kerr, J.E.D., 'The design of flexible pavements,' Proc. of the A.G.M., Eng. Inst. of Canada, 1964.

52. Peattie, K.R.,'Stress and strain factors for three-layer elastic systems,' Bulletin No.342, H.R.B., 1962, pp 215-253.

53. Hveem, F.N., 'Pavement deflections and fatigue failures,' Bulletin No.114, H.R.B., 1955, pp 43-87.

54. 'Thickness design-asphalt pavement structures for highways and streets,' Asphalt Institute Manual series No.1, 7th ed. The asphalt Institute, 1962.

55. Shook, J.F. and Finn, F.N., 'Thickness design relationships for asphalt pavements,' Proc. Int. Conf. on Struct. Des. of Asphalt Pavements, 1962, pp 52-83.

56. Shook, J.F., 'Development of Asphalt Institute thickness design relationships,' Proc. A.A.P.T., 1964, pp 187-217.

57. Highway Research Board, 'The AASHO road test; part 5: Pavement research, ' Special Report No.61E, 1962.

58. Hicks, L.D., 'Structural design of flexible pavements in North Carolina,' Proc. Int. Conf. on Struct. Des. of Asphalt Pavements, 1962, pp 802-811.

59. Tons, E., Chambers, R.E. and Kamin, M.A., 'Layered pavement design method for Massachusetts,' H.R.R. No.71, 1965, pp 193-219.

60. Vesic, A.B., 'The validity of layered solid theories for flexible pavements,' Proc. Int. Conf. on Struct. Des. of Asphalt Pavements, 1962, pp 283-290.

61. Baker, R.F.,'A structural design procedure for pavements,' Proc. Int. Conf. on Struct. Des. of Asphalt Pavements, 1962, pp 464-475.

62. McLeod, N.W., 'Some notes on pavement structural design,' in two parts, H.R.R. No.13, 1963, pp 66-141, and H.R.R. No.71, 1965, pp 85-104.

63. Highway Research Board, 'The WASHO road test; part 1, Design construction and testing procedures,' Special Report No.18, 1954.

64. Highway Research Board, 'The WASHO road test; part 2: Test data, analysis, findings, 'Special Report No.22, 1955.

65. 'Flexible pavement behaviour as related to deflection,' Symposium, Proc. A.A.P.T., 1962, pp 208-399.

66. Saal, R.N.J. and Pell, P.S., 'Fatigue of bituminous road mixes,' Kolloid Zeitschrift, Bd.171, Heft 1, 1960, pp 61-71.

67. Pell, P.S., 'Fatigue characteristics of bitumen and bituminous mixes,' Proc. Int. Conf. on Struct. Des. of Asphalt Pavements, 1962, pp 310-323.

68. Monismith, C.L., 'Fatigue of asphalt paving mixtures,' Proc. 1st Annual Street and Highway Conf., Nevada, 1966.

69. Lucas, A.G., Bazin, P. and Saunier, J., 'The fatigue testing of bituminous mixes,' Revue gen. de Routes Aerodr., 404, Nov. 1964.

70. Dehlen, G.L. 'Flexure of a road surfacing, its relation to fatigue cracking and factors determining its severity,' Bulletin No. 321, H.R.B. 1962, pp 26-39.

71. Pell, P.S., 'Fatigue of bituminous materials in flexible pavements,' Proc. Inst. of Civil Eng's, Vol. 31, July 1965, pp 283-312.

72. 'Soil mechanics for road engineers,' D.S.I.R., Road Research Laboratory, H.M.S.O., 1952, pp 221-225

73. Dearman, H.R. 'The structure of the culm measures at Meldon, near Okehampton, N. Devon,' Quart. Journ. Geol. Soc. of London, Vol. 115, 1959, pp 65-106.

74. Peattie, K.R. and Sparrow, R.W., 'The fundamental action of earth pressure cells,' Journ. Mech. and Phys. of Solids, Vol. 2, 1954, pp 141-155.

75. Sparrow, R.W. 'Depth of ballast. Pilot investigation into the measurement of stresses in the formation,' B. Railways Research Board Report (Eng. Div.) E.200, July 1958.

76. Dunn, C.S. and Billam, J., 'A study of the response characteristics of a new miniature earth pressure cell,' Civil Eng. and Pub. Works Review, 1966, pp 181-186.

77. Redshaw, S.C., 'A sensitive miniature pressure cell,' Jour. Sc. Insts., Vol. 31, 1954, p 467.

78. Private communication from the Road Research Laboratory.

79. Rowe, P.W., and Barden, L., 'The importance of free ends in triaxial testing,' Journ. Soil Mech. and Found. Div., A.S.C.E., Vol. 90, No. S.M.1., 1964, pp 1-27.

80. 'Final report on development of earth strain measuring device.' U.S. Army Eng. Ohio River Div. Lab., 1953.

APPENDIX I DATA PROCESSING

I.1 Primary Results

Tory[11] solved the problem of interpreting a large number of traces by devising a trace reader and encoder unit, which, coupled with a paper tape punch converted experimental readings from analogue to digital form. Once on punched tape, the results could be analysed by a suitable computer program.

This apparatus was originally designed to produce 5-hole paper tape which was the system used by Tory, and was later changed to the 7-hole system as new computing facilities became available on the Atlas machine at Manchester University and subsequently on the KDF9 at Nottingham. The trace reader equipment is shown in Fig. I.1.

The first program developed for work described in this thesis was used to analyse experimental data produced by the trace reading equipment. This program determined contact pressures, total loads and all the stresses, strains and deflections for a complete test run. This basic program was used, with slight modifications, to analyse all the single and

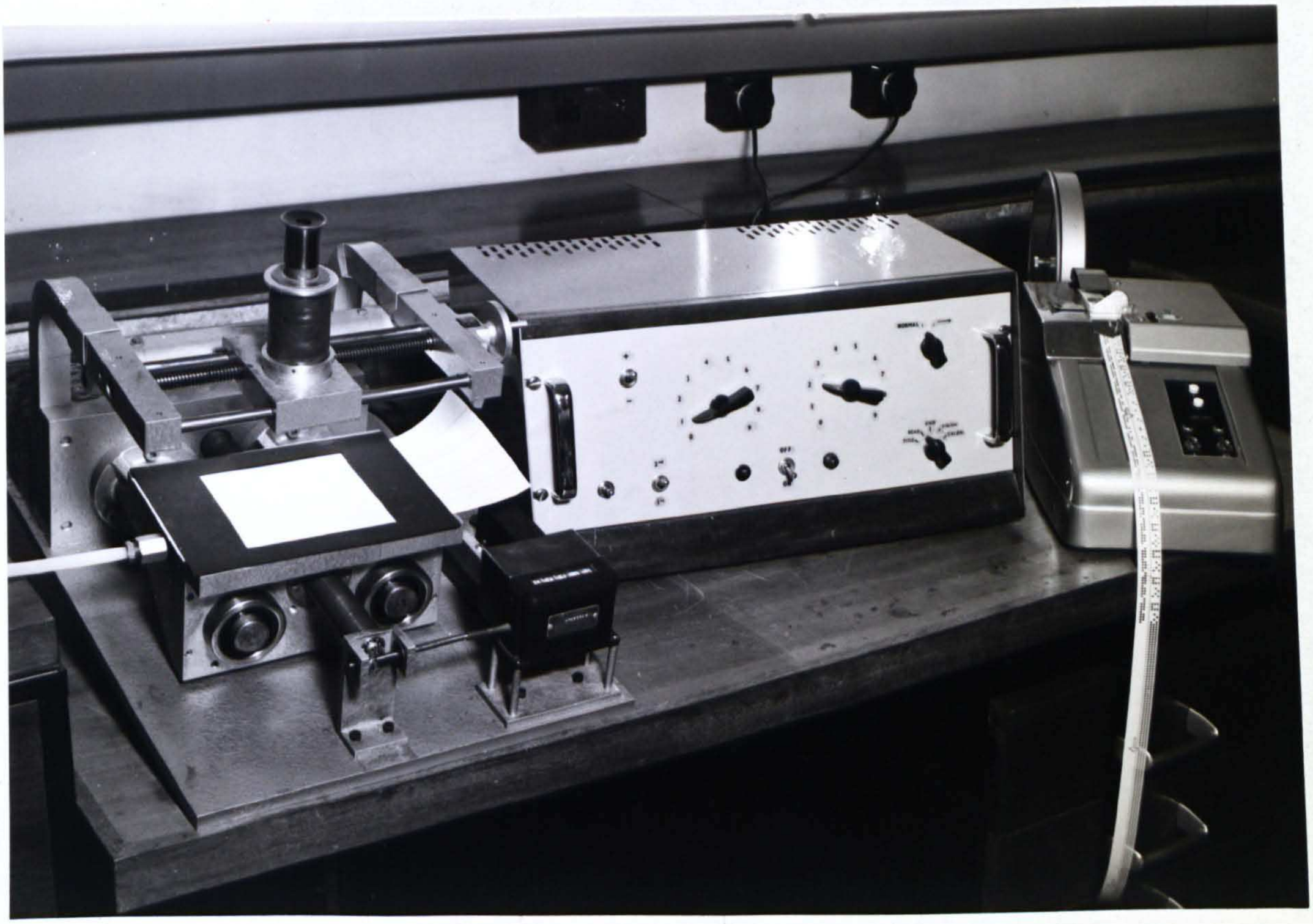

FIG. I.1 TRACE READER, ENCODER UNIT AND TAPE PUNCH

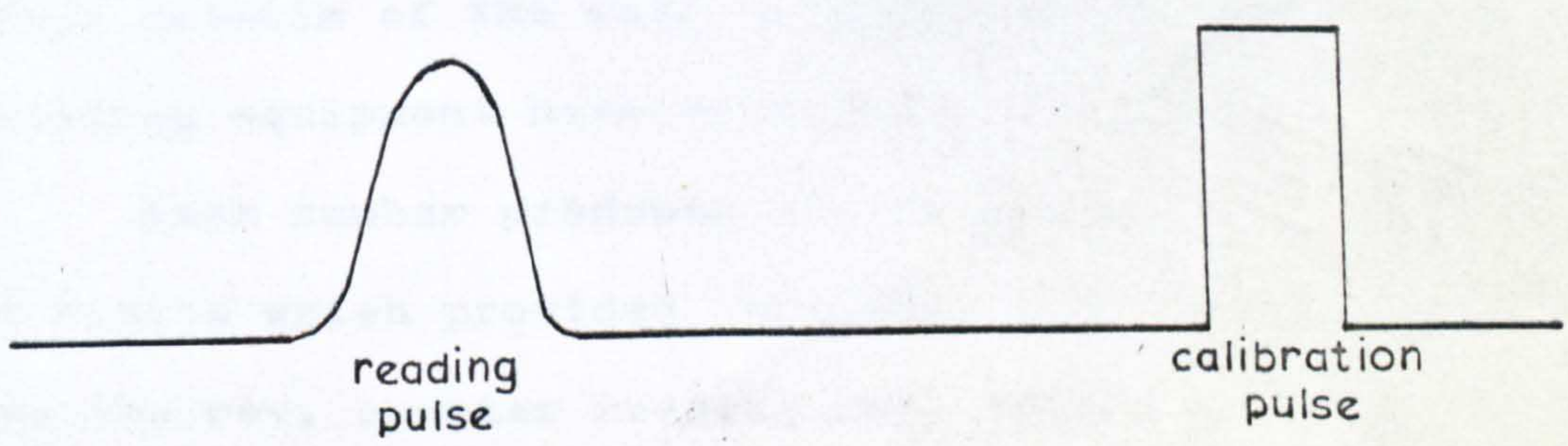

FIG. I.2 TYPICAL TRACE

two-layer system results.

A typical trace for one channel of output is shown in fig. I.2. It consists of a square calibration pulse and a pulse representing the reading being taken. One loading position in the test pit produced at least six such traces. In reading each pulse the paper is held on a movable table by air vacuum and the table moved relative to a microscope eye piece fitted with cross-hairs. The movement of the table, and hence the height of the pulse, is monitored by a special rev. counter connected to the screw which moves the table along. To complete the reading of one trace, the microscope is focussed at the top and bottom of each pulse, and a number punched out each time. This means four numbers, two for the calibration pulse and two for the reading. Full details of the mode of operation of the trace reading equipment have been given by Tory[11].

Each number produced by the equipment consisted of 8 digits which provided labelling information as well as the rev. counter reading and, under certain circumstances, other relevant data. When reading a trace the number was of the following form:- ABCDEFGH.

where A = Label to determine whether a calibration or reading pulse was involved.

B = Label to determine whether the top or bottom of a pulse was being read

CD = Channel number of the trace being used.

EFGH = Rev. counter reading.

A = 6 for a calibration and 5 for a reading

B = 0 for the bottom and 2 for the top of a pulse.

C and D could be any digit from 0 to 9.

Each test run consisted of several applications of load or "tests". The data for each test was, therefore, preceeded by a punched number which took the form:- 1000AB00 where AB referred to the "test" no.

When all the traces for a particular test run had been read and put on punched tape, a terminating number was punched, viz:- 30000000.

Each number was followed by a pair of space symbols and after every fifth, a newline symbol as well. This made the print out of the numbers easy to read, as can by seen in fig. I.3 which shows a small portion of typical test data, for the first two "tests", or loading

```
10000100  60000745  62000669  60010659
62010590  52000458  52010478  50010658  50000742
50130734  52130709  50120694  50250644  52120586
52250514  62250417  62120446  62130466  60250646
60120693  60130733  10000200  60000797  62000722
60010709  62010641  52000508  52010523  50010708
50000791  50130783  52130759  50120744  50250696
52120641  52230578  50230574  52250572  52070477
50070477  62070185  62230324  62250469  60070480
62120497  62130516  60230573  60250698  60120743
60130784  10000300  60000780  62000704  60010691
```

Fig. I.3 PORTION OF TYPICAL DATA FOR PRIMARY PROGRAM

positions, of a test run. The first number is 10000100 indicating "Test 1". This is followed by 10 numbers starting with 6 indicating calibration pulse information and 10 with 5 indicating reading pulse data. The data for test 2 follows preceeded by the number 10000200.

In producing a data tape from the analogue traces, the possibility of human error clearly arose. Some likely mistakes were easily checked by studying the print out of the data tape. The test numbers were located and underlined for clarity and then the number of "numbers" for each test was quickly counted. This was checked against the required number, being four times the number of channels involved, and varied from test to test. This procedure occasionally showed

omissions, but the possibility of punching one number twice and leaving out another remained. Experience showed this to be most unusual, but if it did happen, the error became obvious after the data had been processed by computer, when any unusual results were investigated, to see if they originated from a data tape error.

It would have been possible to incorporate in the computer program a routine to check the data for errors, but since a print out of the data was required anyway, and the procedure above took very little time, this was not considered necessary.

The computer program written to produce primary results from the data tapes is shown in detail in figs. I.4 to I.12, where test D/A has been used as the example. Primary results consist of applied contact pressures, a check on whether the assumed and actual contact areas were equal and all the stresses, strains and deflections directly measured in the test pit. These latter were calculated in their appropriate units as well as in normalised form (see chapter 6). A typical print out of results is shown at the end of

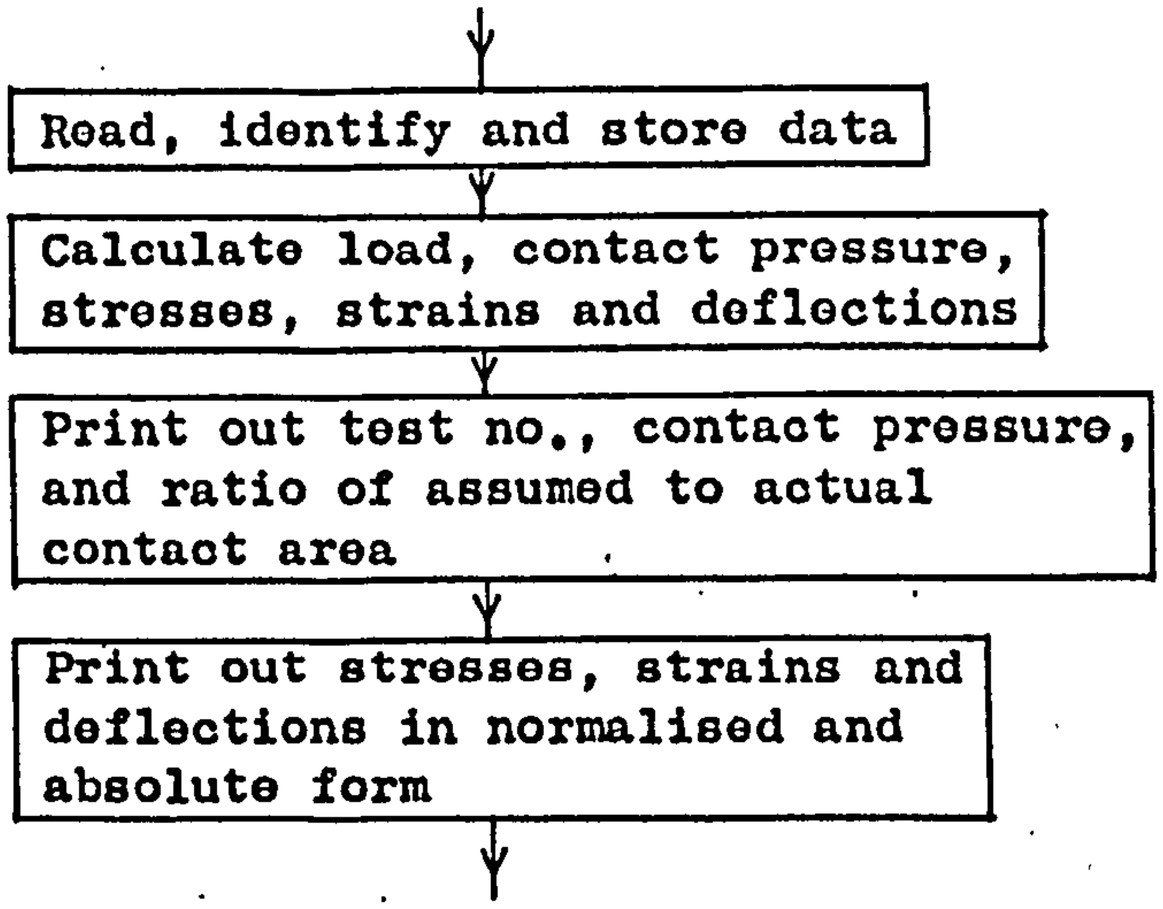

FIG. I.4 MAIN SUBDIVISIONS OF PRIMARY PROGRAM

the program details in fig. I.12.

The basic calculation in the program is very simple and consists of the following equation:-

$$f(m,n) = \frac{d(m,n) - c(m,n)}{b(m,n) - a(m,n)} \times k(n)$$

where f(m,n) refers to the stress, strain, surface deflection, load or contact pressure being calculated. a, b, c and d, with appropriate sufficos, refer to the rev. counter readings for the top and bottom of calibratio and reading pulses. Thus (d - c) is the height of the reading pulse and (b - a) that of the calibration. The suffices (m,n) are used to label each rev. counter reading where m = test number and n = cell number. Thus a(1,3) refers to the rev. counter reading of the

bottom of the calibration pulse for channel 3 in test 1. The suffices are required in order to store all the data in the computer, so that it can be subsequently printed out in the correct order. k(n) is the calibration figure for the channel (i.e. transducer) being used, and is the value of the calibration pulse obtained when the instrument was calibrated prior to installation (See section 3.1).

Tables I.1 and I.2 have been compiled with the aid of a loading programme sheet (fig. 5.3) and a knowledge of the relative positions of load and cells for each load application. They indicate the values of m and n used to identify the stresses and strains measured for this particular test run on the pit. The significance of Tables I.1 and I.2 is that they indicate roughly the way in which the computed results need to be printed out. Table I.1 shows tests numbers for each measurement and the channel numbers of the cells involved. All combinations of cell number and test number produce a result, e.g. for vertical stress with cells 27 and 3, results are as shown in Table I.2. A knowledge of the depth of each cell is required,

TABLE I.1 IDENTIFICATION OF RESULTS FROM THE PRIMARY PROGRAM

Measurement	Cell No's. (n)	Test No's. (m)			
		Radius (in.)			
		0	3	6	9
Vertical Stress	21, 8, 9	13 13	14 12	15 11	16 10
Vertical Stress	27, 3	25 25	26 24	27 23	28 22
Radial Stress	26, 4, 5	29 29	30 28	31 27	32 26
Radial Stress	20, 10, 11	9	10	11	12
Tangential Stress	20, 10, 11	9	8	7	6
45° Stress	23, 7	5	6	7	8
135° Stress	23, 7	5	4	3	2
Vertical Strain	25, 12, 13	1 1	2 32	3 31	4 30
Radial Strain	22, 16, 17	17	16	15	14
Tangential Strain	22, 16, 17	17	18	19	20
45° Strain	24, 14, 15	21	20	19	18
135° Strain	24, 14, 15	21	22	23	24

TABLE I.2 PRIMARY PROGRAM - RESULTS FOR TWO TYPICAL CELLS

Cell No.	Radius (in.)			
	0	3	6	9
27	(25, 27) (25, 27)	(26, 27) (24, 27)	(27, 27) (23, 27)	(28, 27) (22, 27)
3	(25, 3) (25, 3)	(26, 3) (24, 3)	(27, 3) (23, 3)	(28, 3) (22, 3)

and this is provided by a convenient rule of thumb. All cell numbers greater than 20 refer to the centre of the base layer, other even numbers to 3 in. below the interface and odd numbers to 12 in. below the interface. Results at the interface are not included in the table, but have been catered for in the program. Surface deflection measurements do not appear in Table I.1 since none were taken for test. D/A but the procedure for labelling was identical to that indicated for stresses and strains.

Fig. I.4 shows the four main sub-divisions of the computer program. At the end of the first two all

measurements are in the computer store, then the print out of results follows in two parts, as indicated. A detailed flow diagram for each of these subdivisions is shown in figs. I.5 to I.9, and this is followed in fig. I.10 by a print out of the actual program in Atlas Autocode, the computer language which was used. In the flow diagrams, autocode representation has been kept to a minimum, for the better understanding of readers not well versed in Atlas Autocode. The abbreviations used should be self explanatory, but the instruction "switch L(x)" needs explanation. This indicates that control passes to the instruction labelled L(x), where x takes its current value. This provides several possibilities as can be seen, in this case L(2), L(4), L(6) or L(7), these suffices being the only values which x can assume at this stage. A full list of the notation used in the program is shown in fig. I.11.

A print out of a typical output is shown in fig. I.12.

$\frac{P}{T}$ means :- $\frac{\text{contact pressure x assumed contact area}}{\text{applied load}} \times 100$

$= \frac{\text{assumed contact area}}{\text{actual contact area}} \times 100$

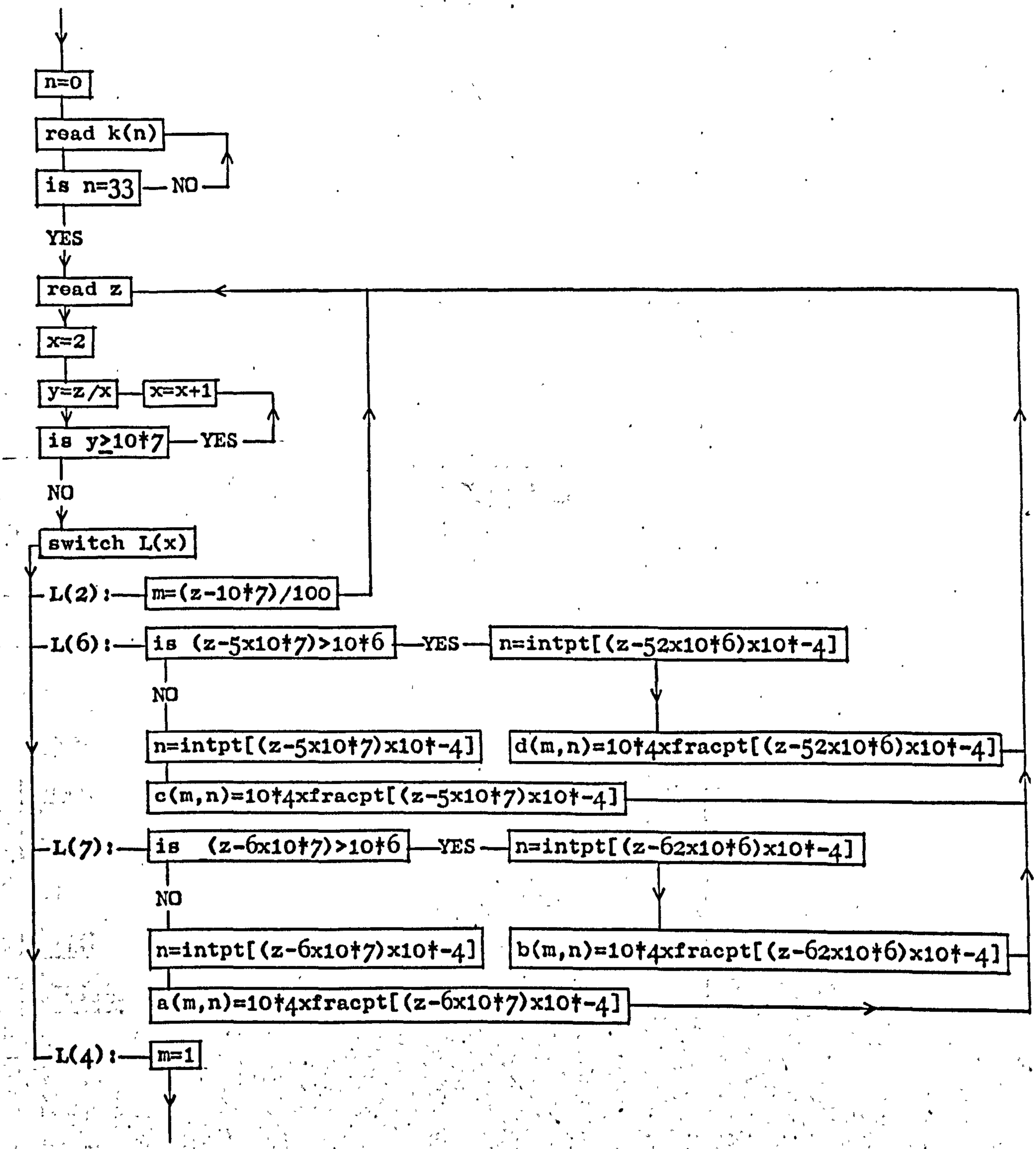

FIG. I.5 FLOW DIAGRAM FOR FIRST PART OF PRIMARY PROGRAM

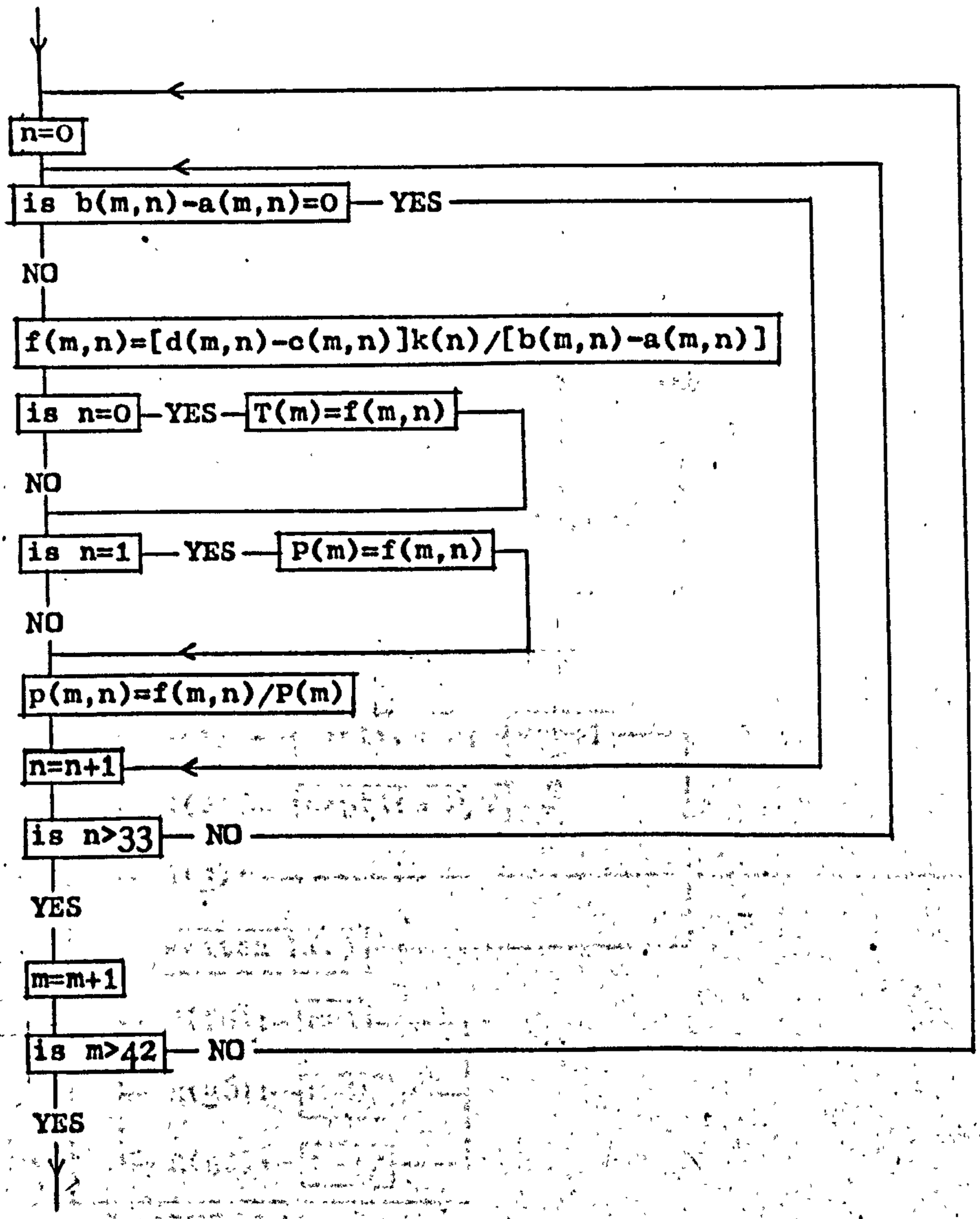

FIG. I.6 FLOW DIAGRAM FOR SECOND PART OF PRIMARY PROGRAM

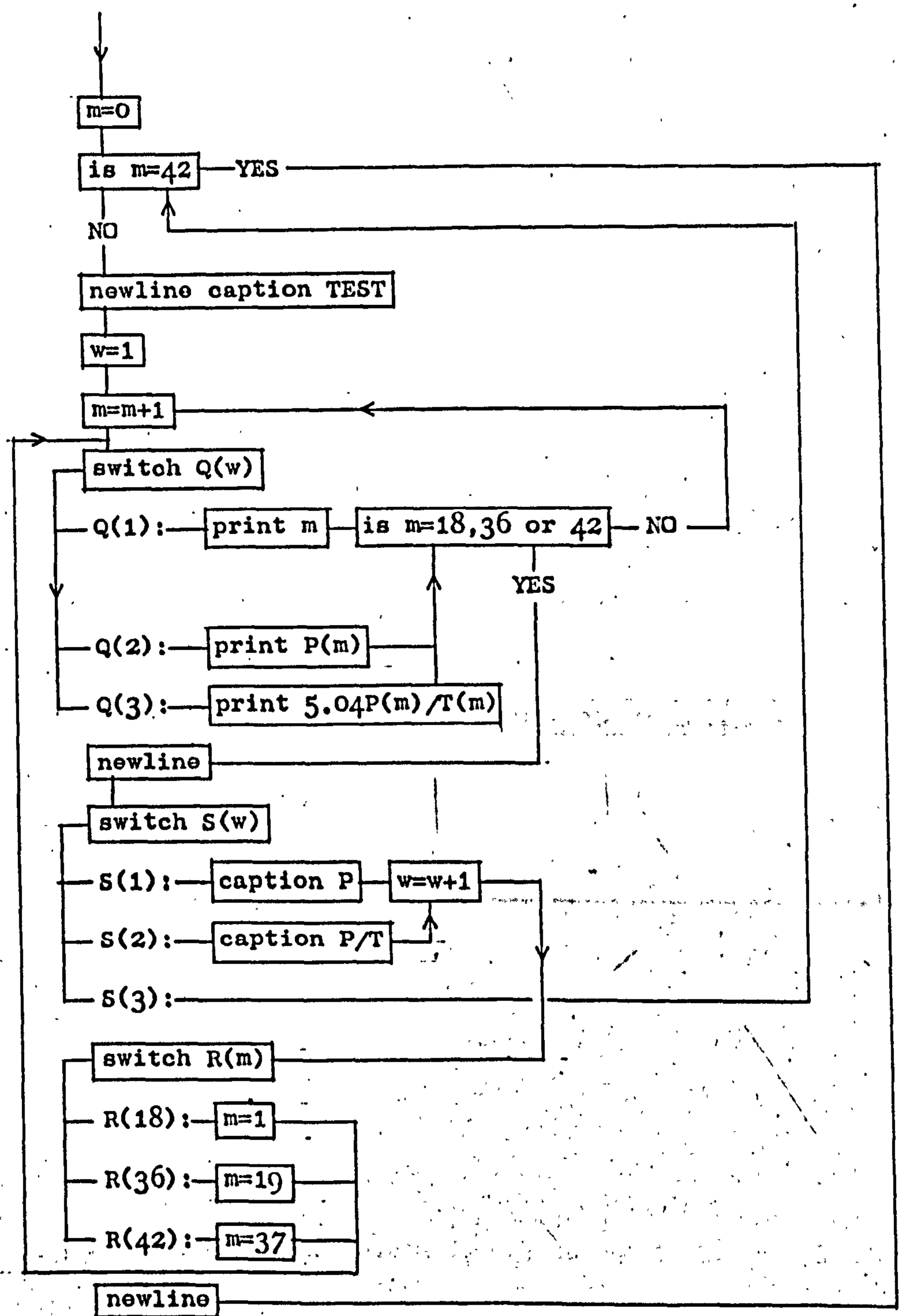

FIG. I.7 FLOW DIAGRAM FOR THIRD PART OF PRIMARY PROGRAM

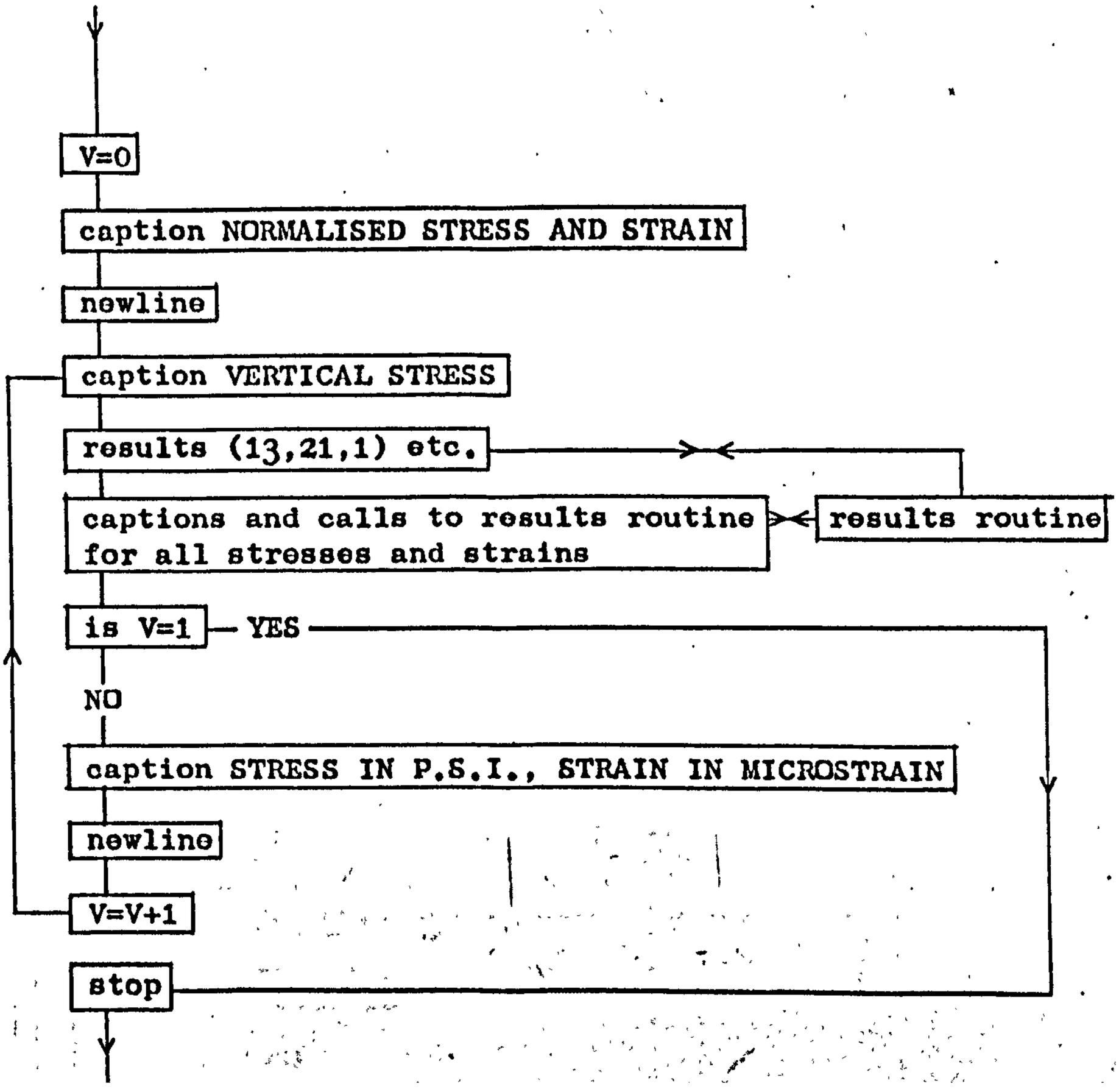

FIG. I.8 FLOW DIAGRAM FOR LAST PART OF PRIMARY PROGRAM

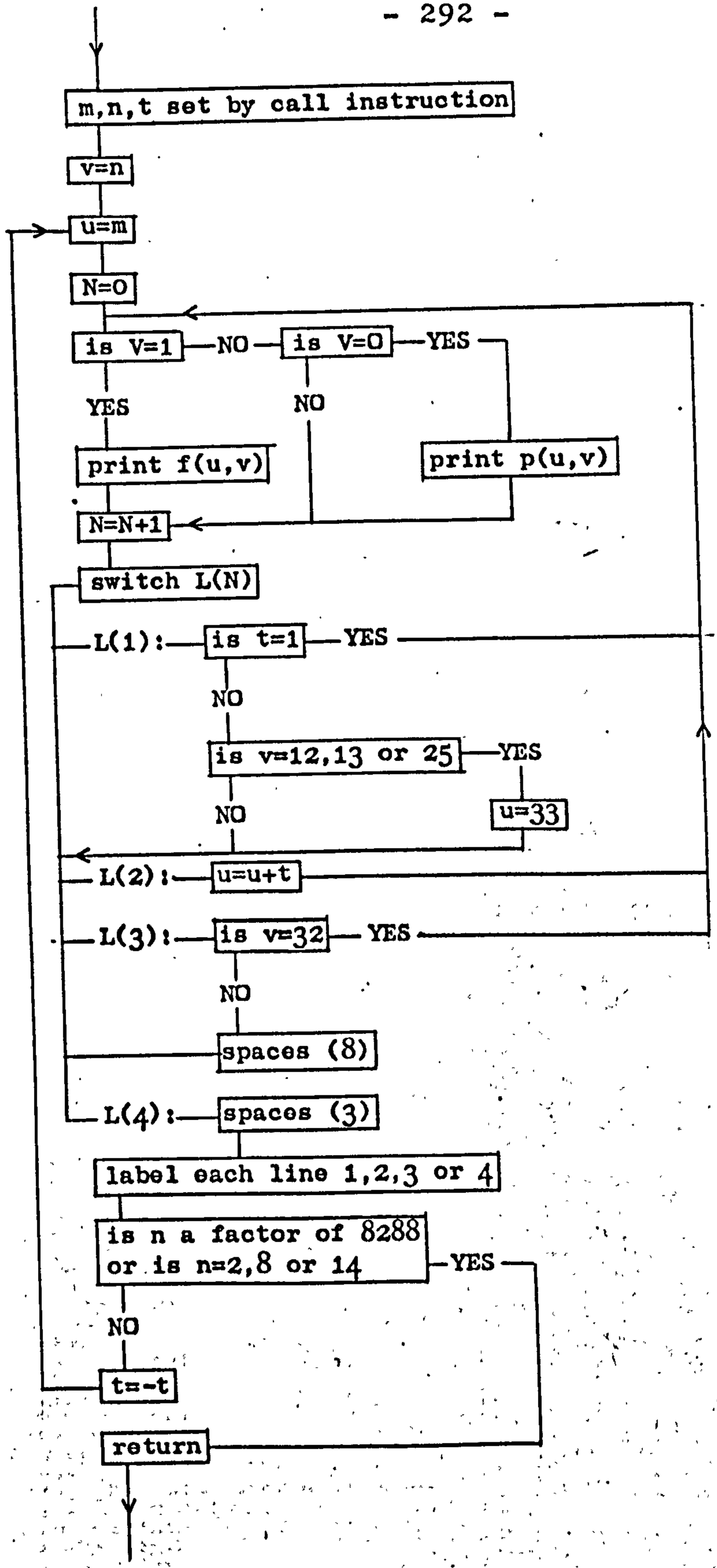

FIG. I.9 FLOW DIAGRAM FOR "RESULTS" ROUTINE - PRIMARY PROGRAM

```
begin
array a,b,c,d,p,f(1:42,0:33),k(0:33),T,P(1:42)
integer x,m,n,z,w,V
real y
switch L(2:7),S,Q(1:3),R(18:42)
routine spec results(integer m,n,t)
cycle m=1,1,42
cycle n=0,1,33
a(m,n)=0;b(m,n)=0;c(m,n)=0;d(m,n)=0;k(n)=0
repeat
repeat
cycle n=0,1,33
read(k(n))
repeat
2:read(z)
x=2
8:y=z/x
if y≥1α7 then ->1
->L(x)
1:x=x+1;->8
L(2):m=(z-1α7)/100
->2
L(6):if (z-5α7)>1α6 then ->9
n=intpt(1α-4(z-5α7))
c(m,n)=1α4fracpt(1α-4(z-5α7))
->2
9:n=intpt(1α-4(z-52α6))
d(m,n)=1α4fracpt(1α-4(z-52α6))
->2
L(7):if (z-6α7)>1α6 then ->10
n=intpt(1α-4(z-6α7))
a(m,n)=1α4fracpt(1α-4(z-6α7))
->2
10:n=intpt(1α-4(z-62α6))
b(m,n)=1α4fracpt(1α-4(z-62α6))
->2
L(4):m=1
19:n=0
20:if b(m,n) - a(m,n)=0 then ->17
f(m,n)=(d(m,n)-c(m,n))k(n)/(b(m,n)-a(m,n))
if n=0 then T(m)=f(m,n)
if n=1 then P(m)=f(m,n)
if f(m,n)>1α4P(m) then ->17
p(m,n)=f(m,n)/P(m)
17:n=n+1
if n>33 then ->18
->20
18:m=m+1
if m>42 then ->21
->19
21:m=0
S(3):if m=42 then ->80
newline
caption TEST
w=1
82:m=m+1
->Q(w)
Q(1):print(m,5,0)
84:if m=18 or m=36 or m=42 then ->81
->82
Q(2):print(P(m),3,1);->84
Q(3):print(5.04P(m)/T(m),5,0);->84
81:newline
->S(w)
S(1):caption ⌀⌀⌀P
83:w=w+1
->R(m)
S(2):caption ⌀P/T
->83
R(18):m=1;->Q(w)
R(36):m=19;->Q(w)
R(42):m=37;->Q(w)
80:newline
V=0
caption NORMALISED⌀STRESS⌀AND⌀STRAIN;newline
23:caption VERTICAL⌀STRESS
results(13,21,1)
results(25,27,1)
results(13,8,1)
results(13,9,1)
results(25,3,1)
caption RADIAL⌀STRESS
results(29,26,1)
results(9,20,1)
results(33,33,1)
results(29,4,1)
results(9,10,1)
results(29,5,1)
results(9,11,1)
caption TANGENTIAL⌀STRESS
results(9,20,-1)
results(9,10,-1)
results(9,11,-1)
caption 45.DEG.STRESS
results(5,23,1)
results(5,7,1)
caption 135.DEG.STRESS
results(5,23,-1)
results(5,7,-1)
caption VERTICAL⌀STRAIN
results(1,25,1)
results(35,32,1)
results(1,12,1)
results(1,13,1)
caption RADIAL⌀STRAIN
results(17,22,-1)
results(38,28,1)
results(42,29,-1)
results(17,16,-1)
results(17,17,-1)
caption TANGENTIAL⌀STRAIN
results(17,22,1)
results(17,16,1)
results(17,17,1)
caption 45.DEG.STRAIN
results(21,24,-1)
results(21,14,-1)
results(21,15,-1)
caption 135.DEG.STRAIN
results(21,24,1)
results(21,14,1)
results(21,15,1)
if V=1 then ->22
caption STRESS⌀IN⌀P.S.I.,⌀STRAIN⌀IN⌀MICROSTRAIN;newline
V=V+1
->23
22:stop
routine results(integer m,n,t)
integer N,u,v
switch L(1:4)
newline
v=n
12:u=m
N=0
4:if V=1 then print(f(u,v),3,3)
if V=0 then print(p(u,v),3,3)
1:N=N+1
->L(N)
L(1): if t=1 then ->2
if 12≤v≤13 or v=25 then u=33
L(2):->2
L(3): if v=32 then ->14;->2
14:spaces(8)
L(4): spaces(3);->3
2:u=u+t;->4
3:if 20≤v≤27 then ->5
if v=28 or v=33 then ->6
if v=29 or 31≤v≤32 then ->7
if intpt(v/2)=(v/2) then ->8
caption (5)
10:print(v,3,0);newline;->9
5:caption (1);->10
6:caption (2);->10
7:caption (3);->10
8:caption (4);->10
9:if intpt(8288/u)=(8288/u) then ->11
13:return
11:if u=2 or u=8 or u=14 then ->13
t=-t;->12
end
end of program
```

FIG. I.10 PRIMARY PROGRAM IN ATLAS AUTOCODE

n = cell number
k = calibration constant
z = any number on data tape
L = label
m = test number
intpt = integral part of
fracpt = fractional part of
a = bottom of calibration pulse
b = top of calibration pulse — rev. counter
c = bottom of reading pulse — readings
d = top of reading pulse
f = stress, strain, deflection, load or contact pressure
T = applied load
P = applied contact pressure
p = normalised stress, strain or deflection
(for stress, 100p is the correct normalised form)
Q,S,R = labels
v = current value of m
u = current value of n
x,y,w,V,N,t = symbols used to fascillitate programing,
eg., counters, current values, etc,
↑ = to the power of... (used in flow diagrams only)

FIG. I.11 NOTATION USED IN PRIMARY PROGRAM

```
TEST      1      2      3      4      5      6      7      8      9     10     11     12     13     14     15     16     17     18
   P   26.4   27.6   27.4   24.2   27.3   27.7   27.8   27.7   27.7   27.0   26.5   26.5   27.3   27.0   26.7   27.8   27.6   27.8
 P/T     87     90     90     79     92     91     90     93     91     89     88     89     87     84     93     89     89     89

TEST     19     20     21     22     23     24     25     26     27     28     29     30     31     32     33     34     35     36
   P   26.9   26.8   24.4   26.9   27.1   27.6   27.2   26.4   27.4   27.9   26.1   26.9   27.1   27.4   27.0   26.9   27.2   27.5
 P/T     86     89     80     88     88     90     88     85     87     87     83     86     86     87     88     87     88     89

TEST     37     38     39     40     41     42
   P   26.7   26.0   27.2   24.9   25.9   27.8
 P/T     91     92     90     87     87     90

NORMALISED STRESS AND STRAIN
VERTICAL STRESS
  0.814  0.805  0.347  0.119  (1) 21
  0.814  0.444  0.265  0.069  (1) 21

  0.660  0.603  0.471  0.176  (1) 27
  0.660  0.934  0.324  0.071  (1) 27

  0.197  0.185  0.143  0.116  (4)  8
  0.197  0.178  0.180  0.100  (4)  8

  0.079  0.078  0.057  0.058  (8)  9
  0.078  0.089  0.064  0.044  (8)  9

  0.081  0.079  0.063  0.063  (8)  3
  0.081  0.083  0.081  0.068  (8)  3
RADIAL STRESS
  0.207  0.190  0.185  0.000  (1) 26
  0.207  0.204  0.180  0.199  (1) 26

  0.292  0.269  0.257  0.221  (1) 20

 -0.024 -0.014 -0.012  0.036  (2) 33

  0.102  0.086  0.094  0.097  (4)  4
  0.102  0.089  0.084  0.072  (4)  4

  0.044  0.057  0.067  0.067  (4) 10

  0.021  0.028  0.016  0.020  (8)  3
  0.021  0.016  0.028  0.025  (8)  3

  0.013  0.017  0.017  0.014  (8) 11

TANGENTIAL STRESS
  0.292  0.274  0.209  0.101  (1) 20

  0.044  0.020 -0.000 -0.024  (4) 10

  0.013  0.007  0.007 -0.003  (8) 11
45.DEG.STRESS
  0.414  0.402  0.406  0.313  (1) 23

  0.021  0.039  0.036  0.042  (8)  7
135.DEG.STRESS
  0.414  0.285  0.082 -0.022  (1) 23

  0.021  0.016  0.000  0.000  (8)  7
VERTICAL STRAIN
 30.078 27.907 18.738  2.253  (1) 25
 30.078 28.522 24.567  7.443  (1) 25

 16.462 14.437  8.943         (3) 32
 16.462 -9.047 11.499         (3) 32

 16.614 17.092 13.019  8.772  (4) 18
 16.614 17.497 13.031  8.920  (4) 18

  4.163  3.818  3.359  3.045  (8) 13
  4.163  3.078  2.102  1.333  (8) 13
RADIAL STRAIN
 -2.281 -0.827  1.560  3.881  (1) 22

 -7.714 -6.367 -2.436 -0.181  (2) 20

 -3.394 -2.941 -0.666  0.000  (3) 29

 -4.121 -2.830 -1.054  0.963  (4) 16

 -1.196 -1.031 -0.689  0.000  (8) 17
TANGENTIAL STRAIN
 -2.281  0.000  0.000  0.000  (1) 22

 -4.121 -4.268 -3.391 -2.264  (4) 16

 -1.196 -1.202 -1.409 -1.068  (8) 17
45.DEG.STRAIN
 14.466 -98.408 32.836 30.378  (1) 24

  8.464  0.000 16.006 16.250  (4) 14

  1.719  2.740  3.800  4.183  (8) 19
135.DEG.STRAIN
 14.466 -0.798 -12.995 -9.936  (1) 24

  8.464  2.164 -0.997 -1.959  (4) 14

  1.719  0.000 -0.386 -0.571  (8) 19
```

```
STRESS IN P.S.I.  STRAIN IN MICROSTRAIN
VERTICAL STRESS
 14.823 13.631  9.994  3.282  (1) 21
 14.823 11.765  7.011  2.397  (1) 21

 17.918 15.928 12.907  4.787  (1) 27
 17.918 14.749  8.786  1.922  (1) 27

  9.372  9.006  4.108  3.197  (4)  8
  9.372  4.715  3.965  2.686  (4)  8

  2.048  2.100  1.640  1.511  (8)  9
  2.048  1.870  1.604  1.198  (8)  9

  2.194  2.093  1.732  1.726  (8)  3
  2.194  2.301  2.194  1.841  (8)  3
RADIAL STRESS
  5.406  5.045  5.013  0.000  (1) 26
  5.406  5.975  4.925  5.269  (1) 26

  8.068  7.248  6.798  5.866  (1) 20

 -0.656 -0.384 -0.329  0.983  (2) 33

  2.670  2.289  2.283  2.660  (4)  4
  2.670  2.426  2.298  1.900  (4)  4

  1.221  1.033  1.764  1.764  (4) 10

  0.844  0.680  0.436  0.846  (8)  3
  0.844  0.435  0.764  0.695  (8)  3

  0.370  0.461  0.463  0.368  (8) 11
TANGENTIAL STRESS
  8.068  7.861  5.647  2.802  (1) 20

  1.221  0.549 -0.221 -0.659  (4) 10

  0.370  0.184  0.184 -0.092  (8) 11
45.DEG.STRESS
 11.298 13.368 10.950  8.666  (1) 23

  0.864  1.070  0.973  1.163  (8)  7
135.DEG.STRESS
 11.298  6.900  2.250 -0.607  (1) 23

  0.864  0.388  0.000  0.000  (8)  7
VERTICAL STRAIN
794.760 780.079 513.837  84.548  (1) 25
794.760 780.831 644.079 197.387  (1) 25

452.830 397.727 238.636         (3) 32
452.830-239.606 310.180         (3) 32

491.903 471.037 356.707 218.349  (4) 18
491.903 476.022 373.000 229.922  (4) 18

110.019 105.284  92.071  73.708  (8) 13
110.019  84.248  56.996  35.338  (8) 13
RADIAL STRAIN
-62.857 -22.764  48.344  96.748  (1) 22

-216.107-173.826 -69.552  -4.678  (2) 20

 -98.746 -76.304 -17.693   0.000  (3) 29

-113.569 -69.630 -30.239  86.015  (4) 16

 -32.967 -28.378 -16.917   0.000  (8) 17
TANGENTIAL STRAIN
 -62.857   0.000   0.000   0.000  (1) 22

-118.569-117.500 -91.052 -87.361  (4) 16

 -32.967 -33.104 -37.833 -28.494  (8) 17
45.DEG.STRAIN
 882.672-2033.716 881.679 836.782  (1) 24

 211.226   0.000 429.767 447.674  (4) 14

  41.908  73.333  93.966 118.238  (8) 19
135.DEG.STRAIN
 882.672 -21.486-388.672-274.618  (1) 24

 211.226  80.198 -27.070 -84.141  (4) 14

  41.908   0.000 -10.476 -15.760  (8) 19
```

FIG. I.12 OUTPUT FROM PRIMARY PROGRAM

The mean contact pressure and value of the area ratio have been calculated separately. In this case mean $\frac{P}{T}$ = 90% i.e. assumed contact area = 0.9 x actual area. This value of 90% is not typical and it indicates that the actual area was larger than that assumed, which is difficult to conceive unless some load was transmitted through the metal rings around the loading platen.

The stresses and strains appear in four columns representing radii of 0, 3 in., 6in., and 9 in. from left to right. Each line is followed by a number in brackets indicating the depth and also the cell number. The interpretation of these depth numbers is shown in Table I.3. Normalised stresses are 100 times less than the definition given in section 6.1, bringing them into line with normalised strain and deflection since all effects are calculated from the same equations.

I.2 Derived results

Several duplicate results emerged from the primary program, and these were averaged in order to produce

TABLE I.3 IDENTIFICATION OF DEPTH NUMBERS ON OUTPUT FROM PRIMARY PROGRAM

No.	Depth (in.)	Location
1	6	Upper layer
2	$\pm 10\frac{1}{2}$	Just above interface
3	$\pm 13\frac{1}{2}$	Just below interface
4	15	Subgrade
5	24	Subgrade

unique values of all the measured stresses and strains. A new data tape was then made with values of vertical, radial, tangential, 45° and 135° stresses and strains for each point and in addition the mean contact pressure for each test. Three of these data tapes were produced for the single layer system, and two for the two layer system each containing information on four test runs, whereas the primary results were processed for one test run at a time. Each tape contained results from tests with the same size of loaded area.

```
begin
array an(0:1)
real ez,er,ec,ed,ep,pz,pr,pd,pp,pc,x,y,A,B,C,D,E,u1,u2,v1,v2,a,b,c,P,p,p1,p3,e1,e3
integer q,r,s,t,u
switch L(-1:2),M(1:4)
caption###x####p1####p3##TORMAX####y#####e1#####e3###GAMAMAX#an(p)#an(e)##p1###J1###I2####E#####eE####nu###enu;newline
caption S/A;newline
cycle r=1,1,4
read(p)
cycle s=1,1,10
read(ez,er,ec,ed,ep,pz,pr,pd,pp,pc)
x=pz+pr-pd-pp
y=ez+er-ed-ep
pz=.01(pz-.1x)
pr=.01(pr-.1x)
pd=.01(pd+.4x)
pp=.01(pp+.4x)
ez=.1(ez-.17y)
er=.1(er-.17y)
ed=.1(ed+.33y)
ep=.1(ep+.33y)
pc=.01pc;ec=.1ec
a=pz;b=pr;c=pd;q=0
3:t=1
an(q)=28.6arctan((a-b),(2c-a-b))
2:P=.5((a+b)+t*sqrt((2c-a-b)^2+(a-b)^2))
u=t+q
->L(u)
L(1):p1=P;->1
L(-1):p3=P;->7
L(2):e1=P;->1
L(0):e3=P;->4
1:t=-1;->2
7:a=ez;b=er;c=ed;q=1
->3
4:print(.01x,2,2);print(p1,1,3);print(p3,1,3);print(.5(p1-p3),1,3);print(.1y,4,2);print(e1,3,2);print(e3,3,2)
print((e1-e3),3,2);print(an(0),3,1);print(an(1),3,1);print(p1*p,3,1);print(p*(p1+p3+pc),3,1)
print(.33p^2*(p1^2+pc^2+p3^2-p1*pc-pc*p3-p3*p1),3,1)
A=1a6(((pc+pr)/ez)+((pc+pz)/er)+((pp+pc)/ed)+((pz+pr)/ec)+((pd+pc)/ep))
B=1a6((pz/ez)+(pr/er)+(pd/ed)+(pc/ec)+(pp/ep))
C=1a12(((pc+pr)/ez)^2+((pz+pc)/er)^2+((pc+pp)/ed)^2+((pz+pr)/ec)^2+((pd+pc)/ep)^2)
D=1a12((pz/ez)^2+(pr/er)^2+(pd/ed)^2+(pc/ec)^2+(pp/ep)^2)
E=1a12((pz*(pr+pc)/ez^2)+(pr*(pz+pc)/er^2)+(pd*(pc+pp)/ed^2)+(pc*(pz+pr)/ec^2)+(pp*(pd+pc)/ep^2))
u1=(5E-A*B)/(5C-A^2)
u2=(5D-B^2)/(5E-A*B)
v1=(B*C-E*A)/(5C-A^2)
v2=u2*(E*B-A*D)/(5D-B^2)
print(.5(v1+v2),5,0);print(50|(v1-v2)|/(.5(v1+v2)),3,1)
print(.5(u1+u2),2,2);print(50|(u1-u2)|/(.5(u1+u2)),3,1)
newline
if s=5 then ->5
->6
5:newline
6:repeat
->M(r)
M(1):caption S/B;->M(4)
M(2):caption S/C;->M(4)
M(3):caption S/D
M(4):newline
repeat
stop
end of program
```

FIG. I.13 PROGRAM FOR DERIVED RESULTS

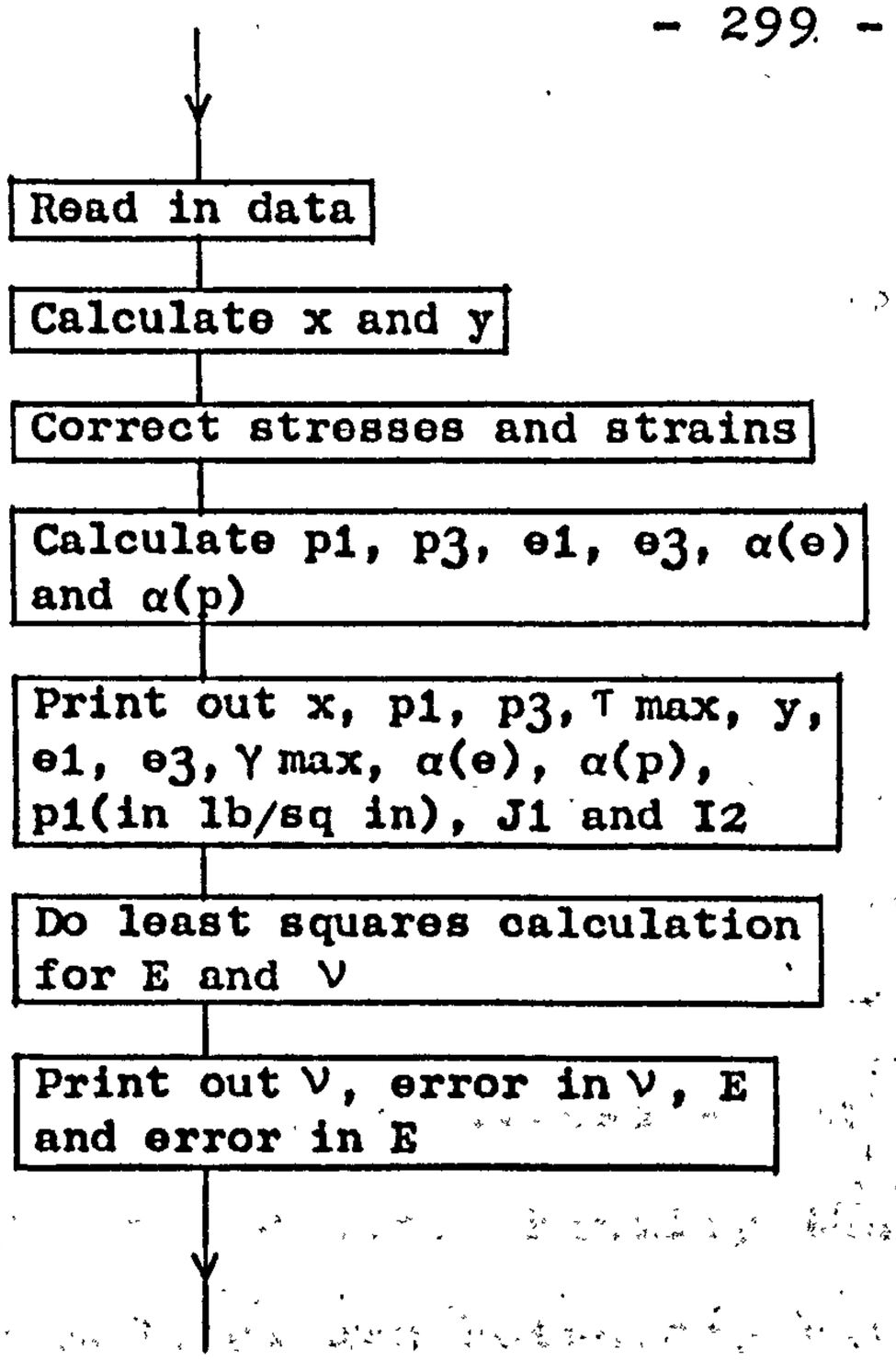

FIG. I.14 FLOW DIAGRAM FOR DERIVED RESULTS PROGRAM

From the data on these new tapes, all the derived results mentioned in section 6.5 were computed as well as certain other useful information. The program used for the purpose is shown in fig. I.13, and a flow diagram in fig. I.14. The stresses and strains are first corrected to eliminate the equilibrium and compatibility errors as shown in section 7.3. Various derived stresses and strains are then computed and printed out. Finally the least squares calculation for modulus and Poisson's ratio is carried out and the results printed. The approach adopted for this least squares calculation is outlined in section 6.6. The error in E has been expressed as:-

$$\frac{\frac{1}{2}(E_1 - E_2)}{\frac{1}{2}(E_1 + E_2)} \times 100\%$$

where E_1 and E_2 are the two values obtained by performing the two regressions. A similar expression has been used for ν.

Output from this program is shown in Fig. I.15, where, with the exception of the right hand value of p_1, and also J_1 and I_2, all stresses and strains are in normalised form, stress again differing from the original definition as explained in I.1 above.

Fig. I.13

X	P1	P3	TORMAX	Y	E1	E3	GAMAMA
S/A							
0.06	0.880	0.472	0.204	-5.30	158.70	-31.80	190.50
0.04	0.874	0.414	0.230	-4.20	166.77	-47.34	214.11
0.09	0.572	0.217	0.177	-5.00	156.32	-55.12	211.44
0.07	0.274	-0.006	0.140	-27.80	70.27	-22.42	92.70
0.02	0.139	-0.002	0.071	1.10	17.53	-5.01	22.54
S/B							
0.09	0.230	0.074	0.078	-30.00	12.30	-4.10	16.40
0.12	0.222	0.050	0.086	-26.30	19.36	-10.42	29.78
0.08	0.214	0.006	0.104	-18.60	23.18	-13.75	36.93
0.10	0.168	-0.012	0.090	-12.90	20.98	-11.30	32.28
0.06	0.134	-0.017	0.076	-3.80	12.24	-5.45	17.68
S/B							
0.11	0.959	0.534	0.212	-62.30	93.89	-31.21	125.10
0.08	0.930	0.467	0.232	-64.80	108.51	-43.88	152.39
0.12	0.640	0.258	0.191	-34.40	140.94	-56.95	197.89
0.05	0.323	-0.020	0.172	-31.10	73.09	-25.02	98.11
0.13	0.151	-0.017	0.084	4.30	22.99	-6.65	29.64
S/C							
0.17	0.273	0.091	0.091	-24.80	9.32	-6.28	15.60
0.10	0.267	0.060	0.103	-19.50	15.47	-8.74	24.20
0.13	0.240	0.023	0.108	-14.90	20.99	-13.23	34.22
0.12	0.196	-0.001	0.099	-11.20	17.84	-10.93	28.78
0.10	0.164	-0.022	0.093	-6.80	12.96	-6.65	19.61
S/C							
0.19	0.810	0.405	0.202	-16.50	80.10	-17.20	97.30
0.12	0.801	0.376	0.212	-28.00	75.26	-15.84	91.10
0.00	0.525	0.211	0.157	-8.70	66.99	-21.33	88.33
0.11	0.274	-0.020	0.147	-17.10	35.19	-10.17	45.36
0.10	0.171	-0.012	0.091	1.50	8.19	-2.20	10.38
S/C							
0.15	0.215	0.035	0.090	-7.20	6.52	-2.28	8.80
0.13	0.219	0.016	0.102	-8.80	7.41	-3.42	10.83
0.19	0.197	-0.011	0.104	-7.30	9.22	-5.53	14.75
0.04	0.148	0.017	0.066	-9.30	9.34	-5.28	14.63
0.02	0.117	0.003	0.057	-5.20	6.29	-1.93	8.22
S/D							
0.15	0.776	0.392	0.192	-10.40	90.47	-14.93	105.40
0.16	0.765	0.322	0.237	-17.70	95.77	-12.15	107.93
0.05	0.548	0.195	0.177	-5.70	71.30	-21.06	92.36
0.15	0.254	0.025	0.115	-17.30	37.27	-7.99	45.26
0.07	0.138	0.002	0.068	1.90	7.63	0.03	7.60
S/D							
0.29	0.192	0.041	0.076	-13.00	6.31	-1.49	7.80
0.15	0.193	0.033	0.080	-9.10	9.25	-3.55	12.80
0.05	0.184	0.017	0.084	-7.20	9.96	-2.41	12.37
0.05	0.148	0.018	0.065	-5.80	9.09	-3.72	12.81

EE	NU	ENU
0.2	0.42	0.2
0.4	0.45	0.3
9.2	0.41	31.0
33.7	0.24	40.1
1.1	0.52	9.0
0.1	0.45	0.8
3.0	0.32	1.0
1.3	0.49	14.5
1.6	0.48	11.1
0.2	0.28	8.9
0.0	0.48	0.0
1.0	0.54	0.4
8.3	0.42	32.0
36.1	0.22	50.8
17.4	1.02	44.2
0.2	0.58	0.1
0.5	0.32	0.0
1.3	0.59	8.9
0.5	0.59	9.9
0.3	0.29	18.2
0.0	0.42	0.0
0.1	0.44	0.4
22.5	0.45	58.5
60.3	-0.58	-98.3
955.5	-0.94	-97.7
0.0	0.42	1.1
4.6	0.25	2.8
8.4	0.52	54.5
19.7	0.67	70.9
10.5	0.42	48.6
0.0	0.40	0.0
0.3	0.39	0.2
24.2	0.38	60.4
8.6	0.22	22.7
20.1	-0.03	-54.2
1.5	0.33	7.3
2.1	0.29	0.8
2.0	0.30	6.6
4.0	0.38	17.5

18.7	-0.04	-56.2	51.0	53.2	1.0	0.9	0.4 33612
			0.080	-5.20	5.04	-1.88	7.72
			-0.03	0.145	-0.015	0.010	

FIG. I.15 OUTPUT FROM DERIVED RESULTS PROGRAM

I.3 Other computer programs

While not coming strictly under the heading of data processing, two other programs were developed to calculate theoretical results, and a third program was used, but not developed, for the same purpose.

Fig. I.16 shows the program developed for calculating theoretical stresses and strains from the tables of Ahlvin and Ulery[27]. The data in this case consisted of values of the constants from the tables and also values of modulus and Poisson's ratio appropriate to the depth being considered. This program was used for producing Boussinesq solutions for both the single and the two layer systems. In addition to the stresses calculated by Ahlvin and Ulery's formulae, derived results for comparison with similar measured values were also computed. Typical output is shown in fig. I.17.

The program which was used, but developed elsewhere, was that for solving the multilayer problem. This program was written in Fortran IV and was on punched cards, facilities for which did not exist at Nottingham. Data cards had to be prepared elsewhere and the program

```
begin
begin;1112,0,0,100:
array A,B,C,D,E,F,G,H(1:9)
real Em,nu,Z,g,v,p,t,z,r
integer a,q,l
caption ##ez###er###ec###ed###ep###e1###e3##gmax##pz#####pr#####pc#####pd#####pp#####p1#####p3###tmax##
/angle#wz;newline
read(a)
q=0
3:read(Em,nu);caption E=;print(Em,5,0);caption ##nu=;print(nu,0,2);newline
cycle l=1,1,9
if q=1 or q=3 then ->1
read(A(l),B(l),C(l),D(l),E(l),F(l),G(l),H(l))
1:z=1α6(1+nu)((1-2nu)*A(l)+B(l))/Em
r=1α6(1+nu)((1-2nu)*F(l)+C(l))/Em
g=2α6(1+nu)*G(l)/Em
print(z,4,0);print(r,4,0)
print(1α6(1+nu)((1-2nu)*E(l)-D(l))/Em,4,0)
print(.5(z+r+g),4,0)
print(.5(z+r-g),4,0)
print(.5(z+r+sqrt((z-r)²+g²)),4,0)
print(.5(z+r-sqrt((z-r)²+g²)),4,0)
print(sqrt((z-r)²+g²),4,0)
v=(A(l)+B(l))1α2
p=1α2(2nu*A(l)+C(l)+(1-2nu)*F(l))
t=1α2G(l)
print(v,3,1);print(p,3,1)
print(1α2(2nu*A(l)-D(l)+(1-2nu)*E(l)),3,1)
print(.5(v+p+2t),3,1);print(.5(v+p-2t),3,1)
print(.5(v+p+sqrt((v-p)²+4t²)),3,1)
print(.5(v+p-sqrt((v-p)²+4t²)),3,1)
print(.5sqrt((v-p)²+4t²),3,1)
print(90arctan((v-p),2t)/π,4,1)
print(1α5(1+nu)(1-nu)*H(l)*a/Em,4,1)
newline
repeat
q=q+1
if q=4 then ->2
newline
->3
2:stop
100:111;85,-,αg;newline;caption β85=;print(g,3,0)
stop
end
end of program
```

FIG. I.16 PROGRAM FOR BOUSSINESQ THEORETICAL RESULTS

ez	er	ec	ed	ep	e1	e3	gmax	pz	pr	pc	pd	pp	p1	p3	tmax	/angle	wz
E= 8465 nu= 0.41																	
76	-22	-22	27	27	76	-22	98	91.1	32.4	32.4	61.7	61.7	91.1	32.4	29.3	0.0	72.9
76	-22	-22	34	20	76	-22	99	90.1	31.6	31.6	65.3	56.5	90.5	31.3	29.6	4.3	72.0
74	-22	-22	42	10	77	-24	101	86.9	29.3	29.3	67.7	48.5	88.5	27.7	30.4	9.2	69.5
69	-20	-21	52	-3	77	-28	104	79.6	26.2	25.2	69.3	36.5	84.2	21.6	31.3	15.8	65.4
55	-12	-20	61	-18	73	-30	104	64.6	24.3	19.3	68.1	20.8	75.5	13.4	31.1	24.8	59.7
31	3	-17	61	-27	63	-29	92	41.7	24.8	12.8	59.5	7.1	60.8	5.7	27.5	36.1	53.2
9	15	-13	46	-23	47	-23	69	20.7	24.0	7.6	43.1	1.6	43.2	1.6	20.8	47.3	46.8
-3	16	-7	23	-11	26	-13	39	6.0	17.1	3.6	21.8	1.4	23.2	-0.0	11.6	59.2	38.6
-3	8	-2	7	-3	10	-5	15	1.0	7.7	1.6	7.4	1.4	8.9	-0.1	4.5	68.9	29.3
E= 8465 nu= 0.41																	
76	-22	-22	27	27	76	-22	98	91.1	32.4	32.4	61.7	61.7	91.1	32.4	29.3	0.0	72.9
76	-22	-22	34	20	76	-22	99	90.1	31.6	31.6	65.3	56.5	90.5	31.3	29.6	4.3	72.0
74	-22	-22	42	10	77	-24	101	86.9	29.3	29.3	67.7	48.5	88.5	27.7	30.4	9.2	69.5
69	-20	-21	52	-3	77	-28	104	79.6	26.2	25.2	69.3	36.5	84.2	21.6	31.3	15.8	65.4
55	-12	-20	61	-18	73	-30	104	64.6	24.3	19.3	68.1	20.8	75.5	13.4	31.1	24.8	59.7
31	3	-17	61	-27	63	-29	92	41.7	24.8	12.8	59.5	7.1	60.8	5.7	27.5	36.1	53.2
9	15	-13	46	-23	47	-23	69	20.7	24.0	7.6	43.1	1.6	43.2	1.6	20.8	47.3	46.8
-3	16	-7	23	-11	26	-13	39	6.0	17.1	3.6	21.8	1.4	23.2	-0.0	11.6	59.2	38.6
-3	8	-2	7	-3	10	-5	15	1.0	7.7	1.6	7.4	1.4	8.9	-0.1	4.5	68.9	29.3
E= 17943 nu= 0.41																	
16	-6	-6	5	5	16	-6	22	28.4	0.7	0.7	14.6	14.6	28.4	0.7	13.9	0.0	13.1
16	-6	-6	7	3	16	-6	22	28.6	1.0	0.4	16.9	12.7	28.7	0.9	13.9	4.3	13.1
15	-6	-6	8	1	15	-6	21	26.8	1.2	0.6	18.1	9.9	27.4	0.6	13.4	8.8	12.4
13	-5	-6	9	-0	14	-6	20	24.8	1.8	0.5	19.1	7.6	26.2	0.5	12.9	13.2	12.7
12	-4	-5	9	-1	14	-6	19	22.4	2.6	0.5	19.4	5.5	24.6	0.4	12.1	17.5	12.4
10	-3	-5	10	-2	12	-5	18	19.6	3.3	0.4	19.2	3.7	22.7	0.2	11.2	21.8	12.0
8	-2	-5	10	-3	11	-5	16	16.7	4.0	0.4	18.4	2.3	20.6	0.1	10.3	25.9	11.6
6	-0	-4	9	-3	10	-4	14	12.7	4.8	0.3	16.5	0.9	17.4	-0.0	8.7	31.6	10.9
3	1	-3	7	-3	7	-3	10	7.3	5.1	0.2	12.5	-0.0	12.6	-0.1	6.4	40.0	9.8
E= 17943 nu= 0.44																	
15	-7	-7	4	4	15	-7	22	28.4	1.0	1.0	14.7	14.7	28.4	1.0	13.7	0.0	12.7
16	-6	-7	6	3	16	-6	22	28.6	1.3	0.7	17.1	12.9	28.8	1.2	13.8	4.4	12.7
14	-6	-6	7	1	15	-6	21	26.8	1.5	0.9	18.2	10.1	27.4	0.9	13.3	8.9	12.0
13	-5	-6	9	-1	14	-6	20	24.8	2.1	0.8	19.2	7.8	26.2	0.8	12.7	13.4	12.3
12	-4	-6	9	-2	13	-6	19	22.4	2.9	0.7	19.6	5.7	24.6	0.6	12.0	17.7	12.0
10	-3	-5	10	-3	12	-5	18	19.6	3.6	0.6	19.3	3.8	22.7	0.4	11.1	22.0	11.6
8	-2	-5	10	-3	11	-5	16	16.7	4.2	0.5	18.6	2.4	20.7	0.3	10.2	26.2	11.2
6	-0	-4	9	-4	10	-4	14	12.7	5.0	0.4	16.6	1.0	17.5	0.1	8.7	32.0	10.6
3	1	-3	7	-3	7	-3	10	7.3	5.4	0.3	12.6	0.1	12.7	-0.0	6.4	40.5	9.5

FIG. I.17 OUTPUT FROM BOUSSINESQ THEORETICAL RESULTS PROGRAM

was run on the IBM 7090 computer at Imperial College in London. This program produced just sufficient information to obtain the complete description of stress and strain at a point. Some of the information required for comparison with experimental results had, therefore to be calculated. The output from the main program consisted of vertical, radial and vertical-radial shear stress and strain. These values were used as data for a program which calculated all the other stresses and strains required for comparison with measured and derived experimental results. The program and typical output are shown in figs. I.18 and I.19.

Finally a relatively simple program was written to determine the best fit straight lines on the various log-log plots used in Chapters 7 and 8.

```
begin
real ez,er,g,a,b,c,q,pz,pr,j
integer x,t,m,n
switch  L(1:4)
caption ADDITIONAL#THEORETICAL#RESULTS,#2#LAYER#SYSTEM;newline
caption POSN##E1#####E45######E3#####E135###GAMAMAX##α(E)####P1#####P45######P3#####P135###TORMAX###
α(P);newline
caption A=6,#E1=13500,#NU1=.35,#E2=12700,#NU2=.41;newline
m=0
5:n=8
6:cycle x=1,1,n
print(x,2,0)
read(ez,er,g)
a=ez;b=er;c=g;q=1
3:t=1
4:print(.5((a+b)+t*sqrt((a-b)²+c²)),4,2)
print(.5(a+b+t*c),4,2)
if t=1 then ->1
print(q*sqrt((a-b)²+c²),4,2)
print(90arctan((a-b),c)/π,3,1)
if q=.5 then ->2
read(pz,pr,j)
a=pz;b=pr;c=2j;q=.5
->3
1:t=-1;->4
2:newline
if m≤1 and x=4 then newline
if 2≤m≤3 and x=5 then newline
repeat
newline
m=m+1
->L(m)
L(1):caption A=6,#E1=13500,#NU1=.35,#E2=25000,#NU2=.41;newline;->5
L(2):caption A=9,#E1=11500,#NU1=.35,#E2=9100,#NU2=.41;newline
7:n=10;->6
L(3):caption A=9,#E1=11500,#NU1=.35,#E2=16500,#NU2=.41;newline;->7
L(4):stop
end of program
```

FIG. I.18 PROGRAM FOR ADDITIONAL MULTILAYER RESULTS

FIG. 1.19 OUTPUT FROM ADDITIONAL MULTILAYER RESULTS PROGRAM

ADDITIONAL THEORETICAL RESULTS, 2 LAYER SYSTEM

POSN	E1	E45	E3	E135	GAMAMAX	%(E)	P1	P45	P3	P135	TORMAX	%(P)
A=6, E1=13500, NU1=.35, E2=12700, NU2=.41												
1	44.10	15.35	-13.40	15.35	57.50	0.0	64.30	35.60	6.90	35.60	28.70	0.0
2	40.94	26.50	-13.24	1.20	54.17	13.9	58.96	44.50	4.74	19.20	27.11	23.3
3	31.14	28.15	-11.54	-8.55	42.69	29.6	43.49	40.45	0.71	3.75	21.39	36.8
4	18.67	18.65	-7.67	-7.65	26.34	43.5	25.52	25.45	-0.92	-0.85	13.22	44.2
5	15.30	4.60	-6.10	4.60	21.40	0.0	19.90	10.30	0.70	10.30	9.60	0.0
6	14.66	7.75	-5.86	1.05	20.52	9.5	19.10	13.20	0.60	6.50	9.25	17.2
7	12.86	9.30	-5.26	-1.70	18.12	18.7	16.80	14.10	0.40	3.10	8.20	28.5
8	10.64	9.25	-4.34	-2.95	14.98	27.3	13.82	13.15	0.28	0.95	6.77	35.1
A=6, E1=13500, NU1=.35, E2=25000, NU2=.41												
1	45.70	15.90	-13.90	15.90	59.60	0.0	66.70	36.90	7.10	36.90	29.80	0.0
2	41.86	26.15	-13.16	2.55	55.02	12.7	60.56	44.85	5.54	21.25	27.51	21.8
3	30.70	27.20	-10.20	-6.70	40.91	28.0	43.45	39.90	2.45	6.00	20.50	35.7
4	17.38	17.35	-5.98	-5.95	23.37	42.8	24.43	24.35	0.97	1.05	11.73	43.9
5	3.90	1.15	-1.60	1.15	5.50	0.0	9.90	4.95	0.00	4.95	4.95	0.0
6	3.88	1.80	-1.58	0.50	5.46	6.9	9.63	5.50	0.07	4.20	4.78	12.7
7	3.58	2.20	-1.46	-0.10	5.05	13.5	9.02	5.65	-0.02	3.35	4.52	23.2
8	3.22	2.40	-1.32	-0.50	4.55	19.8	8.13	5.50	-0.03	2.60	4.08	29.4
A=9, E1=11500, NU1=.35, E2=9100, NU2=.41												
1	59.90	22.60	-14.70	22.60	74.60	0.0	81.30	49.50	17.70	49.50	31.80	0.0
2	59.48	33.15	-16.08	10.25	75.55	8.8	79.40	58.70	15.10	35.80	32.15	16.2
3	53.84	42.60	-16.64	-5.40	70.47	21.5	69.30	63.30	9.30	15.30	30.00	30.8
4	44.78	42.35	-17.78	-15.35	62.57	33.6	54.54	56.70	1.16	-1.00	26.69	39.1
5	28.92	28.90	-12.72	-12.70	41.63	43.9	34.21	37.30	-1.21	-4.30	17.71	44.4
6	36.80	11.20	-14.40	11.20	51.20	0.0	35.50	19.00	2.50	19.00	16.50	0.0
7	35.77	17.75	-14.07	3.95	49.85	8.0	34.41	25.25	2.29	11.45	16.06	14.8
8	32.82	22.10	-13.02	-2.30	45.83	16.1	31.48	28.85	1.82	4.45	14.83	25.8
9	28.45	23.25	-11.55	-6.35	40.00	23.9	27.16	29.00	1.24	-0.60	12.96	32.8
10	23.38	21.50	-9.68	-7.80	33.05	31.2	22.19	26.15	0.81	-3.15	10.69	37.8
A=9, E1=11500, NU1=.35, E2=16500, NU2=.41												
1	62.70	23.60	-15.50	23.60	78.20	0.0	84.90	51.60	18.30	51.60	33.30	0.0
2	61.59	32.65	-16.19	12.75	77.79	7.4	82.31	59.15	16.09	39.25	33.11	14.0
3	53.76	40.75	-15.06	-2.05	68.83	19.2	70.04	62.15	11.46	19.35	29.29	28.9
4	42.76	39.80	-14.76	-11.80	57.51	31.9	53.18	54.45	4.12	2.85	24.53	38.1
5	26.28	26.25	-9.58	-9.55	35.85	43.5	32.02	34.70	1.58	-1.10	15.22	44.2
6	11.60	3.45	-4.70	3.45	16.30	0.0	19.50	9.95	0.40	9.95	9.55	0.0
7	11.39	5.15	-4.59	1.65	15.99	6.3	19.12	11.50	0.38	8.00	9.37	11.8
8	10.81	6.40	-4.41	0.00	15.21	12.4	18.11	12.40	0.29	6.00	8.91	21.2
9	9.90	7.10	-4.10	-1.30	14.00	18.4	16.53	12.55	0.17	4.15	8.18	28.1
10	9.78	7.20	-3.68	-2.10	12.47	24.1	14.61	12.00	0.09	2.70	7.26	32.9

APPENDIX II STRESS-STRAIN RELATIONSHIPS FOR PAVEMENT MATERIALS

II.1 Introduction

The procedure for relating stress and strain measurements, described in section 6.6, assumes that the materials are linear elastic. The simple elastic equations (9-11) result from linear superposition of strains in three orthogonal directions. As a result of these calculations, it has been shown in Chapters 7 and 8 that the materials are in fact non-linear, and that the secant modulus is stress dependent. Because of this conclusion, the initial assumption of linearity is clearly inaccurate, although it was adequate in the context of checking the validity of linear elastic theory, which was the main aim in Chapters 6, 7 and 8. The value of secant modulus calculated at a point was roughly the mean of the values at each stress used in the calculation. Hence the correlation between J_1, which is approximately proportional to the mean of the stresses at a point, and the resulting mean secant modulus shown in figs. 7.2 and 8.1.

The object of this appendix is to relate stress and strain without assuming a linear relationship between

them, in an attempt to indicate more accurately how the materials actually behave under load. This analysis is by no means complete, but does indicate the sort of approach that may be worthwhile pursuing in the future.

II.2 Definitions and Notation

The following expressions are used extensively in this appendix and are, therefore, defined here for convenience.

Shear stress

$$\tau = \frac{p_1 - p_2}{2}$$

Shear strain

$$\gamma = e_1 - e_2$$

with similar expressions for other pairs of principal stresses and strains.

Octahedral shear stress

$$\tau \text{ oct} = \tfrac{1}{3} \sqrt{\{(p_1 - p_2)^2 + (p_2 - p_3)^2 + (p_3 - p_1)^2\}}$$

Octahedral shear strain

$$\gamma \text{ oct} = \tfrac{2}{3} \sqrt{\{(e_1 - e_2)^2 + (e_2 - e_3)^2 + (e_3 - e_1)^2\}}$$

Mean normal stress, (or confining stress)

$$s = \tfrac{1}{3} (p_1 + p_2 + p_3)$$

Dilatation

$$\Delta = e_1 + e_2 + e_3$$

Deviator stress

$$s_1 = p_1 - s$$

with similar expressions for other directions.

II.3 Analysis of results

Since the stress system is three dimensional and the materials are non-linear, a simple relationship between uniaxial stress and strain, required to define secant modulus, is difficult to obtain. It is not particularly useful either, since secant modulus and Poisson's ratio are insufficient information to define the behaviour of the material. The procedure which follows consists of a check on isotropy and, this proven, goes on to relate stress and strain in each of the three principal directions.

At a general point in the material, the three principal stresses are p_1, p_2 and p_3 and the corresponding strains e_1, e_2 and e_3. In section 7.6 and 8.6 principal planes of stress and strain were shown to be coincident, although the correlation was not consistently good. In figs. II.1 and II.2 a further check for isotropy has been carried out by considering shear stress and strain, which are proportional to principal stress and strain differences respectively. Thus $(\frac{p_1 - p_2}{2})$ has been

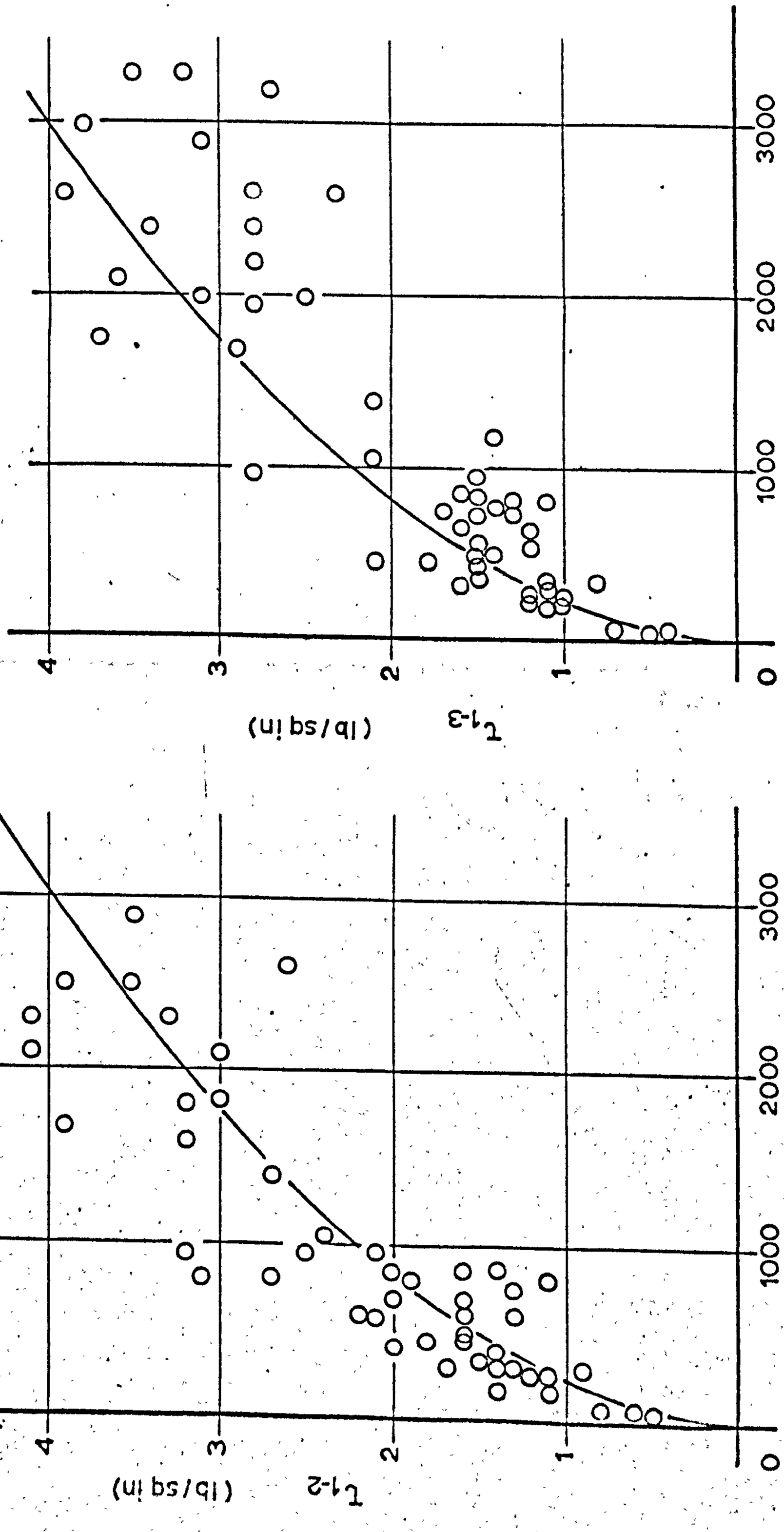

FIG. II.1 SHEAR STRESS AGAINST SHEAR STRAIN FOR KEUPER MARL

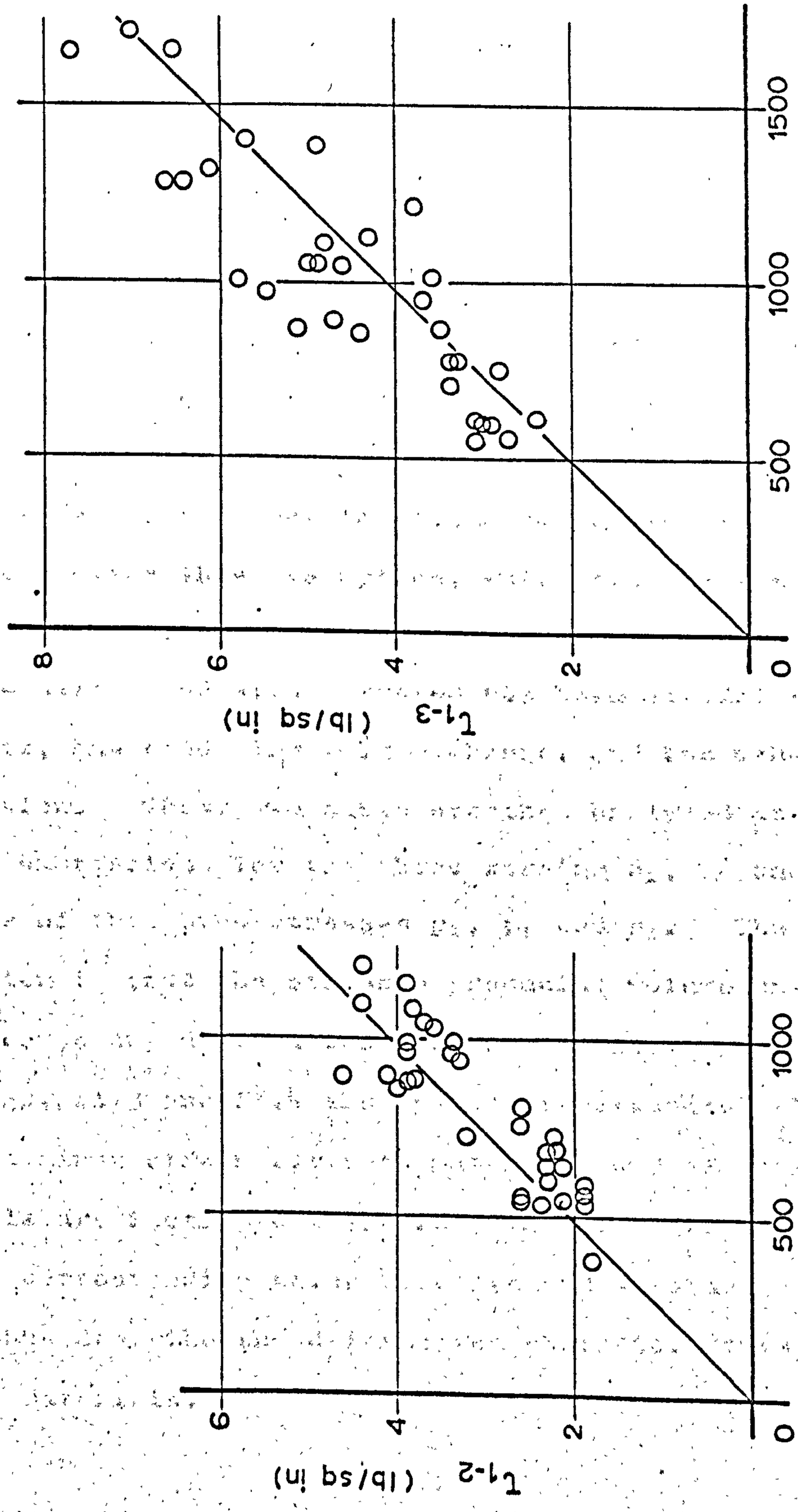

FIG. II.2 SHEAR STRESS AGAINST SHEAR STRAIN FOR MELDON DUST

plotted against ($e_1 - e_2$) and the relationship compared with that obtained by plotting the other two differences. The common factor in each plot is the line fitted to the points on figs. II.2 and II.3 of octahedral shear stress/strain. The relationship is almost the same in each case, although the intermediate and minor principal values are so close as to render this plot of little use and it is not, therefore, included. It was decided that the materials exhibited something close enough to isotropy to proceed using this assumption, which greatly simplifies the calculations.

The stress and strain system has been divided into two parts, one producing volume change, and the other, deformation. These two parts are then analysed to produce expressions for the three strains e_1, e_2 and e_3 in terms of the three stresses p_1, p_2 and p_3. The only assumption is that the stresses producing volume change do not cause any deformation and vice versa.

Figs. II.3 and II.4 show plots of octahedral shear stress against strain for each material, and since the materials are isotropic these relationships are valid for any corresponding shear stresses and strains. These plots thus describe the deformation characteristics of the two materials.

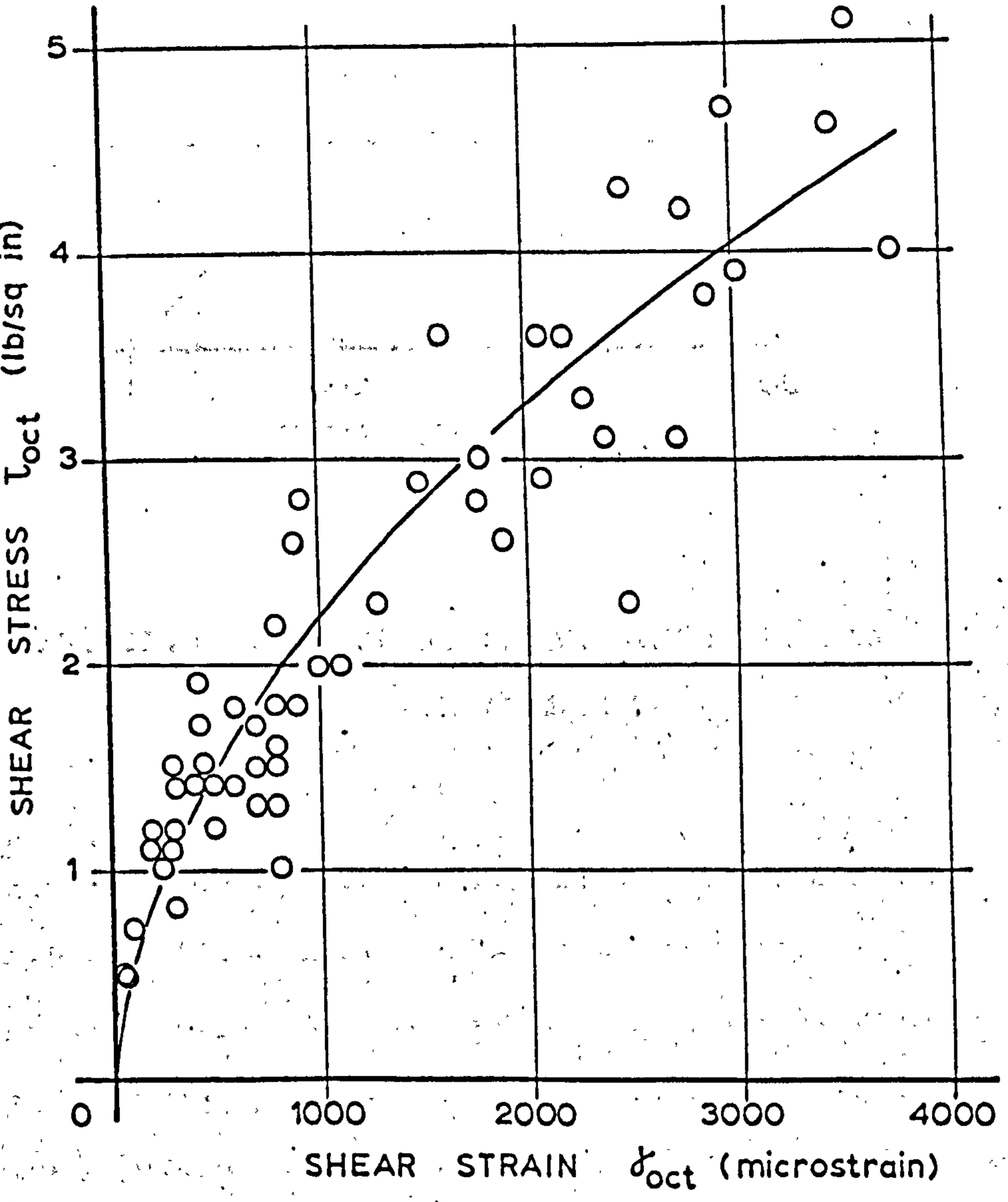

FIG. II.3 OCTAHEDRAL SHEAR STRESS/STRAIN FOR KEUPER MARL

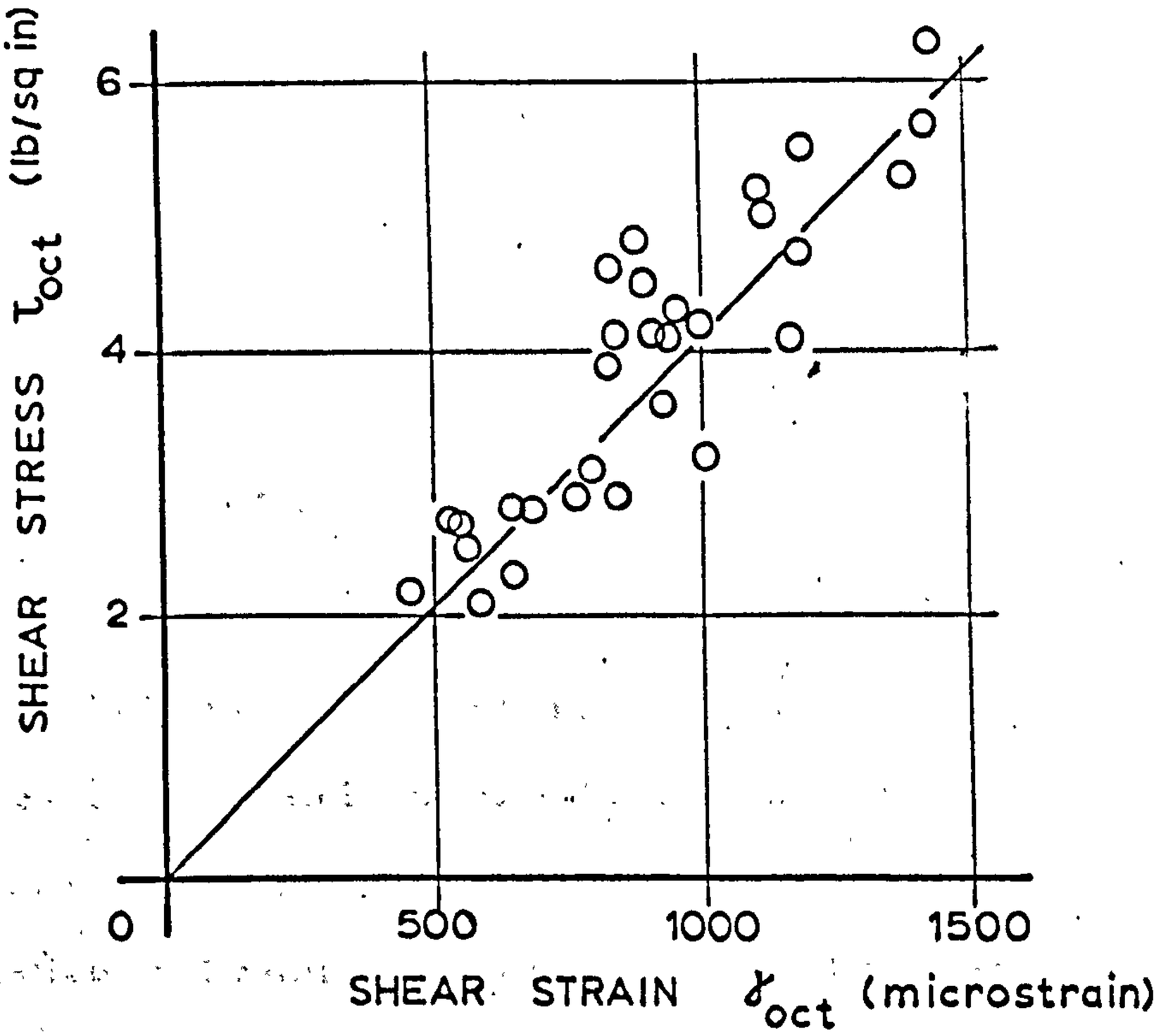

FIG. II.4 OCTAHEDRAL SHEAR STRESS/STRAIN FOR MELDON DUST

The volume change characteristics are shown in figs. II.5 and II.6 where mean normal stress, $s = \frac{1}{3}(p_1 + p_2 + p_3)$ is plotted against the dilatation $\Delta = e_1 + e_2 + e_3$. On the s - Δ plot for Keuper Marl, dilatations less than 200 microstrain have been ignored, since small strain readings were shown to be unreliable (Chapter 4). Curves, or straight lines, have been fitted to the experimental points and are as follows:-

For Keuper Marl:

$$\Delta = 153s \qquad \ldots (12)$$

$$\gamma = 175\ \tau^2 + 50\tau \qquad \ldots (13)$$

For Meldon Dust:

$$1000s = 10\Delta + \frac{6\ \Delta^2}{1000} \qquad \ldots (14)$$

$$\gamma = 242\tau \qquad \ldots (15)$$

where all strains are in microstrain.

The volume change and deformation characteristics for each material are described by these equations. The relationship between confining stress (s) and dilatation (Δ) is the bulk modulus (K), while that between the shear stress (τ) and strain (γ) is the modulus of rigidity (G). It should be noted that, at this stage, K is a constant for the Keuper Marl, and that G is likewise for the Meldon Dust, the other two relationships being quadratics over the range shown.

The strain in each direction is made up of two components, $\frac{\Delta}{3}$ from the volume change, and ϵ from the deformation. Hence

$$e_1 = \frac{\Delta}{3} + \epsilon_1,\ e_2 = \frac{\Delta}{3} + \epsilon_2 \text{ and } e_3 = \frac{\Delta}{3} + \epsilon_3 \qquad \ldots (16)$$

Using equation (12) for Keuper Marl

$$\frac{\Delta}{3} = 51s = 17(p_1 + p_2 + p_3) \qquad \ldots (17)$$

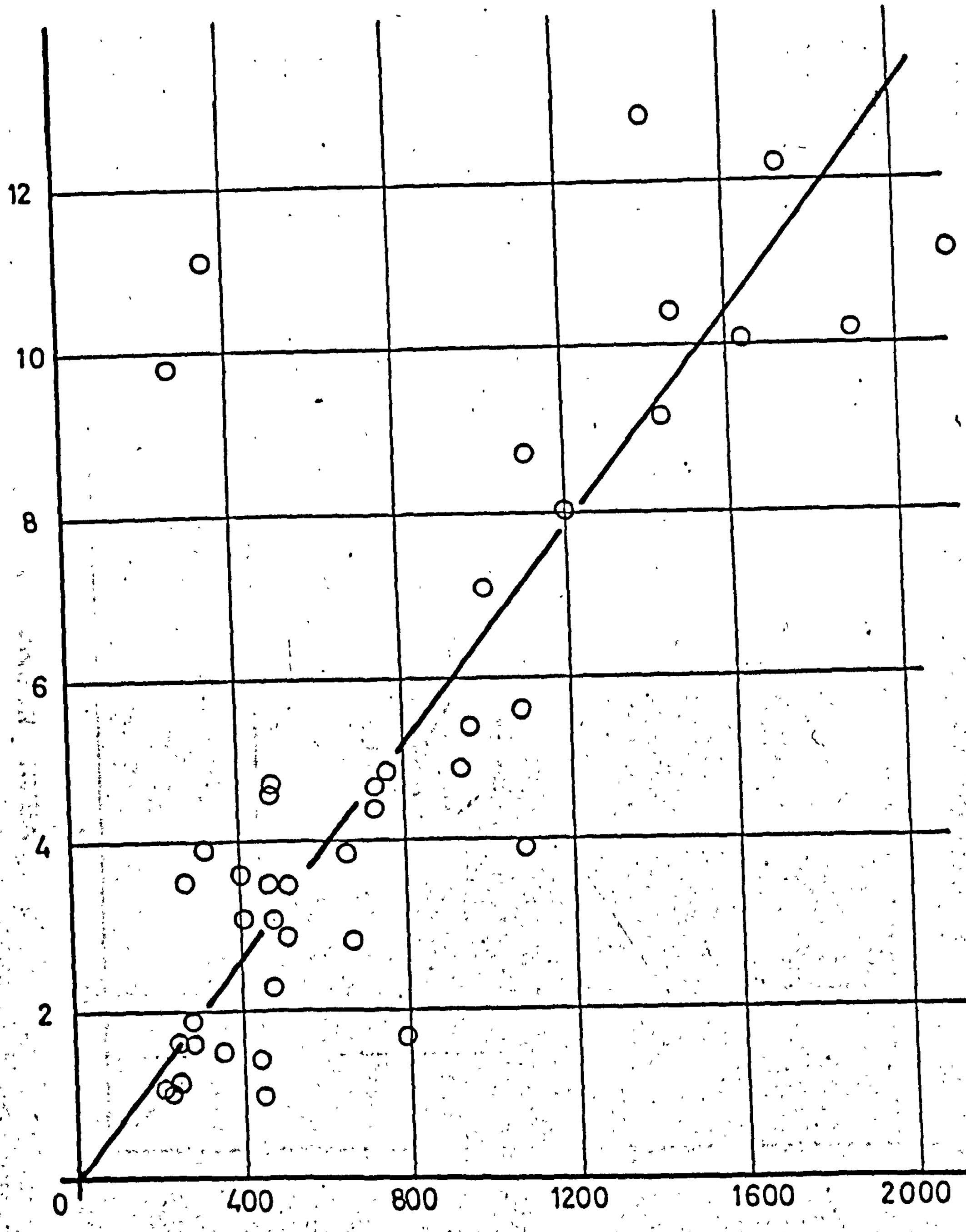

FIG. II.5 MEAN NORMAL STRESS AGAINST DILATATION FOR KEUPER-MARL

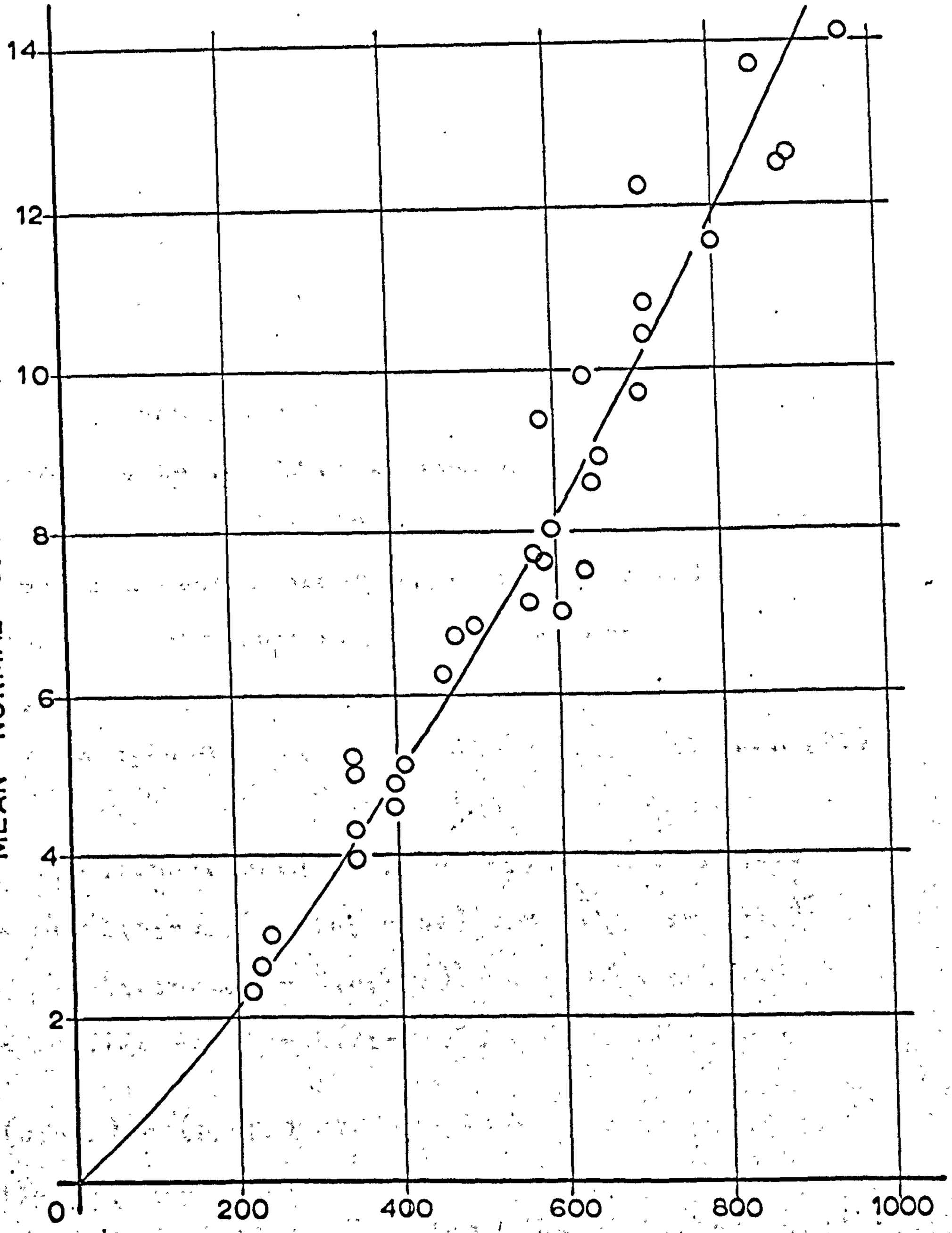

FIG. II.6 MEAN NORMAL STRESS AGAINST DILATATION FOR MELDON DUST

The deviator stresses are:

$$s_1 = p_1 - s,\ s_2 = p_2 - s \text{ and } s_3 = p_3 - s$$

These cause the deformation, resulting in corresponding strains ϵ_1, ϵ_2 and ϵ_3.

From equation (13),

$$\epsilon_1 - \epsilon_2 = 43.8\ (s_1 - s_2)^2 + 25(s_1 - s_2) \quad \ldots (18)$$

$$\epsilon_1 - \epsilon_3 = 43.8\ (s_1 - s_3)^2 + 25(s_1 - s_3) \quad \ldots (19)$$

A third relationship for $\epsilon_2 - \epsilon_3$ is not included since its accuracy is low. This is because $(\epsilon_2 - \epsilon_3) <<< (\epsilon_1 - \epsilon_2)$ or $(\epsilon_1 - \epsilon_3)$ and therefore the assumption of a second order equation for strain difference may introduce significant errors.

As ϵ_1, ϵ_2 and ϵ_3 produce zero volume change,

$$\epsilon_1 + \epsilon_2 + \epsilon_3 = 0 \quad \ldots (20)$$

Solving equations (18) to (20) for ϵ_1, ϵ_2 and ϵ_3 gives

$$\epsilon_1 = 14.6[(s_1-s_2)^2 + (s_1 - s_3)^2] + 8.3(2s_1-s_2-s_3)$$

$$\epsilon_2 = 14.6[(s_1-s_3)^2 - 2(s_1-s_2)^2] + 8.3(2s_2-s_1-s_3)$$

$$\epsilon_3 = 14.6[(s_1-s_2)^2 - 2(s_1-s_3)^2] + 8.3(2s_3-s_1-s_2)$$

Since $(s_1-s_2) = (p_1-p_2)$ and $(2s_1-s_2-s_3) = (2p_1-p_2-p_3)$ equations (16) become:

$$e_1 = 14.6[(p_1-p_2)^2 + (p_1-p_3)^2] + 33.7\ p_1+8.7(p_2+p_3) \ldots (21)$$

$$e_1 = 14.6[(p_1-p_3)^2 -2(p_1-p_2)^2] + 33.7\ p_2+8.7(p_1+p_3) \ldots (22)$$

$$e_3 = 14.6[(p_1-p_2)^2 -2(p_1-p_3)^2] + 33.7\ p_3+8.7(p_1+p_2) \ldots (23)$$

An expression relating stress and the resulting strain in the same direction is required in order to obtain an expression for secant modulus, thus correlating this approach with the linear elastic method, and with triaxial results. This can most easily be done by considering the "unconfined" case, i.e. $p_2 = p_3 = 0$ hence

$$e_1 = 29.2\ p_1^2 + 33.7\ p_1 \qquad \text{... from (21)}$$

$$\therefore \frac{1}{E} = \frac{e_1}{p_1} = 29.2\ p_1 + 33.7$$

The relationship between E and p_1 is shown in fig. II.7, from which it is clear that the earlier calculations indicate a stiffer soil. This comparison may not be entirely accurate since a three dimensional problem has been artificially reduced to a uniaxial one, a case which never occurs in the soil.

If the "unconfined" case is again considered an expression for Poisson's ratio can also be obtained, since

$$e_2 = -14.6\ p_1^2 + 8.7\ p_1 \qquad \text{... from (22)}$$

and

$$\nu = -\frac{e_2}{e_1} = \frac{14.6\ p_1 - 8.7}{29.2\ p_1 + 33.7}$$

$$\text{or } \nu = \frac{p_1 - 0.6}{2\ p_1 + 2.3}$$

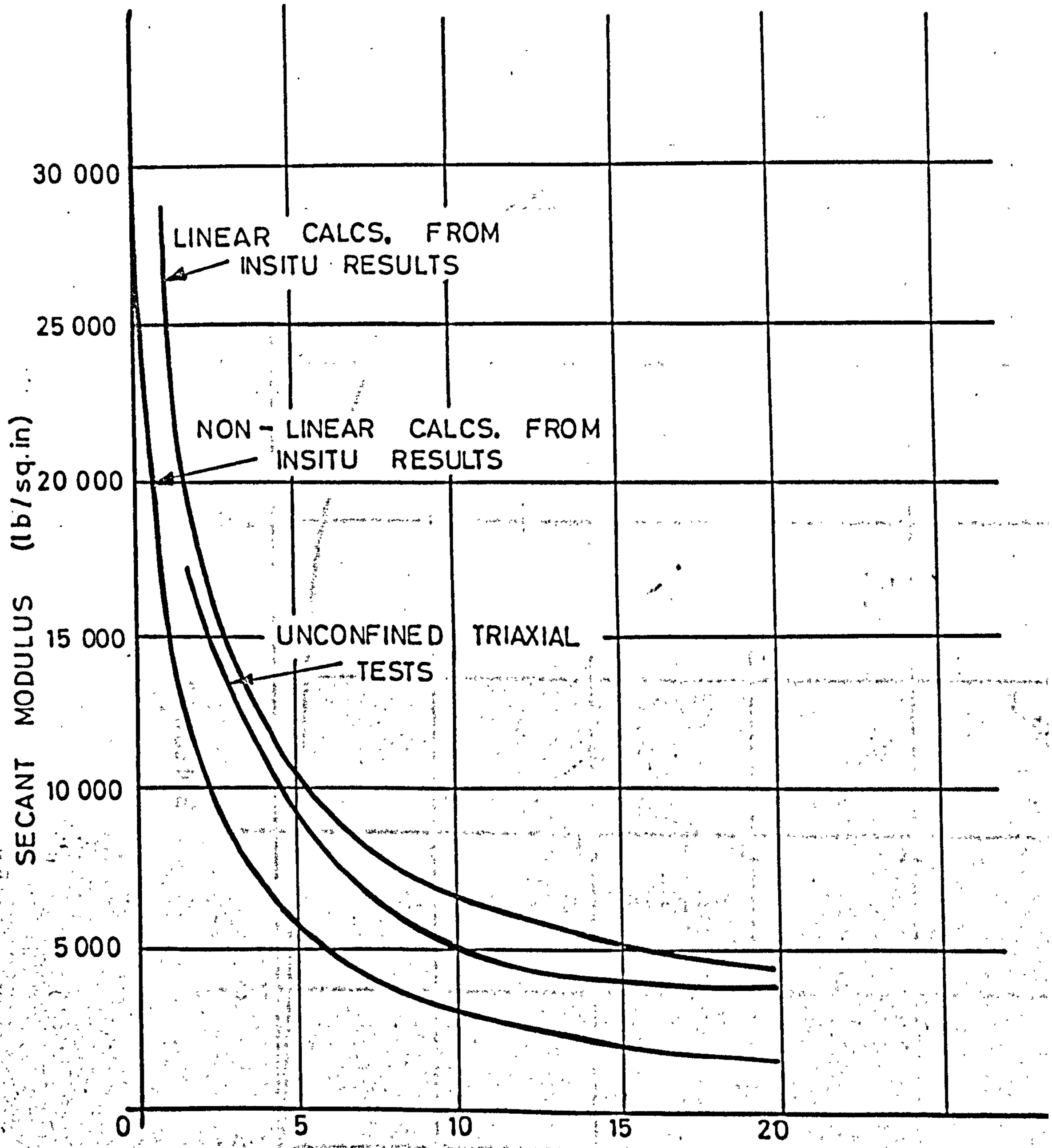

FIG. II.7 SECANT MODULUS AGAINST MAJOR PRINCIPAL STRESS IN THE UNCONFINED CASE FOR KEUPER MARL

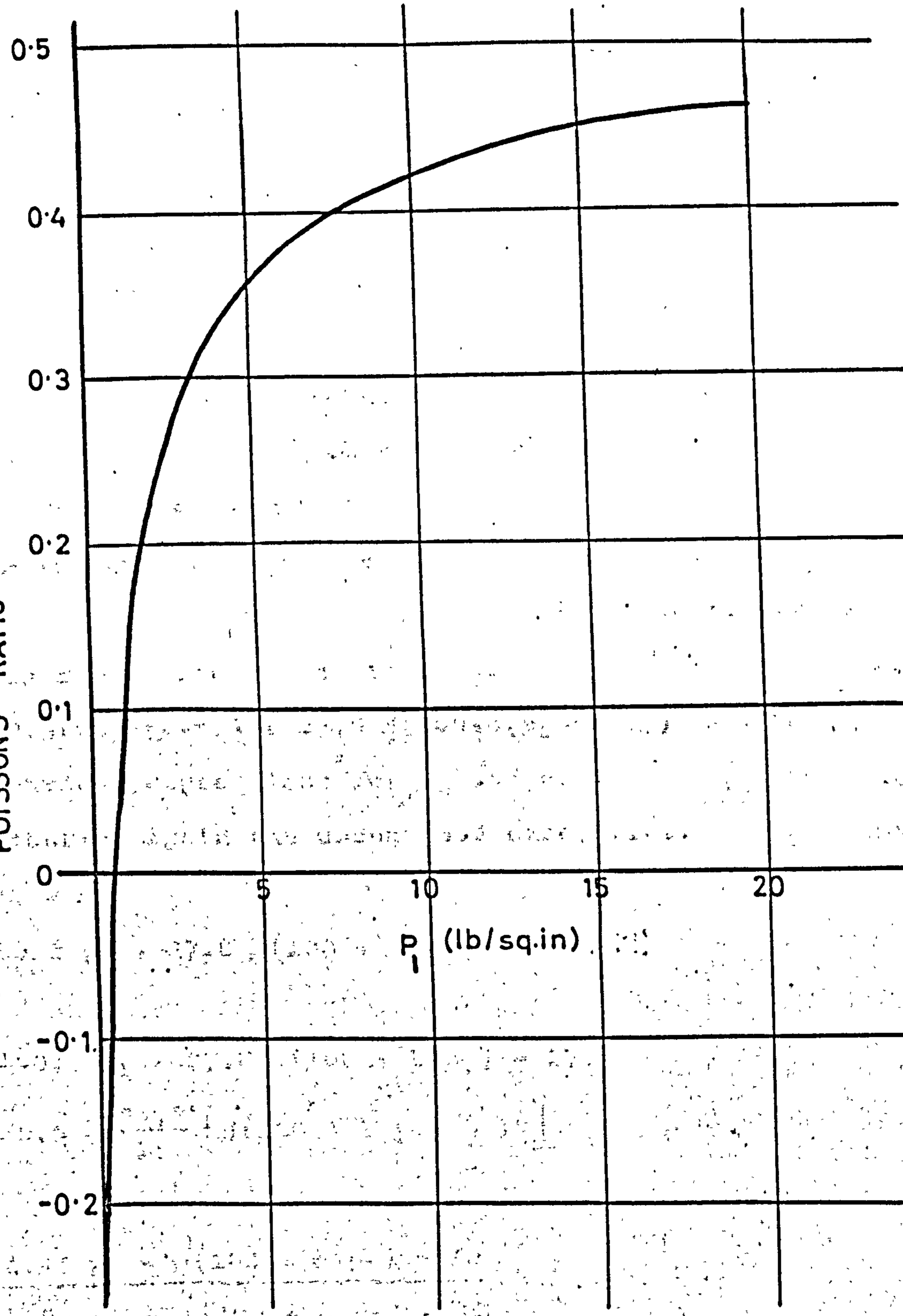

FIG. II.8 POISSON'S RATIO AGAINST MAJOR PRINCIPAL STRESS IN THE UNCONFINED CASE FOR KEUPER MARL

This expression has been plotted in fig. II.8. There is no obvious physical explanation for the negative values of Poisson's ratio at stresses less than 0.6 lb/sq.in. This peculiarity may be a result of the various approximations involved in deriving the expression for ν, especially the imposition of uniaxial conditions, as discussed above. The mean value for Poisson's ratio obtained from the linear elastic calculations was 0.41 which compares favourably with fig. II.8 except for stresses less than about 5 lb/sq.in.

A similar analysis has been carried out for the Meldon Dust, using equations (14) and (15). The resulting expressions for strain are as follows:

$$e_1 = 40.3(2p_1 - p_2 - p_3) + 27.8\sqrt{[100 + 8(p_1 + p_2 + p_3)]} - 278$$

with symmetrical expressions for e_2 and e_3.

Considering again the unconfined case, i.e.,

$$p_2 = p_3 = 0$$

$$e_1 = 80.6\ p_1 + 27.8\sqrt{(100 + 8\ p_1)} - 278$$

and

$$e_2 = -40.3\ p_1 + 27.8\sqrt{(100 + 8\ p_1)} - 278$$

$$\therefore \frac{1}{E} = 80.6 + \frac{27.8}{p_1}\left[\sqrt{(100 + 8\ p_1)} - 10\right]$$

and

$$\nu = \frac{1.45\ p_1 - \sqrt{(100 + 8\ p_1)} + 10}{2.9\ p_1 + \sqrt{(100 + 8\ p_1)} - 10}$$

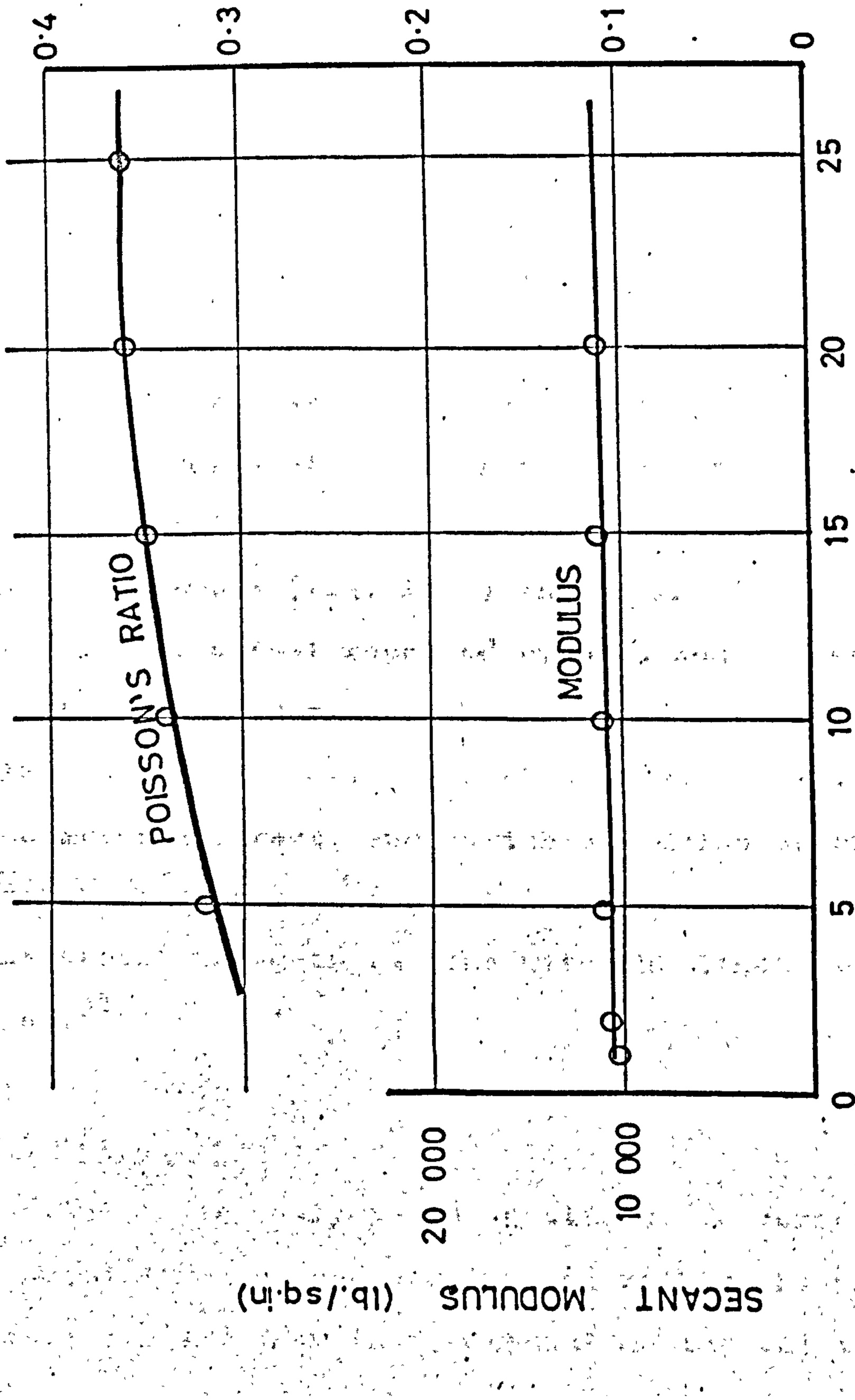

FIG. II.9 SECANT MODULUS AGAINST MAJOR PRINCIPAL STRESS IN THE UNCONFINED CASE FOR MELDON DUST AND POISSON'S RATIO

The variation of E and ν with p_1 is shown in fig. II.9, where it is clear that both functions are almost independent of stress, for the unconfined case. This indicates that for the granular material, secant modulus is independent of the stress causing deformation, i.e., the deviator stress, a conclusion supported by the fact that the modulus of rigidity is constant (see fig. II.4). The bulk modulus of the granular material varies with confining stress (fig. II.6) indicating that secant modulus also varies, a fact reported by Seed and others.[6,15]

The Keuper Marl shows a converse effect; constant bulk modulus indicating secant modulus to be independent of confining stress, and variable modulus of rigidity indicating that secant modulus varies with confining stress. This effect is again in line with the findings of Seed et al.[34]

II.4 Discussion

The above analysis is an attempt to correlate the measured stresses and strains, or rather the principal values derived from them, without making the assumption of linearity used in the main part of the thesis.

The equations for strain as functions of stress at a point, derived above, only apply for the materials used

in this project at the moisture contents which were used. Thus they are restrictive, but are perhaps descriptive of the sort of behaviour to be expected from a silty clay and a crushed stone of small particle size.

The analysis has shown that an exact theoretical solution based on the actual behaviour of soils such as have been used here, is likely to be extremely complicated.

It is difficult to compare the results of this analysis with those based on linear elastic calculations, because this very assumption makes the two approaches quite different. The approximate comparisons carried out for the unconfined case indicate that the Keuper Marl is less stiff than was indicated by linear elastic calculations. The actual value calculated for the Meldon Dust is quite hypothetical since with zero confining stress, its secant modulus is clearly very low. The fact that it is almost independent of stress is, however, interesting as noted in II.3 above.

This analysis does not presume to be complete by any means, but is presented as the basis of a possibly more accurate means of determining the behaviour of the materials in which the stress and strain measurements were taken.